LATE PRECAMBRIAN (HADRYNIAN) ASH-FLOW TUFFS AND ASSOCIATED ROCKS OF THE HARBOUR MAIN GROUP NEAR COLLIERS, AVALON PENINSULA, S. E. NEWFOUNDLAND

CENTRE FOR NEWFOUNDLAND STUDIES

TOTAL OF 10 PAGES ONLY
MAY BE XEROXED

(Without Author's Permission)

GRAHAM T. NIXON

copy 1

100231

CENTRE FOR NFLD. STUDIES
JAN 14 1977
MEMORIAL UNIVERSITY
OF NEWFOUNDLAND

LATE PRECAMBRIAN (HADRYNIAN) ASH-FLOW TUFFS AND ASSOCIATED ROCKS OF THE HARBOUR MAIN GROUP NEAR COLLIERS, AVALON PENINSULA, S. E. NEWFOUNDLAND

by

GRAHAM T. NIXON

A THESIS

Submitted in partial fulfillment of the requirements for the degree of

MASTER OF SCIENCE

Memorial University of Newfoundland

October 1974

© GRAHAM T. NIXON 1976

Frontispiece. Finn Hill, Colliers, viewed from the west.

Table of Contents

	Page
Abstract	I
List of Tables	IV
List of Figures	VI
List of Plates	VIII
List of Photomicrographs	X
CHAPTER I. INTRODUCTION	1
1.1. Location and Access	2
1.2. Historical Background	2
1.3. Physiography and Climate	3
1.4. Geological Setting of Eastern Avalon in the light of Previous Work	3
1.5. General Geology of the Colliers Peninsula	8
1.6. Present Study	9
1.7. Mapping Methods	10
1.8. Acknowledgments	10
CHAPTER II. ASH-FLOW TUFFS OF THE HARBOUR MAIN GROUP	12
2.1. Terminology of the Volcaniclastic Rocks	12
2.2. Ash-Flow Deposits: An Introduction and Field Relationships	15
2.2.1. Bacon Cove Ash-Flow Sequence	17
2.2.2. Weavers Hill Ash-Flow Sequence	25
2.2.3. Finn Hill Ash-Flow Sequence	32

Table of Contents (Cont'd.)

CHAPTER II. (Cont'd.) Page

2.3. Mechanism of Ash-Flow Emplacement 39

2.4. Provenance and Magnitude of the Ash-Flow Deposits 45

CHAPTER III. TEXTURES AND MINERALOGY OF THE ASH-FLOW TUFFS .. 53

3.1. Bacon Cove Ash-Flow Sequence 53

3.1.1. Textures 53

3.1.2. Mineralogy 55

3.2. Weavers Hill Ash-Flow Sequence 56

3.2.1. Textures 57

3.2.2. Mineralogy 59

3.3. Finn Hill Ash-Flow Sequence 59

3.3.1. Textures 60

3.3.2. Mineralogy 63

3.4. Devitrification and Hydration 64

CHAPTER IV. LAVA FLOWS AND HYPABYSSAL INTRUSIVE ROCKS OF THE HARBOUR MAIN GROUP 69

4.1. Felsic Lava Flows 69

4.1.1. Rhyolite 69

4.1.2. Dacite 70

4.2. Mafic Lava Flows 71

4.3. Aphanitic Rhyolite Sills 74

4.4. Porphyritic Sills or "Porphyrites" 76

4.5. Diabase Dykes 81

Table of Contents (Cont'd.)

		Page
CHAPTER IV. (Cont'd.)		
4.6.	Olivine Diabase (Picritic) Sill	82
4.7.	Diabase Sill(?) intrusive into the Conception Group	83
CHAPTER V.	SEDIMENTARY ROCKS	84
5.1.	Epiclastic Deposits of the Harbour Main Group	84
5.1.1.	Volcanic Breccias and Conglomerates	84
5.1.2.	Volcanic Sandstones and Argillaceous Siltstones	86
5.2.	Conception Group	87
5.3.	Cambrian Rocks	89
CHAPTER VI.	STRUCTURE	90
6.1.	Folding and Cleavage	90
6.2.	Faulting	92
6.3.	Summary	94
6.4.	Discussion	95
CHAPTER VII.	ALTERATION AND METAMORPHISM	97
7.1.	Felsic Volcanic Rocks	98
7.2.	Intermediate and Mafic Volcanic Rocks	107
7.3.	Genesis of the Alteration and Metamorphism	109
7.4.	Timing of the Alteration and Metamorphism	113
CHAPTER VIII.	MINERAL AND WHOLE-ROCK CHEMISTRY	116
8.1.	Electron-Probe Microanalysis of Feldspar Phenocrysts	119

Table of Contents (Cont'd.)

CHAPTER VIII. (Cont'd.) Page

8.1.1. Significance of Metamorphic Compositions 129

8.1.2. Significance of Magmatic Compositions 132

8.2. Whole-Rock Analytical Data 135

8.2.1. Rhyolitic Ignimbrites 184

8.2.1.1. Chemical Effects of Alteration 185

8.2.1.2. Quantitative Aspects of Alkali Metasomatism 192

8.2.1.3. Magmatic Trends and Affinities 197

8.2.2. Porphyrites 209

8.2.3. Basaltic Rocks 217

8.2.4. Magmatic Evolution of the Harbour Main Volcanic Suite 243

CHAPTER IX. GENERAL CONCLUSIONS AND A TENTATIVE MODEL FOR LATE PRECAMBRIAN MAGMATISM AND TECTONISM ON AVALON 250

Bibliography 260

Appendix 1. Whole-Rock Analyses (Molecular %) 282

Appendix 2. Feldspar Analyses (Molecular %) 284

Appendix 3. Analytical Procedures 287

Appendix 4. Theoretical Predictions of Trace Element Behaviour 299

Plates i

Photomicrographs xiii

ABSTRACT

Late Precambrian (Hadrynian) volcanic rocks of the western part of the Harbour Main Group near Colliers comprise a thick succession of chiefly rhyolitic ash-flow tuffs overlain by basaltic lavas and intruded by porphyritic sills of intermediate composition. The tuffs form three distinct ash-flow sequences, each composed of a number of simple cooling units. The Bacon Cove sequence at the base of the section, the Weavers Hill sequence in the middle, and the Finn Hill sequence at the top, are each characterised by contrasting phenocryst assemblages consisting of albite + quartz + biotite, albite + quartz, and albite + minor quartz and clinopyroxene, respectively. Concentration of crystals and xenoliths near the base of individual cooling units is a direct result of gravitative settling of the suspended load during ash-flow emplacement together with concomitant winnowing of the fine ash fraction. The majority of the Colliers ash-flow tuffs probably represent the distal deposits of a much larger ash-flow field originally situated to the north of the map area.

Subsequent devitrification and hydration of volcanic glass have preserved vitroclastic textures with remarkable fidelity. The devitrification textures so formed locally resemble structures produced during the experimental devitrification of natural rhyolite glass.

Mild structural deformation dated as Late Hadrynian and post-Cambro-Ordovician involved block-faulting and two distinct periods of

folding and weak penetrative deformation. Metasomatic alteration largely preceded a regional metamorphism of prehnite-pumpellyite grade which may have accompanied Late Precambrian folding.

Electron microprobe analysis of feldspar compositions throughout the complete range of Harbour Main volcanic rocks revealed predominantly albite and K-feldspar of metamorphic origin, and rare igneous anorthoclase and calcic plagioclase.

The chemical effects of alteration processes on the whole-rock analyses have been examined quantitatively where possible prior to classification of magmatic trends and affinities. Localised metasomatism involved mobility of essentially Na_2O, K_2O, CaO, Rb, and Ba. The least mobile constituents are Al_2O_3, TiO_2, total Fe, Zr, Cr, and Ni.

The silicic ash-flow tuffs and granitoid rocks of the Harbour Main Group are very similar in composition and characterised by high total alkalies, Ba, and K/Rb, and low CaO and Rb/Sr. Ba/Sr and Rb/Sr ratios indicate that plagioclase was precipitated early in the differentiation history of rhyolitic magmas and that biotite was a comparatively late phase to arrive on the liquidus. The porphyritic sills or "porphyrites" have relatively high K_2O, Ba, and Rb, and low CaO and Sr, and are very similar in composition to continental interior "andesites". The basaltic rocks are "transitional" to "mildly alkaline" chemical types with typically high Al_2O_3 and low TiO_2. The main rock-types of the Harbour Main Group cannot be related simply by fractional crystallisation of a parental silicate melt.

The accumulated chemical data and prominent bimodal association strongly suggest that the Harbour Main volcanic suite was emplaced in an environment characterised by rifting and distension of continental lithosphere. It is suggested that the ash-flow tuffs and porphyrites originated by partial fusion of the lower continental crust and that the basaltic rocks were derived by partial melting of an upper mantle source region.

List of Tables

Table		Facing Page/ Page
Table 1.	Lithostratigraphic units of the Avalon Peninsula, S.E. Newfoundland	3
Table 2.	Terminology and grain-size for pyroclastic rock fragments	13
Table 3.	Bacon Cove ash-flow sequence	18
Table 4.	Weavers Hill ash-flow sequence	26
Table 5.	Finn Hill ash-flow sequence	33
Table 6.	Electron microprobe partial analyses of feldspar phenocrysts	121
Table 7.	Whole-rock analyses	136
Table 8.	Correlation matrices for 82 whole-rock analyses of Harbour Main Group volcanic rocks, Colliers Peninsula	176
Table 9.	Table of averages	177
Table 10.	Major and trace element compositions of rhyolitic ignimbrites, flows, and granitoid rocks used for comparison with Harbour Main ignimbrites	205
Table 11.	Major and trace element compositions of andesitic lavas and plutonic rocks used for comparison with intermediate intrusive rocks ("porphyrites") of the Harbour Main Group	213
Table 12.	Major element compositions of basalts used for comparison with Harbour Main basaltic rocks	229

List of Tables (Cont'd.)

Table 13. Rank order of basalts used for comparison with feldsparphyric basalts, Harbour Main Group 233

Table 14. Rank order of basalts used for comparison with olivine basalt, Harbour Main Group 236

Table 15. Selected estimates of the average composition of the continental crust 256

Table 16. "Classical" analyses of McGill feldspar standards 288

Table 17. Electron-probe sequence of measurements per analytical run 289

Table 18. Precision of electron-probe analyses 291

Table 19a. Precision of major element analyses 296

Table 19b. Precision of trace element analyses 296

Table 20a. Accuracy of major element analysis as determined by fit of standards to calibration curve 297

Table 20b. Accuracy of major element analysis as determined by comparison of 24 samples analysed by X-ray fluorescence and atomic absorption 297

Table 20c. Accuracy of trace element analysis by fit of standards to calibration curve 298

List of Figures

Figure		Facing Page
Figure 1.	Location map of Colliers Peninsula, S.E. Newfoundland	2
Figure 2.	General geology of Avalon Peninsula, S.E. Newfoundland	3
Figure 3.	General geology of Colliers Peninsula	9
Figure 4.	Location of geochemical sampling sites outside the map area	9
Figure 5.	Or: Ab: An diagram for selected feldspar analyses	127
Figure 6.	Major elements vs. silica for Harbour Main Group volcanic rocks, Colliers Peninsula	183
Figure 7a.	Qz: Ab: Or diagram for felsic volcanic rocks (Bacon Cove ash-flow sequence)	188
Figure 7b.	Qz: Ab: Or diagram for felsic volcanic rocks (Weavers Hill ash-flow sequence)	188
Figure 7c.	Qz: Ab: Or diagram for felsic volcanic rocks (Finn Hill ash-flow sequence)	188
Figure 7d.	Qz: Ab: Or diagram for main compositional fields of felsic volcanic rocks	188
Figure 8.	Na_2O vs. K_2O: ash-flow tuffs and felsic flows	196
Figure 9.	An: Ab: Or diagram for felsic volcanic rocks	200
Figure 10a.	Qz: Or: Ab + An diagram: classification	200
Figure 10b.	Qz: Or: Ab + An diagram for felsic volcanic rocks	200
Figure 10c.	Qz: Or: Ab + An diagram for average compositions of ash-flow tuffs	200

List of Figures (Cont'd.)

Figure 11. An: Ab: Or diagram for mafic and intermediate volcanic rocks 210

Figure 12. Total alkalies vs. alumina for Harbour Main Group volcanic rocks, Colliers Peninsula 210

Figure 13. Trace elements vs. silica for Harbour Main Group volcanic rocks, Colliers Peninsula 210

Figure 14. K/Rb ratios for Harbour Main Group volcanic rocks, Colliers Peninsula 244

Figure 15. Rb/Sr ratios for Harbour Main Group volcanic rocks, Colliers Peninsula 244

Figure 16. Ti/Zr ratios for Harbour Main Group volcanic rocks, Colliers Peninsula 245

Figure 17. Alkali-lime index for Harbour Main Group volcanic rocks, Colliers Peninsula 245

Figure 18. Total alkalies vs. silica diagram for Harbour Main Group volcanic rocks, Colliers Peninsula 246

Figure 19. AFM diagram for Harbour Main Group volcanic rocks, Colliers Peninsula 246

Figure 20. Distribution of chemical analyses and estimated abundances of volcanic rock-types in various environments 247

List of Plates

Plate		Page
Frontispiece	Finn Hill, Colliers	
Plate 1.	Dark green collapsed pumice-lapilli	i
Plate 2.	James Cove, Colliers Bay	ii
Plate 3.	Strike ridges ~~of~~ Finn Hill sequence ignimbrites	ii
Plate 4.	Xenolith of feldsparphyric basalt in welded tuff	iii
Plate 5.	Eutaxitic fiamme, Finn Hill	iii
Plate 6.	Ryans Head and Burkes Cove	iv
Plate 7.	Eutaxitic fiamme, Burkes Cove	iv
Plate 8.	Slump structure in welding, Burkes Cove	v
Plate 9.	Eastern rhyolite sill	v
Plate 10.	Large porphyrite intrusion near Kitchuses	vi
Plate 11.	Xenolith of quartz-monzonite in porphyrite	vi
Plate 12.	Autobrecciated porphyrite	vii
Plate 13.	Brecciated porphyrite intruding reddish siltstones	vii
Plate 14.	Mud ball horizon in thinly-bedded siltstones, Harbour Main Group	viii
Plate 15.	Poorly consolidated cobble conglomerate	viii
Plate 16.	Fine-grained volcanic breccias, sandstones, and siltstones, Harbour Main Group	ix
Plate 17.	Folded Conception siltstones	ix
Plate 18.	Angular unconformity, Bacon Cove	x

List of Plates (Cont'd.)

Plate		Page
Plate 19.	Synform in thinly-bedded sandstones and siltstones, Harbour Main Group	x
Plate 20.	Tight syncline in Conception siltstones	xi
Plate 21.	Red- and green-altered tuff, Campbell Hill	xii
Plate 22.	Green altered volcanic breccias	xii

List of Photomicrographs

Photomicrograph		Page
Photomicrograph 1:	Granophyre xenolith	xiii
Photomicrograph 2:	Pink to pale green mottled fragment of recrystallised tuff in volcanic breccia	xiii
Photomicrograph 3:	Fragment of flow-banded rhyolite in Conception greywacke	xiv
Photomicrograph 4:	Tricuspate, cuspate, and rod-like shards exhibiting open vitroclastic texture	xiv
Photomicrograph 5:	Altered, densely welded crystal-vitric tuff enclosing devitrified platy shards	xv
Photomicrograph 6:	Densely welded vitric tuff	xv
Photomicrograph 7:	Microspherulitic alkalic feldspar in the matrix of a sillar, nucleated preferentially along crystal boundaries	xvi
Photomicrograph 8:	Euhedral paramorph of alpha-quartz after beta-quartz in ignimbrite	xvi
Photomicrograph 9:	Partially resorbed quartz and oxidised biotite phenocrysts in sillar	xvii
Photomicrograph 10:	Altered biotite phenocryst	xvii
Photomicrograph 11:	Deformed biotite phenocrysts	xviii
Photomicrograph 12:	Ragged, comminuted pumice coated with hematite and set in a bleached vitroclastic matrix	xviii
Photomicrograph 13:	Delicate cuspate, platy, and rod-like shards set in a finely comminuted, hematitic matrix	xix
Photomicrograph 14:	Eutaxitic pumice-lapilli exhibiting delicately frayed extremities and recrystallisation to alkalic feldspar and quartz	xix

List of Photomicrographs (Cont'd.)

Photomicrograph 15: Same specimen as photomicrograph 14 xx

Photomicrograph 16: Collapsed pumice-lapilli exhibiting fibres of quartz and alkalic feldspar in axiolitic intergrowth..... xx

Photomicrograph 17: Pumice fragment exhibiting concentric layers of chiefly alkali feldspar with fine axiolitic structure coated with opaque dust and partly replaced by sericite xxi

Photomicrograph 18: Non-welded vitroclastic texture xxi

Photomicrograph 19: Dense welding in central part of dark brown fiamme-bearing ignimbrite xxii

Photomicrograph 20: Perlite cracks in devitrified densely welded ignimbrite xxii

Photomicrograph 21: Same specimen as photomicrograph 20. Perlite cracks developed preferentially in fiamme xxiii

Photomicrograph 22: Same specimen as photomicrograph 20. Welding wraps around lithophysal cavities xxiii

Photomicrograph 23: Same specimen as photomicrograph 20. Crystallisation products impinging on a rock fragment xxiv

Photomicrograph 24: Intensely recrystallised fiamme-bearing ignimbrite xxiv

Photomicrograph 25: Lamellar twinning in clinopyroxene microphenocryst xxv

Photomicrograph 26: Irregular recrystallisation destroying densely welded textures in ignimbrite xxv

Photomicrograph 27: Bleached spherulitic rim to shard remnant exhibiting dense welding xxvi

Photomicrograph 28: Same specimen as photomicrograph 27..... xxvi

Photomicrograph 29: Same specimen as photomicrograph 27. Thin curvilinear "canals" of minor alkalic feldspar in a quartz base xxvii

List of Photomicrographs (Cont'd.)

Photomicrograph 30: Same specimen as photomicrograph 27. Microspherulitic quartz, alkali feldspar, granular magnetite and relict shards xxvii

Photomicrograph 31: Same specimen as photomicrograph 27. Micropoikilitic quartz concentrated near center of spherulite xxviii

Photomicrograph 32: Well-developed perlitic cracks in recrystallised welded tuff xxviii

Photomicrograph 33: Incipient development of microspherulitic alkali feldspar and granophyric quartz in devitrified tuff fragment xxix

Photomicrograph 34: Same specimen as photomicrograph 33. Typical development of "bird's-eye" devitrification textures in welded tuff xxix

Photomicrograph 35: Same specimen as photomicrograph 33. "Bird's-eye" devitrification involving granophyric quartz and microspherulitic alkali feldspar xxx

Photomicrograph 36: Fairly sharp contact between microspherulitic devitrification textures (quartz, alkalic feldspar, opaques) and bleached cryptocrystalline zone in which shard outlines are barely visible xxx

Photomicrograph 37: Same specimen as photomicrograph 36.

Photomicrograph 38: Same specimen as photomicrograph 36. Finely crystalline zone separating coarse and cryptocrystalline devitrification products xxxi

Photomicrograph 39: Amphibole microphenocrysts in dacite oriented subparallel to the flow-banding xxxi

Photomicrograph 40: Subhedral amphiboles in dacite replaced by alkalic feldspar, chlorite, and clay minerals xxxii

Photomicrograph 41: Groundmass olivine in mafic lava flow exhibiting a core of fresh olivine xxxii

List of Photomicrographs (Cont'd.)

Photomicrograph 42: Olivine phenocrysts and microphenocrysts in mafic lava flow xxxiii

Photomicrograph 43: Amygdaloidal top of mafic lava flow..... xxxiv

Photomicrograph 44: Subhedral phenocrysts of albite enclosing tiny inclusions of chlorite (original glass) and exhibiting zonal replacement by epidote xxxiv

Photomicrograph 45: Glomeroporphyritic intergrowth of chlorite pseudomorphous after pyroxene, magnetite, and subhedral apatite xxxv

Photomicrograph 46: Feldsparphyric dyke with hyalophitic texture xxxv

Photomicrograph 47: Sharp contact between successive intrusive phases of a multiple dyke xxxvi

Photomicrograph 48: Olivine diabase containing subhedral olivine phenocrysts xxxvi

Photomicrograph 49: Green biotite phenocryst in sericitised and bleached welded tuff xxxvii

Photomicrograph 50: Albite phenocryst dusted with hematite showing alteration to sericite and clay minerals xxxvii

Photomicrograph 51: Epidotised shards in welded tuff xxxviii

Photomicrograph 52: Intense recrystallisation of dacite to a fine-grained assemblage of "mossy" epidote, quartz, and albite xxxviii

Photomicrograph 53: Incipient welding in sericitised crystal-lithic tuff xxxix

Photomicrograph 54: Same specimen as photomicrograph 53 xxxix

Photomicrograph 55: Mottled albite glomerocryst exhibiting patchy replacement by potassium feldspar and minor sericite xxxx

Photomicrograph 56: K-feldspar spreading from fractures and partly replacing resorbed albite phenocryst .. xxxx

List of Photomicrographs (Cont'd.)

Photomicrograph 57: Well-developed "chequered" twinning in albite phenocryst xxxxi

Photomicrograph 58: Development of chequered twinning in albite xxxxi

Photomicrograph 59: "Tuffisite" pipe transecting welded tuff and carrying rotated fragments and crystals xxxxii

Photomicrograph 60: Same specimen as photomicrograph 59 xxxxii

Photomicrograph 61: Veins of albite and epidote promoting recrystallisation of iron oxide at their margins xxxxiii

Photomicrograph 62: Electron-probe X-ray image photomicrographs showing patchy development of sericite within an albite phenocryst xxxxiv

Photomicrograph 63: Electron-probe photomicrographs of K-feldspar along fractures in an albite phenocryst and partly replacing its host xxxxv

Photomicrograph 64: Electron-probe photomicrographs of K-Na cryptoperthite along fractures and cleavage planes within an albite phenocryst xxxxvi

CHAPTER I

INTRODUCTION

The Avalon Peninsula of southeastern Newfoundland is formed by a northerly trending belt of Late Precambrian (Hadrynian) volcanic, plutonic, and sedimentary rocks that are little deformed and metamorphosed, and that are overlain locally by the eroded remnants of a thin platformal succession of Cambro-Ordovician shales, limestones, and sandstones. The oldest Proterozoic unit (the Harbour Main Group) forms the core (15 miles; 24km wide) of Eastern Avalon, and consists of a subaerial assemblage of felsic and mafic lava flows, silicic ignimbrites, and volcanogenic sediments intruded by hypabyssal rocks (rhyolite and "porphyrite" sills, and diabase dykes) and a granitoid pluton (the Holyrood Plutonic Series). The Harbour Main and Holyrood rocks are unconformably overlain to the east and west by a sequence of marine sediments consisting mainly of greywackes and cherts locally intercalated with volcanogenic material and glaciomarine deposits (the Conception and Connecting Point Groups). The marine sequences are flanked in turn by coarser grained, molasse-type detritus of shallow marine and fluviatile origin (Cabot and Hodgewater Groups).

The study presented below comprises a detailed volcanological and petrological account of the volcanic rocks of the Harbour Main Group with special emphasis placed on the ash-flow deposits.

FIG. 1. Location map of Colliers Peninsula, S.E. Newfoundland (after Brueckner, 1969).

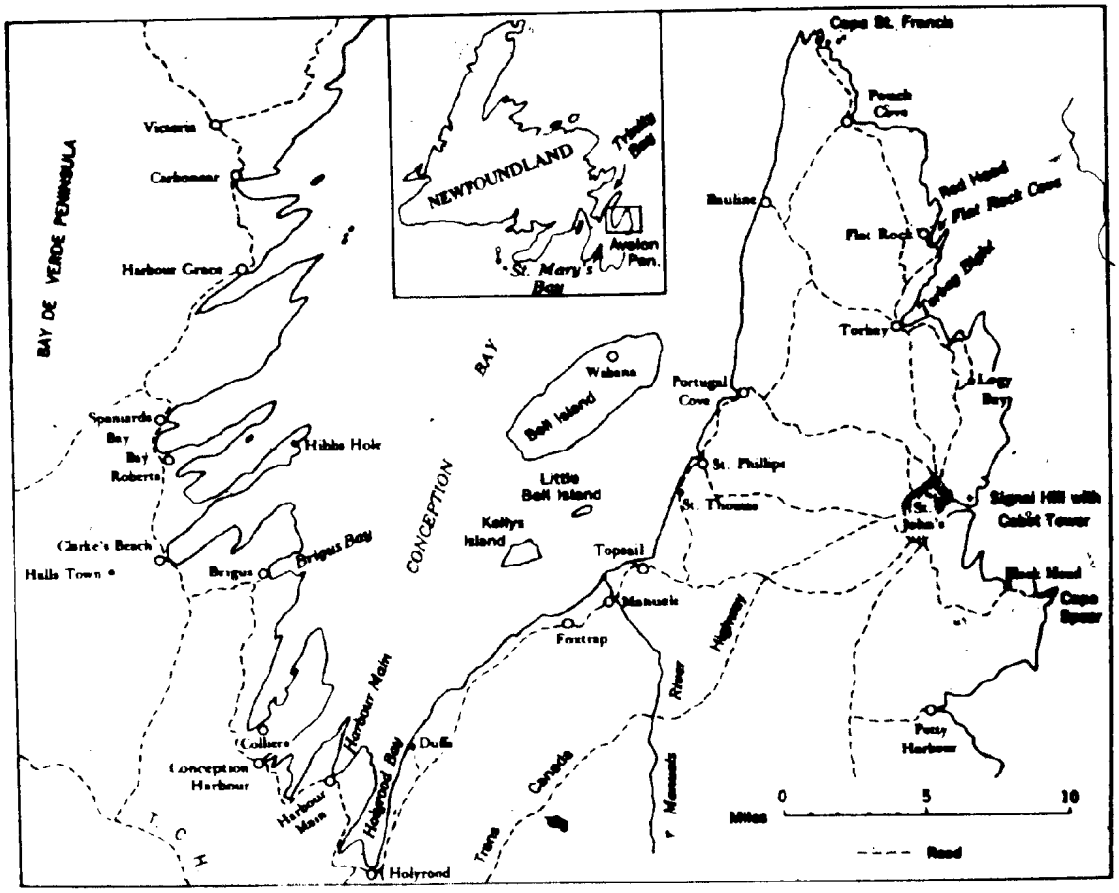

1.1. Location and Access

The Colliers Peninsula is situated in southwestern Conception Bay at latitude 47°28'N, longitude 53°11'W, and forms part of the Peninsula of Avalon, Southeastern Newfoundland. The area lies approximately 42 miles (67.6kms) west of the city of St. John's, the provincial capital (fig. 1). It is easily accessible by road along Highway 60 (the Conception Bay Highway) or alternatively by travelling inland along the Trans-Canada Highway as far as the Avondale access where a gravel road connects with Highway 60. In the western part of the map area the wooden dwellings of Colliers occupy the shores of Colliers Bay; at the base of the peninsula the communities of Conception Harbour, and further north Kitchuses and Bacon Cove, overlook Gasters Bay to the east.

The map area is covered by National Topographic Series sheets 1 N/6 East Half (Holyrood) and 1 N/11 East Half (Harbour Grace) at a scale of 1:50,000. Maps of the general geology include those of Hutchinson (1954), Map 1035A Harbour Grace, and McCartney (1954), Preliminary Map 54-3 Holyrood, on a scale of 1 inch to 1 mile, and McCartney (1967), Map 1168A Whitbourne, on a scale of 1 inch to 4 miles.

1.2. Historical Background

The bay and settlement of Colliers were named after James Collier, one of the first settlers in the area; his grave can be found at James Cove to the north.

FIG. 2. General Geology of Avalon Peninsula, S.E. Newfoundland (after Hughes and Brueckner, 1971).

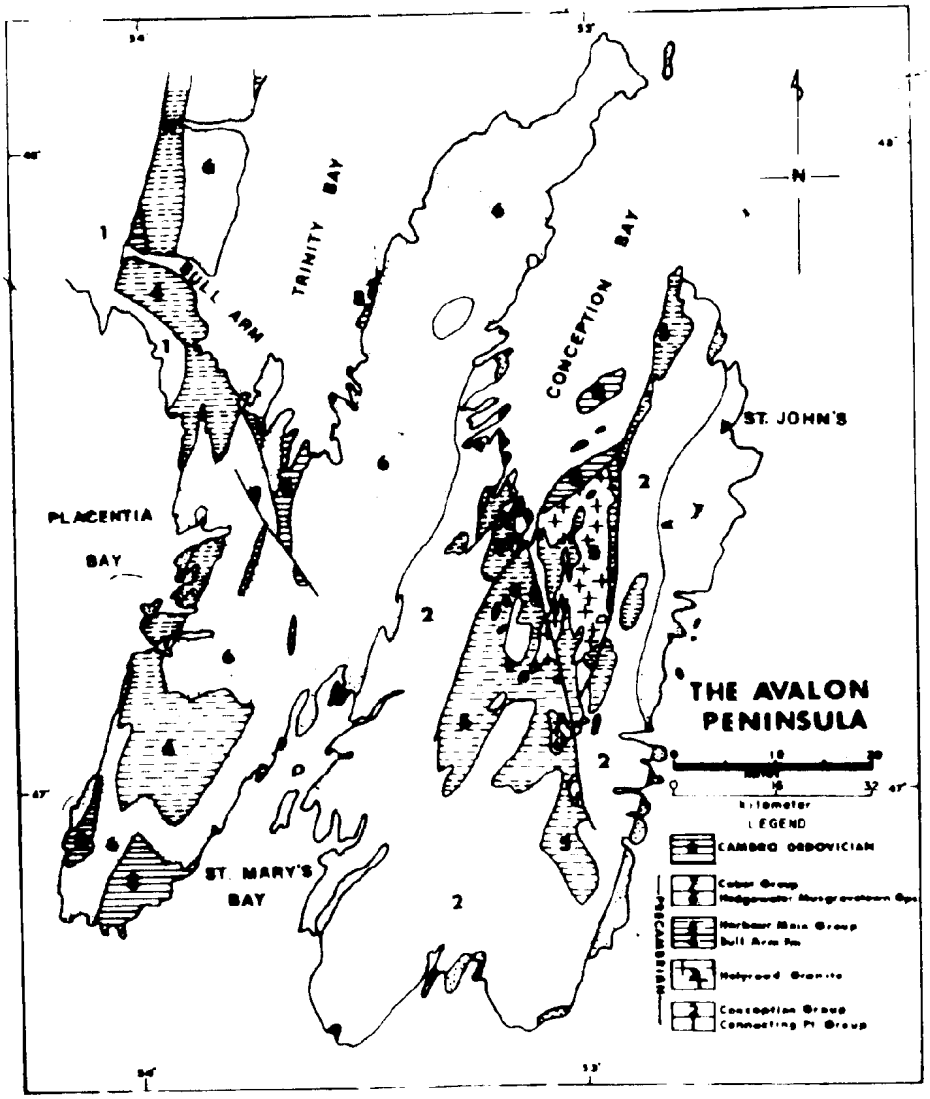

TABLE 1. Lithostratigraphic Units of the Avalon Peninsula, S. E. Newfoundland (modified from McCartney (1967) and Rose (1952)

Age	Approximate Thickness		Western Avalon (McCartney, 1967)	Central & Eastern Avalon	Easternmost Avalon (Rose, 1952)
Early Ordovician	5000ft.	ironstone, shale, limestone and sandstone		Wabana Group Bell Island Group Clarenville Formation	water-cover
Late Cambrian	300ft			Elliot Cove Formation	
Middle Cambrian	780ft		Manuels River Formation Chamberlain's Brook Formation		
Early Cambrian	75ft 522ft		Brigus Formation Smith Point Formation Bonavista Formation		Acadian Series
Eo-Cambrian	0-600ft.	quartzite	disconformity Random Formation	angular unconformity	disconformity
Precambrian	6000ft	conglomerate	disconformity	angular unconformity	
	13400ft	arkose siltstone	Musgravetown Group including Bull Arm Formation	Holyrood Plutonic Series (607 ± 11 m.y.) Hodgewater Group	Cabot Group
	8000ft	felsic to mafic volcanic rocks			disconformity
(Hadrynian)	6000ft 9000ft	siltstone greywacke tillite	Connecting Point Group	Conception Group	
	6000ft	felsic to mafic volcanic rocks, including porphyrites and Holyrood-type granitoid rocks		unconformity Harbour Main Group	

1.3. Physiography and Climate

The map area covers approximately 7.5 square miles (19.4km^2) and has a coastline of about 14 miles (22.5kms) in length with excellent rock exposures. Outcrop inland is also good with about 70% exposure. The highest point in the area, Campbell Hill, rises about 425ft (128.5m) above sea level; Finn Hill, Weavers Hill, and the hills to the west and southwest of Bacon Cove exceed 300ft (91.4m) in height.

Pleistocene glaciers have greatly modified the landscape and rôches moutonnées (for example, Finn Hill), whaleback ridges, and ice-striated rock surfaces generally indicate a northerly to northwesterly direction of ice movement. Glacial till and areas of bog thinly blanket the bedrock in parts of the peninsula; boulder trains and perched erratics up to 8ft (2.4m) in diameter are of local origin. The general glacial features of the Avalon Peninsula have been described in some detail by Henderson (1960) and Jenness (1960).

Contrary to the experiences of McCartney (1967, p. 7) the author enjoyed a hot and somewhat dry field season. Torrential rain fell on June 1st and the next rainstorms occurred on July 24th and again on August 8th. Such summers are indeed rare on the Avalon.

1.4. Geological Setting of Eastern Avalon in the Light of Previous Geological Work

Jukes (1843) published the first geological map and report of Newfoundland as a result of field work undertaken during 1839-40. On

the easternmost part of the Avalon, Jukes (ibid.) recognised an "Upper Slate Formation" (Cambro-Ordovician sediments and Hodgewater Group in part), and a "Lower Slate Formation" (Signal Hill sandstones and St. John's shales). Murray, the first Director of the Geological Survey of Newfoundland, and his Assistant and successor, Howley, published two volumes of progress reports of the Survey and a detailed geological map (Murray and Howley, 1881; Howley and Murray, 1918). They divided the Precambrian rocks of Avalon into "Laurentian gneiss, etc." which represents the main areas of granitic rocks; and "metamorphic slate and sandstones, etc." which corresponds to the Harbour Main Group. Walcott (1899) used the term "Avalon Terrane" for the Precambrian sedimentary rocks overlying the "Archean gneiss" (Harbour Main Group) and introduced the names "Conception Slates" and "Torbay Slates" for the lower two formations of his "Avalonian" or "Avalon series". Buddington (1919) clarified the relations and petrology of the Precambrian plutonic and volcanic rocks with the aid of chemical analysis, and proposed the term "Avondale volcanics" for the "Archean gneiss" of Walcott. However, Howell (1925) suggested the name be replaced by "Harbour Main volcanics". Working on Eastern Avalon, Rose (1952) re-defined the Harbour Main Group to include the volcanic and sedimentary rocks of the "Harbour Main (Avondale) volcanics". He referred to the "Conception slate" and "Torbay slate" as the Conception Group, and included St. John's, Signal Hill, and Blackhead formations in his Cabot Group. Rose's publication was the first of a series of G.S.C. maps and memoirs on

the regional geology of the Avalon by Rose (ibid.), Hutchinson (1953), Jenness (1963), and McCartney (1954, 1967).

Absolute age determinations of Precambrian rocks were carried out by McCartney et al., (1966) using whole-rock Rb-Sr methods to date the Holyrood "granite" (sensu lato). An isochron plot gave an age of 574 ± 11 m.y. (decay constant = 1.47×10^{-11} year^{-1}) which they regarded as the time of emplacement of the granite in Harbour Main and Conception Group rocks. A similar age of 597 ± 42 m.y. was reported by Fairbairn (1965 in McCartney et al., 1966) for a Rb-Sr determination on a potassium feldspar from the same granite. While the exact figures are still subject to some uncertainty (cf. Frith and Poole, 1972), they clearly indicate a Late Precambrian (Hadrynian) age.

The terminology of the lithostratigraphic units of Avalon currently used is that of Rose (1952), though the "Holyrood granite batholith" is more correctly referred to as the Holyrood Plutonic Series (McCartney, 1967). The general relationships of major lithostratigraphic units and correlation of rock-types in other parts of the Avalon are shown in table 1. For other reviews of the geology of Eastern Avalon the reader is referred to McCartney (1967, 1969), and Brueckner (1969).

Recently, Anderson and Misra (1968), Misra (1969), and Brueckner and Anderson (1971) have described soft-bodied metazoan fossils and tillite horizons from the Conception Group; and King (1972) has shown that current directions in the Cabot and Hodgewater

Groups indicate a southerly direction of transport of molasse-type sediments from a source to the north.

Controversy has arisen, however, concerning the original depositional environment and tectonic setting of the Precambrian rocks of Avalon:

Papezik (1969, 1970) carried out the first detailed studies of ash-flow deposits on the Colliers Peninsula at Finn Hill, and presented 22 chemical analyses of rhyolitic and basaltic rocks of the Harbour Main Group. He interpreted their sodic composition in terms of differentiation from an alkali-olivine basalt parental magma in a post-orogenic tectonic setting of the Basin-Range type.

Alternatively, Hughes (1970) and Hughes and Brueckner (1971) have discussed Late Precambrian tectonic movements within the Appalachian belt (the so-called Avalonian Orogeny) in terms of the formation of a volcanic archipelago by calc-alkaline volcanism. They presented a model of island arc-type volcanism in which a "syn-volcanic" constructional phase is represented by four pene-contemporaneous facies - vent, alluvial, marine, and plutonic (corresponding to the Harbour Main Group, Conception Group, and Holyrood Plutonic Series) - thereby attempting to reconcile conflicting age relationships between the isochron age for granite emplacement (McCartney _et al._, 1966) and depositional, erosional, and tectonic events preceding the Lower Cambrian marine transgression (cf. McCartney, 1966, p. 955; 1969, p. 122). The Cabot and Hodgewater

Groups were formed during a "post-volcanic" destructional phase in a marine and alluvial environment.

The "contemporaneous" model of Hughes and Brueckner and the "sequential" model of McCartney have been discussed by Frith and Poole (1972). They regard a date of 607 ± 11 m.y. as a more precise estimate for emplacement of the Holyrood Plutonic Series "since dates calculated by using the first constant (1.39×10^{-11} $year^{-1}$) appear to be more consistent with results of other dating methods" (Frith and Poole, ibid., p. 1059). They pointed out that a time range of 37-57 m.y. between intrusion of Holyrood granite and the beginning of Lower Cambrian deposition on Avalon satisfied both models.

More recently, Hughes and Malpas (1971) and Malpas (1972) have presented evidence for alkali metasomatism, with enrichment of rubidium and potassium, in Doe Hills rhyolite of the Bull Arm Formation on the Isthmus of Avalon. They suggest that metasomatism, involving both the alkalies and calcium, may have been operative on a large scale in rocks of the Harbour Main Group. Consequently, Hughes (1972a) regards the Late Precambrian volcanic rocks of the Avalon Peninsula as part of a "spilite/keratophyre province" resulting from a "bulk" metasomatism broadly coeval with regional metamorphism.

The presence of a low-grade regional metamorphism of prehnite-pumpellyite grade in the Precambrian lithologies of the Avalon has recently been recognised by Papezik (1972a, in press).

It is evident from previous geological work that Avalon geology is indeed complex and somewhat controversial. Any attempt to achieve a better understanding of the geological evolution of Precambrian rocks on Avalon must inevitably deal with some of the controversial issues.

1.5. General Geology of the Map Area

The Colliers Peninsula forms part of the "Western Block" of Brueckner (1969), separated from the "Middle Block" ("Holyrood Horst" of McCartney (1967) and main outcrop of Holyrood Plutonic Series) by a high-angle fault system extending south-southwest from Holyrood Bay (fig. 2). Unfortunately, present knowledge of the stratigraphy and structure of the fault-bounded blocks does not allow firm litho-stratigraphic correlations to be made across the Avalon.

Rocks of the Harbour Main Group underlie a major portion of the Colliers Peninsula; the volcanic pile faces west and dips steeply in that direction (fig. 3). A stratigraphic succession over 7900ft (2408m) in thickness is well exposed and consists of felsic pyroclastic rocks, volcanogenic sediments, and minor lava flows, intruded by transgressive sills of "porphyrite", diabase dykes, and rhyolite, and overlain to the west of the map area by a series of basaltic flows, best exposed along the western shores of Colliers Bay. McCartney (1967) regarded these mafic flows as the youngest part of the Harbour Main Group with an estimated thickness

FIG. 3. General Geology of Colliers Peninsula.

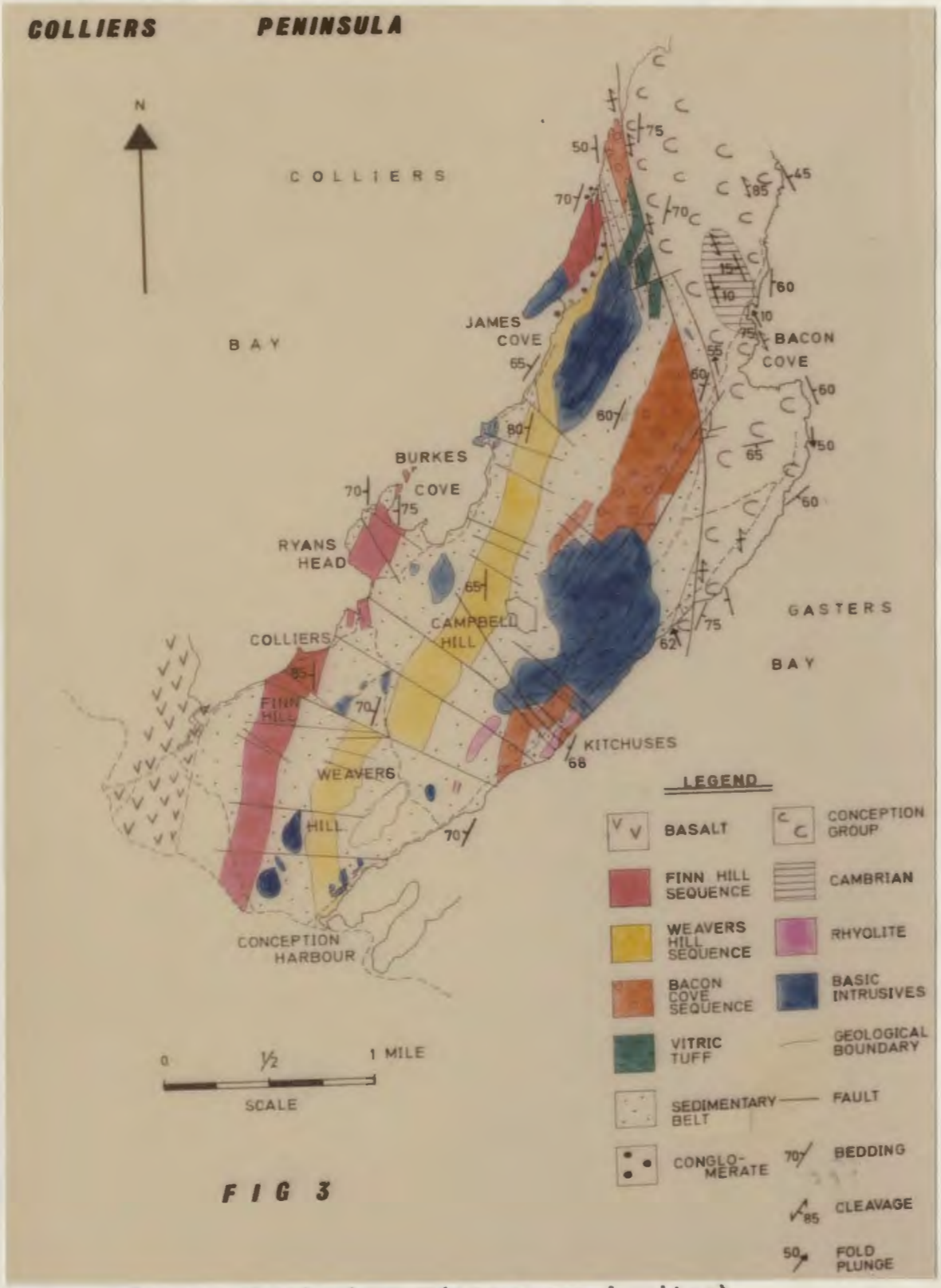

(Note: basic intrusives = porphyrites)

FIG. 4. Location of Geochemical Sampling Sites Outside the Map Area (modified from McCartney, 1967).

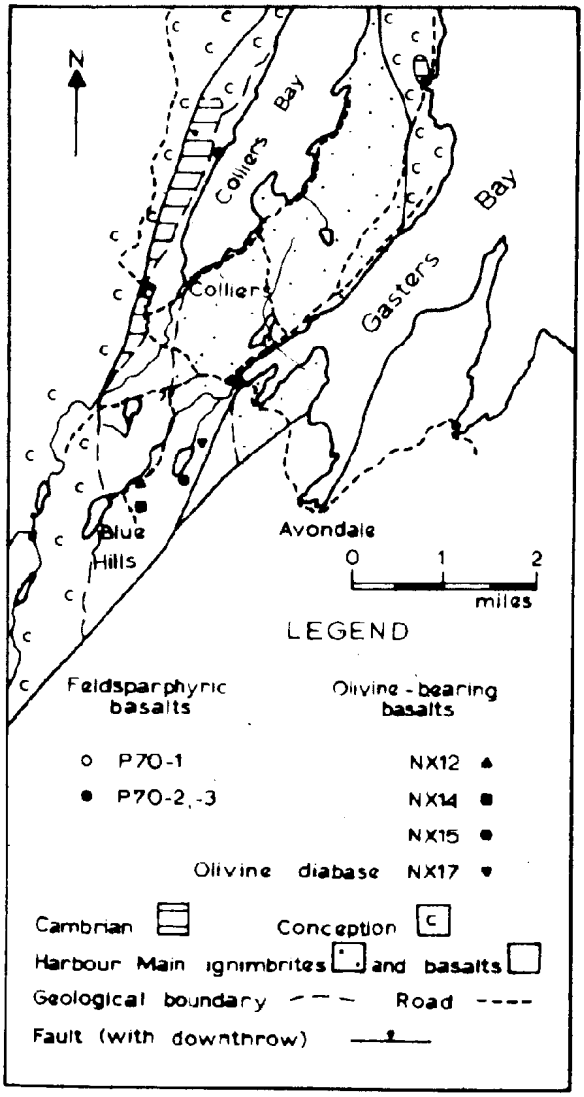

of approximately 1000ft (304.8m). However, reconnaissance of the area around the Blue Hills, 3 miles (4.8kms) south of the map area, indicates that this is best regarded as a minimum thickness for the mafic volcanics at this horizon (cf. fig. 4).

Greywackes, siltstones and minor tillites of the Conception Group in the northern part of the peninsula lie in fault contact with Harbour Main rocks to the south. McCartney (1954) interpreted parts of this contact west of Bacon Cove as an unconformity, mistaking a fault slice of conglomeratic and laharic sediments of the Harbour Main Group for basal Conception conglomerate.

A small synclinal remnant of Lower Cambrian detrital rocks and limestones rests on folded Conception siltstones at Bacon Cove and constitutes the youngest map unit of the area.

1.6. Present Study

The present study comprises a detailed geological account of a well-exposed stratigraphic section of the Harbour Main Group on the western flank of the volcanic belt. The work involved mapping an area of approximately 7.5 square miles (19.4km^2), microscopic study of over 300 thin sections, and 82 complete and 90 partial whole-rock and mineral analyses. An attempt has been made first to examine each aspect of the geology - stratigraphy, structure, metamorphism, petrography, and whole-rock and mineral chemistry - individually; then to relate the data as a whole to present concepts concerning the petrology and tectonic setting of the Harbour Main Group on the Avalon Peninsula.

1.7. Mapping Methods

After three weeks of reconnaissance mapping in August 1971, the main part of the field work was carried out during June to September 1972, when a base camp was established at Bacon Cove. Black and white aerial photographs on a scale of 8 inches to 1 mile and 7.5 inches to 1 mile were obtained from the National Air Photographic Library, Ottawa, and were used as a map base in the field. Rock-types within the Harbour Main Group were mapped in detail, while the Conception Group and Lower Cambrian Strata were mapped on a reconnaissance basis only.

1.8. Acknowledgments

I wish to thank Memorial University of Newfoundland for the award of a University Fellowship 1971-1973; P. Thornley for assistance in the field; J. Vahtra, D. E. Press, and Dianne England for analytical help; G. R. Andrews for contributing 20 whole-rock analyses determined by atomic absorption spectrophotometric methods; Gill Campbell for drafting assistance; W. S. Marsh for outstanding photographic reproduction; Dr. K. D. Collerson for the gift of a specimen of porphyrite breccia containing shards; Dr. D. F. Strong for use of computer programs and unpublished analytical data; and the Geology Department, M. U. N., for providing all facilities and thin sections, and for the use of a boat and outboard engine July to September 1972. Financial assistance in the field and in support of the microprobe work was provided by

N.R.C. Grant A-2131 and G.S.C. Grant 32-65, both to Dr. V. S. Papezik. I am indebted to McGill University, in particular Dr. W. H. MacLean, for permission to use the electron-probe microanalyser and computer; L. Larson and Dr. W. H. MacLean performed the majority of the feldspar analyses and contributed photomicrographs 62, 63, and 64.

I benefited greatly from discussions with faculty and graduate colleagues of the Geology Department, M.U.N., in particular Dr. D. F. Strong, and John G. Malpas; with participants of the 24th International Geological Congress (Montreal) Field Excursion to Newfoundland; with members of the Newfoundland "granite-ophiolite" field trip, June-July 1973; and with participants of the G.A.C. Newfoundland Section Annual Meeting, St. John's, March 1973. Discussions with Drs. W. H. MacLean and R. F. Martin (McGill University), Dr. N. Rast (University of New Brunswick), and William P. Leeman and James D. Hoover (University of Oregon) also proved extremely valuable.

Dr. V. S. Papezik conceived the project and advised during all stages of its development. I sincerely appreciate his guidance and keen criticism of the manuscript.

I deeply appreciate the warm Newfie hospitality shown towards me by the people of Colliers, Bacon Cove, and Kitchuses, especially Mr. and Mrs. Frank Conway of Colliers. My sincerest thanks are extended to Barbie and Ron and Candy for their patience and encouragement during seemingly endless revision and improvement of a preliminary draft of this thesis.

CHAPTER II

ASH-FLOW TUFFS OF THE HARBOUR MAIN GROUP

2.1. Terminology of the Volcaniclastic Rocks

A confusing discrepancy is often apparent in the literature between original definition, classification and current usage of the terms describing the volcaniclastic rocks. This section has been reserved to define the terminology used throughout this thesis.

The grade-size classification and terminology of the pyroclastic rocks favoured here is that proposed by Wentworth and Williams (1932), later modified by Fisher (1961), and presented in table form below (table 2). Fisher (ibid.) described a diversified group of volcanic breccias and re-defined volcanic breccia as a "rock composed predominantly of angular volcanic fragments greater than 2mm in size set in a subordinate matrix of any composition and texture, or with no matrix; or composed of fragments other than volcanic set in a volcanic matrix." (Fisher, 1961, p. 1072). This term is only modified or described further, along the guidelines laid down by Fisher (1958, 1960, 1961) and Wright and Bowes (1963), where the evidence favours a particular mode of emplacement and/or environment of deposition. For example, the epiclastic volcanic rocks of Fisher (1961, p. 1409) contain fragments produced by "weathering and erosion of solidified or lithified volcanic rocks of any type" and include laharic breccias and volcanic conglomerates. Use of the term "tuff-breccia" (Norton, 1917, p. 162) to describe

TABLE 2. Terminology and Grain-Size for Pyroclastic Fragments (after Fisher, 1961)

Grade-Size (mm)	Epiclastic Fragments	Pyroclastic Fragments	
	boulders (and "blocks")	coarse	blocks
256			and
	cobble	fine	bombs
64			
	pebble	lapilli	
2			
	sand	coarse	ash
1/16			
	silt		
1/256		fine	ash
	clay		

a deposit other than one of pyroclastic origin is clearly ambiguous. Fisher (1961, p. 1412) recommended tuff-breccia be used synonymously with lapilli tuff; however, the latter term is preferred here.

The basic depositional unit of ash-flow deposits is the ash flow: it is "the deposit resulting from the passage of one nuée ardente ..... it consists of 50 or more weight per cent of ash and fine-ash exclusive of foreign inclusions" (Smith, 1960, p. 800), where "ash" lies in the size range less than 2mm as defined here. The principal genetic concept relating to ash-flow deposits is that of the cooling unit, an "ash-flow deposit that can be shown to have undergone continuous cooling" (Smith, 1960, p. 801). Recognition of zonal variations in welding and crystallisation features of ash-flow sheets enable distinctions to be made between simple, compound, and composite cooling units (cf. Ross and Smith, 1961). The term ignimbrite (Marshall, 1935) is used here synonymously with ash-flow tuff whether welded or non-welded.

A type of ash-flow tuff referred to as a "sillar", has been described by Fenner (1948) and Jenks and Goldich (1956) from the Peruvian Andes. The sillars are thoroughly indurated due to crystallisation by pneumatolytic action rather than compaction and welding of hot pumice and shards. Although most of the ash-flow tuffs of the Colliers Peninsula preserve welded textures, certain ash-flow deposits lack a distinct zone of welding and appear to have an affinity to the so-called sillars, though not corresponding exactly to descriptions in the literature.

2.2. Ash-Flow Deposits: An Introduction and Field Relationships

An appreciation of the acute problems of recognition involved in the study of Precambrian ash-flow tuffs, as compared to their glassy Cenozoic counterparts, can be gained from the literature. Only since the classical textural studies of geologically recent ignimbrite sheets by Marshall (1935) in New Zealand, and Mansfield and Ross (1935) in Idaho, have reports of Precambrian occurrences become better documented. For example, Hjelmquist (1955) identified Precambrian welded tuffs from Dalarna, Central Sweden; Rittman (1962) recognised welded textures in ignimbrites in eastern Egypt; Ross and Smith (1961) mentioned occurrences in Morocco and in Precambrian basement rocks from Texas oilwells; and more recently, Thieme (1970) has recognised welded tuffs in basement rocks in Zambia cut by a syenitic dome dated at 1930 ± 70 m.y.

Excellently preserved ash-flow tuffs of Hadrynian age on the Colliers Peninsula rank perhaps among the finest examples of Precambrian ash-flow deposits documented. The Harbour Main Group as a whole contains several belts of well-preserved ignimbrites described in some detail by McCartney (1967) and Papezik (1969, 1970).

In the map area, three predominantly pyroclastic sequences, composed essentially of ash-flow tuffs, are interbedded with volcanogenic sediments containing relatively minor amounts of ash-flow material (fig. 3 and geological map in pocket). Ash-flow sequences have been named after measured stratigraphic sections at Bacon Cove, Weavers Hill, and Finn Hill; listed from oldest to youngest, they

are referred to throughout as the Bacon Cove ash-flow sequence, Weavers Hill ash-flow sequence, and Finn Hill ash-flow sequence, respectively (cf. tables 3, 4, and 5). The top and bottom of each ash-flow sequence is marked by epiclastic volcanic rocks (Fisher, 1961) which vary markedly in texture and composition along strike.

In the ignimbrite sheets so far described from the Harbour Main Group, only simple cooling (Ross and Smith, 1961) has been recognised (cf. Papezik, 1969). In the Colliers area, each type-section of an ash-flow sequence has been divided into a succession of simple cooling units; each unit has been numbered for ease of reference in tables 3, 4, and 5. Cross-sections of the ash-flow sequences at selected localities along strike are also presented; thicknesses of individual units were measured in the field and estimated from aerial photographs.

Mineral modes and proportions of pumice and xenoliths were determined visually in thin section and in outcrop (where possible); both methods generally agreed within approximately 5-10% of the quoted value.

2.2.1. Bacon Cove Ash-Flow Sequence

A stratigraphic section located 0.5 mile (0.8km) southwest of Bacon Cove, comprises a succession of ash-flow cooling units (1-9, table 3), which together with laterally equivalent units (10-14) at Kitchuses, are collectively referred to as the Bacon Cove ash-flow sequence. The resistant ash-flow tuffs form a group of narrow ridges aligned northwest-southeast and bounded by en échelon, high-angle faults. The north-northwesterly strike of the deposits crosses these ridges at a low angle.

The Bacon Cove ash-flow sequence is characterised by a repetitive yet distinctive series of crystal tuffs (units 1, 3, and 5; coloured red in table 3); pumiceous crystal tuffs (units 7 and 9; coloured yellow); vitric tuffs (units 4 and 8; coloured green); and extremely crystal-rich sillars (units 2 and 6; coloured orange). Varying proportions of phenocrystic quartz, biotite, and albite appear throughout the sequence. Generally, the lithic component is significant only as a thin basal concentration, which rarely exceeds 15% of the rock. At Bacon Cove, ash-flow deposits are found in erosive contact, while further south at Kitchuses, intercalated tuffaceous sandstones and epiclastic volcanic breccias are volumetrically important.

Units 1, 3 and 5, in the lower part of the Bacon Cove sequence, comprise reddish grey to dark red crystal tuffs exhibiting a zonal pattern of welding (Ross and Smith, 1961). Generally, a thin (5-10

TABLE 3. Bacon Cove Ash-Flow Sequence.

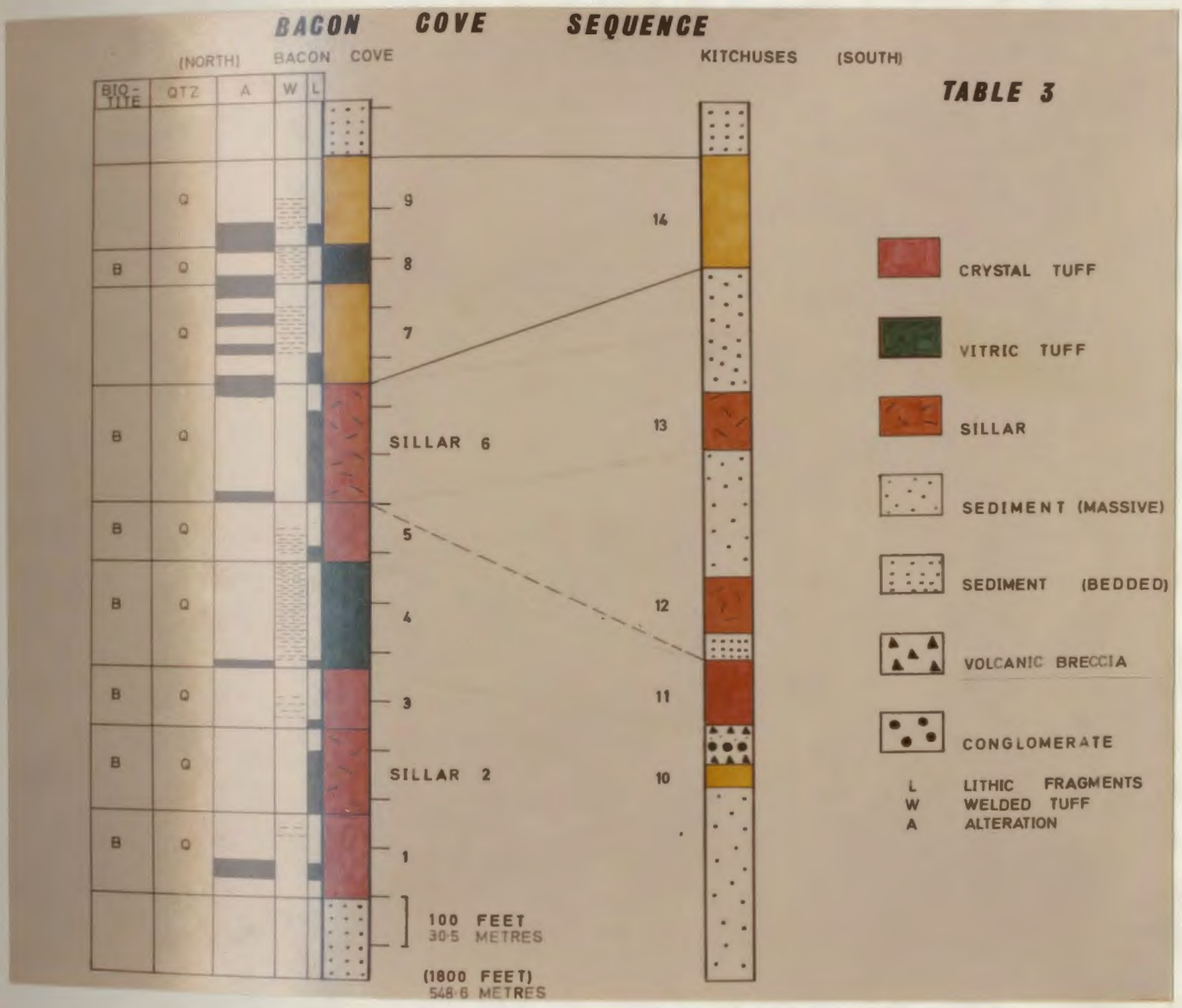

(Note: pumiceous cooling units coloured yellow)

ft; 1.5-3m) basal zone contains 5-10% lithic fragments less than 1.5 inches (3.8cm) in diameter set in a non-welded shard and crystal matrix, largely obscured by iron-oxide dust. Xenoliths consist mainly of quartz- and biotite-bearing crystal tuff and non-welded vitric tuff; sedimentary rock-lapilli, some showing a green alteration, are common in the thick basal layer of unit 1, and a rare granophyre fragment occurs in unit 3 (photomicrograph 1). At the base of unit 5, which occupies a depression at the top of unit 4, lapilli of densely welded vitric tuff derived from the underlying unit have been plastically deformed by welding and lie within the plane of compaction. The transition from non-welded to welded textures near the base of these ignimbrite sheets is fairly sharp, occurring within a zone about 1-2ft (0.3-0.6m) in thickness. Welded crystal tuff grades upward into a partly welded counterpart, and eventually into a non-welded, fine-grained crystal tuff at the top of the cooling unit.

Vertical gradations in welding can be matched with systematic changes in crystal accumulation and mineral proportions. Phenocryst content at the base reaches approximately 40% by volume of quartz (10%), biotite (3%), and albite (remainder). A non-welded upper zone marks a gradual decrease in crystals (10%) set in a finely comminuted shard matrix heavily impregnated with hematite; the relative proportions of quartz and biotite are 3% and 1%, respectively. The size of phenocrysts also diminishes upward from 2-3.5mm at the base to less than 0.5mm at the top of the unit.

Locally, the thin (up to 3ft; 0.9m) basal layer of unit 3 attains a crystal concentration of 60%, composed of about 15% quartz, 5% biotite and 40% albite. Only the higher content of hematite dust, sharp contact, and slightly smaller (0.5-2mm) crystals distinguish this basal layer from the underlying sillar (unit 2). However, the welded textures so common in the central parts of units 1, 3 and 5 have not been observed in the sillars.

Units 2 and 6 are unique to the Bacon Cove ash-flow sequence; conspicuously rich in crystals of quartz, biotite, and albite set in an intensely recrystallised vitroclastic matrix, they strongly resemble the sillar-type ash-flow tuffs described in the literature (cf. chapter II, section 2.1.). These deposits are typically massive and lack any form of internal stratification; welding has not been detected. Colour generally varies from reddish brown to buff, though pale green mottling is conspicuous near the top and base of unit 6. The base of unit 2 is not exposed and the horizon sampled texturally resembles the top and middle of unit 6.

Extensive outcrops of unit 6 are to be found along a broad ridge in the centre of the type-locality. It represents the thickest (240ft; 73.2m) cooling unit of the Bacon Cove sequence and may comprise several ash-flows. The base of this unit overrides ash-flow tuffs in the lower part of the sequence (units 4 and 5) and encloses them as subangular to rounded lapilli; sedimentary and mafic xenoliths are comparatively rare. Small (6mm) rock fragments of similar origin are distributed chaotically throughout the unit.

Locally, veins and patches of reddish-brown jasper form a prominent "node" with a pitted surface due to weathering, and superficially resemble xenoliths.

Vertical variations in crystal concentration and phenocryst proportions within this cooling unit can be traced in the field. Rounded crystals of quartz (1.5-3.5mm), biotite "books" (up to 3mm), and broken albite (0.5-4mm) set in a recrystallised shard matrix constitute 30% (at the top of the unit) to 75% (towards the base) by volume of the deposit. The proportion of phenocrysts in the xenolithic basal zone averages about 30%, of which quartz forms 15%, biotite 4%, iron-oxide 2-3%, the remainder being albite. An upward decrease in the amount and size of lithic fragments is accompanied by an increase in the proportion of crystals, reaching a maximum concentration between 10-70ft (3-21.4m) above the base of the unit.

Units 4 and 8 are vitric ash-flow tuffs, typically purplish grey or salmon-pink in colour. Unit 4 is a compact, densely welded ignimbrite sheet strongly resembling a massive rhyolite flow. However, the use of a hand-lens on a weathered surface reveals deformed and slightly flattened shards which define a compaction foliation due to welding. At the base, a thin zone of partial welding (4-10ft; 1.2-3m) contains approximately 10-15% crystals of albite (0.5-2mm), quartz (0.5-2mm), and rare flakes of biotite (<1mm). This basal layer grades fairly abruptly into a zone of dense welding above, which encloses tiny (less than 0.5mm) broken albite crystals and

small (2-4mm) subangular lithic fragments which form about 1% and 3%, respectively, of the rock. Welded vitric tuff continues upward to the base of the overlying ash-flow tuffs (units 5 and 6) with no observed textural change. The original thickness of the cooling unit must clearly have exceeded the maximum 210ft (64.1m) recorded in the type-section.

The upper vitric tuff (unit 8) is preserved in a series of discontinuous outcrops along the easternmost ridge of the type-locality and varies from 0-50ft (0-15.3m) in thickness. Dark green lenses of collapsed pumice are conspicuous in a purplish grey, densely welded vitroclastic matrix, and constitute about 5% of the unit. Other textural and mineralogical features are similar to those recorded from unit 4.

Units 7 and 9, well-exposed in the ridges to the extreme west, consist of greyish red to dark red crystal tuff; a zonal pattern of welding is characteristic. The presence of pumice-lapilli megascopically distinguishes these ignimbrite sheets from cooling units 1, 3 and 5 lower in the sequence. Dark green to yellowish brown pumice, constituting 5-10% of the rock, are preferentially eroded to form a conspicuous but poorly developed foliation in the interior of the sheet, without appreciable staining of the dark red shard matrix. An assortment of lithic fragments (<30mm across), concentrated in a mottled pale green to buff basal layer, includes quartz- and biotite-bearing welded tuff, igneous rock fragments with phenocrysts of albite and pyroxene (partly altered to chlorite and quartz), tuffaceous sandstone,

and sparse basalt and rhyolite. Green and pink mottling in unit 7, though most extensive at the base, occurs sporadically throughout the unit.

Mineralogical changes are marked by the disappearance of biotite and an increase in the albite:quartz ratio. Crystal content gradually decreases with height above the base of the cooling unit, ranging 25-15% in unit 7 and 30-20% in unit 9; the xenolithic basal zone contains approximately 10-25% crystals. Crystal size commonly varies from 2.5mm at the base to less than 1mm at the top of the unit.

The salient features of a stratigraphic section at Kitchuses, 2 miles (3.2kms) south of the type-locality, are shown in table 3. Although intrusive rhyolite sills and intense faulting complicate stratigraphic relationships, 5 cooling units (10-14, table 3) have been recognised. Units 10, 11 and 14 exhibit zonal variations in welding; units 12 and 13 are sillars, texturally identical to units 2 and 6 described earlier. Lateral correlation, however, is tentative since thick wedges of volcanogenic sediments replace many of the ash-flow sheets at Bacon Cove.

The base of the section is particularly well-exposed east of Kitchuses in coastal cliffs overlooking Gasters Bay. Unit 10 forms a greyish green ash-flow sheet, about 40ft (12.2m) thick, with collapsed pumice-lapilli, scattered xenoliths of red crystal tuff (5-30mm), and crystals (25-30%) of quartz (5-10%) and albite (20%). Unit 11, a dark purplish red ignimbrite with a pale green xenolithic

base (4ft; 1.2m thick), contains comparatively fewer crystals (15-25%) and less quartz (5%); biotite has not been recorded from either of these cooling units. Unit 12, the lower sillar, has been partly altered to a greyish green to pale green colour; noticeable mineralogical differences include a lower average crystal content (40-50%) than similar units further north, phenocrysts of pale golden mica (altered biotite), and sparse cubes of pyrite. Crystal concentration near the base of unit 13 is conspicuous, reaching approximately 50% of the rock (15% quartz, 15% biotite, and 20% albite), and progressively decreases to about 35% (10% quartz, 5% biotite, and 20% albite) near the top of the unit. The larger (2-3.5mm) quartz crystals occur in the basal zone together with biotite (3mm), albite (1-3mm), and minor xenoliths (3-15mm). Unit 14 is a reddish grey pumiceous ash-flow tuff with a marked concentration of xenoliths at the base. It strongly resembles unit 7 in both texture and mineralogy.

Ash-flow deposits exposed in fault blocks to the north of the Bacon Cove sequence strongly resemble certain cooling units in the type-section (table 3). A grey- to pink-weathering vitric tuff, about 270ft (82.4m) thick (map ref. 3575,6190), is identical to unit 4 at Bacon Cove. For the most part shards are densely welded, though a non-welded zone is preserved at the top of the cooling unit. Broken crystals of albite (up to 2mm) and biotite (<2mm) are only conspicuous at the base, and form about 15% of the rock.

The unit thins rapidly towards the south, and an isolated outcrop of pink vitric tuff east of Campbell Hill (map ref. 3475,5860) may represent its far-travelled equivalent. Dark red to reddish grey crystal tuffs overlying this ignimbrite probably comprise more than a single cooling unit. Angular to rounded crystals of quartz (1-2mm), biotite (0.5-2mm), and albite (1-2mm) occur sporadically, and welded textures have been identified.

Considering these deposits along with underlying ash-flow sheets at Bacon Cove, it is evident that a cyclical pattern of ash-flow deposition had been established in the area at this time. The significance of this pattern is poorly understood since it may represent:

a) real variations in the crystallisation history of the magma.

b) the cyclical nature of types of eruptive activity dominant at the vent(s).

c) variations in the distance of source vents from the Colliers area.

d) combinations of a, b, and c.

2.2.2. Weavers Hill Ash-Flow Sequence

The Weavers Hill ash-flow sequence, with a strike length a little over 4 miles (6.4kms), is the most extensive of the ash-flow sequences that form the Colliers Peninsula. It is particularly well-exposed at Weavers Hill (the type-locality), at Campbell Hill, and in coastal cliffs south of James Cove (fig. 3). It is terminated in the north by faulting and intrusion of porphyritic sills, and blanketed by glacial drift at the southern edge of the map area.

Of the textural criteria applied to distinguish individual cooling units in the field, the relative abundance of enclosed pumice, the degree of welding, the horizon of marked xenolithic concentration (if any), and the crystal:glass (devitrified) ratio were particularly useful in subdividing this ash-flow sequence. Colour is certainly no guide, though pumiceous ash-flow tuffs do appear susceptible to a greenish alteration whatever their level in the pile (for example, units 7, 9, 10, and 14, table 3; units 48-50, 52, 54, and 57, table 5); their markedly pumiceous nature was probably an important contributing factor (plate 1).

The Weavers Hill ash-flow sequence is characterised by a monotonous group of drab greyish green to greenish grey ignimbrite sheets (units 17-26 and laterally equivalent units 29-35 and 36-40, table 4) locally altered to shades of red, pink, and green, and conspicuously rich in variably compacted, dark green to yellowish brown, limonite-stained pumice, which constitute approximately 5-15% of a single cooling unit. Pumice-lapilli only rarely enclose

TABLE 4. Weavers Hill Ash-Flow Sequence.

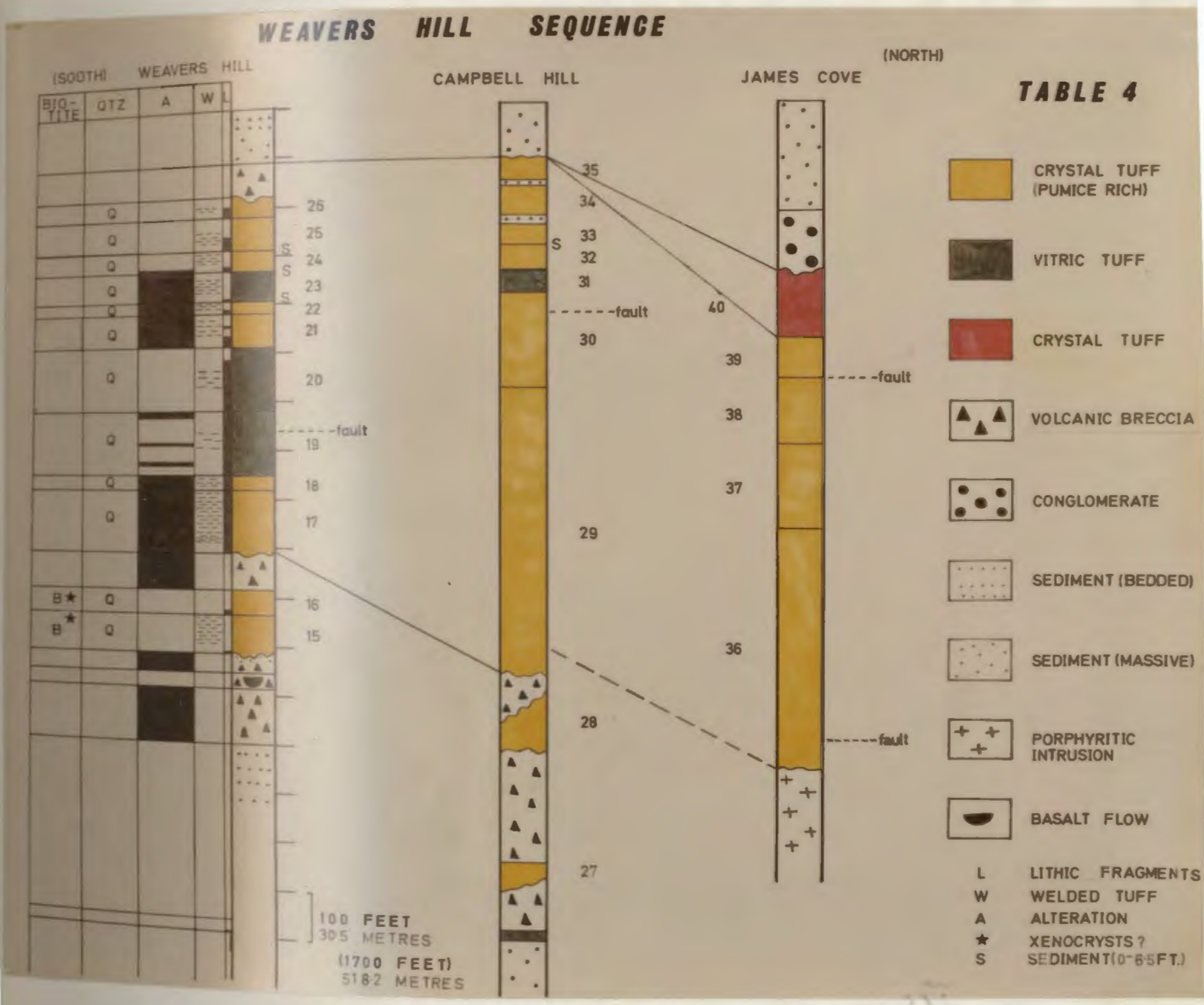

crystals and where concentrated in the upper part of a unit, presumably indicate rafting of lighter pumice toward the top (and sides) of the ash flow (cf. Kuno, 1964; Ono, 1966; Fisher, 1966; Lipman, 1967; and Walker, 1972).

Although systematic variations in crystal content have been detected and are particularly noticeable in the thick vitric tuffs of the Weavers Hill sequence (units 19 and 20; coloured green in table 4), mechanical sorting of the crystal fraction has generally been less efficient than that implied by vertical variations in crystal:shard ratios of Bacon Cove ash flows. The amount of crystals and proportion of mafic minerals differ considerably in each case, and rock fragments of comparable size and specific gravity are more chaotically distributed throughout the entire ash-flow sequence.

The mineralogy of this sequence is remarkably uniform: angular to rounded albite crystals (many of them broken and less than 3mm in diameter) are common, and resorbed crystals of quartz (0.2-2mm) locally form up to 4% of the rock; biotite is rare, occurring only as xenocrysts in basal ash flows at Weavers Hill, but as a cognate phase in ash-flow tuffs at the top of the sequence at James Cove.

At Weavers Hill, adequate exposure and the occurrence in the upper part of the section of thinly bedded lenses of tuffaceous sandstones and siltstones (representing breaks in ash-flow emplacement) facilitate subdivision of the sequence into its component cooling

units (units 17-26, table 4). The top of the sequence is marked by an irregular erosion surface mantled by a light reddish brown epiclastic volcanic breccia (Fisher, 1961) containing rock fragments up to 10mm in diameter; this breccia is overlain in turn by reddish brown, thinly bedded volcanic arkoses and siltstones. Red pumiceous crystal tuffs (units 15 and 16), 0-90ft (0-27.5m) below basal Weavers Hill ash flows (units 17 and 18), are interbedded with dark brown to pale green volcanic conglomerates and breccias of diverse origins.

Units 17 and 18, 126ft (38.4m) and 34ft (10.4m) thick, respectively, are strongly transgressive towards the south onto ash-flow tuffs lower in the pile (units 15 and 16). They comprise at least two cooling units of coarsely xenolithic ash-flow material: angular to subrounded blocks and lapilli of accidental and accessory origin (terminology of Macdonald, 1972, p. 123) measure up to 14 inches (35cm) average diameter and constitute approximately 20% by volume of the rock. Xenoliths include abundant greyish white and purplish grey flow-banded rhyolite, quartz- and biotite-bearing welded tuff, dark red crystal tuff, "porphyrite", tuffaceous sandstone, and rare basalt. In the lower part of the zone of welding, pumice-lapilli are squeezed between rock fragments and moulded around crystals, assuming a variety of shapes and orientations; higher in these units the pumice:xenolith ratio decreases and pumice fragments are consistently flattened within a compaction foliation. Crystals of rounded quartz, albite, and sporadic large (2.5mm) flakes of biotite,

probably xenocrysts, comprise about 25-30% of the unit and are distributed chaotically throughout the unit.

Units 19 and 20 are composed of dark greenish grey to pink- and red-mottled vitric tuff and are distinctive in their comparative lack of crystals (2-20%) and completely chaotic assortment of subangular lithic inclusions (locally 15-20%). Xenoliths are generally of fine lapilli-size (cf. table 2) with a slight concentration in a non-welded basal zone up to 30ft (9.2m) thick. Red- and green-altered rock fragments are common; clasts of pink quartzofeldspathic sandstone and basalt occur sporadically. Crystal concentration gradually increases from about 3% near the top to 10-20% in the lower part of each unit. A sharp increase in crystal content (20-35%) in a dark red, non-welded tuff (up to 13ft; 4m thick) at the top of unit 20 possibly represents a separate ash flow within this cooling unit. A zone of intense shearing and brecciation about 200ft (61m) across and oriented parallel to the pumice foliation does not appear to affect the logical progression of welding (Smith, 1960a; Ross and Smith, 1961) and therefore the stratigraphic position of cooling units; it may, however, affect the thickness.

Units 21-26 comprise pale green to dark red ignimbrite sheets containing approximately 10-30% crystals and separated by thin veneers of tuffaceous sandstones, locally contorted and enclosed as rip-up clasts within the base of these ash flows. A slight concentration of crystals and lithic fragments occurs in a thin basal non-welded layer about 2-3ft (0.6-0.9m) thick in units 22, 24, 25, and 26, and

in a somewhat thicker welded zone (about 50ft; 15.3m thick) in the central part of unit 21; unit 23 is a vitric ash-flow tuff with a crystal content of approximately 10% by volume of the rock.

In addition to the measured section at Weavers Hill, two stratigraphic sections of the Weavers Hill ash-flow sequence at Campbell Hill and James Cove are presented in table 4. Lateral correlation of cooling units is also shown where possible.

About 0.25 mile (0.4km) north of Weavers Hill, the lower part of the ash-flow sequence (not shown in table 4) comprises a comparatively thin (less than 600ft; 183m) succession of dark red ignimbrites. Xenolithic tuffs at the base are thinner (less than 100ft; 30.5m) than similar deposits (units 17 and 18) at Weavers Hill, and only one cooling unit of vitric tuff (158ft; 48.2m thick) has been recognised.

At Campbell Hill the sequence thickens to approximately 1000ft (305m) of greyish green pumiceous ignimbrite sheets (units 29-35). A more chaotic distribution of crystals and pumice, and a paucity of sedimentary partitions between cooling units, hamper attempts to subdivide the lower part of the ash-flow sequence. A single cooling unit of vitric tuff occurs near the top of a predominantly crystal-bearing sequence of ash-flow sheets averaging about 20-30% crystals of quartz and albite.

At James Cove, the north-northeasterly strike of the pumice foliation trends subparallel to the shoreline (plate 2). In the

south, a dark greenish grey crystal tuff (unit 36), locally exhibiting pinkish albite crystals, lies in fault contact with volcanic sandstones and siltstones. Irregularities in the trend of compacted pumice are probably due to rotation of small fault blocks antithetic to the main fault. The most conspicuous mineralogical and textural variations are found in northern outcrops. Dark red, pumice-poor crystal tuffs locally "cap" the sequence; densely welded textures are common and at least one cooling unit measures over 100ft (30.5m) in thickness (unit 40). The total crystal content is about 30%, consisting of quartz (4%), feldspar (22%), and biotite (2-3%); the lithic fraction constitutes 5-10% of the unit.

Small but consistent amounts of biotite (1-2%) are also found in a dark red, pumice-rich crystal tuff (unit 39) directly underlying unit 40. Also a dark purplish red ignimbrite (unit 41, table 5) within the overlying sediments locally contains about 2% biotite. It is of interest to note that the presence of biotite as a cognate mineral in these ash-flow tuffs is accompanied by changes in the degree of welding; relatively thin, pumice-poor and pumice-rich ignimbrite sheets exhibit zones of dense welding in their interiors, whereas in the thicker pumice-rich cooling units lower in the sequence, compaction and welding are less intense (though a foliation due to welding is more easily recognised in the field).

Below the basal ash-flow deposits of the Weavers Hill sequence, but included here for convenience, dark red to pale green crystal tuffs

(units 15, 16, 27, and 28, table 4) are preserved in shallow topographic depressions that existed in epiclastic volcanic deposits at the time of ash-flow emplacement. On the eastern slopes of Weavers Hill two such ignimbrites (units 15 and 16) are found in erosive contact. Unit 15 reaches a maximum thickness of 73ft (22.3m), and is truncated within the upper zone of incipient welding (Ross and Smith, 1961) by a dark red crystal tuff (unit 16) which is entirely non-welded and forms a conspicuously pitted surface on weathering. The absence of stratification within unit 16, the concentration of lithic fragments (5%) and sharp contact at the base justify subdivision into two cooling units, and moreover, suggest an ash-flow origin. The central zone of unit 15 is densely welded and liphophysal cavities (up to 5mm in diameter) at the base are locally filled with spherulitic quartz and calcite. Vesiculation may have been promoted by the passage of a hot pyroclastic flow over wet volcanic breccias below. Crystals of quartz (2.5mm) are comparable in size to the larger crystals in Bacon Cove ash flows and form about 5% of a total crystal content of 25-30%, which includes 1% biotite, the remainder being albite. Units 27 and 28 on the eastern slopes of Campbell Hill exhibit textural and mineralogical features similar to unit 15, and these deposits probably represent the eroded remnants of formerly much more extensive ignimbrite sheets. Textural and mineralogical features of these deposits are more reminiscent of crystal tuffs at Bacon Cove and contrast markedly with typical Weavers Hill ignimbrites.

2.2.3. Finn Hill Ash-Flow Sequence

The Finn Hill ash-flow sequence (units 43-60, table 5) comprises all known cooling units of ash-flow tuff (interbedded with epiclastic volcanic rocks) that lie stratigraphically above a basal ash-flow tuff (unit 43) exposed on the southern shore of Dock Cove (cf. fig. 3 and geological map). A stratigraphic column over 2100ft (640.5m) thick has been compiled from a series of sections measured across the extrapolated length (3.5 miles; 5.6kms) of the ash-flow sequence.

A considerable variety of ash-flow deposits has been recognised, including pumice-poor tuffs with large (up to 4.5mm) crystals of albite (units 43-47, 51, 53, 55, and 56; coloured red in table 5); lapilli-tuffs enclosing variably compacted pumice and abundant rock fragments (units 48-50, 52, 54, and 57; coloured yellow); and two ignimbrites with highly unusual textures exposed at Finn Hill (units 58 and 59). An important difference between the Finn Hill ash-flow sequence and those described previously is the increased proportion of epiclastic volcanic material in the type-section; a natural division can conveniently be made between a lower (units 43-46) and an upper (units 47-60) group of ignimbrite cooling units.

The lower part of the Finn Hill sequence at Dock Cove comprises over 480ft (146.4m) of predominantly greenish grey to purplish grey crystal tuffs (units 43-46) interbedded with volcanic breccias and sandstones. Zonal variations in welding have only been detected in unit 45, which exhibits a densely welded interior. However, a crude

TABLE 5. Finn Hill Ash-Flow Sequence.

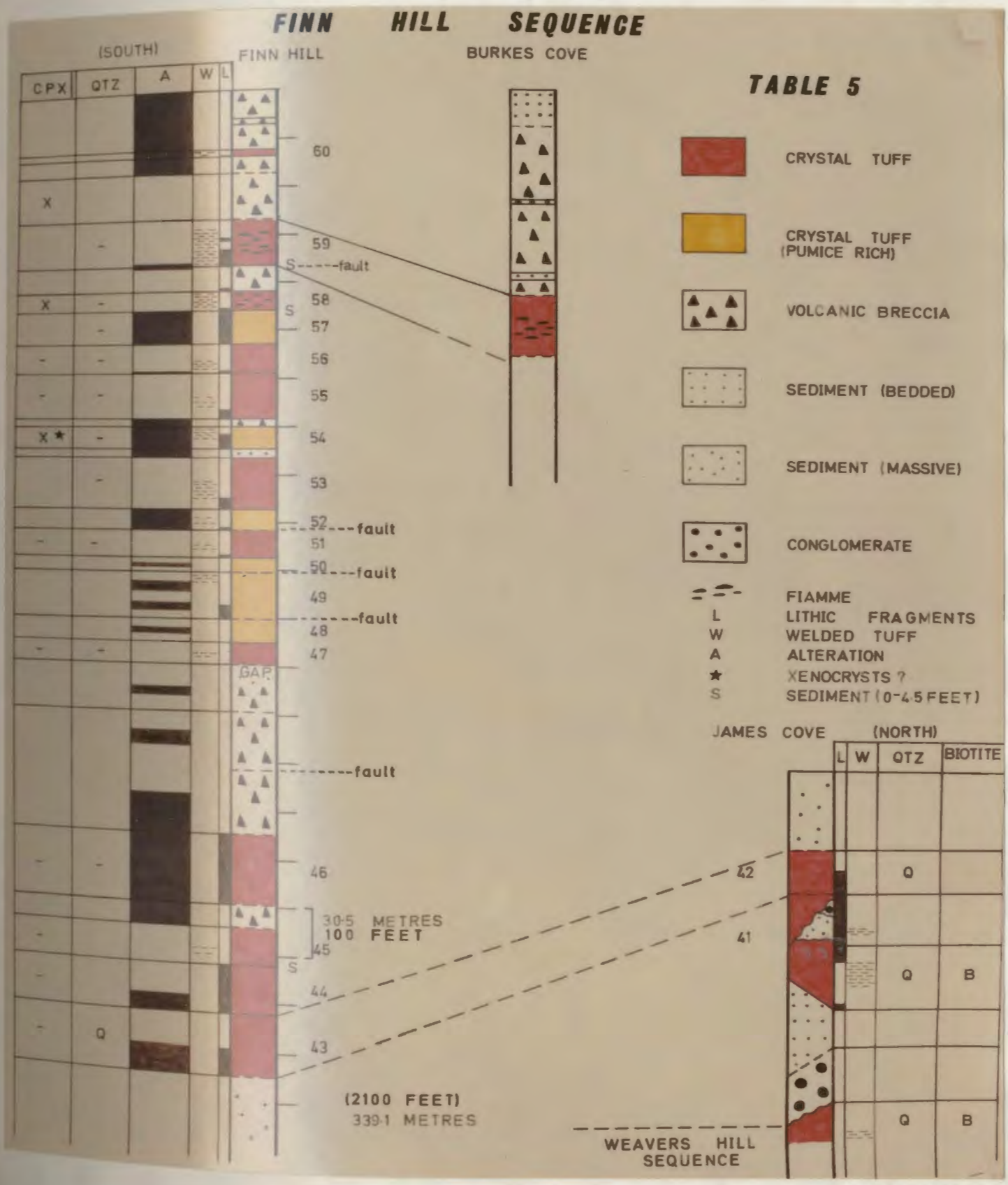

alignment of pumice-lapilli (about 2% by volume) has been observed within the green altered base of unit 43. Angular to subangular xenoliths (average diameter about 8 inches; 20.3cm) constitute approximately 10-15% of each cooling unit, and commonly consist of red- and green-altered crystal tuffs, reddish brown to dark brown tuffaceous sandstones, and amygdaloidal basalt and diabase; fragments of flow-banded rhyolite are present but comparatively rare. The mineralogy is remarkably simple: euhedral to subhedral and broken crystals of albite (2-4.5mm) form 25-40% of the rock and are typically the only crystals present; partially resorbed crystals of quartz have been recorded from unit 43 where they form 1-4% of the unit.

At Finn Hill, the upper part of the ash-flow sequence is exceptionally well preserved and has been described in detail by Papezik (1969), who presented a measured section over 800ft (243.8m) thick across a succession of dark red to reddish grey ignimbrite sheets separated by volcanic breccias of various origins and minor tuffaceous sandstones. This section has been incorporated into the stratigraphic column in table 5 with only slight modification (cf. Papezik, 1969, p. 1407).

Ash-flow tuffs on the eastern slopes of Finn Hill form strike ridges trending north-south and offset by east-west zones of faulting and dyke intrusion (plate 3). Units 47, 51, 53, 55, and 56 comprise reddish grey ignimbrite sheets containing large (up to 4mm) euhedral to subhedral and broken albite crystals (25-35%) and an assortment of

rock-lapilli (5-10%) set in a well-preserved shard matrix. Xenoliths commonly consist of basalt and dark red crystal tuff of accidental and accessory origin, respectively. Welded textures at the centre of the sheet generally grade into partly welded and non-welded margins. An interior zone of dense welding characteristically exhibits a conspicuous alignment of the long axes of albite crystals which provide a guide to welding in the field. Units 53 and 55 contain rounded grains consisting of intersecting plates of hematite in a base of chlorite, which possibly represent pseudomorphs after olivine. The basal part of unit 56 exhibits a distinctive red and green mottling which partly obscures welded textures at this horizon. Alteration of this nature is discussed in detail later (chapter VII).

Units 48-50, 52, 54, and 57 represent ash-flow tuffs of a different type. They consist of pale brown to pale green lapilli-tuffs enclosing pumice (5-10%) and angular to rounded rock fragments (10-20%) composed largely of rhyolite, tuffaceous sandstones and siltstones, fragments formed by mosaic intergrowths of quartz and albite, porphyritic rocks with albite phenocrysts, and rare basalt. Albite crystals are usually small (0.5-2mm) and form about 25-40% of a unit; crystals are commonly anhedral to subhedral in habit and set in an altered shard matrix. Where welded textures are preserved (units 49, 52, and 54) dark green to yellowish brown pumice-lapilli are flattened to form a weakly eutaxitic structure. Rare clinopyroxene crystals (<1mm) have been recorded from unit 54 and probably represent xenocrysts.

Units 58 and 59 are intercalated with thickly bedded volcanic breccias interpreted as volcanic mudflows or lahars. Crystal content is somewhat lower (10-20%), and lithic lapilli vary from 5-20% in unit 59 to 5-15% in unit 58. Unit 58 is a conspicuous dark reddish brown to almost black crystal tuff, 35ft (10.7m) thick, exhibiting a strongly eutaxitic foliation which curves around crystals and rock fragments and is best seen in thin section. The mineralogy consists of crystals of albite (1-3mm) and small (0.5-1mm) clinopyroxene crystals which occur as a decidedly cognate phase forming approximately 0.5% of the rock. A chocolate-brown volcanic breccia overlying unit 58 contains angular fragments of welded tuff derived from the unit below, and found up to 6 inches (15.2cm) above the base of this lahar; the contact is sharp and distinct.

Textural variations typical of ignimbrite cooling units (Ross and Smith, 1961) are well preserved in unit 59. Angular to subangular xenoliths (0.5-4inches; 1.3-10.2cm across) are for the most part chaotically distributed except for a slight concentration in the middle of the zone of welding (plate 4). Megascopic textural features are rather striking: dark grey to black lenses measuring up to 14 inches (35.5cm) in length, with rounded or delicately frayed extremities, define a strongly eutaxitic foliation. They commonly enclose euhedral albite crystals (up to 3mm) and appear pancake-shaped in three dimensions (plate 5). Similar textures are found on a microscopic scale in unit 58. The inclusions described resemble the "fiamme" or "flame structures" of "tuff lavas" from the Phlegrean Fields, Italy

(Cook, 1966); collapsed pumice in the "eutaxites" documented from Gran Canaria (Schmincke and Swanson, 1967); and dense glassy inclusions in pantelleritic ignimbrites at Fant'Ale volcano, Ethiopia (Gibson and Tazieff, 1967; Tazieff, 1969; Gibson, 1970; McBirney, 1968).

Unit 60 consists of a pale red to pale green altered crystal tuff containing about 20% crystals of albite (less than 2mm) set in a partly welded shard matrix.

Lateral correlations of ash-flow cooling units in the Finn Hill sequence are shown in table 5.

At James Cove a reddish grey ignimbrite (unit 42) transgresses a volcanic conglomerate to rest with marked disconformity on a dark purplish grey ignimbrite sheet (unit 41) further south. Unit 42 contains angular to subangular rock-lapilli comprising dark red crystal tuff, dark brown tuffaceous sandstone, basalt, diabase, and rare rhyolite. Large (1-4mm) crystals of albite and small (1-2mm) quartz crystals (3%) form about 30-40% of the rock. A swarm of dark green to pale brown eutaxitic pumice-lapilli occur within a thin (10-20ft; 3.1-6.1m) zone of welding in the lower part of the unit. Unit 42 has been correlated with unit 43 at the base of the Finn Hill ash-flow sequence on the basis of comparable textures, and in particular the occurrence of crystals of quartz.

Unit 41, by definition therefore, lies below the base of the Finn Hill ash-flow sequence. Although the central part of the unit exhibits a zone of dense welding, intense recrystallisation locally destroys shard outlines (cf. chapter III). Crystals of albite (<2.5mm)

constitute 10% (near the top) to 30% (at the base) of the unit; biotite (<1mm) also occurs but forms less than 1%.

Excellent exposures of the topmost part of the Finn Hill sequence are found at Ryans Head and along the western shore of Burkes Cove. Epiclastic volcanic breccias and conglomerates overlie a fiamme-bearing ignimbrite correlated with unit 59 in the section at Finn Hill (plate 6). Megascopically distinct fiamme protrude slightly from the surface of glacially scoured outcrops due to differential erosion of inclusion and matrix (plate 7). A concentration of rock-lapilli near the centre of the cooling unit forms a discontinuous layer 0-3ft (0-0.9m) in thickness. Densely welded textures persist as far as the upper and lower margins of this layer and in general the boundaries of the zones of welding parallel the "bedding planes" indicated by the lithic horizons. Irregularities at the base of this bed are reflected by gentle warping of the compaction foliation. This is interpreted as the result of slumping due to rapid loading by an overriding ash flow while the lower ash-flow unit was still hot and capable of plastic deformation (plate 8). Thus, cooling unit 59 can be divided into a lower and an upper ash-flow unit separated by a layer of rock-lapilli probably representing a deposit formed by gravity settling of denser lithic fragments toward the base of the younger ash flow. Gibson (1970) has described xenolithic horizons of similar nature in ash-flow sheets at Fant'Ale. The internal chemistry of unit 59 is presented later (chapter VIII and table 7) and suggests that its multiple flow history may also record

compositional variations that existed in the magma reservoir immediately preceding its eruption.

2.3. Mechanism of Ash-Flow Emplacement

The first detailed account of a nuée ardente-type eruption is credited to Lacroix who described the eruption of Mont Pelée on the island of Martinique on May 8th, 1902 (cf. Macdonald, 1972, p. 142, for a brief resumé of this eruption). On the previous day, Anderson and Flett had witnessed similar eruptions at La Soufrière on St. Vincent, and later that same year at Mont Pelée on July 9th. Although no scientifically observed nuées ardentes have produced recognisable welded ash-flow deposits, the geological evidence overwhelmingly favours a gas-emitting particulate flow as the agent of transport. According to Ross and Smith (1961), ash-flow deposits are typically chaotic and in this respect resemble rather closely pyroclastic deposits at Finn Hill and Weavers Hill, interpreted as ash-flow sequences. However, systematic vertical variations of included crystals and rock fragments are a distinctive macroscopic feature of the Bacon Cove ash-flow sequence. Textural characteristics such as these appear to demand density sorting during emplacement akin to mechanisms of deposition postulated from graded textures in the distal ends of submarine density currents.

Ash-flow sheets interbedded with marine sedimentary sequences are known from the literature, and in certain cases have been taken as evidence for subaqueous eruption and emplacement of fluidised silicic magma. Graded textures in such deposits appear to lend weight to this argument. For example, textures of this nature in pyroclastic flows of Miocene age have been recorded by Fiske and

Matsuda (1964) from the Wadaira Tuff Member of the Tokiwa Formation, Japan. Density sorting in the thicker ash-flow deposits has resulted in concentration of partly vesiculated fragments of dacite near the base and shredded pumice-lapilli toward the top of each unit. Furthermore, it has been shown quite convincingly that where pyroclastic flows enter water pumice-lapilli are preferentially oriented parallel to the direction of flow, a texture which is genetically remote from their orientation by compaction and welding (cf. Fiske, Hopson, and Waters, 1963, p. 16). Similar deposits in which welding does occur, however, have been described from the Ordovician (Caradocian) marine strata of North Wales by Francis and Howells (1973), from the Vati Group on Rhode Island, Greece, by Mutti (1965; cf. in particular fig. 9, p. 280), and by Fiske (1969) from ash flows of Miocene age in Puerto Rico (Fiske, ibid., plate 3, fig. 2). In the latter examples, however, it is difficult to conceive how welding can take place to any great extent in a submarine environment, and in this respect the ignimbrites of North Wales have sparked a great deal of controversy.

Gravitational sorting in terrestrial ash-flow deposits has been described, for example, by Hay (1959) from La Soufrière, by Fisher (1966) from distal parts of the Picture Gorge ignimbrite of north-central Oregon, by Ono (1966) and Lipman (1967) from ash-flow sheets of the Aso Caldera, Japan, and by Walker (1972) in a comprehensive study of crystal concentration in ignimbrites. In particular, Fisher (1966) related lateral variations in phenocryst proportions and size of included rock fragments to their specific gravities or "settling

velocities", which, he argued, governed sorting and sedimentation in a turbulent pyroclastic flow. Some measure of laminar flow during transport was invoked by him (Fisher, ibid., p. 360) and this mechanism has also been suggested by Gibson (1970, p. 199) to explain sorting of xenoliths in Ethiopian ash flows at Fant'Ale. Likewise, Elston and Smith (1970) attributed the formation of primary directional fabrics in the Bandelier Tuff and Battleship Rock ash-flow sheets of the Valles Caldera, New Mexico, to laminar flowage in a highly mobile medium. Examples are known, therefore, of density stratification within a moving ash flow which has been preserved and recognised upon deposition.

Concerning the textural characteristics of the Bacon Cove ash-flow sequence, it seems reasonable to postulate that sorting occurred at the distal parts of these ash flows. Evidence in support of this hypothesis comes from the section at Kitchuses where many of the ash-flow cooling units are missing and were probably not deposited (cf. table 3). In addition to a number of complex factors governing the mode and intensity of a particular eruption and the consequent nature of the pyroclastic debris (cf. Verhoogen, 1951), it is likely that the preservation of textures resulting from primary laminar flowage would only occur where the surface of deposition was relatively uniform. Considerations involving the relief over which an ash flow has travelled might explain in part at least the fabrics recorded from ash-flow cooling units in the upper part of the Weavers Hill section (units 19-26 in table 4) and at Bacon Cove (units 3, 5, 7, and 9, table

3) as compared with those found in the lower part of the Weavers Hill section (notably units 17 and 18, table 4).

At this point, let us consider the sillars of the Bacon Cove ash-flow sequence. Crystal concentration in these sillars could be explained simply by gravitative sorting of crystals during flow in an originally much thicker ash-flow deposit. This mechanism is indeed plausible since textures comparable with those found in the sillars have been observed at the base of an ignimbrite sheet (unit 3, table 3) in the type-section at Bacon Cove. Moreover, delicate wisps of devitrified glass adhering to many of these crystals strongly suggest derivation from freshly erupting magma rather than the scrapings of a weathered regolith.

One of the earliest detailed studies of crystal-rich, glowing avalanche deposits was made by Hay (1959) at La Soufrière. Hay compared the concentration of phenocrysts in scoria and bombs with their concentration in the ash fraction of these deposits. He found that about one fifteenth of the total material erupted had been incorporated in the ash flow and that approximately one third had been lost as finely comminuted ash (predominantly vitric) to the cloud overriding the basal avalanche, resulting in marked enrichment of crystals. In particular, the ferromagnesian minerals had more than doubled their initial concentration in the magma. The ash flow itself had separated into a denser fraction consisting of blocks, lapilli, and crystals, and a lighter fraction comprised chiefly of expanding gas and shards. Furthermore, these textures could be traced to within a

few hundred yards of the vent, implying that segregation in the vertical eruptive column had taken place almost immediately. Lipman (1967) and Walker (1972) have also appealed to selective removal of shards and their subsequent deposition at the extremities of an ash-flow deposit.

Winnowing of shards is certainly a more appealing mechanism for producing the textures observed in the sillars of the Bacon Cove ash-flow sequence since there is no evidence for extensive erosion of a crystal-poor zone at the top of these cooling units. Although the sillars are much thinner 2 miles (3.2kms) further south at Kitchuses, there is no significant decrease in the crystal:shard ratio and textures are comparable with the deposits at Bacon Cove. This strongly suggests that a considerable amount of volcanic ash was distributed well beyond the confines of the map area during eruption and emplacement of the sillars. However, the problem of estimating the relative amount of pyroclastic material produced during a single eruption is greatly increased where welded textures are lacking. For example, the greater thickness of sillars at Bacon Cove might be attributed to a number of undetected ash-flow units within a single cooling unit; such phenomena have been observed where welding is present in unit 59 of the Finn Hill ash-flow sequence.

In conclusion, it has been argued that many of the textural features of individual cooling units within the map area have been produced by processes involving density sorting during ash-flow emplacement. In particular, density stratification has played a

major role in the formation of textures in Bacon Cove ash-flow tuffs, especially the sillars. It should be mentioned, however, that although crystal enrichment in these deposits invites an erroneous interpretation concerning their original concentration in the magma prior to eruption, the size of the larger crystals in the sillars is comparable with the average grain size in granitic phases of the Holyrood Plutonic Series (with which the sillars are compared chemically in chapter VIII) and suggests that they were derived from a magma in a relatively advanced state of crystallisation. This magma has subsequently undergone crystal fractionation resulting from post-magmatic eruptive processes.

2.4. Provenance and Magnitude of the Ash-Flow Deposits

The sites of former volcanic edifices that supplied what must have been considerable volumes of ash-flow material have not been recognised in the map area. It would be fortuitous, indeed, if the eroded remnants of an ash-flow source were exposed in cross-section, and such a structure has yet to be observed in the Harbour Main Group. Although ash-flow sheets cannot be traced to their source, it is possible to use indirect geological evidence to infer the general direction of provenance of many of the ash-flow deposits and to predict the minimum number of source vents active at any one time. Perhaps the most pertinent features to consider are stratigraphic variations of both single cooling units and entire ash-flow sequences along strike, and variability of xenolith assemblages. Compositional variations are considered later (chapter VIII).

The Bacon Cove ash-flow sequence thins markedly toward the south where many cooling units in the type-section are replaced by thick wedges of tuffaceous sandstone and siltstone. Ash-flow tuffs mineralogically and texturally identical to vitric and crystal tuffs at Bacon Cove are exposed in fault blocks in the extreme north of the map area. Fine-grained clastics along strike to the south are enriched in shards and crystals of quartz and biotite, and represent proximal deposits of reworked pyroclastic material, no doubt derived largely from the unconsolidated upper zones of ignimbrite cooling units. Strictly stratigraphic evidence, therefore, requires that the source vent(s) for Bacon Cove ash flows was located to the north

of present exposed limits of Colliers ignimbrites. Combining the arguments above with textural evidence presented earlier (section 2.3.) it appears that the Bacon Cove ash-flow sequence was deposited at the distal parts of a much more extensive ash-flow field to the north.

In the case of Weavers Hill ash-flow tuffs, the stratigraphic evidence for a particular direction of provenance is less compelling. The sequence attains a maximum thickness at Campbell Hill and a minimum in the south; its thickness in the north is unknown. The effects of erosion and palaeotopography are complex and difficult to evaluate. The presence of a thick unit of crystal tuff (unit 40, table 4) at the top of the sequence at James Cove and its absence to the south suggest that at least this ignimbrite had its origin to the north. Local conglomeratic horizons at James Cove suggest that a region of higher elevation existed here immediately succeeding ash-flow deposition. Similarly, laharic breccias interbedded with thin conglomeratic horizons located east of Campbell Hill, pass into fine-grained volcaniclastic deposits further south. Since volcanic mudflows, like nuées ardentes, flow predominately under the influence of gravity, a topographic high to the north is again inferred. If this region of higher relief persisted throughout deposition of Weavers Hill ash-flow tuffs, as the evidence suggests, it is likely that the source of the ash flows was also located in the north since they retain their sheet-like form and do not pinch out along strike as would be expected if they had flowed from south to north and gradually buried a pre-existing topographic high.

Prolific fragments of flow-banded rhyolite found in these ash-flow tuffs and laharic breccias suggest a common source area. Contrasting assemblages of xenoliths in Bacon Cove and Weavers Hill ignimbrites (i.e. predominantly crystal and vitric tuff-lapilli in the former, and mainly flow-banded rhyolite in the latter) could be interpreted as indicating:

a) different source areas for each ash-flow sequence, or
b) the same source area with an intervening period of extrusion/intrusion of viscous rhyolite at the vent(s).

In any case, it is evident that not all the extrusive/intrusive episodes at source vents are recorded by the volcanic stratigraphy presently exposed. Density stratification of crystals, pumice, and rock fragments has been noted in a number of ash-flow sheets at Weavers Hill (though less pronounced than comparable textures in Bacon Cove ignimbrites) but has not been observed at Campbell Hill or James Cove. These observations suggest that, all other factors being equal, the Weavers Hill ash-flow tuffs are comparatively nearer their source.

The highly diverse nature of ignimbrites comprising the Finn Hill sequence and relatively short lateral extent of the upper and lower groups of cooling units preclude conclusions as to the location of source vents. Interfingering of cooling units at Finn Hill with contrasting textures and xenolith suites provide evidence for at least two separate source regions concurrently active. Pumiceous crystal tuffs (units 48-50, 52, 54, and 57, table 5) strongly resemble those

of the Weavers Hill sequence but contain a greater proportion of rock fragments and clay-size material. Sparse xenoliths of flow-banded rhyolite are found in the pumiceous tuffs and laharic breccias; however, crystal tuffs and fiamme-bearing ignimbrites of the sequence (coloured red in table 5) lack rhyolite, though basaltic xenoliths are common. Consequently, the former ignimbrites were probably derived from a waning source area that may have previously supplied Weavers Hill ash-flow tuffs, whereas the latter deposits were derived from a separate source.

Considerations of the volumes of ash-flow fields generally lead to conclusions involving the nature of source vents. For example, in an excellent review of ash flows, Smith (1960, p. 819) summarised the orders of magnitude of some well-known Tertiary and younger ash-flow deposits. Ash-flow deposits of small volume (maximum of 1-10km^3) and restricted distribution he categorised as either eruptions at open craters, for example, Mayon volcano, 1968; and La Soufrière, 1902; or craters with domes, for example, Mt. Pelée, 1902; Bezymianny, 1956; and Hibokhibok, 1951. Voluminous ash-flow deposits are commonly products of eruptions through fissures, either linear or arcuate, associated with multiple source regions or volcano-tectonic depressions. Ash-flow fields of this type generally exceed 100km^3 and many have been estimated to range 1000-10000km^3, for example, San Juan ash-flow field, Colorado (Luedke and Burbank, 1961); Yellowstone (Boyd, 1961); and Lake Toba volcanic field in Sumatra (Van Bemmelen, 1949). Intermediate volumes are usually associated with calderas, for example, Aso caldera,

Japan (Lipman, 1967); Valles Caldera, Jemez Mountains, New Mexico (Smith and Bailey, 1966); and Timber Mountain, Nevada (Ekren, 1968).

Original volumes of Colliers ignimbrites are unknown since they are incompletely preserved in cross-section only; however, some speculations concerning their original magnitude are worthwhile since there appears to be a crude correlation between the volume of ash-flow fields, i.e. the nature of the source vents, and the thickness and textural characteristics of cooling units.

Nuée ardente type or Peléean activity in historic time is characterised by eruptions through central or pipe vents (Macdonald, 1972, p. 199) or from lateral cones or fissures of a composite volcano at a mature stage of growth. The deposits are usually of rhyolitic compositions and relatively small volumes, and thoroughly welded textures are lacking. Furthermore, ash flows commonly follow the course of river valleys eroded into the flanks of the main cone; seldom do they form extensive deposits at lower elevations on surrounding plains, which are more commonly blanketed by laharic breccias. A river valley is clearly not a favourable location for the preservation of loosely consolidated pyroclastic material, and streams soon excavate new channels at a fairly rapid rate. Perhaps a somewhat unusually violent and voluminous ash-flow eruption for a large stratovolcano was the paroxysmal eruption of prehistoric Mt. Mazama (Williams, 1942), which produced flat-lying sheets of pumice extending 35 miles (56.3kms) to the east. Though fossil fumaroles indicate that the pumice flows were hot when they came to rest, the deposits are entirely non-welded and the eruption produced a caldera

6 miles (9.7kms) in diameter, now occupied by Crater Lake. In contrast, the rhyolitic ash-flow deposit which formed the Valley of Ten Thousand Smokes in 1912 was considered to have a fissure source on the flanks of Mt. Katmai (Fenner, 1923; Bordet, Marinelli, Mittempergher, and Tazieff, 1963). Macdonald (1972, p. 240) described the Katmai eruption as "the closest approach to a rhyolitic flood eruption that we have had in recent centuries", yet this deposit only produced a zone of incipient welding at the base.

Strong evidence that ash-flow tuffs of the Weavers Hill sequence were derived from a single source is provided by a suite of rhyolitic xenoliths common to all cooling units. Similar textural and mineralogical characteristics further strengthen this argument. Furthermore, the general lack of sedimentary partings between cooling units and preservation of non-welded upper margins in the majority of these ignimbrite sheets suggest rapid emplacement during a period of intense volcanic activity. The earliest deposits at the base of the sequence (units 17 and 18, table 4) appear to have been restricted to topographic lows allowing later deposits to spread laterally as continuous, almost horizontal sheets in much the same manner as the Aso III sheet, a compound cooling unit, accomplished in a single eruptive episode (Lipman, 1967). Assuming a minimum thickness of 1000ft (305m) for the entire Weavers Hill sequence and that the deposits blanketed a uniform topography for a distance normal to strike equal to the exposed strike length, i.e. 4 miles (6.4kms), then the volume of tuff produced during this eruptive episode is about 3.03 cubic miles (7.84km^3). This

estimate is approximately double the size of Japanese ash-flow fields erupted through craters (Smith, 1960, p. 819), and is much greater than recent estimates of the "great sand-flow" at Katmai National Monument (compare Fenner, 1923, with Gedney, Matteson, and Forbes, 1970); however, it falls short of the volumes of pumice flows calculated for Crater Lake by Williams (1942). Although the volumetric evidence is entirely speculative, the form and textures of cooling units comprising the Weavers Hill ash-flow sequence are considered incompatible with their origin at a crater in the summit region of a composite volcano (if past experience of such eruptions is adequate); instead, the evidence is more consistent with a fissure/caldera source and deposition in a subsiding basin or trough. Present knowledge concerning the tectonic regime at the time of ash-flow deposition is in accord with this interpretation (cf. chapter VI). If this view is correct, it can probably be extended to include the other ash-flow sequences, though their origins are obviously more complex.

Based on the available stratigraphic and textural evidence, doubt has already been cast on the proximity of source vents for Bacon Cove and Weavers Hill ash-flow tuffs. In the type-sections described earlier (tables 3, 4, and 5), component cooling units that exhibit welded textures, and can therefore be recognised with a high degree of confidence, rarely attain 200ft (61m) in thickness (units 4 and 7, table 3). The problems of subdividing non-welded tuffs into cooling units have already been examined (section 2.3.) and it is of interest that the thickest "cooling unit" in a measured section is a

sillar (unit 6, table 3). In many ignimbrite sheets, however, the level of erosion locally extends down to the interior zone of welding and original thicknesses must have been greater. In comparison, individual cooling units of volcano-tectonic depressions and giant calderas may attain thicknesses as great as that of Bacon Cove or Weavers Hill sequences, and ash-flow fields commonly exceed the thickness of the entire volcanic pile presently exposed on the Colliers Peninsula; compound and composite cooling units (Ross and Smith, 1961) are also common and contrast markedly with the thin, simple cooling units of Colliers ignimbrites. Thus, it appears that the Bacon Cove, Weavers Hill, and Finn Hill ash-flow sequences may well have originated from source vents similar to the smaller calderas cited by Smith (1960), since they bear little resemblance to the proximal deposits of the more voluminous ash-flow fields. The nature of the peripheral deposits of such regions, however, is poorly documented, and it is quite possible that Colliers ash-flow deposits occupy such a position.

CHAPTER III

TEXTURES AND MINERALOGY OF THE ASH-FLOW DEPOSITS

A guide to the predominant textural and mineralogical features of the Bacon Cove, Weavers Hill, and Finn Hill ash-flow sequences is provided by tables 3, 4, and 5, respectively. Albite phenocrysts are ubiquitous and have not been tabulated. Variations of texture and mineralogy within individual cooling units have been described previously (chapter II); the descriptions below, therefore, are generalised with examples taken from specific cooling units.

3.1. Bacon Cove Ash-Flow Sequence

Textures characteristic of ignimbrite cooling units (Ross and Smith, 1961) have been recognised in all but units 2 and 6 (table 3). Crystals of biotite, quartz, and albite are found throughout the sequence, though units 7 and 9 at Bacon Cove and units 10 and 14 at Kitchuses contain no biotite.

3.1.1. Textures

Vitroclastic matrices in ash-flow tuffs of the Bacon Cove sequence generally exhibit well-preserved shards approximately 0.02-0.4mm across and up to 3mm in length coated by a thin layer of iron-oxide particles. Zonal variations in welding in units 1, 3-5, and 7-9 can be traced

by progressive deformation of the shards by compaction during cooling. An upper zone with open vitroclastic textures is composed of platy shards, representing the vesicle walls of fragmented pumice-lapilli, set in a finely comminuted matrix dusted with iron-oxide (photomicrograph 4). This zone passes downwards through a zone of incipient welding into densely welded textures in the middle and lower parts of the ignimbrite. Shards have been plastically deformed and are draped around crystals and xenoliths (photomicrograph 5). Non-welded textures in the basal zone are common and incipient welding has been observed. In vitric tuffs (units 4, 8, and ignimbrite to the north) shards are densely welded though eutaxitic textures are poorly developed (photomicrograph 6).

Quite contrasting textures are found in the crystal-rich sillars (units 2 and 6). Intense microspherulitic devitrification consisting of fibrous quartz and alkalic feldspar, partly replaced by sericite, has destroyed all trace of shard outlines in the lower and central parts of the units (photomicrograph 7); open vitroclastic textures are preserved at the top. In several specimens collected near the base of unit 3, where crystals form up to 40% of the rock, wisps of iron-oxide dust locally outline bent and welded shards in the interstices between crystals. No trace of shard outlines can be detected where opaques have been leached. The possibility remains that the sillars may in fact have been consolidated by welding, and that the prominent recrystallisation textures are a product of secondary hydration and devitrification. If future work should reveal welding, then the comparisons made earlier (chapter II,

section 2.1.) between these deposits and classical sillars described by Fenner (1948) and Jenks and Goldich (1956) are no longer valid. Enrichment of crystals probably inhibited welding and possibly exerted a greater influence on the development of welded textures than low temperature emplacement.

Units 7, 8, and 9 at Bacon Cove, and units 10 and 14 at Kitchuses have distinct textural and mineralogical affinities to overlying ash-flow tuffs of the Weavers Hill sequence. Megascopic pumice is conspicuous and biotite is lacking (except for a small amount in unit 8).

3.1.2. Mineralogy

Phenocrysts of quartz range from about 0.2mm in the vitric tuffs to 3.5mm in the sillars; biotite forms minute flakes less than 0.1mm to large tabular crystals up to 3mm across; crystals of albite range from less than 0.5mm where broken to 4mm in monomineralic intergrowth. Minor magnetite, hematite, and zircon (rare) are disseminated throughout the matrix. Quartz crystals are usually resorbed, showing rounding and intricate embayment; they invariably occur as alpha-quartz paramorphs after beta-quartz, though euhedral crystals are rare (photomicrograph 8). In the sillars, euhedral to subhedral biotite phenocrysts are characteristically impregnated with magnetite and hematite along cleavage planes, and appear almost opaque where sectioned parallel to the basal pinacoid (photomicrograph 9). Relatively soft biotites are commonly broken down and dispersed as ragged

flakes in the vitric tuffs, though larger crystals occur near the base (photomicrograph 10). In sillars, and at the base of unit 3, crystals of biotite are locally deformed by impinging quartz and albite (photomicrograph 11); abrupt truncation by microshears is probably a feature of later deformation during folding. Albite phenocrysts are generally broken and rounded in sillars, but euhedral to subhedral in vitric and crystal tuffs. Albite and Carlsbad twinning is preserved and crystals rarely form glomeroporphyritic intergrowths. Accessory zircon is euhedral to subhedral in habit, and either set in large biotite phenocrysts or at random in the groundmass.

3.2. Weavers Hill Ash-Flow Sequence

Greenish grey, pumiceous ash-flow tuffs of the Weavers Hill sequence are typified by eutaxitic textures in the central parts of cooling units and non-welded margins (cf. table 4). A small amount of quartz is characteristic (usually less than 4%), accompanied by phenocrysts of albite (10-35%). Crystals of biotite occurring in units 15 and 16 are probably of xenocrystic origin. However, a little biotite (less than 2%) is present in a red crystal tuff at James Cove (unit 40). Lithic fragments (up to 20% of the rock) are chaotically distributed in the lower part of the sequence (units 17-20), but form basal concentrations in units 21-26 above.

3.2.1. Textures

Vitroclastic textures are well-preserved in these pumiceous ignimbrites though leaching of opaque dust and alteration to sericite and clay minerals is generally more pronounced than in the other ash-flow sequences. Particles of iron-oxide, mainly hematite at the margins of cooling units and magnetite in their interiors, coat the margins of shards and pumice-lapilli (photomicrograph 12). A well-defined foliation in the vitric tuffs (units 19 and 20) is largely a result of the preferred orientation of pumice fragments within a moving ash flow rather than a feature caused by compaction and welding. Non-welded textures preserved in the upper zones of units 19 and 20 exhibit cuspate, platy, and slender rod-like shards commonly 0.06-0.8mm thick and up to 3mm in length which represent the extremely thin walls of tube-vesicles in fragmented pumice (photomicrograph 13). Shards enclosing rounded vesicles probably represent cross-sections of the more typical tube-vesicles. Incipient welding in a zone below grades downwards into a densely welded interior zone with eutaxitic pumice-lapilli. Progressive collapse of pumice under lithostatic loading is accompanied by elimination of pore space until only a smear of opaque dust marks the former presence of tube-vesicles (photomicrograph 14). Coarse recrystallisation consisting chiefly of alkalic feldspar and quartz with mosaic to weak microspherulitic structure is preferentially located within collapsed pumice-lapilli (photomicrograph 15). Similar textures in recent ignimbrites, for example, at Pant'Ale (Gibson, 1970), suggests

that the recrystallised areas are products of vapour-phase crystallisation during cooling and genetically related to expulsion of volatiles trapped within the pumice. Textural features of this type have also been observed in microscopic fiamme of unit 58 at Finn Hill, and it is suggested that pumice and fiamme are not necessarily inclusions with distinct modes of origin. Axiolitic and spherulitic devitrification structures, composed of alkalic feldspar partly replaced by sericite and clay minerals, are common in less densely welded zones (photomicrographs 16 and 17). Rare fractures within the pumice are dusted with iron-oxide particles and oriented perpendicular to the eutaxitic foliation. Schmincke and Swanson (1967) have described similar "tension" cracks in relatively brittle pumice from eutaxites of Gran Canaria which originated during secondary viscous creep on steeply inclined slopes.

An important feature of units 19, 20, and 26 is the local orientation of drawn out pumice-lapilli at a high angle to the foliation (photomicrograph 18), and which begin to lose their attitude and shape on welding. It is of genetic significance to note that although these units are among the thickest of the sequence (apart from unit 26 whose thickness is unknown) and were evidently derived from the same poorly crystallised, presumably high-temperature magma, eutaxitic textures are not as well-developed in these ignimbrites as similar textures in thinner units above. Clearly the mode of eruption, whether it be a vertical eruption column as envisaged by Smith (1960) or a directed blast as witnessed by

Anderson and Flett (1903), played a major role in the cooling history of these ash-flow deposits.

3.2.2. Mineralogy

Phenocrysts of quartz are generally rounded and embayed, and somewhat smaller (<2mm) than crystals in Bacon Cove ignimbrites. Albites are usually subhedral and broken; Carlsbad and lamellar twinning is common. Pumice-lapilli sporadically enclose euhedral to subhedral albite phenocrysts, and many crystals have shreds of devitrified glass adhering to them. Apatite and iron ore are common accessory minerals; zircon has only been found in a biotite-bearing ignimbrite (unit 40) at James Cove. Biotite crystals (<0.8mm) are generally pleochroic from green to colourless, and the prominent dusting of opaques along cleavage planes is lacking, though alteration to chlorite and leucoxene is common.

3.3. Finn Hill Ash-Flow Sequence

Zonal variations in welding have been observed in all units apart from units 43, 44, 46, 48, 50, and 57 (table 5). The development of welded textures in the lower group of ignimbrites has only been recognised in unit 45; however, zones of dense welding characterise many of the ignimbrites above. Albite crystals are most pronounced in this ash-flow sequence and locally occur to the exclusion of other phenocryst phases. Crystals of clinopyroxene are found in units 54 and 58.

3.3.1. Textures

Highly variable but distinct textural features divide these cooling units into three groups: pumiceous tuffs resembling ignimbrites of the Weavers Hill sequence (units 48-50, 52, 54, 57); ignimbrites lacking pumice and characterised by minute shards and densely welded interiors (coloured red in table 5); units 58 and 59 with inclusions of devitrified glass (fiamme) unique to these ignimbrites.

The non-welded base of an ash-flow tuff at James Cove (unit 42) contains tiny rod-like and platy shards (0.1-0.8mm in length and 0.03-0.1mm across) and sporadic pumice fragments (1.8-3.5cm maximum dimension) which become progressively flattened upwards until weakly eutaxitic and curving around crystals and rock fragments. Cuspate shards coated with a film of opaque dust are found toward the top of this unit.

At Finn Hill, units 49, 52, and 54 contain a thin interior zone of eutaxitic pumice (1.5-4.5cm in length) bending around accidental lithic inclusions and broken crystals; welding has not been detected in units 48, 50, and 57. Pumice-lapilli in non-welded margins are commonly rounded and may be derived from older pyroclastic deposits. Shard outlines are almost completely destroyed by intense leaching of iron-oxide from their margins, and the matrix is usually clouded by clay-size particles. These ignimbrites have strong textural affinities to those of the Weavers Hill sequence described earlier (section 3.2.1.)

Units 47, 51, 53, 55, and 56 forming the eastern slopes of Finn Hill and ridges to the north exhibit strongly welded central zones with elongate shards (0.1-0.5mm in length) enclosing subhedral phenocrysts (cf. Papezik, 1969, figs. 11 and 12). Gradations into open vitroclastic textures at the margins of these units are best seen in the upper parts of the ignimbrite sheet; rod-like shards partly squeezed between crystals gradually assume cuspate and fork-shaped forms (up to 0.3mm in length). Pumice-lapilli have not been observed.

Ignimbrites near the top of the Finn Hill sequence have been documented in detail by Papezik (1969). Papezik (ibid., p. 1411, unit 6) describes unit 56 as "strongly recrystallised, resembling in part a typical 'feldspar porphyry', and the outlines of shards are only rarely preserved". The most striking welded textures, however, occur in unit 58 (cf. Papezik, ibid., unit 9, figs. 3, 4, 6-8, and 10). A predominantly cryptocrystalline groundmass appears dark brown even in thin section due to pervasive iron-oxide dust. Strongly eutaxitic shards and dark obsidian-like fiamme, some with delicately frayed extremities, are so flattened and drawn out that locally they simulate flow lines. Microspherulitic devitrification products appear to nucleate preferentially within fiamme and are aligned along the direction of flow (photomicrograph 19). Perlitic cracking is well-developed in the matrix (photomicrograph 20), and also occurs extensively in fiamme, thereby proving their glassy origin (photomicrograph 21). In the upper and central parts of this unit, cavities of lithophysal origin are filled with coarsely

spherulitic epidote rimmed by mosaic quartz, individual grains of which preserve a faint microspherulitic structure (photomicrograph 22). The eutaxitic shard foliation curves around the lithophysae, which clearly must have been formed immediately preceding or during welding (photomicrograph 23). These textures, therefore, are most likely a result of vapour-phase crystallisation of metastable mineral phases during initial cooling. Closely comparable features have been described by Gibson (1970, fig. 10a) in geologically recent pantelleritic ignimbrites at Fant'Ale. Though quartz rims probably represent original high-temperature polymorphs such as tridymite or cristoballite, the central cavity-filling epidote probably crystallised later during low-grade metamorphism, the effects of which are discussed later (chapter VII). Many of the "nodular" structures of Caradocian ignimbrites in North Wales, for example, represent hollow lithophysal cavities rimmed by spherulitic quartz paramorphic after tridymite and partially filled by quartz mosaics during later processes of silicification.

In unit 59 above, intense recrystallisation has destroyed all trace of shard outlines, though margins of fiamme measuring 0.2-35.5cm in length and up to 10cm thick are usually marked by a thin film of iron-oxide particles (photomicrograph 24; also cf. Papezik, 1969, unit 12, fig. 5). Unlike ash-flow tuffs at Weavers Hill, no evidence remains for the collapse of vesiculated pumice, and in this case an alternative origin might be one involving lava-fountaining at the vent and incorporation of liquid "clots" that were either volatile-

poor or did not have chance to vesiculate prior to welding, as described, for example, by Gibson and Tazieff (1967).

3.3.2. Mineralogy

Phenocrysts of albite (0.1-3.5mm) within the margins of these ash-flow tuffs are generally anhedral to broken, yet commonly subhedral in densely welded interior zones. However, albites in pumiceous tuffs of this sequence are usually anhedral to subhedral throughout, while those crystals enclosed within fiamme are characteristically euhedral (photomicrograph 24). Twinning on the Albite and Carlsbad laws is common. Subhedral glass-charged crystals of albite occur locally in unit 58. The only ferromagnesian mineral identified is found in units 54 and 58; it is a fresh, colourless to pale green clinopyroxene (0.2-1mm), biaxially +ve, with a 2V of approximately 50° (visual determination); this is probably augite. Subhedral to broken clinopyroxenes locally form 0.5% of the rock, and lamellar twinning has been observed (photomicrograph 25). Glomeroporphyritic intergrowths of clinopyroxene, albite, and apatite are reminiscent of multimineralic clots found in the intrusive "porphyrites". The rare crystals of clinopyroxene found in unit 54 are probably xenocrysts. Accessory minerals include abundant iron ore and needles of apatite; zircon has not been recorded. A small amount of phenocrystic quartz (less than 2%) in unit 43 forms the mineralogical basis for correlating this unit with unit 42. Rounded grains of pale green chlorite cut by intersecting platas of hematite have been recorded from units 53 and

55 by Papezik (1969, units 2 and 4), and possibly represent pseudomorphs after olivine.

3.4. Devitrification and Hydration

Since ash-flow tuffs by their very nature are predominantly glassy, they are thermodynamically unstable and will devitrify if given sufficient time. Descriptions of the crystalline derivatives of geologically old glasses are becoming increasingly better documented (for example, Anderson, 1969, 1970a, 1970b) and occasionally resemble textures produced during experimental studies on the devitrification of natural glasses (in particular, Lofgren, 1971a, 1971b).

Certain textural features of ash-flow tuffs on the Colliers Peninsula appear to be the products of crystallisation processes operating "below the glass transition temperature" (Shaw, 1965, p. 123) or more specifically "at temperatures below the thermodynamic solidus temperature" (Lofgren 1971a, p. 111). Although it is well-known that recrystallisation of hot shards and pumice frequently takes place in the interiors of ash-flow sheets during an initial period of cooling, the textures described below are believed to be of secondary origin, i.e. closely linked with devitrification and hydration of consolidated, yet apparently still glassy, ash-flow deposits during diagenesis and burial.

On the eastern slopes of Finn Hill, at the base of unit 55, a distinctive mottled zone, about 5ft (1.6m) thick, consists of small (1-8mm) rounded "blebs" of red welded tuff in a pale yellowish green

to greenish grey fine-grained matrix (cf. Papezik, 1969, unit 6). The reddish areas are irregular in detail, with hematite dust coating densely welded shards aligned in roughly the same direction in all "fragments" (photomicrograph 26). Alteration is marked at the edges of these fragments by removal of hematite until shard outlines are no longer visible (photomicrographs 27 and 28). The removal of hematite is accompanied by intense recrystallisation involving the formation of fibres of alkali feldspar and quartz with distinct microspherulitic structure. Apparently, the hematite dust does not move very far (in the order of millimeters) and recrystallises as minute aggregates of magnetite, rarely with subhedral habit, near the outer parts of spherulites or "pinned" at their margins. The spherulites themselves are separated from each other locally by a thin film of cryptocrystalline felsitic material, largely quartz where determinable (photomicrographs 30 and 31) and textures resemble a more mature development of "orb textures" described by Lofgren (1971, figs. 2 and 3a). Development of microspherulitic feldspar generally precedes complete removal of hematite, which may record successive stages of spherulite growth. Perlitic cracks commonly act as sites for incipient bleaching and recrystallisation (photomicrograph 32). It is of interest that many of the microscopic features of Finn Hill ignimbrites resemble rather closely textures illustrated by Boulton (1904, plate XL, figs. 1 and 2, and plate XLI, fig. 2) from Uriconian rhyolitic tuffs (welded) at Pontesford Hill, Shropshire.

Recrystallisation textures of a somewhat different nature are well-developed in a dark purplish red, densely welded ash-flow tuff (unit 41) at James Cove. These textural features, however, are not noticeable in the field, and only detected with the aid of a microscope. Particles of iron-oxide (largely magnetite) coat the extremities of confocally radiating fibres of alkalic feldspar and quartz, producing a delicately crenulate pattern, a "negative" image in plane-polarized light of spherulites best seen under crossed nicols at high magnification (photomicrograph 33). More advanced stages of recrystallisation produce microspherulitic feldspar, or mosaics of feldspar and sparse chlorite, enclosed by granophyric quartz. Individual quartz grains rarely preserve sweep extinction indicating their fibrous heritage. Locally, they coalesce to form a clear rim (with uniform extinction) around feldspar spherulites giving a "bird's-eye" texture (photomicrographs 34 and 35). This rather striking texture bears a strong resemblance to the micropoikilitic and microgranophyric textures described by Lofgren (1971a, fig. 7) during hydrothermal devitrification of natural rhyolite glass. Quartz of similar habit has been described by Anderson (1970a, fig. 1) as "snowflake" textures from Cambrian and Precambrian ash-flow tuffs in the Wichita Mountains of Oklahoma and St. Francis Mountains, Missouri.

Microspherulitic and "bird's-eye" textures may exhibit sharp to finely gradational contacts with very fine grained to cryptocrystalline felsitic areas in which opaque particles have largely been removed, though a part may remain as leucoxene (photomicrographs 36 and 37). Contacts are generally irregular with a narrow transition zone (less

than 0.5mm wide) between the comparatively coarse-grained microspherulitic textures and cryptocrystalline material (photomicrograph 38). Textures of the latter type are identical to crystallisation features of the "devitrification front" illustrated by Lofgren (1971a, figs. 1A, 1B, and 4) which marked a spherulite-glass contact.

Of the granophyric or micropoikilitic textures described, Lofgren (1971a, p. 118) states "micropoikilitic quartz is the result of the initial crystallisation of a glass or a silicate melt at subsolidus temperatures. The possibility that micropoikilitic quartz could be secondary, resulting from silica introduced from an outside source, is not ruled out but is considered unlikely". Removal of iron-oxide by leaching is almost certainly later or penecontemporaneous with spherulite growth, which probably served to stabilise opaque particles by recrystallisation to magnetite granules.

Estimates for the time required for complete devitrification of a natural glass vary considerably, but the rarity of glasses older than Cretaceous (or approximately 135 m.y.) suggests that most natural glasses devitrify within a comparatively short span of geological time. Marshall (1961) suggested that water plays an important role in the devitrification of natural glass since "thermal reconstitution alone would take 10^{60} years at 25°C (assuming 100Kcal/mole to be the activation energy of natural rhyolite glass) and 10^{9} years at 750°C." (Marshall, ibid., p. 1503). However, the rates of

hydrothermal reconstitution of natural rhyolite glass are greatly increased by the presence of alkali-rich solution (Lofgren, 1971a, p. 111). It is considered likely, therefore, that during a burial metamorphism involving migrating solutions enriched in the alkalies and calcium, originally glassy Harbour Main ash-flow tuffs could have devitrified entirely within the probable age span of Precambrian time on Avalon.

CHAPTER IV

LAVA FLOWS AND HYPABYSSAL INTRUSIVE ROCKS OF THE HARBOUR MAIN GROUP

4.1. Felsic Lava Flows

Only two isolated outcrops of felsic lava flows, representing periods of eruptive activity less violent than that accompanying associated ash-flow deposits, have been recognised in the map area.

4.1.1. Rhyolite

A rhyolite flow lying stratigraphically above the Bacon Cove ash-flow sequence forms a small crag about 500ft (152.5m) east of the Conception Harbour-Kitchuses road (map ref. 3440,5730). The dark reddish grey rock is distinctly porphyritic and exhibits contorted millimeter-scale flow banding. The high state of oxidation and occurrence of phenocrysts distinguish this flow from aphanitic rhyolite sills to the north.

In thin section, the flow contains phenocrysts of highly resorbed quartz (0.5-2mm), subhedral albite (0.3-4.5mm) exhibiting fine lamellar twinning, and green pleochroic biotite (<1mm) set in a devitrified groundmass of alkalic feldspar and subordinate quartz. Euhedral zircon and granular opaques occur as accessory minerals. The irregular flow banding is defined by crystallites of iron-oxide

segregated into darker coloured bands; the originally glassy groundmass exhibits mosaic and microspherulitic devitrification textures. Modal proportions of albite, quartz, and biotite are estimated at 10%, 2%, and 0.5%, respectively. This flow has petrographic affinities to ash-flow tuffs of the Bacon Cove sequence and quartz- and biotite-bearing ignimbrites at James Cove (unit 40, table 4; and unit 41, table 5); cf. chemical analysis GC52, table 7.

4.1.2. Dacite

A dacite flow occurs as large rafts enclosed within a complex porphyritic intrusion at Old Schoolhouse Point, 0.5 mile (0.8km) north of Burkes Cove (map ref. 3460,6040). Greyish white to dark grey laminar flow banding is conspicuous, with light and dark layers spaced approximately 0.5-3.5 inches (1.3-8.9cm) apart. The extrusive origin of this rock is indicated by a flow-brecciated base in addition to a monolithic sedimentary breccia above comprised of angular flow-banded fragments of dacite (up to 7 inches; 17.8cm in length) enclosed in a red siltstone matrix.

Incipient breakup of this flow into rafts within the "porphyrite" has resulted in differential rotation of these rafts through an angle of approximately 58° as recorded by a sharp deflection in the flow banding; one raft measuring 4ft (1.2m) in length by 3ft (0.9m) across now lies at right-angles to its parent.

The rock contains euhedral to subhedral and resorbed albite phenocrysts ranging about 0.2-2mm in length and locally forming

glomeroporphyritic aggregates up to 4mm across. Microphenocrysts of partially resorbed acicular amphibole (up to 2mm in length) are completely replaced by chlorite, calcite, and clay minerals, and a concentration of opaque dust occurs at their margins (photomicrograph 39). Amphibole cross-sections and relict cleavage leave little doubt as to their original composition (photomicrograph 40). Accessory apatite is common; zircon has not been observed. A well-defined flow banding consists of alternating concentrations of iron ore partly altered to leucoxene and pilotaxitic albite microlites set in a felsic groundmass (quartz and alkalic feldspar where determinable); cf. chemical analysis GC12, table 1.

4.2. Mafic Lava Flows

To the west and southwest of the map area, a thick sequence of mafic lava flows striking approximately north-south and dipping steeply to the west are the youngest volcanic rocks of the Harbour Main Group (cf. McCartney, 1967, p. 19). These flows were sampled along the western shores of Colliers Bay (map ref. 3260,5950), at the mouth of Colliers River (map ref. 3245,5820), and about 3 miles (4.8km) south of the map area near the Blue Hills; localities are shown in fig. 4. The contact between the basaltic flows and volcanic breccias overlying the Finn Hill sequence is not seen in the map area.

Flows range from almost black to reddish grey in colour, and widely spaced reddened and brecciated flow-tops have been observed. Trachytic or diabasic textures are common and amygdales measuring up

to 0.5 inch (13mm) in diameter are generally filled with prehnite, epidote, calcite, adularia, chlorite, sphene, and rarely pumpellyite and quartz (Papezik, written comm., 1974; cf. photomicrograph 41).

Feldsparphyric basalts at western Colliers Bay are characterised by trachytic textures formed by laths and subequant phenocrysts of albite (up to 15mm in length) which locally exhibit fine lamellar twinning according to albite and (rarely) pericline twin laws. A groundmass of albite laths encloses opaque ore and minor interstitial glass altered to chlorite. Chlorite pseudomorphous after rare olivine in the groundmass, and phenocrysts of clinopyroxene with the composition of calcic augite (Papezik, pers. comm., 1972), have been recorded from these flows (cf. chemical analyses P70-1, P70-2, and P70-3, table 7).

Specimens collected near the Blue Hills are olivine-bearing basalts. Olivine commonly occurs as subhedral to anhedral micro-phenocrysts (<2mm) in the groundmass accompanied by a colourless to pale green clinopyroxene; both are enclosed by interlocking albite laths up to 4mm in length (cf. NX12 and NX15, table 7). Groundmass olivine is usually replaced by serpentine, iddingsite, and iron-oxide; fresh olivine is rarely preserved (photomicrograph 41). Phenocrysts of olivine (2-3mm) have been recorded from only one flow (NX14, table 7) and are completely altered to iron-oxide, chlorite, and iddingsite; a rim of straw-yellow pleochroic serpentine and iron-oxide is a conspicuous textural feature (photomicrograph 42). Amygdaloidal potassium feldspar is considered responsible for an anomalously high potassium content in sample NX15 (table 7).

An unusual outcrop consisting of a dark grey to purplish black basaltic lava flow is located about 550ft (167.8m) northeast of the triangulation point on Weavers Hill (map ref. 3330,5725). The cross-sectional area of outcrop is crudely semicircular, and the flow is enveloped by brown, pink, and green volcanic breccias below basal ash-flow tuffs of the Weavers Hill sequence. Phenocrysts of albite up to 15mm in length exhibit trachytic texture in the upper part of the flow; angular rock fragments (0.25-0.75 inch; 6-19mm) are included in a flow-breccia at the base. Although the occurrence of a single feldsparphyric flow at this horizon is somewhat anomalous, the dimensions of the outcrop and the incorporation of rounded cobbles (up to 6 inches; 15.2cm. in diameter) of this rock in the base of a volcanic breccia immediately above suggest a flow origin in situ.

The chemistry of the basaltic flows has an important bearing on the later stages of magmatic evolution in the Harbour Main Group. Flows in western Colliers Bay have been described by Papezik (1970) as hawaiites and mugearites. The occurrence of appreciable amounts of olivine in the groundmass of flows to the south and the lack of a reaction relationship between olivine and pyroxene have been regarded as the petrographic expression of an alkali-olivine basalt (for example, Kuno, 1959, 1960). A rim of serpentine and iron-oxide surrounding olivine phenocrysts in flows near the Blue Hills (which contain abundant olivine microphenocrysts) possibly mimics an oxidation reaction between olivine phenocryst and groundmass due to rapid eruption

of magma from depth. Reactions of this type have been observed in alkalic basalts of La Grille and Kartala volcanoes, Comores Archipelago (Strong, pers. comm., 1973).

4.3. Aphanitic Rhyolite Sills

Two aphanitic rhyolite sills (coloured pink in fig. 3) aligned northeast-southwest, intrude the Kitchuses section of the Bacon Cove ash-flow sequence, and are themselves cut by east-west trending faults, diabase dykes, and "porphyrite" intrusions (cf. geological map). The sills lie approximately 0.25 mile (0.4km) apart, with a minimum length of 1400-1500ft (427-457.5m) and a maximum width of 180-300ft (54.9-91.5m). Intrusive contacts are best seen along the eastern margins of these sheets; contacts are sharp and locally sheared. A cream to pale brown rock is pale grey on fresh surfaces; conspicuous flow banding is accompanied locally by autobrecciation.

The western rhyolite sill is poorly exposed. Pinkish grey, angular to rounded fragments of flow-banded rhyolite are enclosed in a dark reddish grey matrix of finely comminuted material stained with hematite. Laminar flow banding is preserved in outcrops along the northeastern margin (map ref. 3460,5790).

The eastern rhyolite sill forms a distinct line of cream to white crags running parallel to the shoreline of Gasters Bay (plate 9). Flow banding and small-scale folds generated during viscous flow are well developed in the interior of this sheet and pass outwards into a brecciated envelope. Measurements of the mean

attitude and orientation of the less-disturbed flow banding are comparable with those recorded for bedding and cleavage surfaces in surrounding volcanic breccias and tuffs.

A rhyolite dyke up to 6ft (1.8m) maximum width can be seen intruding a sillar of the Bacon Cove ash-flow sequence (unit 12, table 3) in outcrops 500ft (152.5m) north of the northernmost tip of the eastern sill (map ref. 3520,5815).

The textures and mineralogy of these rocks are very similar. Microphenocrysts of albite (<1.5mm) and resorbed quartz (<0.5mm) are rare; minute crystals of opaque ore commonly occur in a felsitic groundmass. Laminar segregations of iron-oxide define the conspicuous flow banding which is accentuated by a marked orientation of feldspar microlites. A cryptocrystalline groundmass includes coarser zones of microspherulitic devitrification involving quartz and alkalic feldspar. Autobrecciation at the margins of these sheets is accompanied by locally more intense development of mosaic quartz in the groundmass. Veins of albite (1-3mm in width) are believed to have modified the composition of a specimen collected from the eastern rhyolite sill (GC31, table 7).

The relative geological age of these intrusions can be pinpointed quite accurately: they are older than ash-flow deposits of the Bacon Cove ash-flow sequence, which they intrude, and younger than the porphyrites and diabase dykes. It is notable that an abundance of cream to white fragments of flow-banded rhyolite occur in volcanic breccias immediately below and within ash-flow tuffs of

the Weavers Hill sequence. It is suggested, therefore, that the rhyolite sills are penecontemporaneous with and possibly genetically related to rhyolite of extrusive or intrusive origin recorded as abundant xenoliths in Weavers Hill ash flows. The chemical evidence presented later (chapter VIII) supports this interpretation; cf. chemical analyses GC4 and GC31, table 7.

4.4. Porphyritic Sills or "Porphyrites"

Porphyrites (coloured blue in fig. 3) are by far the most common and voluminous intrusions in the map area. Intrusions of this type occupy the more barren, treeless areas largely covered by glacial drift (plate 10). The margins of many of the smaller bodies are controlled by the bedding-plane surfaces of their wall-rocks; however, the larger porphyrites are strongly transgressive.

Xenoliths are quite common at the margins of these intrusions, and range from large rafts of green altered porphyrite with pseudomorphed feldspars sheared along a locally intense cleavage (map ref. 3555,5835) to small inclusions of thinly-bedded sandstone about 6ft (1.8m) in length (map ref. 3315,5725) and small (usually 2-10 inches; 5.1-25.4cm) subrounded to rounded rock fragments of green and red volcanic breccias and greyish red crystal tuffs (map ref. 3515,6140). A small porphyrite forming the western promontory of James Cove carries an assortment of xenoliths up to 14 inches (35.6cm) in diameter, comprising reddish grey welded tuff, greenish grey porphyrite, and cobbles of quartz-monzonite with dark brown oxidised rims (plate 11). These rims provide an important clue to the origin

of the quartz-monzonite, since identical textures have been observed in volcanic conglomerates on the opposing shore of James Cove and from similar deposits further north (cf. section 5.1.1.). The conglomerates, therefore, provide a suitable source for these xenoliths, whose origin would otherwise necessitate derivation from a granitic intrusion at depth.

The most striking feature of the porphyrites, however, is the widespread occurrence of an autoclastic intrusion breccia (Fisher, 1961, p. 1411) comprising angular, roughly equidimensional blocks of porphyrite set in a fine-grained, locally xenocrystic groundmass, probably a marginal chill. Evidently, a late magmatic pulse resulted in brecciation of previously consolidated porphyrite (plate 12). On the southwestern slopes of Weavers Hill (map ref. 3315,5720) and the western shore of James Cove, porphyrites have intruded thinly-bedded sandstones and siltstones, and angular blocks of intrusion breccia measuring up to 12 inches (30.5cm) in length have been emplaced in relatively undisturbed sediment. The igneous matrix surrounding the blocks is gradually replaced by a sedimentary one in which the original bedding has been preserved (plate 13). Gradation between the two extremes is represented by a rock in which commingling of igneous and sedimentary matrices has taken place. Furthermore, at Old Schoolhouse Point, devitrified rod-like shards have been preserved in gently contorted laminae of reddish brown siltstone which occupy the interstices of intrusive porphyrite blocks. Textures such as these require relatively passive intrusion of magma into wall-

rocks which quite clearly could not have been consolidated at the time of emplacement. The more violent explosive activity associated with diatremes can be ruled out since not only would delicate shards be destroyed but all trace of bedding would be removed. The marginal autoclastic breccias described here have affinities to the "pépérite breccia" mentioned by Fisher (1960) and defined by him as resulting "from shallow intrusion of fluid magma into unconsolidated or poorly consolidated sediments or rocks" (Fisher, 1960, p. 975). Thus, it is not surprising that a strong stratigraphic control is exerted on these intrusive bodies; only the larger porphyrites manage to cut across the ash-flow sequences, consolidated by welding at the time of deposition.

Considering the extensive outcrops of xenolithic and auto-brecciated porphyrite, it appears that the margins of many of these intrusions have only recently been uncovered by erosion.

Although the porphyrites show a wide geographic distribution in this part of the Harbour Main Group, many of their petrographic characteristics are similar; their chemistry, however, varies according to the proportion and nature of phenocryst phases, the extent of contamination by extraneous material, and the degree of alteration (cf. chemical analyses of porphyrites, table 7). The more leucocratic porphyrites free from xenocrysts contain phenocrysts of albite exhibiting locally hiatal to seriate textures set in a mesostasis of devitrified glass and minor iron-oxide (map refs. 3555, 5835,3470,6030, and 3560,5890; analyses GC8, GC10, and GC41, respectively).

subordinate amounts of pyroxene have been identified in specimens collected in the east (map ref. 3560,5890; analysis GC41) and south (map refs. 3285,5670 and 3315,5725; analyses GC40 and GC25, respectively) of the map area, and in a distinctly melanocratic porphyrite located at Colliers school (map ref. 3350,5870; analysis GC51). Modal proportions (estimated visually) of the more common leucocratic porphyrites average 0-4% pyroxene, 20-40% albite, and 1-2% opaque ore. Alteration of the primary mineral assemblages to sericite, clay minerals, calcite, chlorite, epidote, albite, and leucoxene is common (photomicrograph 44).

Subhedral to resorbed albite phenocrysts generally form individual subequant grains averaging 2-4mm in length, or glomeroporphyritic intergrowths up to 7mm across; lamellar twinning along the (010) composition plane occurs locally. Minute inclusions of devitrified glass and opaques are commonly oriented parallel to crystal outlines. A green pleochroic chlorite with greyish blue polarization colours is pseudomorphous after pyroxene (0.2-2mm in length) which generally occurs as single crystals with euhedral to anhedral habit. Phenocrysts of pyroxene in the melanocratic porphyrite (GC51, table 7) form multimineralic intergrowths (1-2.5mm across) with magnetite and apatite (photomicrograph 45).

Xenocrysts of subhedral to highly corroded quartz, and biotite pleochroic in greens and browns, are particularly common at hematitic margins of these intrusions (for example, GC6, GC7, GC30, and P70-8, table 7). Cognate albite phenocrysts locally exhibit irregular frac-

tures stained with hematite. The brecciated marginal chill of a porphyrite along the northeastern contact of the eastern rhyolite sill (map ref. 3505,5770) contains xenocrysts of biotite largely oxidised to magnetite and partially altered to secondary muscovite (GC6, table 7). Some euhedral biotite xenocrysts have been internally reconstituted to form an intergrowth of magnetite crystallites and alkalic feldspar. Similar crystals are found in the surrounding sediments and tuffs, and this texture may be of pre-inclusion origin. In a specimen collected farthest from the contact, a few biotite pseudomorphs have lost their euhedral habit, possibly due to incipient breakdown within the porphyrite melt.

It is immediately evident that the porphyrites pose a considerable problem of sampling for chemical analysis, not only with respect to xenolithic and xenocrystic contamination but also because of their varying degree of alteration to secondary mineral assemblages. Greyish green porphyrite enclosed as rafts within the large intrusion north of Kitchuses contains albite phenocrysts replaced by calcite, chlorite, and sericite set in an intensely saussuritised groundmass (GC7, table 7). In general, alteration is confined to incipient development of clay minerals and sericite, though in one specimen (map ref. 3555,5835) a small amount of epidote has recrystallised in the groundmass (GC8, table 7). Also, in an attempt to sample and analyse a block of the marginal intrusion breccia, it became obvious that the effects of present day weathering have to be carefully considered (GC25, table 7).

The porphyrites form a very important cogenetic suite of intrusive rocks since they represent the only rocks of intermediate nature

so far described from the Harbour Main Group. As we shall see later, in the section devoted to geochemical characteristics of the Harbour Main volcanic suite (chapter VIII), they transform a strictly bimodal basalt-rhyolite association into a chemically more coherent series of rock-types.

4.5. Diabase Dykes

Greenish grey to almost black diabase dykes are widely distributed in the map area. The dykes cut all other rock-types of the Harbour Main Group including porphyrites and rhyolite sills. The majority have a steep attitude and strike east-west; however, in coastal exposures north of Ryans Head (map ref. 3380,5980) and Old Schoolhouse Point (map ref. 3490,5965) dykes have shallow (10-20°) dips. At the latter locality, a multiple dyke exhibits centimetre-scale banding. Contacts between bands pinch and swell but are quite sharp, and one-sided chilled margins are well-developed.

In contrast to the pseudomorphed phenocrysts in the porphyrites, pyroxenes in the dykes remain unaltered. Where pyroxene is present, it occurs as granular crystals of clinopyroxene (0.2-2mm) forming an intergranular to intersertial texture with albite laths about 1-3mm in length (cf. chemical analyses GC9, GC11, GC21, and GC26, table 7). Rare subhedral phenocrysts of clinopyroxene (1.5-2mm) have been observed in a dyke at Weavers Hill (map ref. 3325,5720; GC21, table 7). Dykes that completely lack clinopyroxene are feldsparphyric types consisting of interlocking or locally pilotaxitic albite crystals

approximately 0.5-3.5mm in length (GC2, GC13, GTN31t, and GTN31u, table 7). Subhedral to anhedral and resorbed albite phenocrysts usually exhibit fine lamellar twinning; fretted margins and "spongy" interiors are due to tiny inclusions of chlorite (replacing former glass, photomicrograph 46). The multiple dyke contains glomeroporphyritic albite phenocrysts (2mm across) with hiatal texture (H165, table 7; photomicrograph 47). Granular iron ore partly altered to leucoxene is a common accessory mineral in all the dykes; interstitial glass has recrystallised to chlorite, accompanied locally by minor epidote and albite. Amygdaloidal textures have been observed in dykes north of Old Schoolhouse Point (map ref. 3490,5963) and at Finn Hill (map ref. 3295,5810). Amygdales are usually filled with calcite, albite, and chlorite.

4.6. Olivine Diabase (Picritic) Sill

A greyish green to pale green mafic sill with diabasic texture and conspicuous dark brown to red- and orange-weathering olivine phenocrysts was observed intruding amygdaloidal basaltic flows approximately 0.5 mile (0.8km) south of the map area (cf. fig. 4). In thin section, serpentine, hematite, and orange pleochroic iddingsite are pseudomorphous after subhedral to anhedral olivine phenocrysts (2-3mm) and microphenocrysts (<1mm) of the groundmass. Euhedral to anhedral, pale green clinopyroxene (0.2-1mm) exhibiting simple and lamellar twinning is enclosed subophitically by laths of albite (0.5-2mm) altered in part to sericite and clay minerals. Interstitial

glass has recrystallised largely to epidote, with lesser amounts of chlorite and clear patches of alkalic feldspar (photomicrograph 48). It is the epidote in the groundmass that imparts the distinctive green colour to this rock; cf. chemical analysis NX17, table 7.

4.7. Diabase Sill(?) Intrusive into the Conception Group

A greenish grey to almost black, medium- to fine-grained rock with diabasic texture, interpreted as a sill, intrudes greenish grey Conception siltstones on the northeastern shore of Colliers Bay 1.25 miles (2.0kms) north of James Cove. The intrusion was described by Hutchinson (1953, p. 27) as a "diorite plug", and represents the only intrusive rock on the Harbour Grace map sheet (Map 1035A). Microscopic pyroxenes (replaced by chlorite) and albite laths (up to 3mm in length) are set in a chloritic groundmass enclosing minor amounts of sphene. A narrow (10 inches; 25.4cm) zone of hornfelsing at the contact predates the impression of a regional cleavage (S_2; cf. chapter VI), and apparently represents the youngest igneous event in the map area.

CHAPTER V

SEDIMENTARY ROCKS

5.1. Epiclastic Deposits of the Harbour Main Group

Volcanogenic sedimentary rocks interbedded with the main ash-flow sequences of the Colliers Peninsula represent periods of quiescent volcanic activity in the region.

5.1.1. Volcanic Breccias and Conglomerates

Epiclastic volcanic breccias (Fisher, 1961) are well-exposed at Finn Hill and Ryans Head, on the eastern slopes of Weavers Hill, and 0.25 mile (0.4km) southeast of Campbell Hill. Certain of these deposits have been interpreted as volcanic mudflows or lahars, and two types of laharic breccia have been identified.

At Finn Hill, a chocolate-brown lahar (50ft; 15.3m thick) located between cooling units 58 and 59 (unit 10 of Papezik, 1969), lies in sharp erosional contact with unit 58 and contains angular fragments of welded tuff and clinopyroxene crystals derived from it. A similar laharic breccia (about 100ft; 30.5m thick) overlies a reddish grey ignimbrite sheet (unit 59; unit 13 of Papezik, ibid.); the contact is depositional and completely gradational, preserving a non-welded zone at the top of this cooling unit. Angular to subangular and rounded rock-lapilli are chaotically distributed throughout the deposit, and commonly consist of dark red crystal tuff, amygdaloidal

and trachytic-textured basalt, a variety of sedimentary rocks, and rare granophyre set in a finely comminuted matrix containing microscopic lunate and rod-like shards. Crystals of albite (0.5-2mm) in various stages of alteration to clay minerals and white mica, are crudely aligned in the interior of the deposit, and pale brown laminated mudstone fragments, only partly consolidated at the time of incorporation within the mudlow, have been elongated parallel to bedding surfaces. Internal foliation of comparable type has been described in the "hot mud flows" of Van Bemmelen (1949), and possibly suggests relatively rapid emplacement of Finn Hill lahars rather than designate a specific temperature of deposition.

At Burkes Cove, the upper lahar is thinner (15ft; 4.6m) and a distinct accumulation of rounded cobbles, probably concentrated by winnowing of the clay-size matrix, occurs along its upper surface. Thinly-bedded, water-washed volcanic breccias overlie this lahar.

At Pyans Head, brown, green, and pink laharic breccias (correlated with similar deposits on the western slopes of Finn Hill) are interbedded with thin (1-2ft; 0.3-0.6m) volcanic conglomerates containing cobbles up to 10 inches (25.6cm) in diameter, dark brown sandstones, and red siltstones; dessication cracks and mud ball horizons are locally well-developed (plate 14). The lahars contain exotic rafts of older volcanic breccias measuring 3-5ft (0.9-1.5m) in length and 2-3ft (0.6-0.9m) across which were only partly consolidated at the time of incorporation. The southern margins of these blocks are crenulated and frayed; this is probably indicative of flow

from the north. Clasts of red- and green-altered crystal tuff (photomicrograph 2), tuffaceous sandstone, basalt, diabase, and rare granite form about 15% of the rock.

A similar volcanic mudflow 0.25 mile (0.4km) southeast of Campbell Hill (map ref. 3465,5840) encloses rip-up clasts (up to 18 inches; 45.7 cm in length) of thinly-laminated siltstone contorted and injected by a dark brown, ill-sorted matrix containing sand-, silt-, and clay-size particles. In general, lahars of this type texturally resemble the cold mudflows or "normal lahars" documented by Van Bemmelen (1949).

Volcanic conglomerates form sea cliffs at the eastern shore of James Cove and in Colliers Bay about 0.25 mile (0.4km) to the north (plate 15). Cobbles and boulders (up to 18 inches; 45.7cm in diameter) of red crystal tuff, basalt, diabase, and intermediate rocks with albite phenocrysts are enclosed in a dark brown to greenish brown, poorly consolidated matrix made up of polished sand grains and pebbles. Locally, rims of cobbles are oxidised to a dark reddish brown rind extending to a depth of about 0.5 inch (1.3cm).

Thin (1-3ft; 0.3-0.9m) conglomeratic horizons are quite common in Harbour Main sedimentary rocks along the coast north of James Cove and on the shores of Gasters Bay at Kitchuses.

5.1.2. Volcanic Sandstones and Argillaceous Siltstones

The finer clastics of the Harbour Main Group generally form topographic lows occupied by thick deposits of glacial drift and

dense vegetation. The most extensive exposures are found in coastal outcrops or along fault scarps (plate 16). Pale brown to reddish brown, thinly-bedded arkosic sandstones and argillaceous siltstones are well-exposed along the cemetery road (map ref. 3375,5835). A wealth of sedimentary structures include intraformational breccias consisting of mudstone flakes in a sandstone matrix, load-and-flame structures, slump structures, and minor channel cut-and-fill. Graded bedding, small-scale cross-laminations, and flute casts are westward-facing, and inferred current directions are from north and south.

Graded bedding is a common feature of thinly-bedded sandstones along the coast north of James Cove (map ref. 3560,6270), and trough cross-bedding occurs in tuffaceous sandstones near the base of the Bacon Cove ash-flow sequence at Kitchuses (map ref. 3520,5790).

5.2. Conception Group

Rocks of the Conception Group underlie the extreme north and northeastern parts of the Colliers Peninsula, separated from the Harbour Main Group by a major fault (fig. 3 and geological map). The main rock-types consist of greenish grey laminated siltstones and mudstones, greenish grey to dark brown greywackes, and reddish brown to dark brown sandstones (plate 17). Basal Conception conglomerate is exposed in cliffs west of Colliers Bay at Maryvale (map ref. 3400,6290) where it disconformably overlies mafic lavas of the Harbour Main Group, enclosing rounded cobbles of basalt and diabase in a fine-grained chloritic matrix.

A distinctive reddish brown sandstone facies exposed on the coast 0.5 mile (0.8km) south of Bacon Cove (map ref. 3702,5990) contains a rudite horizon at its southern margin. Rounded pebbles, cobbles, and boulders of Harbour Main-type volcanic rocks are chaotically distributed throughout an ill-sorted sandstone and mudstone matrix. Rock fragments include dark red crystal tuff, reddish grey rhyolite, amygdaloidal basalt, brown tuffaceous sandstone, and a large (18 inches; 45.7cm in diameter) well-rounded boulder of quartz-monzonite. Rudaceous and arenaceous horizons of this nature have been interpreted as tillites and glaciomarine deposits by Brueckner (1969) and Brueckner and Anderson (1971), an interpretation that the author favours to explain the origin of the deposits described above. At the southern extremity of this tilloid (tops unknown) a thin (6-18 inches; 15.2-45.7cm) greyish white calcareous horizon contains algal structures that extend into the sandstone over a distance of about 1-3 inches (2.5-7.6cm), and appear to form an encrustation. A zone of shearing separates this bed from white-weathering, silicified argillaceous siltstones further south.

Sandstone horizons containing isolated pebbles occur along the northeastern shore of Bacon Cove harbour (map ref. 3670,6140) and at Colliers Point. In thin section, the rocks are greywackes containing rounded to subangular grains of albite (0.2-1mm), quartz (0.4-0.8mm), and small rock fragments (<3mm) in a fine-grained matrix (10-15%). A rounded clast (2.5mm) of flow-banded rhyolite contains albite phenocrysts partly replaced by sericite and potassium feldspar; crystals

of chlorite and sphene are pseudomorphous after biotite (photomicrograph 3).

5.3. Cambrian Rocks

Only one small outlier of Cambrian sedimentary rocks occurs within the map area.

At Bacon Cove, excellent coastal exposures in the core of a downfaulted syncline reveal Lower Cambrian rock-types resting with marked angular unconformity on greenish grey siltstones of the Conception Group (plate 18). A basal conglomerate (0-3ft; 0-0.9m thick) occupies irregular pockets in the Precambrian regolith, and contains angular to subrounded pebbles and boulders up to 12 inches (30.5cm) average diameter in a matrix of calcareous arkose with polished and rounded quartz grains (0.5-1.5mm) and volcanic fragments (<8mm). A bed of pink limestone (about 5ft; 1.5m thick) exhibiting possible algal mounds overlies the conglomerate. The succession continues upwards with thinly-bedded, fine-grained calcareous sandstones, red shales, and algal beds, all probably correlative with the Smiths Point Formation (McCartney, 1967; King, pers. comm., 1972; cf. table 1).

CHAPTER VI

STRUCTURE

Critical structural relationships between major lithostratigraphic units are well-exposed within the map area and along the western shores of Colliers Bay. The region has been subjected to repeated intervals of folding and faulting, and fold style varies markedly with lithology.

6.1. Folding and Cleavage

On the Colliers Peninsula a westward-dipping, westward-facing stratigraphic section of the Harbour Main Group forms part of the western limb of a large antiform whose axis strikes approximately north-south and lies to the east of the map area. A cleavage (S_1), axial-planar to this fold (F_1), is particularly well-developed in argillaceous siltstones and mudstones at Ryans Head; in sandstones and siltstones exposed along the cemetery road in the southern part of the peninsula; and in the poorly consolidated matrix of a volcanic conglomerate at James Cove. In the ash-flow sheets and massive, coarser clastics, most of the strain has been relieved by shearing along bedding surfaces (So) during folding. Corrugations on the flanks of this antiform occur in sedimentary rocks exposed along the coast north of James Cove: a small synform plunging 10° to 155° probably reflects the attitude of the larger structure (plate 19).

Fold closures in Conception rocks have been observed at several localities; for example, immediately west of the road junction at Bacon Cove (map ref. 3630,6075) and along the coast to the north (map refs. 3675,6155 and 3690,6220). Medium-scale, moderate to tight folds plunge steeply (50-62°) to the north-northwest or south-southeast, contrasting markedly with the predominantly large-scale structures in Harbour Main rocks. Although a fault separates Harbour Main and Conception rocks in the map area, their stratigraphic relationship can be seen in western Colliers Bay at Maryvale. Here basal Conception conglomerate disconformably overlies mafic volcanics at the top of the Harbour Main Group (McCartney, 1967; Papezik, 1970). McCartney (1967, p. 97) reported a folded angular unconformity between these lithologies at Woodfords 2 miles (3.2km) south of Holyrood; however, recent field work indicates that the poorly exposed contact could be interpreted as a faulted disconformity (B. O'Brien, pers. comm., 1973).

At Bacon Cove, flat-lying basal Cambrian conglomerate in the core of a shallow syncline rests with angular unconformity on Conception siltstone. A penetrative cleavage (S_2) is axial-planar to gently plunging open folds (F_2) of the Cambro-Ordovician succession. Although the matrix of the conglomerate lacks a cleavage, a few pebbles of Conception siltstone have taken up the S_2 fabric, which passes through them without deviation into the underlying Conception Group. Where cleavage has been impressed on Conception rocks in areas remote from Cambrian outcrop, only one penetrative fabric can be detected; this fabric has the same attitude as S_2 and is considered one and the same.

At the northern tip of the main fault-zone, small (1-3 inches; 2.5-7.6cm) chert pebbles have been flattened in the plane of the S_2 foliation; major and minor axes of the pebbles average 2:1, respectively, and the orientation of major axes lies close to vertical. Where the competence of the pebble approaches that of the matrix, deformation of the pebbles should reflect the shape of the deformation ellipsoid of bulk finite strain in the host rock (Flinn, 1956, 1962; Gay, 1968, 1969).

6.2. Faulting

Two sets of high-angle faults can be recognised in the map area; faults trending east-west and northwest-southeast and interpreted as the earliest structures; faults striking roughly north-south or northeast-southwest and succeeding F_1. Two lines of evidence suggest that many of the faults mapped at a high angle to the strike of Harbour Main rocks were penecontemporaneous with volcanism and sedimentation:

a) Included in the sediments composed entirely of Harbour Main detritus are rounded clasts of hypabyssal (diabase, feldsparphyric intermediate rocks) and plutonic rocks (quartz-monzonite and granite, s.s.), too abundant and widely distributed to be explained solely as xenoliths enclosed within an erupting magma and subsequently derived as products of erosion. Also, their mode of occurrence as monolithic aggregates of up to five boulders enclosed in the coarser volcanic conglomerates, suggests an extensive source area, uplifted and eroded

down to plutonic (epizone) levels of the volcanic pile. Since evidence for a period of folding during deposition of the Harbour Main Group on Eastern Avalon is lacking, large-scale uplift must have involved block-faulting, which presumably accompanied volcano-tectonic uplift and collapse.

b) A green alteration, demonstrably penecontemporaneous with ash-flow deposition and effected by percolating metasomatic solutions (cf. chapter VII), locally pervades fault planes which acted as channelways for the fluids. Alteration of this type has not been seen to affect post-F_1 fault zones.

In the map area, Harbour Main and Conception rocks are separated by a major fault, marked by a zone of intense shearing and brecciation 300-900ft (91.5-274.5m) wide and best exposed on the coast and at Bacon Cove. On the shores of Gasters Bay, Harbour Main clastics and Conception siltstones lie juxtaposed and the brecciation is largely confined to the Conception Group. Here, a fault slice of tightly folded, greenish grey Conception siltstones has been emplaced within red siltstones and volcanic conglomerates of the Harbour Main Group, thereby setting a maximum age limit for the main movement along this fault, i.e. post-F_1 (plate 20). In coastal cliffs at the extreme northern end of the main fault the trend of the shear zone closely approaches that of the S_2 fabric and chert pebbles in Conception siltstone are consistently flattened in the plane of the foliation across the fault zone, thereby setting a minimum age limit, i.e. pre-F_2. Although known stratigraphic relationships indicate downthrow of Conception rocks, the magnitude of this movement is unknown.

Faulting in the Bacon Cove ash-flow sequence oriented northeast-southwest appears to be related to movement along the main fault, possibly taken up in part by secondary shear planes or Reidel shears. In a sedimentary fault slice within the main fault-zone a cleavage has been impressed subparallel to the trend of these faults and boudinaged mafic dykes lie in the plane of the foliation. Reactivation of pre-F_1 fault planes has produced a marked deflection in the trend of the main fault.

6.3. Summary

A chronology of structural events in the map area has been established.

Early high-angle faulting in Harbour Main time probably continued into latest Precambrian; at least one period of compressive deformation (D_1) involved folding (F_1) and impression of a regional cleavage (S_1). Uplift and erosion of Precambrian rocks was succeeded by deposition of a transgressive Cambro-Ordovician succession of shelf sediments. A second period of deformation (D_2), post-dating Early Ordovician depositional events, i.e. Bell Island and Wabana Groups (cf. table 1), resulted in the development of open folds (F_2) and axial-plane cleavage (S_2), and probably tightened earlier Precambrian folds of similar trend. Major movement along the main fault-zone post-dated D_1 but pre-dated D_2 structures.

The entire deformational history of the map area prior to deposition of Lower Cambrian sedimentary rocks is regarded as evidence for the Avalonian Orogeny.

6.4. Discussion

Although a period of orogenic movement, the Avalonian Orogeny, affecting Late Precambrian rocks of Avalon has long been recognised (Jukes, 1843; Murray and Howley, 1881; Buddington, 1919; Rose, 1952; Lilley, 1966; McCartney, 1967, 1969; Brueckner, 1969), the precise nature and timing of the deformation are controversial (cf. Rodgers, 1967; Poole, 1967; and Hughes, 1970). The Avalonian Orogeny has been regarded as a period of orogenic movement dominated by block-faulting (McCartney, 1967, 1969; Brueckner, 1969; Hughes, 1970); as a period of pre-Conception folding followed by Conception, Cabot-Hodgewater deposition (Poole, 1967); and as "two periods of at least local orogenic movement, one accompanying the metamorphism and granite intrusion (of the Harbour Main Group), the other during or just preceding the deposition of the arkosic units (Cabot and Hodgewater Groups)" (Rodgers, 1968, p. 410). Part of this confusion undoubtedly arises from the fragmentary nature of the structural data presently available. For example, the penetrative/semi-penetrative or "patchy" style of Hadrynian and later deformation in Avalon could simply be a result of exposures at different structural levels of the sedimentary pile, accomplished by large-scale movements of fault-bounded blocks.

From the structural evidence presented above, it is quite clear that the Avalonian Orogeny as such involved both extensional and compressional tectonic episodes. Although only a single period of Hadrynian deformation (D_1) involving lateral shortening has been recognised within the map area, the structural history of Late Precambrian

rocks in Avalon is obviously more complex. For example, in contrast to the marked angular unconformity that exists between Conception and Cambrian lithologies at Bacon Cove, Williams et al. (1972, p. 217-218) state of Western Avalon that "Cambro-Ordovician rocks were deformed along with the Hadrynian and no structural break exists between the two". These authors are in fact referring to the broadly conformable nature of the contact between the Pandom Formation of Trinity Bay and conformable Cambrian strata above, and the underlying arkosic sequences of the Hodgewater Group (interpreted by McCartney, 1967, p. 100, as a disconformity; cf. table 1).

The intensity of Early Paleozoic deformation in Newfoundland is symmetrically disposed about the axis of the Central Mobile Belt (Williams et al., 1972). The Colliers region is located in Zone H of Williams et al. (ibid.), the most easterly tectonostratigraphic division of the Northern Appalachians in Newfoundland, near the eastern limit of Acadian structures. The style of D_2 within the map area closely resembles that attributed to Acadian deformation, i.e. steep penetrative to semi-penetrative cleavage and upright folds. In northern Avalon at least, the intensity of deformation of Cambro-Ordovician rocks, i.e. D_2 of the map area, increases toward the west, whereas at Manuels River, 20 miles (32.2kms) to the east (cf. fig. 1), fossiliferous Cambrian beds are essentially undeformed. These data are discussed later (chapter IX) where models purporting to explain the tectonic evolution of the Avalon are critically reviewed.

CHAPTER VII

ALTERATION AND METAMORPHISM

In common with other geologically old volcanic rocks and their sedimentary derivatives, the Harbour Main Group has undergone various forms of alteration leaving the rocks coloured distinctive shades of red, pink, grey, and green. For alterations that lead to such reddish and greenish volcanic rocks, the term "anchi-metamorphic" has been used by German authors (for example, Tröger, 1935, in Streckeisen, 1967) to imply epizonal processes of alteration operating between the zone of weathering and incipient metamorphism. This term appears to be broadly equivalent to the processes of "propylitisation" described by Moorhouse (1964, p. 197) and originally applied to altered andesites in Nevada.

The physicochemical conditions prevailing during metamorphism can be broadly defined by reference to diagnostic mineral assemblages or metamorphic facies. Known occurrences of prehnite and pumpellyite filling amygdales in basalts west of Colliers Bay (Papezik, written comm., 1974), and pumpellyite observed in veins cutting ignimbrites at Finn Hill, suggest that the limits of "anchi-zone metamorphism" (Fritsch, 1966) in the map area did not exceed the P and T stability field of prehnite-pumpellyite mineral assemblages. Recrystallisation in response to purely deuteric alteration can be ruled out since the same alterations affect rocks of very different initial composition,

i.e. mafic, felsic, and intermediate volcanic rocks. Furthermore, alterations of the same nature are a distinctive and widespread feature of the sedimentary sequences in the Harbour Main Group.

The various forms of alteration coloured greenish grey, pale green, and pink, are grouped together and shown in black where they affect the measured sections (tables 3, 4, and 5). Dark grey to almost black, brownish- and reddish-coloured rock-types are not indicated.

The secondary minerals formed in felsic pyroclastic rocks are quartz, chlorite, albite, colourless mica, carbonate, epidote, sphene, leucoxene, potassium feldspar, hematite, magnetite, limonite, clay minerals, and rare pyrite; diagnostic metamorphic minerals such as prehnite, pumpellyite, and stilpnomelane (?) are found in late-stage fractures. Mafic to intermediate rocks contain all the above minerals plus serpentine, iddingsite, and sporadic copper sulphides and carbonates; prehnite, pumpellyite, and K-feldspar have been observed filling amygdales in basaltic lava flows. The primary phases that completely or partially preserve their igneous compositions include clinopyroxene, magnetite, biotite, quartz, and rare calcic plagioclase in ignimbrites and felsic lava flows, and clinopyroxene and rare olivine in mafic volcanic rocks.

7.1. Felsic Volcanic Rocks

In ignimbrite sheets at Bacon Cove and Finn Hill, systematic gradations in colour from dark grey or reddish grey in densely welded

interiors, to dark red or pale reddish brown at their margins, are due to an increase of hematite dust in the shard matrix, largely the result of advanced oxidation of magnetite granules. Pale brown to pink coloured rocks generally indicate mild leaching of iron-oxide and partial recrystallisation of remaining opaques to hematite and leucoxene.

Secondary phases accompanying the formation of the devitrification textures described earlier (chapter III, section 3.4.) are generally limited to quartz, microspherulitic alkalic feldspar, magnetite, hematite, sparse leucoxene, minor sericite, chlorite, and clay minerals, and rare sphene. Biotite phenocrysts are particularly sensitive to devitrification and alteration, and a progression of internal textural modifications can be consistently matched with spherulitic recrystallisation and local bleaching of the vitroclastic matrix. Deep brown, pleochroic biotite dusted with hematite and magnetite along cleavage planes is altered to green ferriferous biotite with strong to weak pleochroism (photomicrograph 49). Advanced alteration commonly reduces biotite to a fine-grained assemblage of magnetite crystallites altered in part to leucoxene, colourless mica (probably muscovite), and alkalic feldspar (cf. photomicrographs 10 and 11). Where "bird's-eye" devitrification textures are well-developed, for example in a purplish grey ignimbrite at James Cove (unit 41), tiny biotite crystals have been reconstituted to chlorite, magnetite, and sphene. Similar recrystallisation features that formed during mesothermal alteration of biotite phenocrysts in monzonites have been described by Schwartz (1958).

Phenocrysts of albite are generally dusted with clay minerals and minute flakes of sericite. Twinning on the Albite, Carlsbad, and Carlsbad-Albite laws is well preserved. Many albite crystals in reddish-coloured rocks are characterised by a patchy alteration to clay minerals and sericite in core regions and an extremely narrow rim of clear albite (photomicrograph 50). An untwinned phenocryst of Ca-plagioclase (analysis H85M, 2C and 2P, table 6) was discovered in unit 58 at Finn Hill during electron microprobe investigation of feldspar compositions and heterogeneity. Although its present composition is obviously magmatic in origin, it is impossible to decide on the basis of a single crystal whether it represents a xenocryst or the pre-metamorphic composition of albite phenocrysts in this ignimbrite. The ubiquitous occurrence of albitic compositions in sedimentary and volcanic rocks alike strongly favours a metamorphic origin for the albite, particularly in view of the low metamorphic grade at which albite is stable. Analytical data relevant to the origin of albite phenocrysts are presented later (chapter VIII).

A greyish green, pale green, or yellowish green alteration preferentially affects the margins, particularly xenolithic basal zones, of ignimbrite cooling units (cf. tables 3, 4, and 5). Contacts between red and green rocks may be sharp or gradational over a distance of several centimetres (plate 21) and they locally parallel bedding surfaces for distances up to 60ft (18.3m) along strike. In hand specimen it is usually difficult to distinguish tuff from sediment, since recrystallisation of the matrix generally destroys pre-existing

vitroclastic textures. However, xenoliths and crystals are only marginally affected and reveal the original clastic nature of the rock. Fragments of rhyolite and crystals of albite either take on a milky white appearance, or acquire a pink or pale green colouration. Staining of this nature in albites is due to hematite globules or chlorite, respectively, partly replacing crystal margins. Accessory xenoliths of deep red, oxidised tuff are locally altered to a pale red or pink colour due to leaching of hematite; mafic rock fragments remain dark grey or black. Dark green pumice-lapilli in ash-flow tuffs of the Weavers Hill sequence are conspicuous in pale green matrices and generally no trace remains of more finely comminuted vitric material.

Contacts between the various forms of alteration in greenish rocks generally correspond to the following scheme: sharp where yellow-green alteration lies juxtaposed to all other types; completely gradational over several metres between greenish grey and greyish green rocks; and gradational on a scale of centimetres where pale green alteration occupies a zone intermediate between the former types. Changes in rock colour are strongly dependent upon mineral assemblages. In particular, epidote is the principal phase in yellow-green rocks, whereas chlorite, sericite, and potassium feldspar are more prominent in zones of greyish green alteration.

Yellowish green rocks generally contain epidote, colourless carbonate, quartz, albite, leucoxene, sphene, magnetite, clay minerals, sericite, and rare chlorite, in order of decreasing abundance. Epidote is commonly a colourless to pale green variety (clinozoisite has been

identified in certain cases), with weak pleochroism and anomalous blue and green interference colours. It commonly preserves delicate shard and pumice textures in the matrix (photomicrograph 51). Intense epidotisation, however, locally obliterates pre-existing igneous textures. For example, at Old Schoolhouse Point, pistachio-green pods with irregular margins and up to 3.5ft (1.1m) in maximum dimension, consisting of epidote, quartz, and albite in mosaic intergrowth, cut across laminar flow banding in dacite. All phases except magnetite and relict phenocrysts of albite with finely crenulated margins have recrystallised to the new mineral assemblage (photomicrograph 52). Similar textures have been illustrated, for example, by Amstutz (1968, plate 1, types A and B) in rocks of spilitic chemistry, and described by Smith (1968, p. 197-198) in altered mafic lavas of Ordovician age in Australia. Minerals found chiefly in the matrix include carbonate, minor quartz, sphene, leucoxene, magnetite, and chlorite. Sericite and clay minerals are generally confined to primary sites, i.e. replacing primary volcanic phenocrysts and groundmass minerals. Albite occupies all primary plagioclase sites and sporadically forms clear mosaics in the matrix. Chlorite is usually restricted to primary sites, replacing originally glassy inclusions in feldspar phenocrysts. Potassium feldspar has not been observed.

Greenish grey to greyish green rocks contain abundant sericite, lesser amounts of chlorite, quartz, albite, clay minerals and potassium feldspar, subordinate epidote, ferruginous carbonate, sphene, leucoxene,

iron ore, and rare pyrite. Authigenic sericite and clay minerals normally form mimetic overgrowths replacing axiolitic and spherulitic alkali feldspar in vitroclastic matrices. Shard outlines are seldom discernible in plane-polarized light, but are easily seen under crossed nicols (photomicrographs 53 and 54). Sericitisation of albite phenocrysts is markedly less intense.

The most diagnostic mineralogical feature of this alteration is the presence of low-temperature potassium feldspar forming microcrystalline growths in the vitric matrix and partially replacing crystals of albite. Poorly birefringent K-feldspar is usually clearly distinguishable from the albite, but staining with sodium cobaltinitrite was found extremely useful in determining the amount of K-feldspar in the phenocrysts, and was virtually indispensable for differentiating it in the groundmass. Where primary-sited crystallisation of K-feldspar is relatively well-advanced the groundmass takes on a deep yellow stain. However, replacement is generally far from complete, and potash never becomes the predominant phase. Cleavage planes or minute fractures are commonly affected first by the invading K-feldspar, and replacement proceeds by the formation of discrete patches in a milky white albite host, imparting a distinctive mottled appearance to reconstituted phenocrysts (photomicrographs 55 and 56). Clay minerals and tiny flakes of sericite are rarely restricted to either albite or K-feldspar, and commonly replace both. Twinning has not been observed in albite-potash feldspar pseudomorphs, but fine lamellar twins are preserved in adjacent albites unaffected by K-feldspar crystallisation. It is

of interest that the presence of a K-feldspar is not always optically detectable. Scanning electron-beam photomicrographs of an albite phenocryst without visible K-feldspar revealed replacement along cleavages by a distinctly potash-rich phase (photomicrograph 64). In this case, the invading feldspar is a cryptoperthitic potash-soda variety.

A rare occurrence in zones of intense recrystallisation are euhedral crystals, undoubtedly of magmatic origin, that exhibit a well-developed "chequered" pattern of fine lamellar twins. The chequered structure is twinned on the Albite law with stubby, slightly disoriented lamellae which either wedge out or are abruptly truncated by planes parallel to (001). Chequered albite may occupy the whole area of the phenocryst, or form only a part, the remainder exhibiting alteration to sericite and calcite (photomicrograph 57). In certain cases, the pseudomorphous origin of chequered crystals is questionable. For example, a "composite" crystal consisting of complex intergrowths of albite with weakly developed chequered structure and devitrified glass preserving "bird's-eye" devitrification texture was found in the strongly recrystallised upper margin of unit 19 at Weavers Hill (photomicrograph 58). The edges of the crystal in relation to its matrix are sharp to gradational and scalloped. This crystal may represent in situ growth of albite in an originally glassy or devitrified groundmass. Similar mineralogical and textural features have been recognised for example, by Battey (1955) in a detailed study of alkali metasomatism in keratophyres of New Zealand, and by Malpas (1972), and Hughes and Malpas (1971) in hydrothermally

altered rhyolites of the Bull Arm Formation, Isthmus of Avalon.

Clearly, the weight of evidence demands broadly contemporaneous mobility of significant amounts of at least potassium, sodium, and calcium ions (the latter two presumably occupying plagioclase sites) in solution at some stage(s) during alteration and metamorphism. However, it is not immediately clear why potash feldspar consistently replaces albite and never vice versa; fluid chemistry may have been such that potassium ions enjoyed a longer residence time in the aqueous phase relative to sodium ions. Whatever the cause, present mineral and whole-rock compositions are potentially a function not only of original magmatic chemistry but also of later processes of alteration.

Pale green rocks are mineralogically and commonly spatially transitional between zones of greyish green and yellow-green alteration; however, the diverse suite of alteration products in these rocks are more similar to assemblages described for greyish green rock-types. Noticeable differences include a greater proportion of carbonate, epidote, and leucoxene, and a decrease in the amount of K-feldspar. A localised zone of pale green alteration affecting the base of unit 59 at Finn Hill exhibits pipe-like offshoots that penetrate several centimetres into hematitic welded tuff above. In thin section, these pipes show sharp contacts with their host and contain rotated fragments of tuff and broken crystals set in a coarsely crystalline groundmass consisting mainly of mosaic quartz and albite (photomicrograph 59 and 60). Such features are likely the result of gas-streaming and brecciation, and have been referred to as "tuffisites"

(for example, Hughes, 1971). If in this case they represent primary fumarolic deposits formed during an initial period of cooling following ash-flow emplacement, they were probably caused by a build up of volatiles beneath an impermeable cover of welded tuff, since they clearly post-date the welding. Alternatively, if they are related to later alteration and served as active channelways for migrating volatiles, locally elevated vapour pressures during subsequent hydrothermal activity can be inferred.

Minerals that occupy secondary sites such as fractures or vesicles, include epidote, albite, quartz, prehnite, pumpellyite, and a micaceous phase, possibly stilpnomelane. Veins of albite, quartz, and epidote locally dusted with iron-oxide are common throughout the map area. A yellowish green variety of epidote forming elongate bladed crystals with strong pleochroism fills fractures and the interior zones of lithophysal cavities in unit 58 at Finn Hill. Pumpellyite in the veinlets forms radiating acicular crystals with blue-green polarisation colours and trichroism with the formula colourless to pale green to pale brownish green. A colourless to pale yellowish mica, resembling stilpnomelane, coexists with quartz and minor albite in veins cutting a pink-weathering vitric tuff in the extreme north of the map area.

An interesting textural feature of an albite-epidote veinlet in welded tuff is the marked concentration and recrystallisation of iron-oxide along its completely gradational upper margin (photomicrograph 61). Textures of this type have been considered earlier (chapter III, section 3.4.) as resulting from hydration and devitrification of

glassy matrices. This similarity emphasises the fact that secondary devitrification and hydrothermal reconstitution were contemporaneous processes.

7.2. Intermediate and Mafic Volcanic Rocks

Alteration to deep purplish reds and yellowish greens in porphyrites, basaltic flows, and diabase dykes is not extensive. Pistachio green and pale green domains are localised along fault planes and brecciated horizons, or form irregular pods cross-cutting primary igneous textures; reddish zones are chiefly restricted to flow tops. Secondary minerals include chlorite, albite, epidote, carbonate, sericite, clay minerals, serpentine, iddingsite, iron ore, sphene, leucoxene, copper sulphides and carbonates; potassium feldspar, prehnite and pumpellyite commonly occupy cavities. Mafic dykes generally lack macroscopically visible alteration, but the same mineralogical features are apparent when examined under a microscope.

Groundmass alteration of interstitial glass to dark green pleochroic chlorite is usually accompanied by authigenic growths of clear albite, pale green epidote, and calcite. Primary albitised feldspar sites are flecked with sericite and clay minerals; relict calcic plagioclase has not been identified. Chilled margins of porphyrites have commonly recrystallised to a fine-grained aggregate of alkalic feldspar, quartz, chlorite, and minor epidote. Locally intense alteration leads to extensive sericitisation and chloritisation of feldspar phenocrysts and microlites. Albites commonly preserve

lamellar twinning; interlocking mosaics or other subgrain boundaries on primary sites are lacking. The margins of albite phenocrysts are sporadically replaced by sericite which forms a distinct rim around dusty albite, strongly resembling incipient forms of alteration described by Jolly (1970, figs. 4a and 4b) from his Ca-plagioclase (relict)-sericite zone in basaltic andesites of the Robles Formation, south-central Puerto Rico. However, albite phenocrysts with rims of clear albite and thoroughly devoid of sericite or clay minerals are just as common (photomicrograph 47). Such textures are more characteristic of Jolly's descriptions of albite-prehnite-pumpellyite-epidote-quartz-hematite assemblages in the same rocks. Epidote replacing the cores of albite crystals is probably indicative of their former more calcic composition; zonal patterns of replacement possibly represent relict oscillatory-zoned phenocrysts (photomicrograph 44). Pseudomorphs after olivine normally consist of orange pleochroic iddingsite, iron-oxide, and serpentine, pleochroic from colourless to pale yellow; rarely olivine is replaced by alkalic feldspar, chlorite, and quartz. Metastable relict igneous compositions are clinopyroxene and rare olivine. Pyroxenes of porphyritic intrusives, with the notable exception of an olivine diabase described earlier (section 4.6.), are completely altered to chlorite.

K-feldspar of adularia habit locally infills amygdales and forms a patchy replacement of primary-sited albite. Prehnite is also a common mineral in secondary sites, where it occurs as blocky grains enclosing turbid albite. Pumpellyite is generally fibrous in habit with colourless to pale green to bright green trichroism. Prehnite

and pumpellyite have not been observed replacing the primary minerals of rocks in the map area.

The occurrences of copper sulphides (chalcopyrite and bornite (?)), and copper carbonates (malachite and azurite) are restricted to fault zones and joint systems in the basaltic flows.

7.3. Genesis of the Alteration and Metamorphism

The type of regional low-grade metamorphism that affected the Harbour Main Group has been referred to as "burial metamorphism", a term first introduced by Coombs (1960) for similarly affected rocks of Permo-Triassic age in southern New Zealand. Coombs demonstrated that prehnite-pumpellyite mineral assemblages intervene in geologic position and metamorphic grade between rocks of the zeolite facies and typical lower greenschist assemblages. Metamorphic zones of similar disposition and mineralogy have been described, for example, by Seki (1965), Otalora (1964), Smith (1968, 1969), Levi (1969), Surdam (1969, 1973), and Jolly (1970). The field and petrographic information revealed by all these studies are broadly consistent with the patterns of alteration and metamorphism observed in Harbour Main rock-types.

The origin of mineral parageneses in rocks of this type have traditionally been related to differences in the geothermal gradient, in fluid pressure, or more accurately the activity of water (a_{H_2O}), in the chemical potential of CO_2 relative to H_2O (i.e. $\mu CO_2/\mu H_2O$), in the kinetics of reactions, and in the chemical composition of the host rock. These parameters are examined more closely below.

The P and T stability of metamorphic index minerals such as prehnite and pumpellyite has been used to estimate the thickness of overburden during burial metamorphism (for example, Smith, 1969; Jolly, 1970; Papezik, 1972a). Since no correlation has been recognised between metamorphic mineral assemblages and stratigraphic depth in the Colliers cross-section of the Harbour Main Group, the thickness of this section (2.7kms: 2400m rhyolite + 300m basalt) can be taken as the minimum stratigraphic extent of prehnite-pumpellyite parageneses. Assuming a geothermal gradient of 28°C/km and dehydration of the zeolite wairakite to produce prehnite, as suggested by Liou (1971), an overburden of 11.4kms is predicted. The fact that a relatively thin sequence of basaltic lavas occurs at the top of a predominantly silicic succession should not seriously affect the calculation, which has been solved for lithologies of upper crustal density and heat flow properties. Accordingly, the computed value appears to be anomalously high and requires most of this thickness to have been removed by erosion and subsequent deposition of a succession of Cambrian shelf sediments. Similar inconsistencies between predicted and inferred "depths of burial" of critical mineral assemblages occur in regions of low-grade metamorphism throughout the world (cf. Surdam, 1973; Levi, 1969).

Permeability and porosity were apparently decisive factors governing the formation of secondary mineral assemblages in the map area. Brief inspection of tables 3, 4, and 5 reveals that the permeable margins of ash-flow sheets and the more porous volcanic

breccias were most susceptible to secondary recrystallisation. This indicates that phase relationships as defined by P and T alone are inadequate to explain the distribution of secondary mineral assemblages observed in Harbour Main rocks of the Colliers Peninsula, and that other factors have to be considered.

Zen (1961) demonstrated that if CO_2 and H_2O are perfectly mobile constituents in a hydrous silicate system, then at high values of μCO_2 relative to μH_2O kaolinite-calcite or pyrophyllite-calcite assemblages would be favoured over Ca-zeolites. Coombs *et al.* (1970), following Zen, projected these relationships into the field of prehnite-pumpellyite stability. They deduced that μCO_2-μH_2O relationships in the system CaO-Al_2O_3-SiO_2-H_2O-CO_2 are such that it is possible to pass progressively, isothermally and isobarically, at decreasing values of μH_2O(μCO_2 being low), through assemblages representative of zeolite, prehnite-pumpellyite, and lower greenschist facies. At increasing values of μCO_2 clay-carbonate assemblages are favoured over a wide range of μH_2O relative to calcium zeolites, prehnite, and zoisite, and that a direct transition to prehnite or greenschist parageneses is possible. However, studies in active geothermal regions of the formation of partial mineral sequences analogous to many of the secondary mineral assemblages found in Harbour Main ignimbrites, suggest that even where CO_2 is a significant chemical component of the hydrothermal system their development is very strongly temperature-dependent (cf. White and Sigvaldason, 1963; Steiner, 1963; Muffler and White, 1969; Browne and Ellis, 1970).

Chemical variations in attendant fluids produced by interaction with their surrounding wall-rocks may also promote variations in mineral parageneses. Relative enrichment in potassium (K-feldspar + sericite + albite = greenish grey to greyish green to pale green alteration), sodium (albite + quartz = dark grey to reddish grey alteration), and calcium (epidote + calcite = yellow-green alteration) could result primarily from different initial whole-rock compositions. The chemical potential of the fluids would be strongly influenced by complex reactions with these multicomponent silicate systems, though the course of metasomatism is predominantly controlled by the effective activity of the hydrogen ion. In fact hydrogen ion metasomatism (Hemley and Jones, 1964) is responsible for most hydrothermal alterations caused by geochemical processes, and is the main mechanism of mass transfer of chemical components in open systems (compare "infiltration zoning" as conceived by Korzhinskii, 1959). Movement and segregation of elements involved in exchange reactions may have taken place over a distance of millimetres, as in the case of albitisation of primary plagioclase sites and crystallisation in amygdales within volcanic rocks of the Harbour Main Group, or much greater distances, as indicated by zones of intense epidote enrichment. Relative evaluations of the distances involved can be made using textural and geochemical criteria to investigate individual rock specimens, cooling units, or entire ash-flow sequences.

In addition to the parameters above, reaction kinetics may well be more important than is generally realised. For example, since the

early descriptions of Coombs (1960) it is commonly accepted that mineral assemblages in "burial" metamorphic environments are the result of a progressive series of dehydration reactions. However, recent work by Surdam (1973) has challenged this concept as it applies to the formation of mineral assemblages in the Karmutsen Group. Surdam demonstrated that alteration of basaltic glass in the tuffaceous rocks involved hydration and solution, not dehydration. While glass at the top of the stratigraphic section altered to laumontite + phyllosilicate, vitric material at the base altered directly to prehnite + phyllosilicate. He explained this by a high rate of sedimentation which enabled glass at the bottom of the section to pass through the stability fields of heulandite and laumontite into the region of prehnite stability. Solution chemistry, therefore, may be of considerable importance in locally controlling the observed mineral assemblages and geochemical characteristics of volcanic lithologies during metasomatism and low-grade metamorphism.

7.4. Timing of the Alteration and Metamorphism

The timing of the alteration and metamorphism of the Harbour Main Group is an extremely complex problem. Certain lines of evidence suggest that these events were quite distinct:

a) Alteration was contemporaneous with intrusion of porphyrites in the Harbour Main Group since blocks of intrusion breccia are locally altered whereas an igneous matrix of identical composition remains unaffected (plate 12).

b) A clast of Harbour Main rhyolite with albite phenocrysts partly replaced by K-feldspar lies enclosed in Conception metagreywacke containing unaltered albite crystals and devoid of potash in the matrix (photomicrograph 3). Similar textures have been described from K-rich rhyolitic ash-flow tuffs of the Weavers Hill ash-flow sequence (compare photomicrographs 55 and 56). This evidence indicates that alteration of this type pre-dated at least part of the depositional history of the Conception Group.

c) The ubiquitous occurrence of detrital albite crystals in the Cambro-Ordovician sedimentary successions of Conception Bay (J. Douglas, pers. comm., 1973) record erosion of previously metamorphosed (and deformed) Late Precambrian lithologies, since comparatively mild deformation and recrystallisation in Cambrian rocks is demonstrably later (chapter VI).

Since the structural relationships between the Conception and Harbour Main Groups are not well-known, it is tentatively assumed that folding and metamorphism of both rock-types was accomplished by the same event. This leads to the conclusion that hydrothermal alteration of the Harbour Main Group was certainly initiated and largely preceded Late Precambrian metamorphism and the first recognisable period of regional folding and weak penetrative deformation, i.e. D_1 (chapter VI).

Certain lines of evidence tentatively support this suggestion:

d) Hydrothermal alteration began while the rocks were only partly consolidated since alteration of volcanic breccias which have since been lithified preferentially affects fine-grained matrices leaving xenoliths and crystals little altered (plate 22).

e) Prolific fragments of red- and green-altered tuffs admixed with unaltered fragments of similar composition in volcanic breccias and lithic tuffs suggest that alteration was penecontemporaneous with ash-flow emplacement.

f) The formation of non-diagnostic mineral assemblages in Harbour Main ignimbrites is associated with secondary hydration and devitrification (section 3.4.); minerals diagnostic of metamorphic grade such as prehnite and pumpellyite are comparatively scarce and restricted to late-stage fractures.

g) The formation of prehnite in the Cabot Group of the Eastern Block is closely associated with late-stage development of joint systems (Papezik, 1972a). If the Cambro-Ordovician sequences maintain the same unconformable relationship with Precambrian rocks to the east, as the decreasing intensity of deformation in that direction suggests, this would place the metamorphism as a Late Precambrian event.

A definitive knowledge of the metamorphism obviously requires a detailed investigation on a regional scale. However, it is interesting to note that if prehnite-pumpellyite facies metamorphism of the Precambrian rocks of Avalon did in fact accompany or outlast the folding, as (g) above suggests, many of the classical concepts of "burial metamorphism", particularly "depth of burial" would need revision.

CHAPTER VIII

MINERAL AND WHOLE-ROCK CHEMISTRY

Collections of compositional data for the predominantly volcanic Harbour Main Group on Avalon are not as complete as hypotheses purporting to explain the magmatic evolution of the Group might suggest (for example, Papezik, 1970; Hughes and Brueckner, 1971; Hughes, 1972a). The only published analyses of extrusive and hypabyssal rocks include 10 whole-rock analyses for major elements given by Buddington (1916; 1919), only 2 of which lie outside a zone of pyrophyllitisation at the eastern margin of the Holyrood pluton; 22 analyses of lava flows, ignimbrites, volcanic breccias, and sills presented by Papezik (1969; 1970, Table I); and 7 partial analyses for K_2O, Na_2O, CaO, Rb, and Sr reported by Hughes and Malpas (1971). However, the analytical data of Papezik (1970) and Hughes and Malpas (ibid.) include 5 analyses (Table I, nos. 17-21) and 3 analyses (Table II, nos. H.77, M.79, and M.86), respectively, from rhyolitic and basaltic rocks of the Eastern Block (cf. chapter I, section 1.4.). Though generally correlated with the Harbour Main Group (Rose, 1952; Hughes and Brueckner, 1971) rocks of the primarily subaqueous Eastern Block are separated from type localities of the Harbour Main Group by a major shear-zone, the Topsail Fault (cf. fig. 2), and more recent work indicates that they are likely younger than terrestrial volcanic lithologies in the west (Papezik, pers. comm., 1973). This would of course invalidate all but

the most generalised petrogenetic conclusions based on a suite of Harbour Main rocks including such data, and any similarities could be purely incidental. In fact precise stratigraphic control between sampling sites has been demonstrated solely by Papezik (1969; 1970) for 8 analyses at Finn Hill and western Colliers Bay.

Compositional data for the granitic phases of the Holyrood pluton have recently become more numerous. Previous analyses have been published by Buddington (1919), Barning (1965; cf. Papezik, 1970, Table II), and Hughes (1971, Table 1, 2 analyses). A recent study of geochemical variability within the Holyrood intrusion by Strong et al. (1973) provided the most complete collection of major and trace element data now available for granitoid rocks intruding the Harbour Main Group.

All former work on the composition of feldspar phenocrysts in the Harbour Main Group has relied upon optical determinations or X-ray diffraction techniques. McCartney (1967, p. 17-20) reported phenocrysts of oligoclase and orthoclase in Harbour Main ignimbrites and andesine-labradorite compositions in "andesite flows, breccias, and tuffs", but made no mention of albite occurrences. Papezik (1969, p. 1412) used oil immersion methods and XRD to determine the compositions of plagioclase crystals (An_3-An_5) in ignimbrites at Finn Hill and albite-oligoclase phenocrysts (Papezik, 1970, p. 1491) in mafic flows at western Collers Bay. No crystals of K-feldspar were observed apart from a patchy replacement of primary albite sites and an indistinct potash phase in the matrix of a specimen from the Weavers

Hill ash-flow sequence (Papezik, 1970, Table I, analysis no. 12; referenced below as analysis P70-12 in table 7).

Rock specimens for analysis during the present investigation were collected under the strict stratigraphic control offered by the measured sections described earlier (tables 3, 4, and 5), and by the sequence of intrusion within the map area, which is known to be rhyolite-porphyrite-diabase in order of decreasing age. Sample locations are shown on the geological map (rear pocket). Additional specimens were collected from basalts overlying the ignimbrite sequences at sites located on fig. 4. Field observations of oxidised and vesicular flow tops are consistent with the view that basalts further west are progressively younger (McCartney, 1967; Papezik, 1970).

The range of compositions encountered in both phenocryst and whole-rock material require that the effects of alteration and low-grade metamorphism recognised previously (chapter VII) be taken into consideration. Petrogenetic conclusions are seriously impaired by failure to allow for chemical modification of originally "pristine" magmatic compositions. Furthermore, a strictly quantitative approach (for example, Papezik, 1970; Hughes, 1972a) might be misleading without additional inferences based on a comprehensive knowledge of the chemical processes that determine specific magmatic and metamorphic signatures. Since the significance of previous analytical results in rocks of the Harbour Main Group has sparked so much controversy (Papezik, 1970; Hughes and Malpas, 1971; Hughes, 1972a; 1972b) an attempt has been made in this study to impose the necessary chemical

constraints upon interpretation of the data. However, it is not claimed here that the techniques employed are completely discriminatory or that they can be applied indiscriminately to analogous geochemical problems.

Before proceeding further, it must be realised that the area of study represents less than 2% of the total area of outcrop of the Harbour Main Group. However, the map area straddles a narrow transition zone between early rhyolitic and late basaltic volcanism in the Harbour Main Group. Accordingly, if the general style of magmatic evolution within the Harbour Main Group is represented by the stratigraphic section examined herein, as comparisons with analogous volcanic provinces suggest, the petrogenetic conclusions of this study take on regional significance.

8.1. Electron-Probe Microanalysis of Feldspar Phenocrysts

An electron-probe investigation of feldspar phenocrysts in Harbour Main rock-types of the region was aimed at establishing their precise compositional range and homogeneity. The analytical data reveal that phenocrysts of albitic compositions predominate in all rock-types analysed, though K-feldspar locally occupies primary phenocryst sites. Albite and K-feldspar compositions are believed to represent metamorphic alteration of feldspars derived from volcanic liquids. However, the rare occurrence of compositions corresponding to igneous anorthoclase and calcic plagioclase indicate that neither

age nor P and T conditions adequately account for the processes of albitisation.

The method of analysing core and rim regions of phenocryst material generally provides a reliable measure of the degree of zoning or intra-grain homogeneity that existed in crystals growing in silicate melts immediately prior to eruption. While point analyses located along traverses provide valuable information concerning compositional zonations within grains of relatively fresh igneous rocks, the application of this technique to rocks affected by alteration and low-grade metamorphism is severely limited since there is no guarantee that inhomogeneities are distributed systematically about the perimeter of the crystal. However, well-documented coverage of the whole phenocryst allows a distinction between heterogeneities caused by solid solution, incipient development of alteration products, and partial replacement of crystals by a newly formed mineral. It is just as important to consider these compositional effects as the inter-grain variability within and between successive thin sections. Accordingly, phenocryst compositions were investigated in this study by a series of point analyses distributed evenly throughout the core region and around the rim, at a distance of approximately 20-40μm from crystal margins. Further descriptions of the analytical procedures and the instrument are given in appendix 3 together with an estimate of the precision and accuracy attained.

Element abundances for K_2O, Na_2O, CaO, and SiO_2 were measured directly; Al_2O_3 was determined stoichiometrically. The data include

TABLE 6. Electron Microprobe Partial Analyses of Feldspar Phenocrysts (In Weight Percent)

Specimen No.	NX1M					
Rock-Type	B.C.S. sillar (unit 6)					
Phenocryst	1 Rim	1 Core	2 Rim	2 Core	3 Rim	3 Core
SiO_2	67.59	68.14	69.12	69.20	67.94	67.75
Al_2O_3	18.94	19.00	19.33	19.42	19.07	19.04
CaO	0.47	0.26	0.38	0.19	0.43	0.36
Na_2O	10.87	11.27	11.29	11.58	11.05	11.18
K_2O	0.19	0.00	0.07	0.04	0.11	0.01
Total:	98.06	98.67	100.20	100.42	98.61	98.33

Specimen No.	H188M						
Rock-Type	B.C.S. ignimbrite (unit 8)						
Phenocryst	1 Rim	1 Core	1 K-feldspar patch	2 Rim	2 Core	3 Rim	3 Core
SiO_2	69.06	68.80	64.17	69.58	69.26	69.97	68.99
Al_2O_3	19.24	19.59	17.84	19.52	19.40	19.96	19.31
CaO	0.52	0.38	0.03	0.53	0.34	0.29	0.21
Na_2O	11.02	11.42	1.23	11.17	11.29	11.74	11.39
K_2O	0.17	0.13	14.55	0.18	0.20	0.13	0.20
Total:	100.01	100.32	97.81	100.98	100.48	102.10	100.10

Specimen No.	H105M						
Rock-Type	W.H.S. ignimbrite (unit 15)						
Phenocryst	1 Rim	1 Core	2 Rim	2 Core	3 Rim	3 Core Turbid	3 Core Clear
SiO_2	69.77	69.21	67.86	68.74	67.34	68.08	68.46
Al_2O_3	19.98	20.25	20.03	19.44	18.96	19.22	18.68
CaO	0.53	0.42	0.56	0.20	0.43	0.22	0.04
Na_2O	11.51	11.76	11.29	11.59	10.98	11.37	11.32
K_2O	0.09	0.15	0.42	0.02	0.13	0.11	0.00
Total:	101.88	101.79	100.16	100.00	97.84	99.01	98.50

TABLE 6. (Cont'd.)

Specimen No.	H157M			
Rock-Type	W.H.S. ignimbrite (unit 32)			
Phenocryst	1 Rim	1 Core	2 Core	3 Core
SiO_2	67.79	67.76	68.93	68.54
Al_2O_3	20.13	19.08	20.34	20.19
CaO	0.53	0.58	0.67	0.65
Na_2O	11.58	10.84	11.54	11.46
K_2O	0.12	0.20	0.14	0.16
Total:	100.14	98.46	101.62	101.00

Specimen No.	H176M				
Rock-Type	F.H.S. ignimbrite (unit 41)				
Phenocryst	1 Rim	1 Core	2 Rim	2 Core	3 Rim
SiO_2	68.89	69.26	67.82	67.15	67.21
Al_2O_3	19.61	19.49	19.25	18.88	18.78
CaO	0.44	0.38	0.33	0.35	0.30
Na_2O	11.34	11.34	11.24	11.01	10.90
K_2O	0.16	0.15	0.15	0.12	0.19
Total:	100.44	100.62	98.79	97.52	97.45

Specimen No.	H186M			
Rock-Type	F.H.S. ignimbrite (unit 42)			
Phenocryst	1 Rim	1 Core	2 Rim	2 Core
SiO_2	69.35	68.93	68.98	68.96
Al_2O_3	18.94	19.33	19.74	19.57
CaO	0.32	0.31	0.31	0.28
Na_2O	11.04	11.30	11.47	11.44
K_2O	0.21	0.17	0.29	0.23
Total:	99.85	100.05	100.80	100.48

TABLE 6. (Cont'd.)

Specimen No.	C63M						
Rock-Type	F.H.S. ignimbrite (unit 56)						
Phenocryst	1 Rim	1 Core	1 Core Clear	2 Rim	2 Core	3 Rim	3 Core
SiO_2	68.60	67.88	67.90	68.48	68.95	68.06	67.75
Al_2O_3	19.58	19.59	19.45	19.75	20.00	19.80	18.82
CaO	0.28	0.29	0.15	0.31	0.26	0.33	0.27
Na_2O	11.52	11.54	11.62	11.56	11.78	11.54	11.67
K_2O	0.13	0.09	0.07	0.18	0.15	0.21	0.15
Total:	100.10	99.39	99.19	100.27	101.14	99.94	99.66

Specimen No.	C68M			
Rock-Type	F.H.S. ignimbrite (unit 57)			
Phenocryst	1 Rim	1 Core	2 Rim	2 Core
SiO_2	65.45	64.57	66.27	62.14
Al_2O_3	19.35	19.16	18.97	20.27
CaO	0.76	1.00	0.65	1.70
Na_2O	10.78	10.41	10.58	9.15
K_2O	0.21	0.20	0.37	1.96
Total:	96.56	95.35	96.83	95.23

Specimen No.	C85M			
Rock-Type	F.H.S. ignimbrite (unit 58)			
Phenocryst	1 Rim	1 Core	2 Rim	2 Core
SiO_2	60.64	66.23	58.00	57.89
Al_2O_3	20.62	20.08	27.84	28.47
CaO	2.40	1.20	9.74	10.28
Na_2O	8.01	10.46	5.75	5.71
K_2O	2.85	0.65	0.62	0.36
Total:	94.52	98.63	101.95	102.71

TABLE 6. (Cont'd.)

Specimen No.	C88M						
Rock-Type	F.H.S. ignimbrite (unit 59)						
Phenocryst	1 Rim	1 Core	1 K-feldspar along fracture	2 Rim	2 Core	3 Rim	3 Core
SiO_2	67.63	67.72	62.14	65.93	65.48	66.98	66.39
Al_2O_3	19.01	18.96	18.37	19.42	19.10	19.46	19.42
CaO	0.98	1.00	0.00	1.00	0.84	0.88	0.71
Na_2O	10.35	10.41	0.36	10.65	10.65	10.59	10.83
K_2O	0.19	0.03	16.43	0.10	0.07	0.41	0.31
Total:	98.16	98.13	97.30	97.09	96.14	98.32	97.65

Specimen No.	H81M			
Rock-Type	Western Rhyolite Sill			
Phenocryst	1 Rim	1 Core	2 Rim	2 Core
SiO_2	66.53	66.57	66.12	67.02
Al_2O_3	18.43	18.70	18.76	18.72
CaO	0.57	0.36	0.50	0.47
Na_2O	10.50	10.86	10.70	10.78
K_2O	0.12	0.17	0.24	0.13
Total:	96.15	96.67	96.31	97.13

Specimen No.	H80M					
Rock-Type	Porphyrite (intrudes Western Rhyolite Sill)					
Phenocryst	1 Rim	1 Core	2 Rim	2 Core	3 Rim	3 Core
SiO_2	69.03	68.69	68.21	68.12	68.30	68.22
Al_2O_3	19.21	19.52	18.86	19.54	19.10	19.53
CaO	0.43	0.61	0.31	0.46	0.31	0.32
Na_2O	11.12	11.08	10.97	11.29	11.18	11.45
K_2O	0.13	0.18	0.24	0.14	0.15	0.11
Total:	99.92	100.09	98.59	99.55	99.04	99.63

TABLE 6. (Cont'd.)

Specimen No.	H163M					
Rock-Type	Porphyrite (fine-grained)					
Phenocryst	1 Rim	1 Core	2 Rim	2 Core	3 Rim	3 Core
SiO_2	67.30	67.94	68.66	66.61	63.86	64.72
Al_2O_3	17.23	17.38	18.76	18.51	19.94	20.29
CaO	0.39	0.23	0.61	0.06	0.61	0.60
Na_2O	10.03	10.31	10.68	11.19	11.10	11.67
K_2O	0.02	0.02	0.10	0.00	0.53	0.01
Total:	94.96	95.88	98.81	96.37	96.05	97.30

Specimen No.	GC1M			
Rock-Type	Diabase Dyke			
Phenocryst	1 Rim	1 Core	2 Rim	2 Core
SiO_2	64.93	64.62	66.33	64.89
Al_2O_3	19.23	19.72	19.66	19.44
CaO	1.21	1.36	1.18	1.37
Na_2O	10.27	10.38	10.56	10.25
K_2O	0.14	0.17	0.14	0.09
Total:	95.78	96.25	97.86	96.03

Specimen No.	P71-46M			
Rock-Type	Basalt			
Phenocryst	2 Rim	2 Core	3 Rim	3 Core
SiO_2	67.02	67.61	67.37	67.55
Al_2O_3	19.38	19.51	19.39	19.34
CaO	0.47	0.32	0.45	0.45
Na_2O	10.95	11.37	11.17	11.14
K_2O	0.48	0.21	0.19	0.19
Total:	98.31	99.02	98.58	98.67

TABLE 6. (Cont'd.)

Specimen No. GC20M
Rock-Type Basalt (70 ft. below unit 15)

Phenocryst	1 Rim	1 Core	2 Core Clear	2 Core Turbid
SiO_2	68.39	62.19	67.06	61.84
Al_2O_3	18.83	19.95	18.37	20.14
CaO	0.04	1.00	0.08	1.62
Na_2O	11.34	8.86	11.02	8.83
K_2O	0.12	3.24	0.10	2.47
Total:	98.70	95.28	96.63	94.90

Specimen No. C29M
Rock-Type W.M.S. ignimbrite

Phenocryst	1 Rim	1AB1 Core	1 K-feld-spar patch	1AB2 Core	2 Core	3 Rim	3 Core
SiO_2	67.00	67.75	65.39	67.48	67.10	66.30	67.22
Al_2O_3	19.20	19.55	22.65	18.78	18.94	19.42	20.81
CaO	0.37	0.40	0.05	0.28	0.40	0.38	0.44
Na_2O	11.12	10.06	2.21	11.02	10.91	11.22	10.18
K_2O	0.23	2.12	17.48	0.13	0.25	0.27	3.02
Total:	97.91	99.87	107.79	97.69	97.60	97.58	101.66

FIG 5 OR/AB/AN DIAGRAM FOR SELECTED FELDSPAR ANALYSES (recalculated to 100 mol %)

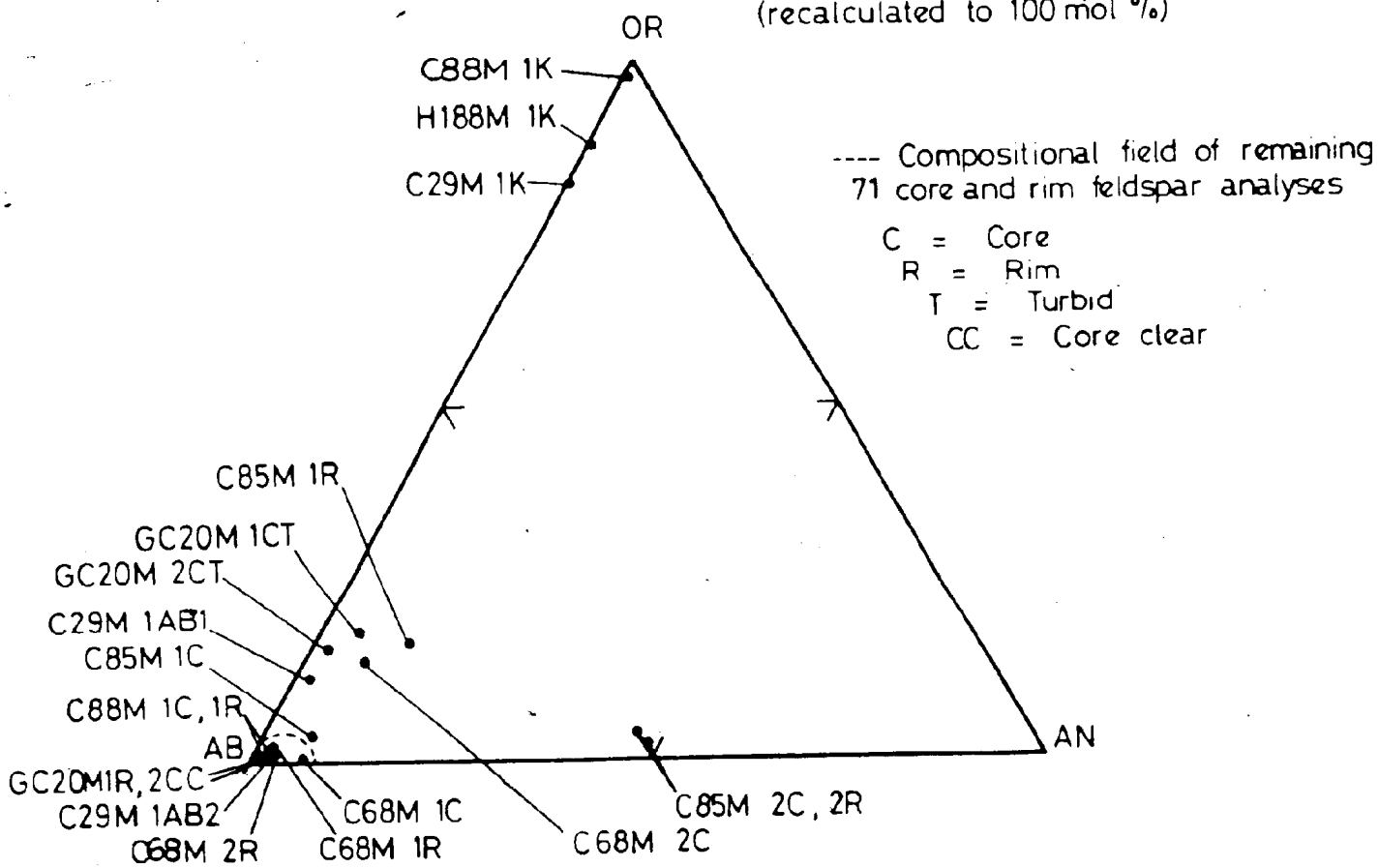

core and rim analyses of 90 phenocrysts from 11 rhyolitic ignimbrites, 1 rhyolite sill, 2 porphyrites, 1 diabase dyke, and 2 basaltic flows. The analytical results are presented in table 6 in weight percent. Analyses have also been recalculated in terms of molecular percentages (appendix 2) and plotted in the system An-Ab-Or (fig. 5).

The majority of phenocryst analyses with respect to ternary feldspar compositions range from $An_{0.3}$ $Ab_{99.7}$ Or_0 (analyses H105M-3CC, and H163M-2C in table 6 and appendix 2) to $An_{5.1}$ $Ab_{93.6}$ $Or_{1.3}$ (C68M-1C) and define the main compositional field for Harbour Main feldspar phenocrysts (fig. 5). Phenocryst compositions are essentially those predicted by the petrographic observations recorded earlier (chapters III and IV). The abundances of Ca and K in solid solution remain predominantly at background levels of detection and there is no difference between the purity of albites in rhyolitic ignimbrites, porphyrites, basalts, or diabase dykes. Most individual plagioclase grains show no appreciable zoning and variations in composition can largely be accommodated within the range of analytical error. However, certain compositional differences cannot be attributed solely to analytical errors. On the scale of the analysed samples, a triangular plot of analyses in the feldspar system (fig. 5) reveals considerable scatter extending beyond the field of albite compositions. It is possible to distinguish a potassium feldspar of variable purity (C29M-1K, H188M-1K, and C88M-1K); a plagioclase of calcic-andesine composition (C85M-2C and C85M-2R); and anorthoclase (C85M-1R); and a cluster of points extending along the Ab-Or join close to the albite end-member molecule. These data are examined in more detail below.

Analyses of basalt specimen GC20M demonstrate the compositional variations detected in turbid core (GC20M-1CT) and clear rim (GC20M-1R) of phenocrysts and those recorded in core regions (GC20M-2CC and GC20M-2CT) of groundmass feldspar laths which resulted from the use of a 20μm beam diameter. These differences are induced by varying proportions of finely crystalline alteration assemblages, notably clay minerals and sericite (photomicrograph 62). The presence of such minerals on primary feldspar sites will seriously affect the assumed stoichiometry and undoubtedly contribute to the consistently low totals of these analyses. This problem is enhanced somewhat by the difficulty to achieve a compromise between a beam size small enough to exclude alteration products and yet of sufficient diameter to avoid volatilisation of alkali elements. Similar effects are evident for specimen C68M to the extent that alteration invites an erroneous interpretation of an anorthoclase composition (C68M-2C).

C29M-1AB1(An_2 Ab_{86} Or_{12}) and C29M-1AB2($An_{1.4}$ $Ab_{97.9}$ $Or_{0.7}$) record differences chiefly in K_2O (and hence Na_2O) due to submicroscopic domains of K-feldspar. Detailed inspection of Teletype chart records confirms that potash occurs as a discrete phase rather than in ternary solid solution.

C29M-1K($An_{0.3}$ $Ab_{16.1}$ $Or_{83.6}$), H188M-1K(An_0 $Ab_{11.5}$ $Or_{88.5}$) and C88M-1K(An_0 $Ab_{3.2}$ $Or_{96.8}$) represent analyses of K-feldspar sited on albite phenocrysts. Most of the potash in specimen C29M can be detected with the petrographic microscope. However, part of the K-feldspar exists in solid solution as K-Na cryptoperthite (not analysed)

located along cleavage planes and detected by X-ray scanning techniques (photomicrograph 64). Purer varieties of K-feldspar invade minute fractures in albite phenocrysts of unit 8 at Bacon Cove (C188M-1K) and unit 59 at Finn Hill (C88M-1K; photomicrograph 63). In particular, C88M-1K closely approaches the pure potash end-member and is similar in composition to the "pure" low-temperature K-feldspar (determined by XRD) found in potassic keratophyres of New Zealand (Battey, 1955).

C85M-2C (An_{49} Ab_{49} Or_2) and C85M-2R ($An_{46.8}$ $Ab_{49.8}$ $Or_{3.4}$) represent a phenocryst (?) of igneous composition within the densely welded central zone of cooling unit 58 at Finn Hill. Systematic zoning was noted in a second phenocryst from the same cooling unit: a clear homogeneous rim of anorthoclase (C85M-1R) surrounds an albitic core (C85M-1C). The composition of C85M-1R is comparable to that given by Carmichael (1963, Table 2, analysis no. 6) for an anorthoclase phenocryst in Icelandic pitchstones.

8.1.1. Significance of Metamorphic Compositions

The spatial and lithological distribution of albite phenocrysts that define the main compositional field of feldspars in Harbour Main volcanic rocks obviates the need for intensive discussion regarding their origin. Since natural processes of differentiation in high-temperature silicate melts cannot account for the ubiquitous occurrence of albitic compositions in rocks of such diverse chemical identities, they are interpreted as the result of low-grade metamorphism. This conclusion is supported by the pioneer work of Bowen (1913), later

augmented by experiments of Tuttle and Bowen (1958) in the systems $KAlSi_3O_8$-$NaAlSi_3O_8$-(H_2O) and $KAlSi_3O_8$-$NaAlSi_3O_8$-SiO_2-(H_2O), and by the studies of Carmichael (1960; 1963) in naturally-occurring volcanic rock series. A more extensive argument for the metamorphic origin of albite phenocrysts in Late Precambrian rhyolites of the Bull Arm Formation, Isthmus of Avalon, has been advanced by Malpas (1972).

Analyses lying outside this restricted field of albite compositions require further consideration. GC20M-1CT, GC20M-2CT, C29M-1AB1, and C68M-2C fall outside the limits of natural solid solution for feldspar phenocrysts in volcanic liquids (Carmichael, 1963) and close to the Ab-Or join (fig. 5). Contamination of these analyses by later alteration products has already been demonstrated and they clearly warrant a metamorphic origin. The albitic core (C85M-1C) of an anorthoclase phenocryst closely approaches the main compositional field of Harbour Main albites and must be interpreted likewise. In this case, albitisation could be achieved by the introduction of sodium and concomitant release of most of the potassium and lesser amounts of calcium. However, the mechanism by which a phenocryst core is modified while its rim preserves a volcanic composition is not readily understood. K-feldspar compositions represented by C29M-1K, H188M-1K, and C88M-1K are all low-temperature microcrystalline varieties partially replacing albite on primary feldspar sites. A cryptoperthitic K-rich feldspar in specimen C29M readily conforms with albite cleavages. In view of the mobility of alkalies in this environment it is believed to be an intermediate stage in the process

of replacement rather than an exsolution texture. The range of solid solution and extreme purity of C88M-1K also provoke this interpretation (cf. Tuttle, 1952), and Battey (1955) has reported identical features in some New Zealand keratophyres.

Recent experimental work has shown that the fluid phase exerts a strong influence on the formation and properties of albite in low temperature environments. For example, an investigation into the hydrothermal crystallisation of low albite by Martin (1969) demonstrated that under the same P-T conditions synthesis of albite is favoured where increased amounts of water interact with appropriate starting materials, in this case glasses on the join $NaAlSi_3O_8$-$Na_2Si_2O_5$. Furthermore, the obliquity of albites so produced is considerably lowered in the presence of persodic solutions in runs of geologically short duration. Similarly, conversion of Ca-plagioclase of high structural state to fully ordered albite during low-grade metamorphism of Harbour Main volcanic rocks would be promoted by the presence of sodic aqueous solutions. The ultimate effects of continued interaction with even weakly sodic fluids of unlimited volume would invariably produce a pure albite of minimum obliquity, and in extreme cases would be expected to transform originally glassy volcanic matrices to albitic compositions, as demonstrated for experimentally devitrified glasses (Martin, 1969). The extreme case of albitisation where whole-rock compositions of silicic ignimbrites and lava flows are essentially those of included albite phenocrysts will be illustrated in the following discussions concerning whole-rock chemistry.

On the scale of an individual phenocryst, therefore, the microprobe data provide ample evidence for ionic transfer in the fluid phase involving both alkalies and calcium. Furthermore, the strict succession of feldspar replacement on primary sites, i.e. incongruent breakdown of Ca-plagioclase to form albite followed by partial replacement of albite by K-feldspar, indicates that Ca^{++} is permanently lost from phenocryst domains. If stoichiometry is to be preserved during albitisation the required exchange is a coupled substitution of Na^{+}-Si^{+++} in the aqueous phase for Ca^{++}-Al^{+++}. The case for K-feldspar replacing albite involves a less complex exchange of Na^{+} for K^{+} (cf. Orville, 1963). Where cations travel only short distances and ionic exchange is essentially confined to phenocryst/matrix systems, i.e. isochemical metamorphism, whole-rock compositions may be expected to faithfully preserve their magmatic heritage. However, the scale of mobility of feldspar components is unknown until quantitatively defined by geochemical techniques. In the extreme case of an open system, the scale of material transfer exceeds that of the geochemical sample or area of sampling.

8.1.2. Significance of Magmatic Compositions

Although selection of material for analysis was strongly biased toward those crystals that were either untwinned or displayed only simple Carlsbad twinning, there is no textural or chemical evidence for the former existence of potassium feldspar phenocrysts in volcanic rocks of the Harbour Main Group. This inevitably leads to the conclusion

that a plagioclase or lime-bearing alkali feldspar were the only feldspar phases obtained on the liquidus throughout the entire differentiation history of source magmas in the region. While this is not such a surprising conclusion for basaltic and intermediate volcanic liquids, it does appear somewhat anomalous throughout the rhyolitic ignimbrite sequences, particularly oversaturated potassic differentiates of the Weavers Hill ash-flow sequence (cf. table 7). This point requires careful examination since experimental studies in the system $KAlSi_3O_8$-$NaAlSi_3O_8$-NaCl-KCl-H_2O have demonstrated that pure feldspar end-members can readily form by exchange of K^+ and Na^+ under hydrothermal conditions (Orville, 1963). The possibility remains, therefore, that albite on primary sites in rhyolitic rocks is pseudomorphous after phenocrysts of K-feldspar. If it can be simply demonstrated that K-feldspar was not required as a phase on the liquidus in these rocks, then reactions of the type envisaged by Orville (ibid.) resulting in complete replacement of K-feldspar by albite need no longer be a factor of consequence.

The experimental work of Tuttle and Bowen (1958) in the systems $NaAlSi_3O_8$-$KAlSi_3O_8$-(H_2O) and $NaAlSi_3O_8$-$KAlSi_3O_8$-SiO_2-(H_2O) has shown that an alkali feldspar minimum in the binary system extends into the ternary system as a thermal trough projecting from the alkali feldspar minimum to the quartz-feldspar boundary curve on the liquidus surface. Carmichael (1963) has traced the paths of crystallisation for feldspar phenocrysts in equilibrium with salic volcanic liquids in the systems $NaAlSi_3O_8$-$KAlSi_3O_8$-$CaAl_2Si_2O_8$ and $NaAlSi_3O_8$-$KAlSi_3O_8$-$CaAl_2Si_2O_8$-SiO_2 for a wide range of igneous rock series. The extent of solid solution

among An-Ab-Or end-members depends upon the temperature of crystallisation and the composition of the parental liquid. In response to a decrease in temperature the solidus fractionation paths for feldspars in equilibrium with differentiating volcanic liquids will proceed down the thermal valley towards the alkali feldspar minimum in these respective systems.

The complete lack of K-rich volcanic feldspars in rhyolitic ignimbrites of the Harbour Main Group strongly suggests that the compositions of parental melts fall in the field for equilibrium crystallisation of one feldspar (a plagioclase). In a ternary feldspar plot, this one feldspar field lies between the Ab-An join and the limit of natural solid solution (Tuttle and Bowen, 1958, p. 132), or above the two feldspar boundary surface in the four-component system (Carmichael, 1963, fig. 4). The lack of obvious resorption textures in albite "phenocrysts" together with the total absence of K-feldspar on the liquidus (assuming conditions of equilibrium fractionation) imply that differentiating volcanic liquids never reached the two-feldspar surface. This may be ascribed to K/Na ratios of initial liquids, as suggested by Carmichael (1963), or result from insufficient cooling of the melt.

It is also possible to reconcile the markedly contrasting compositions of feldspar phenocrysts (C85M-2C,2R and C85M-1R) in a rhyodacitic ignimbrite (unit 58) by considering successive stages of equilibrium fractionation along a single solidus path for an appropriate initial liquid composition. Crystallisation of calcic-

andesine would invariably move the feldspar fractionation path in the direction away from An, parallel with the An-Ab join to eventually curve toward the minimum feldspar composition for the system. In nature, the apex of this path never reaches the field of albite compositions and further growth of Ca-bearing feldspars would necessitate the incorporation of appreciable amounts of potassium in ternary solid solution. In this way, the compositions of C85M-2C,2R possibly represent a phenocryst in equilibrium with a less differentiated part of the magma than that required for the equilibration of lime-anorthoclase (C85M-1R). It is interesting to note that the ignimbrite directly overlying unit 58 is a multiple flow unit which shows significant compositional variation between its upper and lower subdivisions.

8.2. Whole-Rock Analytical Data

The 82 new chemical analyses are presented in table 7 and include determinations of both major oxides and selected trace elements. Supplementary analytical data (major oxides only) for ignimbrites at Finn Hill and basaltic rocks at western Colliers Bay have been taken from Papezik (1970, table 1). Whole-rock analyses in weight percent are expressed as molecular percentages in Appendix 1. Prior to computation of CIPW norms (table 7), all analyses were recalculated to 100 wt. % on a volatile-free basis and total iron (ΣFe_2O_3) was converted to FeO. This prevented the appearance of magnetite and and hematite, and resulted in a more undersaturated normative composition.

TABLE 7

WHOLE-ROCK ANALYSES

Bacon Cove Ash-Flow Sequence

Specimen No.	GC39a	GC39b†	GC37a*	GC37b*	GC42	GC38‡	NX1
Unit	3	3	4	4	5		6
(Wt. %)							
SiO_2	67.00	70.30	78.20	78.10	72.20	72.70	72.00
Al_2O_3	14.80	14.80	11.60	13.30	14.00	13.80	15.40
ΣFe_2O_3	3.98	3.98	1.36	1.15	2.44	3.43	3.25
CaO	0.87	1.05	0.15	0.01	0.37	0.43	0.91
Na_2O	3.60	4.13	0.39	0.52	3.66	4.38	4.49
K_2O	4.39	4.24	6.15	6.25	3.45	3.53	3.17
MgO	1.30	0.30	0.90	0.40	0.60	0.33	1.00
MnO	0.05	0.07	0.02	0.02	0.05	0.02	0.06
TiO_2	0.77	0.44	0.13	0.15	0.32	0.40	0.47
P_2O_5	-	0.02	-	-	-	-	-
L.O.I.	1.42	1.38	0.71	0.84	0.98	1.01	0.60
Total:	98.18	100.69	99.61	100.74	98.07	100.03	101.35
(p.p.m.)							
Rb	152	127	164	179	130	108	105
Sr	158	199	-	-	141	106	200
Ba	1366	1256	1776	1580	1403	1291	1511
Zr	189	171	96	102	191	156	163
Cu	2	3	2	1	2	10	11
Zn	55	53	32	36	51	40	69
Cr	20	26	20	15	19	17	22
Ni	4	4	2	1	3	3	5
K/Rb	240	277	311	290	220	271	251

TABLE 7 (Cont'd.)

Specimen No.	GC39a	GC39b†	GC37a*	GC37b*	GC42	GC38†	NX1
Unit	3	3	4	4	5	6	6
			C I P W Norms				
Q	23.93	24.94	50.39	45.85	35.49	30.39	28.04
Or	26.94	25.35	36.83	37.05	21.07	21.16	18.67
Ab	31.60	35.32	3.34	4.41	31.98	37.56	37.83
An	4.27	5.13	0.75	0.05	1.90	2.16	4.50
Ag	-	-	-	-	-	-	-
Hy	8.96	6.80	4.37	2.69	5.26	5.95	7.77
Ilm	1.52	0.85	0.25	0.29	0.63	0.77	0.89
Ap	-	0.05	-	-	-	-	-
C	2.71	1.57	4.07	5.67	3.69	2.02	2.91

Total iron given as ΣFe_2O_3 and converted to FeO in calculation of CIPW norms.

*Omitted from chemical variation diagrams unless otherwise stated and excluded from calculation of averages (Table 9).

L.O.I. = Loss on ignition.

†Analysed by atomic absorption spectrophotometry.

TABLE 7 (Cont'd.)

Ash-Flow Tuffs Underlying Weavers Hill Ash-Flow Sequence

	(Biotite Phenocrysts)			(No Biotite Phenocrysts)	
Specimen No.	GC34*+	GC35*	GC36*+	GC32*+	GC53*
Unit	27	28	28		
(Wt. %)					
SiO_2	76.30	74.60	81.30	79.10	69.20
Al_2O_3	11.90	13.30	10.90	12.20	15.30
ΣFe_2O_3	1.74	2.15	1.00	2.41	2.58
CaO	1.00	0.56	0.32	0.09	0.37
Na_2O	4.06	5.29	3.40	0.14	7.16
K_2O	2.14	3.82	2.40	3.36	0.57
MgO	-	0.50	0.11	1.30	0.60
MnO	0.05	0.05	0.02	0.05	0.10
TiO_2	0.21	0.26	0.18	0.22	0.34
P_2O_5	-	-	-	-	-
L.O.I.	0.76	0.69	0.48	1.38	1.85
Total:	98.16	101.22	100.12	100.25	98.07
(p.p.m.)					
Rb	85	94	87	142	20
Sr	192	145	137	-	204
Ba	809	1102	958	695	216
Zr	194	217	169	174	203
Cu	7	4	-	8	3
Zn	29	43	11	47	81
Cr	17	17	19	17	26
Ni	3	2	-	2	7
K/Rb	209	337	231	196	237

TABLE 7 (Cont'd.)

Specimen No.	GC34*+	GC35*	GC36*+	GC32*+	GC53*
Unit	27	28	28		
		C I P W Norms			
Q	42.33	26.03	51.02	62.45	22.84
Or	13.02	22.52	14.38	20.15	3.51
Ab	35.33	44.62	28.90	1.20	63.13
An	5.10	1.25	1.60	0.45	1.91
Ag	-	1.30	-	-	-
Hy	2.70	3.79	1.65	7.05	5.61
Ilm	0.41	0.49	0.34	0.42	0.67
Ap	-	-	-	-	-
C	1.12	-	2.11	8.28	2.33

Total iron given as Fe_2O_3 and converted to FeO in calculation of CIPW norms.

L.O.I. = Loss on ignition.

*Omitted from chemical variation diagrams unless otherwise stated and excluded from calculation of averages (Table 9).

+Silicified.

TABLE 7 (Cont'd.)

Weavers Hill Ash-Flow Sequence

Specimen No. Unit	GC28a 19	GC28b 19	GC29 ‡ 21	GC22 23	GC23 24
(Wt. %)					
SiO_2	71.80	71.30	74.70	74.40	73.40
Al_2O_3	14.80	14.80	14.20	13.50	14.60
ΣFe_2O_3	2.91	2.89	2.40	2.02	2.18
CaO	0.25	0.29	0.22	0.38	1.16
Na_2O	1.38	1.44	5.42	2.48	2.56
K_2O	6.18	5.96	2.21	3.73	3.95
MgO	0.20	0.20	0.30	0.80	0.70
MnO	0.07	0.06	0.03	0.06	0.06
TiO_2	0.28	0.28	0.22	0.16	0.19
P_2O_5	-	-	-	-	-
L.O.I.	1.05	0.96	1.04	0.76	0.68
Total:	98.92	98.18	100.74	98.29	99.66
(p.p.m.)					
Rb	192	175	94	148	170
Sr	53	64	178	259	521
Ba	1915	2097	832	946	1076
Zr	128	184	204	186	236
Cu	6	32	6	9	5
Zn	61	58	36	57	60
Cr	18	15	19	18	25
Ni	5	-	4	4	7
K/Rb	267	283	195	209	193

TABLE 7 (Cont'd.)

Specimen No. Unit	GC28a 19	GC28b 19	GC29‡ 21	GC22 23	GC23 24
		C I P W Norms			
Q	38.15	38.33	32.30	43.39	38.85
Or	37.46	36.34	13.14	22.67	23.70
Ab	11.96	12.57	46.11	21.56	21.97
An	1.27	1.49	1.10	1.94	5.84
Ag	-	-	-	-	-
Hy	5.10	5.08	4.43	5.32	5.26
Ilm	0.54	0.55	0.42	0.31	0.37
Ap	-	-	-	-	-
C	5.51	5.52	2.53	4.82	4.06

Total iron given as ΣFe_2O_3 and converted to FeO in calculation of CIPW norms.

L.O.I. = Loss on ignition.

‡Analysed by atomic absorption spectrophotometry.

TABLE 7 (Cont'd.)

Weavers Hill Ash-Flow Sequence (cont'd.)

Specimen No. Unit	GC24* 25	CWT 29	H157 31	P70-12 36	GC48† 36
(Wt. %)					
SiO_2	73.70	70.80	74.10	73.30	73.60
Al_2O_3	13.00	15.10	15.00	14.50 (1.12)	14.20
ΣFe_2O_3	1.50	2.57	1.52	0.58	1.98
CaO	0.18	1.11	0.26	0.48	0.40
Na_2O	6.55	3.27	1.99	2.76	5.26
K_2O	0.91	5.52	5.63	5.47	2.27
MgO	0.60	0.50	0.60	0.35	0.28
MnO	0.01	0.07	0.02	0.04	0.03
TiO_2	0.16	0.32	0.20	0.13	0.15
P_2O_5	-	-	-	0.08	-
L.O.I.	0.97	1.61	0.75	0.70	2.03
Total:	97.58	100.87	100.07	99.51	100.54
(p.p.m.)					
Rb	41	135	182		180
Sr	52	202	77		71
Ba	257	1142	1598		1367
Zr	199	194	188	n.d.	200
Cu	6	20	-		14
Zn	16	54	39		48
Cr	19	20	19		18
Ni	4	4	-		2
K/Rb	184	339	257		243

TABLE 7 (Cont'd.)

Specimen No.	GC24*	CWT	H157	P70-12	GC48†
Unit	25	29	31	36	36
		C I P W Norms			
Q	30.92	26.02	38.82	35.34	37.47
Or	5.59	27.98	33.58	32.70	31.65
Ab	57.45	27.95	16.99	23.60	19.54
An	0.95	5.56	1.30	1.88	3.73
Ag	-	-	-	-	-
Hy	3.87	5.56	3.74	0.88	3.84
Ilm	0.31	0.61	0.38	0.09	0.29
Ap	-	-	-	0.19	-
C	0.95	1.74	5.20	3.39	3.48

Total iron given as ΣFe_2O_3 and converted to FeO in calculation of CIPW norms.

L.O.I. = Loss on ignition.

P70-1 etc. = Papezik, 1970, anal. 1; presented without BaO, ZrO_2, V_2O_5.

( ) = FeO determined separately.

n.d. = not determined.

*Omitted from chemical variation diagrams unless otherwise stated and excluded from calculation of averages (Table 9).

†Analysed by atomic absorption spectrophotometry.

Weavers Hill Ash-Flow Sequence (cont'd.)

Specimen No.	GC47*+	GC14	GC15	GC16	GC17‡
Unit	36	36	37	38	38
(Wt. %)					
SiO_2	76.30	74.10	68.00	73.60	70.00
Al_2O_3	11.50	13.80	13.60	13.10	13.40
ΣFe_2O_3	1.42	1.75	3.82	1.72	1.68
CaO	0.40	0.98	1.58	0.53	0.40
Na_2O	2.07	2.24	2.52	3.53	3.50
K_2O	3.76	4.70	3.69	4.55	4.55
MgO	0.40	0.60	2.70	0.20	0.29
MnO	0.03	0.04	0.06	0.02	0.03
TiO_2	0.15	0.18	0.50	0.42	0.11
P_2O_5	-	-	0.02	-	-
L.O.I.	1.77	1.10	1.57	1.47	1.07
Total:	98.06	99.49	98.06	99.14	101.03
(p.p.m.)					
Rb	136	167	145	136	129
Sr	36	60	70	106	84
Ba	1217	1373	1458	1385	1532
Zr	144	183	179	188	172
Cu	22	11	13	4	31
Zn	37	36	35	38	33
Cr	18	16	16	16	17
Ni	2	2	2	3	2
K/Rb	230	234	211	278	293

TABLE 7 (Cont'd.)

Specimen No.	GC47*+	GC14	GC15	GC16	GC17‡
Unit	36	36	37	38	38
			C I P W Norms		
Q	49.45	39.56	30.49	34.06	35.92
Or	23.19	28.31	22.71	27.60	26.92
Ab	18.27	19.30	22.19	30.63	29.62
An	2.07	4.95	8.02	2.70	1.99
Ag	-	-	-	-	-
Hy	3.29	4.24	12.82	2.75	3.37
Ilm	0.30	0.35	0.99	0.82	0.21
Ap	-	-	-	-	-
C	3.44	3.30	2.74	1.44	1.99

Total iron given as ΣFe_2O_3 and converted to FeO in calculation of CIPW norms.

L.O.I. = Loss on ignition.

*Omitted from chemical variation diagrams unless otherwise stated and excluded from calculation of averages (Table 9).

+Silicified.

‡Analysed by atomic absorption spectrophotometry.

TABLE 7 (Cont'd.)

Ash-Flow Tuffs with Biotite Phenocrysts, Top of Weavers Hill Ash-Flow Sequence, James Cove

Specimen No.	GC18	GC19‡	GC43	P70-16*+	GC44	GC45*
Unit	39	39	40	40	40	41
(Wt. %)						
SiO_2	67.80	72.00	75.30	76.60	72.80	73.40
Al_2O_3	16.20	14.40	12.80	11.64 (1.24)	13.30	13.80
ΣFe_2O_3	3.28	2.36	2.84	1.44	2.02	4.01
CaO	0.51	0.28	0.51	0.40	0.32	0.58
Na_2O	5.16	5.63	4.78	4.03	5.08	6.00
K_2O	3.01	3.32	3.16	2.50	3.55	1.10
MgO	1.00	0.09	0.70	0.69	0.20	0.20
MnO	0.08	0.03	0.03	0.08	0.02	0.04
TiO_2	0.42	0.26	0.33	0.29	0.31	0.62
P_2O_5	-	-	-	0.12	-	0.02
L.O.I.	0.85	0.47	0.28	0.96	0.44	0.47
Total:	98.29	98.84	100.73	99.99	98.04	100.24
(p.p.m.)						
Rb	114	75	62		80	50
Sr	162	151	174		140	145
Ba	1041	1390	1625		1376	1284
Zr	188	164	152	n.d.	161	180
Cu	3	8	18		4	19
Zn	84	45	36		36	53
Cr	22	18	17		20	26
Ni	6	4	4		2	5
K/Rb	219	368	423		268	183

TABLE 7 (Cont'd.)

Specimen No.	GC18	GC19‡	GC43	P70-16*+	GC44	GC45*
Unit	39	39	40	40	40	41
			C I P W Norms			
Q	22.87	24.66	31.29	41.69	29.00	30.41
Or	18.33	20.01	18.66	15.10	21.56	6.55
Ab	44.95	48.54	40.38	34.81	44.13	51.09
An	2.61	1.42	2.53	1.22	1.63	2.76
Ag	-	-	-	-	-	-
Hy	7.58	3.82	5.94	4.44	3.45	6.21
Ilm	0.82	0.50	0.63	0.56	0.61	1.19
Ap	-	-	-	0.28	-	0.05
C	3.63	1.05	0.59	1.90	0.53	1.74

Total iron given as ΣFe_2O_3 and converted to FeO in calculation of CIPW norms.

L.O.I. = Loss on ignition.

P70-1 etc. = Papezik, 1970, anal. 1; presented without BaO, ZrO_2, V_2O_5.

( ) = FeO determined separately.

n.d. = not determined.

*Omitted from chemical variation diagrams unless otherwise stated and excluded from calculation of averages (Table 9).

+Silicified.

‡Analysed by atomic absorption spectrophotometry.

TABLE 7 (Cont'd.)

Finn Hill Ash-Flow Sequence

Specimen No.	GC46a	GC46b‡	GC49	GC50	GTN17*	P70-13**
Unit	42	42	43	43	43	437
(Wt. %)						
SiO_2	69.80	70.10	68.10	70.50	62.10	73.75
Al_2O_3	13.10	14.80	14.60	15.00	12.30	13.30
ΣFe_2O_3	2.94	3.05	3.64	3.81	2.91	(0.56) 1.57
CaO	1.14	1.05	1.23	1.13	1.64	0.18
Na_2O	4.56	4.45	6.09	6.00	4.85	6.19
K_2O	2.20	2.99	1.66	1.56	1.80	2.52
MgO	1.90	1.32	0.70	1.50	0.70	0.27
MnO	0.08	0.10	0.06	0.07	0.08	0.02
TiO_2	0.50	0.51	0.57	0.56	0.45	0.27
P_2O_5	-	-	-	-	-	0.12
L.O.I.	2.14	2.27	1.93	1.17	1.92	0.48
Total:	98.36	100.64	98.58	101.30	88.75	99.23
(p.p.m.)						
Rb	96	120	28	38	39	
Sr	263	229	317	330	334	
Ba	550	890	1086	1011	1451	
Zr	189	206	182	178	185	n.d.
Cu	7	4	4	24	9	
Zn	60	59	57	59	50	
Cr	23	20	26	29	22	
Ni	6	6	8	11	8	
K/Rb	190	207	492	341	383	

TABLE 7 (Cont'd.)

Specimen No. Unit	GC46a 42	GC46b‡ 42	GC49 43	GC50 43	GTN17* 43	P70-13** 43?
			C I P W Norms			
Q	28.85	27.07	21.06	22.52	24.13	26.56
Or	13.57	18.04	10.20	9.25	12.30	15.12
Ab	40.22	38.39	53.51	50.89	47.42	52.12
An	5.90	5.31	6.34	5.62	7.48	0.11
Ag	-	-	-	-	1.64	-
Hy	9.29	7.82	7.20	9.26	6.05	3.94
Ilm	0.99	0.99	1.12	1.07	0.99	0.52
Ap	-	-	-	-	-	0.28
C	1.19	2.38	0.57	1.39	-	0.35

Total iron given as Fe_2O_3 and converted to FeO in calculation of CIPW norms.

L.O.I. = Loss on ignition.

P70-1 etc. = Papezik, 1970, anal. 1; presented without BaO, ZrO_2, V_2O_5.

( ) = FeO determined separately.

n.d. = not determined.

*Omitted from chemical variation diagrams unless otherwise stated and excluded from calculation of averages (Table 9).

**Omitted from averages only.

‡Analysed by atomic absorption spectrophotometry.

TABLE 7 (Cont'd.)

Finn Hill Ash-Flow Sequence (cont'd.)

Specimen No. / Unit	GTN16 / 44	GTN16t / 44	GTN11 / 45	GTN19 / 45	P70-14 / 56	P70-9 / 58
(Wt. %)						
SiO_2	63.60	70.60	75.90	72.30	74.35	64.08
Al_2O_3	16.50	15.20	13.50	12.30	13.33 (1.76)	16.92 (2.38)
ΣFe_2O_3	3.87	4.59	2.82	3.49	0.66	1.91
CaO	3.19	1.71	0.75	1.10	0.68	1.72
Na_2O	3.97	4.96	6.88	5.90	5.55	6.61
K_2O	2.37	1.69	0.52	0.89	1.88	2.34
MgO	2.00	0.40	-	-	0.25	1.41
MnO	0.07	0.08	0.01	0.06	0.07	0.16
TiO_2	0.64	0.79	0.58	0.79	0.52	0.90
P_2O_5	0.05	0.03	-	0.03	0.07	0.21
L.O.I.	1.07	0.92	0.40	1.25	0.75	1.06
Total:	97.33	100.97	101.36	98.11	99.87	99.70
(p.p.m.)						
Rb	81	62	17	12		
Sr	967	396	177	141		
Ba	629	526	203	419		
Zr	238	156	192	85	n.d.	n.d.
Cu	12	1	14	-		
Zn	64	65	17	55		
Cr	25	29	23	23		
Ni	10	10	6	4		
K/Rb	243	226	303	616		

TABLE 7 (Cont'd.)

Specimen No. Unit	GTN16*– 44	GTN16t 44	GTN11 45	GTN19 45	P70-14 56	P70-9 58
			C I P W Norms			
Q	20.09	28.29	30.39	31.49	31.95	8.71
Or	14.62	10.04	3.06	5.46	11.23	14.06
Ab	35.04	42.14	57.82	51.72	47.43	56.80
An	16.17	8.32	3.70	4.61	2.94	7.27
Ag	-	-	-	0.75	-	-
Hy	10.90	7.46	3.70	4.34	4.18	10.03
Ilm	1.29	1.51	1.09	1.56	1.00	1.74
Ap	0.12	0.07	-	0.07	0.16	0.50
C	1.80	2.18	0.26	-	1.11	0.90

Total iron given as Fe_2O_3 and converted to FeO in calculation of CIPW norms.

L.O.I. = Loss on ignition.

P70-1 etc. = Papezik, 1970, anal. 1; presented without BaO, ZrO_2, V_2O_5.

( ) = FeO determined separately.

n.d. = not determined.

*Omitted from chemical variation diagrams unless otherwise stated and excluded from calculation of averages (Table 9).

–Xenocrystic/xenolithic.

Finn Hill Ash-Flow Sequence (cont'd.)

Specimen No. Unit	GTN23a 59	GTN23b* 59	GTN23c 59	GTN23d 59	GTN23e 59	GTN23f* 59
(Wt. %)						
SiO_2	66.80	58.80	64.50	66.40	65.10	64.10
Al_2O_3	14.90	14.50	15.40	14.90	14.70	14.10
ΣFe_2O_3	5.30	7.40	5.36	4.19	4.85	4.47
CaO	1.03	1.42	1.45	0.75	1.01	1.04
Na_2O	6.90	7.69	7.73	7.14	7.03	7.54
K_2O	1.93	0.68	1.09	1.92	1.82	1.21
MgO	1.10	2.10	2.20	0.80	1.20	1.10
MnO	0.10	0.09	0.11	0.08	0.09	0.09
TiO_2	0.89	1,06	0.97	0.82	0.82	1.04
P_2O_5	0.17	0.19	0.04	0.09	0.07	0.02
L.O.I.	0.91	0.99	1.04	1.09	1.44	1.14
Total:	100.03	94.92	99.99	98.18	98.13	95.75
(p.p.m.)						
Rb	31	36	15	28	30	23
Sr	129	155	116	147	109	119
Ba	685	657	336	658	593	332
Zr	155	199	172	186	150	181
Cu	7	4	13	-	-	4
Zn	93	94	127	94	83	93
Cr	28	26	35	24	32	32
Ni	9	8	11	4	12	11
K/Rb	517	157	603	569	504	437

TABLE 7 (Cont'd.)

Specimen No. Unit	GTN23a 59	GTN23b* 59	GTN23c 59	GTN23d 59	GTN23e 59	GTN23f* 59
		C I P W Norms				
Q	12.69	1.70	6.41	12.84	11.09	10.61
Or	11.58	4.32	6.56	11.75	11.19	7.59
Ab	59.22	69.82	66.52	62.49	61.83	67.68
An	4.04	3.26	4.18	3.04	3.31	1.12
Ag	0.01	2.51	2.40	0.17	1.21	3.58
Hy	10.35	15.76	11.96	7.89	9.59	7.28
Ilm	1.72	2.16	1.87	1.61	1.62	2.10
Ap	0.40	0.47	0.09	0.22	0.17	0.05
C	-	-	-	-	-	-

Total iron given as ΣFe_2O_3 and converted to FeO in calculation of CIPW norms.

L.O.I. = Loss on ignition.

*Omitted from chemical variation diagrams unless otherwise stated and excluded from calculation of averages (Table 9).

TABLE 7 (Cont'd.)

Finn Hill Ash-Flow Sequence (cont'd.)

Specimen No. Unit	GTN23h* 59	GTN23i* 59	GTN23l*- 59	GTN22t‡ 59	GTN22c* 59	GTN34* 59
(Wt. %)						
SiO_2	72.00	72.00	58.70	68.60	68.90	67.40
Al_2O_3	13.50	13.80	16.00	14.40	13.20	13.80
ΣFe_2O_3	3.69	3.28	9.21	4.18	3.59	3.48
CaO	0.78	0.89	2.10	1.60	0.94	1.18
Na_2O	6.40	7.49	7.58	7.72	7.48	6.67
K_2O	1.51	0.18	0.53	0.16	0.12	1.34
MgO	0.20	-	1.40	0.74	0.10	1.90
MnO	0.05	0.04	0.13	0.07	0.05	0.19
TiO_2	0.75	0.69	1.13	0.76	0.70	0.72
P_2O_5	0.07	0.05	0.22	-	0.07	-
L.O.I.	0.73	0.84	1.24	1.26	1.13	1.38
Total:	99.68	99.26	98.70	99.49	96.28	98.66
(p.p.m.)						
Rb	26	2	10	2	2	22
Sr	94	83	93	122	81	229
Ba	492	46	103	70	49	400
Zr	155	176	96	145	160	176
Cu	4	7	59	-	-	102
Zn	55	48	109	76	72	100
Cr	24	25	41	25	25	28
Ni	7	6	14	6	8	8
K/Rb	482	747	440	623	498	506

TABLE 7 (Cont'd.)

Specimen No. Unit	GTN23h* 59	GTN23i* 59	GTN23l*- 59	GTN22t‡ 59	GTN22c* 59	GTN34- 59
			C I P W Norms			
Q	25.32	24.59	0.65	17.11	22.36	16.95
Or	9.06	1.09	3.26	0.97	0.75	8.23
Ab	0.17	64.60	66.76	66.78	66.77	58.58
An	3.46	3.58	8.40	4.27	2.21	3.90
Ag	-	0.53	0.81	3.31	1.97	1.80
Hy	5.53	4.16	17.36	6.10	4.36	9.12
Ilm	1.45	1.37	2.23	1.48	1.40	1.42
Ap	0.17	0.12	0.53	-	0.17	-
C	0.09	-	-	-	-	-

Total iron given as ΣFe_2O_3 and converted to FeO in calculation of CIPW norms.

L.O.I. = Loss on ignition.

*Omitted from chemical variation diagrams unless otherwise stated and excluded from calculation of averages (Table 9).

-Mafic xenoliths.

‡Analysed by atomic absorption spectrophotometry.

Finn Hill Ash-Flow Sequence (cont'd.)

Specimen No.	P70-11	GTN29*
Unit	59	60
(Wt. %)		
SiO_2	68.59	69.40
Al_2O_3	15.12	13.50
ΣFe_2O_3	3.35	3.03
CaO	1.13	1.16
Na_2O	5.42	7.02
K_2O	3.64	0.70
MgO	0.74	-
MnO	0.12	0.06
TiO_2	0.72	0.70
P_2O_5	0.13	-
L.O.I.	0.70	0.98
Total:	99.58	96.55
(p.p.m.)		
Rb		11
Sr		425
Ba		330
Zr	n.d.	236
Cu		-
Zn		54
Cr		22
Ni		4
K/Rb		528

TABLE 7 (Cont'd.)

Specimen No. Unit	P70-11 59	GTN29* 60
	C I P W Norms	
Q	18.13	23.24
Or	21.83	4.35
Ab	46.50	62.35
An	4.82	3.42
Ag	-	2.34
Hy	6.52	2.92
Ilm	1.37	1.40
Ap	0.31	-
C	0.53	-

Total iron given as ΣFe_2O_3 and converted to FeO in calculation of CIPW norms.

L.O.I. = Loss on ignition.

P70-1 etc. = Papezik, 1970, anal. 1; presented without BaO, ZrO_2, V_2O_5.

n.d. = not determined.

*Omitted from chemical variation diagrams unless otherwise stated and excluded from calculation of averages (Table 9).

TABLE 7 (Cont'd.)

Volcanic Breccias

Specimen No. Unit	GC33*	WHT*	GTN24n* (15 ft. above 59)	P70-7* (50 ft. above 59)	P70-10* (35 ft. above 60)
(Wt. %)					
SiO_2	73.40	76.20	54.00	62.25	66.07
Al_2O_3	13.70	13.50	15.50	16.74 (1.52)	15.99 (1.70)
ΣFe_2O_3	0.93	1.09	10.39	3.91	2.39
CaO	0.12	0.19	2.03	2.07	3.22
Na_2O	1.76	5.57	6.60	6.67	3.10
K_2O	5.06	4.68	1.48	1.54	2.69
MgO	-	0.60	2.10	2.31	1.40
MnO	0.04	0.03	0.22	0.14	0.12
TiO_2	0.11	0.11	1.26	0.89	0.81
P_2O_5	-	-	0.29	0.30	0.12
L.O.I.	0.84	0.48	1.40	1.32	2.39
Total:	95.96	102.45	95.34	99.66	100.00
(p.p.m.)					
Rb	165	158	30		
Sr	101	97	110		
Ba	1101	989	531		
Zr	46	31	98	n.d.	n.d.
Cu	-	-	18		
Zn	39	28	123		
Cr	17	24	43		
Ni	3	2	15		
K/Rb	255	246	410		

TABLE 7 (Cont'd.)

Specimen No. Unit	GC33*	WHT*	GTN24n* (15 ft. above 59)	P70-7* (50 ft. above 59)	P70-10* (35 ft. above 60)
	C I P W Norms				
Q	45.11	25.69	-	6.83	27.07
Or	31.50	27.19	9.42	9.28	16.34
Ab	15.70	42.57	60.75	57.50	26.93
An	0.63	-	8.59	8.46	15.60
Ag	-	0.77	0.18	-	-
Hy	1.50	2.73	4.09	14.40	9.72
Ilm	0.22	0.20	2.58	1.72	1.58
Ap	-	-	0.72	0.71	0.29
C	5.37	-	-	1.08	2.48

Total iron given as ΣFe_2O_3 and converted to FeO in calculation of CIPW norms.

L.O.I. = Loss on ignition.

P70-1 etc. = Papezik, 1970, anal. 1; presented without BaO, ZrO_2, V_2O_5.

( ) = FeO determined separately.

n.d. = not determined.

*Omitted from chemical variation diagrams unless otherwise stated and excluded from calculation of averages (Table 9).

TABLE 7 (Cont'd.)

	Dacite Flow	Rhyolite Flow	Rhyolite Sills	
Specimen No.	GC12†	GC52 (Biotite Phenocrysts)	GC4*- (East)	GC31 (West)
(Wt. %)				
SiO_2	65.50	72.60	74.30	74.40
Al_2O_3	16.90	14.10	14.60	14.10
ΣFe_2O_3	4.25	1.97	1.82	2.73
CaO	1.22	0.48	0.06	0.55
Na_2O	8.00	7.58	3.20	1.83
K_2O	1.05	0.39	1.67	3.13
MgO	0.83	-	0.20	0.70
MnO	0.07	0.03	0.05	0.07
TiO_2	0.67	0.31	0.07	0.25
P_2O_5	-	-	-	-
L.O.I.	0.91	0.82	1.38	1.08
Total:	99.40	98.28	97.35	98.84
(p.p.m.)				
Rb	44	11	106	116
Sr	204	241	37	265
Ba	331	158	462	972
Zr	183	130	87	149
Cu	-	-	4	7
Zn	49	18	32	30
Cr	23	19	19	18
Ni	5	4	2	2
K/Rb	213	294	131	238

TABLE 7 (Cont'd.)

Specimen No.	GC12‡	GC52 (Biotite Phenocrysts)	GC4*- (East)	GC31 (West)
		C I P W Norms		
Q	8.51	25.41	49.59	48.84
Or	6.33	2.37	10.31	18.99
Ab	69.02	65.94	28.27	15.88
An	6.17	2.45	0.31	2.80
Ag	-	-	-	-
Hy	8.27	2.88	3.64	6.13
Ilm	1.30	0.61	0.14	0.49
Ap	-	-	-	-
C	0.39	0.35	7.74	6.87

Total iron given as ΣFe_2O_3 and converted to FeO in calculation of CIPW norms.

L.O.I. = Loss on ignition.

*Omitted from chemical variation diagrams unless otherwise stated and excluded from calculation of averages (Table 9).

-Albite veins.

‡Analysed by atomic absorption spectrophotometry.

TABLE 7 (Cont'd.)

Porphyrites

Specimen No.	GC6*-	GC7*-	GC8‡	GC10†	GC25*++	GC30*
(Wt. %)						
SiO_2	69.70	66.90	60.90	61.90	50.60	55.50
Al_2O_3	15.90	16.60	16.00	16.30	22.40	17.20
ΣFe_2O_3	6.15	5.19	5.58	5.80	7.02	7.93
CaO	0.55	1.31	4.05	1.53	5.84	2.71
Na_2O	4.73	0.95	2.67	3.30	3.71	4.49
K_2O	2.46	2.78	2.46	4.52	2.55	2.27
MgO	1.20	1.40	1.33	2.57	4.00	3.20
MnO	0.05	0.19	0.08	0.12	0.31	0.19
TiO_2	0.57	0.54	0.55	0.80	0.91	0.81
P_2O_5	-	0.02	0.05	0.04	0.29	-
L.O.I.	0.73	2.52	5.76	2.75	2.33	2.79
Total:	102.03	98.94	99.43	99.63	99.96	97.09
(p.p.m.)						
Rb	89	98	77	150	84	50
Sr	122	74	221	290	484	357
Ba	626	615	542	1767	815	1301
Zr	122	98	119	156	210	122
Cu	6	13	13	26	21	8
Zn	55	78	66	74	123	93
Cr	26	28	25	26	35	39
Ni	5	4	4	9	17	13
K/Rb	230	236	265	250	252	377

Specimen No.	GC6*-	GC7*-	GC8‡	GC10‡	GC25*++	GC30*
		C I P W Norms				
Q	25.38	44.28	23.19	15.06	-	4.91
Or	14.45	17.24	15.63	27.82	15.56	14.36
Ab	39.74	8.43	24.26	28.99	32.38	40.63
An	2.71	6.68	21.23	7.61	27.93	14.38
Ne	-	-	-	-	-	-
Ag	-	-	-	-	-	-
Hy	12.22	12.08	12.64	15.46	8.44	21.48
Ol	-	-	-	-	-	-
Ilm	1.08	1.08	1.12	1.58	1.78	1.65
Ap	-	0.05	0.13	0.10	0.69	-
C	4.42	10.16	1.83	3.40	3.73	2.60

Total iron given as ΣFe_2O_3 and converted to FeO in calculation of CIPW norms.

L.O.I. = Loss on ignition.

*Omitted from chemical variation diagrams unless otherwise stated and excluded from calculation of averages (Table 9).

-Xenolithic/xenocrystic (principally quartz).

++Weathered

‡Analysed by atomic absorption spectrophotometry.

Porphyrites (cont'd.)

Specimen No.	GC40†	GC41†	GC51†	P70-8*-
(Wt. %)				
SiO_2	59.20	61.60	58.40	62.75
Al_2O_3	18.10	16.20	18.10	15.74 (1.24)
ΣFe_2O_3	5.76	5.94	7.80	5.00
CaO	1.60	2.37	1.41	1.80
Na_2O	3.96	4.61	4.19	4.92
K_2O	4.10	1.51	3.60	2.44
MgO	3.00	2.57	2.80	2.62
MnO	0.14	0.12	0.14	0.08
TiO_2	0.67	0.53	0.67	0.70
P_2O_5	0.13	0.09	-	0.23
L.O.I.	3.03	3.82	2.93	2.06
Total:	99.69	99.36	100.04	99.58
(p.p.m.)				
Rb	127	55	116	
Sr	354	322	188	
Ba	1857	339	963	
Zr	165	122	129	n.d.
Cu	13	31	39	
Zn	89	71	79	
Cr	32	29	29	
Ni	14	5	14	
K/Rb	268	228	258	

TABLE 7 (Cont'd.)

Specimen No.	GC40‡	GC41‡	GC51‡	P70-8*-
		C I P W Norms		
Q	9.34	17.03	7.85	13.75
Or	25.24	9.41	22.11	14.88
Ab	34.87	41.08	36.80	42.91
An	7.38	11.76	7.26	7.65
Ne	-	-	-	-
Ag	-	-	-	-
Hy	16.80	16.39	19.74	16.54
Ol	-	-	-	-
Ilm	1.32	1.06	1.32	1.37
Ap	0.31	0.22	-	0.55
C	4.73	3.04	4.93	2.35

Total iron given as ΣFe_2O_3 and converted to FeO in calculation of CIPW norms.

L.O.I. = Loss on ignition.

P70-1 etc. = Papezik, 1970, anal. 1; presented without BaO, ZrO_2, V_2O_5.

( ) = FeO determined separately.

n.d. = not determined.

*Omitted from chemical variation diagrams unless otherwise stated and excluded from calculation of averages (Table 9).

-Xenolithic/xenocrystic.

‡Analysed by atomic absorption spectrophotometry.

TABLE 7 (Cont'd.)

Specimen No.	Porphyritic Sill (Western Block) P70-4 (a)	(b)	Olivine Diabase (Cumulate Rock) NX17‡ (a)	(b)
(Wt. %)				
SiO_2	50.91	53.33	45.40	47.64
Al_2O_3	17.84	18.69	13.80	14.48
ΣFe_2O_3	(4.67)	-	10.86	-
ΣFeO	(5.47)	10.13	-	10.26
CaO	5.75	6.03	7.25	7.61
Na_2O	5.10	5.34	1.90	1.99
K_2O	0.70	0.73	2.46	2.58
MgO	4.27	4.47	12.85	13.48
MnO	0.09	0.09	0.25	0.26
TiO_2	0.86	0.90	0.88	0.92
P_2O_5	0.28	0.29	0.73	0.78
L.O.I.	3.28	-	4.81	-
Total:	99.22	100.00	101.19	100.00
(p.p.m.)				
Rb			54	
Sr			457	
Ba			1997	
Zr		n.d.	159	
Cu			30	
Zn			103	
Cr			559	
Ni			458	
K/Rb			378	

TABLE 7 (Cont'd.)

Specimen No.	P70-4	NX17[‡]
	C I P W Norms	
Q	-	-
Or	4.84	15.27
Ab	45.20	14.63
An	24.85	22.94
Ne	-	1.21
Ag	2.62	7.94
Hy	1.73	-
Ol	18.87	34.48
Ilm	1.71	1.75
Ap	0.68	1.78
C	-	-

Total iron given as ΣFe_2O_3 and converted to FeO in calculation of CIPW norms.

L.O.I. = Loss on ignition.

ΣFeO = total iron given as FeO.

[‡]Analysed by atomic absorption spectrophotometry.

(a) Includes volatiles.

(b) Recalculated to 100% on a volatile-free basis.

( ) = Fe determined separately.

P70-1 etc. = Papezik, 1970, anal. 1; presented without BaO, ZrO_2, V_2O_5.

n.d. = not determined.

TABLE 7 (Cont'd.)

Diabase Dykes

Specimen No.	GC2 ‡ (a)	GC2 ‡ (b)	GC9*	GC11† (a)	GC11† (b)	GC13 (a)	GC13 (b)	GC21*
(Wt. %)								
SiO_2	51.00	52.79	47.80	47.20	49.78	47.50	50.74	53.70
Al_2O_3	17.10	17.70	15.30	16.20	17.08	18.20	19.44	16.00
ΣFe_2O_3	7.49	-	11.67	12.51	-	12.02	-	7.49
ΣFeO	-	6.17	-	-	11.87	-	11.56	-
CaO	9.31	9.62	6.23	6.72	7.08	3.63	3.88	3.64
Na_2O	4.18	4.35	4.31	4.35	4.59	5.45	5.82	5.19
K_2O	1.20	1.24	1.04	0.73	0.77	0.87	0.93	1.52
MgO	4.88	5.09	3.90	5.70	6.01	4.70	5.02	4.80
MnO	0.18	0.19	0.24	0.19	0.20	0.34	0.37	0.20
TiO_2	1.55	1.60	1.88	2.05	2.16	1.75	1.87	1.13
P_2O_5	0.45	0.46	0.41	0.43	0.46	0.34	0.37	0.28
L.O.I.	3.31	-	3.10	3.20	-	3.68	-	3.10
Total:	100.65	100.00	95.88	99.28	100.00	98.48	100.00	97.05
(p.p.m.)								
Rb		12	27	20		33		29
Sr		736	368	249		264		400
Ba		250	528	393		283		577
Zr		209	158	165		167		233
Cu		79	68	60		72		50
Zn		96	98	106		120		29
Cr		80	66	64		129		76
Ni		29	36	38		75		65
K/Rb		830	320	303		219		435

TABLE 7 (Cont'd.)

Specimen No.	GC2‡	GC9*	GC11‡	GC13	GC21*
			C I P W Norms		
Q	-	-	-	-	-
Or	7.35	6.72	4.55	5.50	9.65
Ab	35.48	39.80	35.40	44.93	47.11
An	25.22	21.10	23.75	16.86	17.03
Ne	0.62	-	1.85	2.35	-
Ag	16.09	8.18	7.03	-	0.31
Hy	-	3.54	-	-	18.88
Ol	11.15	15.72	22.27	23.29	4.02
Ilm	3.01	3.90	4.09	3.55	2.30
Ap	1.08	1.04	1.05	0.84	0.70
C	-	-	-	-	-

Total iron given as ΣFe_2O_3 and converted to FeO in calculation of CIPW norms.

ΣFeO = total iron given as FeO.

L.O.I. = Loss on ignition.

*Omitted from chemical variation diagrams unless otherwise stated and excluded from calculation of averages (Table 9).

‡Analysed by atomic absorption spectrophotometry.

(a) Includes volatiles.

(b) Recalculated to 100% on a volatile-free basis.

TABLE 7 (Cont'd.)

Diabase Dykes (cont'd.)

Specimen No.	GC26‡ (a)	GC26‡ (b)	GTN31t*	GTN31u*	H165‡ (a)	H165‡ (b)
(Wt. %)						
SiO_2	50.20	52.49	52.10	51.20	49.00	52.58
Al_2O_3	17.20	17.99	16.30	19.00	18.10	19.41
ΣFe_2O_3	9.53	-	10.57	8.43	9.21	-
ΣFeO	-	8.97	-	-	-	8.90
CaO	4.20	4.39	1.36	1.53	4.45	4.78
Na_2O	5.56	5.82	6.39	5.59	6.00	6.44
K_2O	1.09	1.14	0.52	1.35	1.06	1.14
MgO	6.72	7.03	4.00	4.40	3.92	4.21
MnO	0.18	0.19	0.36	0.42	0.28	0.30
TiO_2	1.42	1.49	0.97	1.09	1.76	1.89
P_2O_5	0.46	0.49	0.14	0.13	0.33	0.35
L.O.I.	3.87	-	3.53	3.83	5.41	-
Total:	100.43	100.00	96.24	96.97	99.52	100.00
(p.p.m.)						
Rb		20	17	56		40
Sr		321	179	215		305
Ba		532	347	420		349
Zr		178	91	119		170
Cu		39	68	54		68
Zn		107	111	224		110
Cr		98	95	86		110
Ni		76	36	27		70
K/Rb		452	254	200		220

TABLE 7 (Cont'd.)

Specimen No.	GC26‡	GTN31t*	GTN31u*	H165‡
		C I P W Norms		
Q	-	-	-	-
Or	6.74	3.36	8.65	6.73
Ab	44.32	58.99	51.24	44.31
An	18.64	6.36	7.30	20.74
Ne	2.63	-	-	5.51
Ag	-	-	-	0.53
Hy	-	15.76	18.24	-
Ol	23.28	9.80	5.64	17.78
Ilm	2.92	2.01	2.24	3.59
Ap	1.12	0.35	0.33	0.82
C	-	3.37	6.36	-

Total iron given as ΣFe_2O_3 and converted to FeO in calculation of CIPW norms.

ΣFeO = total iron given as FeO.

L.O.I. = Loss on ignition.

*Omitted from chemical variation diagrams unless otherwise stated and excluded from calculation of averages (Table 9).

‡Analysed by atomic absorption spectrophotometry.

(a) Includes volatiles.

(b) Recalculated to 100% on a volatile-free basis.

TABLE 7 (Cont'd.)

Basalts

Specimen No.	NX12‡ (a)	NX12‡ (b)	NX14 (a)	NX14 (b)	NX15+ (a)	NX15+ (b)
(Wt. %)						
SiO_2	48.00	50.69	47.00	49.38	51.60	53.77
Al_2O_3	16.20	17.04	17.40	18.28	17.30	18.03
ΣFe_2O_3	12.71	-	12.17	-	10.05	-
ΣFeO	-	12.04	-	11.52	-	9.53
CaO	5.87	6.17	6.80	7.15	2.82	2.94
Na_2O	4.45	4.68	3.53	3.71	3.47	3.62
K_2O	0.27	0.28	0.53	0.56	5.39	5.61
MgO	6.29	6.62	6.80	7.15	4.50	4.70
MnO	0.18	0.19	0.18	0.19	0.19	0.20
TiO_2	1.84	1.93	1.51	1.59	1.05	1.10
P_2O_5	0.35	0.36	0.44	0.47	0.50	0.50
L.O.I.	4.34	-	3.74	-	3.03	-
Total:	100.50	100.00	100.10	100.00	99.90	100.00
(p.p.m.)						
Rb	13		25		111	
Sr	225		379		246	
Ba	242		285		2258	
Zr	103		113		126	
Cu	50		43		23	
Zn	120		110		102	
Cr	188		143		93	
Ni	147		144		66	
K/Rb	172		176		403	

TABLE 7 (Cont'd.)

Specimen No.	NX12‡	NX14	NX15+
		C I P W Norms	
Q	-	-	-
Or	1.68	3.30	33.26
Ab	39.67	31.39	29.07
An	24.70	31.61	11.18
Ne	-	-	0.84
Ag	2.98	0.69	-
Hy	4.07	8.17	-
Ol	22.36	20.73	20.46
Ilm	3.68	3.01	2.08
Ap	0.86	1.07	1.21
C	-	-	1.90

Total iron given as ΣFe_2O_3 and converted to FeO in calculation of CIPW norms.

ΣFeO = total iron given as FeO.

L.O.I. = Loss on ignition.

+K-feldspar filling amygdales.

‡Analysed by atomic absorption spectrophotometry.

(a) Includes volatiles.

(b) Recalculated to 100% on a volatile-free basis.

TABLE 7 (Cont'd.)

Basalts (cont'd.)

Specimen No.	P70-1 (a)	P70-1 (b)	P70-2 (a)	P70-2 (b)	P70-3 (a)	P70-3 (b)
(Wt. %)						
SiO_2	48.13	50.03	49.29	52.30	49.42	51.60
Al_2O_3	20.14	20.94	18.32	19.18	15.95	16.66
ΣFe_2O_3	(1.36)	-	(9.22)	-	(7.22)	-
ΣFeO	(5.74)	7.24	(0.52)	9.23	(3.77)	10.72
CaO	6.43	6.69	6.74	7.06	6.28	6.56
Na_2O	4.35	4.53	4.78	5.01	4.54	4.75
K_2O	1.16	1.20	0.79	0.83	1.50	1.57
MgO	6.32	6.57	4.82	5.05	5.78	6.04
MnO	0.18	0.19	0.07	0.07	0.06	0.06
TiO_2	2.14	2.22	1.04	1.08	1.61	1.68
P_2O_5	0.38	0.39	0.18	0.19	0.35	0.36
L.O.I.	3.15	-	2.38	-	4.10	-
Total:	99.48	100.00	99.22	100.00	100.58	100.00
(p.p.m.)						
Rb						
Sr						
Ba						
Zr	n.d.		n.d.		n.d.	
Cu						
Zn						
Cr						
Ni						
K/Rb						

TABLE 7 (Cont'd.)

Specimen No.	P70-1	P70-2	P70-3
		C I P W Norms	
Q	-	-	-
Or	7.06	4.95	9.26
Ab	34.24	39.68	35.23
An	30.27	27.77	19.53
Ne	1.97	1.73	2.64
Ag	-	5.31	8.81
Hy	-	-	-
Ol	20.39	17.97	20.49
Ilm	4.18	2.09	3.12
Ap	0.91	0.44	0.85
C	0.98	-	-

Total iron given as ΣFe_2O_3 and converted to FeO in calculation of CIPW norms.

ΣFeO = total iron given as FeO.

L.O.I. = Loss on ignition.

P70-1 etc. = Papezik, 1970, anal. 1; presented without BaO, ZrO_2, V_2O_5.

( ) = Fe determined separately.

n.d. = not determined.

(a) Includes volatiles.

(b) Recalculated to 100% on a volatile-free basis.

TABLE 8. CORRELATION MATRICES FOR 82 WHOLE-ROCK ANALYSES OF HARBOUR MAIN GROUP VOLCANIC ROCKS, COLLIERS PENINSULA

	SiO_2	Al_2O_3	ΣFe_2O_3	CaO	Na_2O	K_2O	MgO	MnO	TiO_2	P_2O_5	Rb	Sr	Ba	Zr	Cu	Zn	Cr	Ni
Ni	-51	10	45	45	-16	-15	69	52	27	65	-11	39	17	6	32	41	99	100
Cr	-48	8	42	42	-15	-14	66	54	26	62	- 7	45	21	15	36	47	100	
Zn	-27	19	30	15	12	-14	26	55	27	26	12	65	26	61	62	100		
Cu	-42	30	42	40	2	-21	39	68	43	41	- 9	52	-1	27	100			
Zr	37	-34	-36	-36	-16	27	29	-7	-34	-33	63	58	61	100				
Ba	35	-29	-34	-40	-59	74	-19	-19	-48	-24	84	21	100					
Sr	-20	9	15	26	- 8	-14	24	38	12	24	13	100						
Rb	52	-31	-48	-50	-70	80	-39	-32	-58	-47	100							
P_2O_5	-90	59	85	85	3	-37	90	74	78	100								
TiO_2	-87	73	88	81	31	-58	72	76	100									
MnO	-75	67	75	61	15	-34	68	100										
MgO	-93	60	86	86	- 2	-42	100											
K_2O	52	-29	-50	-53	-71	100												
Na_2O	-16	14	14	3	100													
CaO	-92	67	87	100														
ΣFe_2O_3	-95	79	100															
Al_2O_3	-79	100																
SiO_2	100																	

Total iron given as ΣFe_2O_3. Values given above are expressed as 100x product-moment correlation coefficient (r). All values for r greater than ±22 are significant at the 95% level of confidence (c.f. Dixon and Massey, 1957, Table A30a).

TABLE 9. TABLE OF AVERAGES

Specimen No.	POR-Q		FHS-R		FHS-S		FHS-T		FHS-U	
Unit(s)			59 (upper flow unit)		59 (lower flow unit)		43		42	
No. of Analyses	(5)		(4)		(2)		(2)		(2)	
	(a)	(b)	(a)	(b)	(a)	(b)	(a)	(b)	(a)	(b)
(Wt. %)										
SiO_2	60.40	62.93	65.70	67.18	68.00	69.77	69.30	69.98	69.95	71.89
Al_2O_3	16.94	17.65	14.98	15.32	14.10	14.47	14.80	14.95	13.95	14.34
ΣFe_2O_3	6.18	6.44	4.80	4.91	3.83	3.93	3.73	3.77	3.00	3.08
CaO	2.19	2.28	1.06	1.08	1.39	1.43	1.18	1.19	1.10	1.13
Na_2O	3.75	3.91	7.20	7.36	7.20	7.39	6.05	6.11	4.51	4.63
K_2O	3.24	3.38	1.69	1.73	0.75	0.77	1.61	1.63	2.60	2.67
MgO	2.45	2.55	1.33	1.36	1.32	1.35	1.70	1.72	1.61	1.65
MnO	0.12	0.13	0.10	0.10	0.13	0.13	0.07	0.07	0.09	0.09
TiO_2	0.64	0.67	0.85	0.87	0.74	0.76	0.57	0.58	0.51	0.52
P_2O_5	0.06	0.06	0.09	0.09	-	-	-	-	-	-
L.O.I.	3.66	-	1.12	-	1.32	-	1.55	-	2.21	-
Total:	99.63	100.00	98.92	100.00	98.78	100.00	100.56	100.00	99.53	100.00

TABLE 9. TABLE OF AVERAGES (Cont'd.)

Specimen No.	POR-Q	FHS-R	FHS-S	FHS-T	FHS-U
Unit(s)		59 (upper flow unit)	59 (lower flow unit)	43	42
No. of Analyses	(5)	(4)	(2)	(2)	(2)
(p.p.m.)					
Rb	105	26	12	33	108
Sr	275	125	176	324	246
Ba	1094	567	235	1049	720
Zr	138	166	161	180	198
Cu	24	10	51++	14	6
Zn	75	99	88	58	60
Cr	28	30	27	28	22
Ni	9	9	7	10	6
K/Rb	254(228-268)+	548(504-603)+	565(506-623)+	405(341-492)+	199(190-207)+
Rb/Sr	0.38	0.21	0.07	0.10	0.44
Ba/Sr	3.98	4.54	1.34	3.24	2.93

TABLE 9. TABLE OF AVERAGES (Cont'd.)

Specimen No. Unit(s)	POR-Q	FHS-R 59 (upper flow unit)	FHS-S 59 (lower flow unit)	FHS-T 43	FHS-U 42
No. of Analyses	(5)	(4)	(2)	(2)	(2)
			C I P W Norms		
Q	12.84	10.82	17.00	20.73	27.88
Or	19.17	10.27	4.57	9.66	15.85
Ab	34.45	62.60	62.75	51.90	39.33
An	11.56	3.66	4.06	5.94	5.63
Ag	-	0.96	2.56	-	-
Hy	17.10	9.81	7.61	9.72	8.55
Ilm	1.34	1.66	1.45	1.10	1.00
Ap	0.12	0.22	-	-	-
C	3.42	-	-	0.97	1.77

Total iron given as ΣFe_2O_3 and converted to FeO in calculation of CIPW norms.

L.O.I. = Loss on ignition.

+Range of values.

++Anomalously high Cu value of GTN34 (102 p.p.m.).

(a) Includes volatiles

(b) Recalculated to 100% on a volatile-free basis.

TABLE 9. TABLE OF AVERAGES (Cont'd.)

							Holyrood Pluton			
Specimen No.	WHS-V		WHS-W		BCS-X		Y		Z	
Unit(s)	28,39,40		19,21,23,24,29 31,36,37,38		3,5,6		"Granite"		"Quartz-Monzonite"	
No. of Analyses	(4)		(13)		(5)		(25[x])		(7[x])	
	(a)	(b)	(a)	(b)	(a)	(b)	(a)	(b)	(a)	(b)
(Wt. %)										
SiO_2	71.80	72.89	73.02	74.30	70.84	71.84	72.36	72.76	68.83	71.15
Al_2O_3	14.30	14.52	14.20	14.45	14.56	14.77	14.14	14.22	13.62	14.09
ΣFe_2O_3	2.45	2.49	2.25	2.29	3.42	3.47	1.68	1.69	2.76	2.85
CaO	0.42	0.43	0.62	0.63	0.73	0.74	1.59	1.60	1.98	2.05
Na_2O	5.29	5.37	2.95	3.00	4.05	4.11	4.31	4.33	4.38	4.53
K_2O	3.43	3.48	4.49	4.57	3.76	3.81	4.19	4.21	3.76	3.87
MgO	0.45	0.46	0.46	0.47	0.71	0.72	0.95	0.96	1.00	1.03
MnO	0.05	0.05	0.05	0.05	0.05	0.05	0.09	0.09	0.09	0.09
TiO_2	0.31	0.31	0.24	0.24	0.48	0.49	0.12	0.12	0.20	0.21
P_2O_5	-	-	-	-	-		0.02	0.02	0.13	0.13
L.O.I.	0.61	-	1.15	-	1.08		0.90	-	1.98	-
Total:	99.11	100.00	99.43	100.00	99.68	100.00	100.35	100.00	98.73	100.00

TABLE 9. TABLE OF AVERAGES (Cont'd.)

Specimen No. Unit(s)	WHS-V 28,39,40	WHS-W 19,21,23,24,29 31,36,37,38	BCS-X 3,5,6	Holyrood Pluton Y "Granite"	Holyrood Pluton Z "Quartz-Monzonite"
No. of Analyses	(4)	(13)	(5)	(25^x)	(7^x)
(p.p.m.)					
Rb	79	139*	124	125	108
Sr	150	146*	161	110	228
Ba	1232	1288*	1365	1181*	1774
Zr	183	182*	174	138	117
Cu	5	11*	6	0	8
Zn	52	48*	54	14	31
Cr	19	19*	21	16	26
Ni	4	3*	4	0	21
K/Rb	313(219-368)+	255(193-339)+	252(220-277)+	294(224-423)+	314(245-376)+
Rb/Sr	0.53	0.95	0.77	1.14	0.47
Ba/Sr	8.21	8.82	8.48	10.74	7.78

TABLE 9. TABLE OF AVERAGES (Cont'd.)

Specimen No.	WHS-V	WHS-W	BCS-X	Holyrood Pluton Y	Holyrood Pluton Z
Unit(s)	28,39,40	19,21,23,24,29, 31,36,37,38	3,5,6	"Granite"	"Quartz-Monzonite"
No. of Analyses	(4)	(13)	(5)	(25^x)	(7^x)
		C I P W	Norms		
Q	25.11	35.79	28.50	25.60	22.95
Or	20.65	27.09	22.64	24.96	23.05
Ab	45.55	25.45	34.87	36.73	38.41
An	2.12	3.14	3.69	6.90	6.62
Ag	-	-	-	0.76	2.26
Hy	4.83	4.65	6.84	4.77	6.00
Ilm	0.60	0.47	0.93	0.23	0.39
Ap	-	-	-	0.05	0.31
C	1.14	3.42	2.54	-	-

Total iron given as ΣFe_2O_3 and converted to FeO in calculation of CIPW norms.

L.O.I. = Loss on ignition.

*Average of 12 analyses.

+Range of values.

-Only 1 analysis presented.

xTaken from Strong (unpublished data); rock names based on field criteria of Strong et al., 1973.

(a) Includes volatiles.

(b) Recalculated to 100% on a volatile-free basis.

FIG 6 MAJOR ELEMENTS VS SILICA FOR HARBOUR MAIN GROUP VOLCANIC ROCKS, COLLIERS PENINSULA

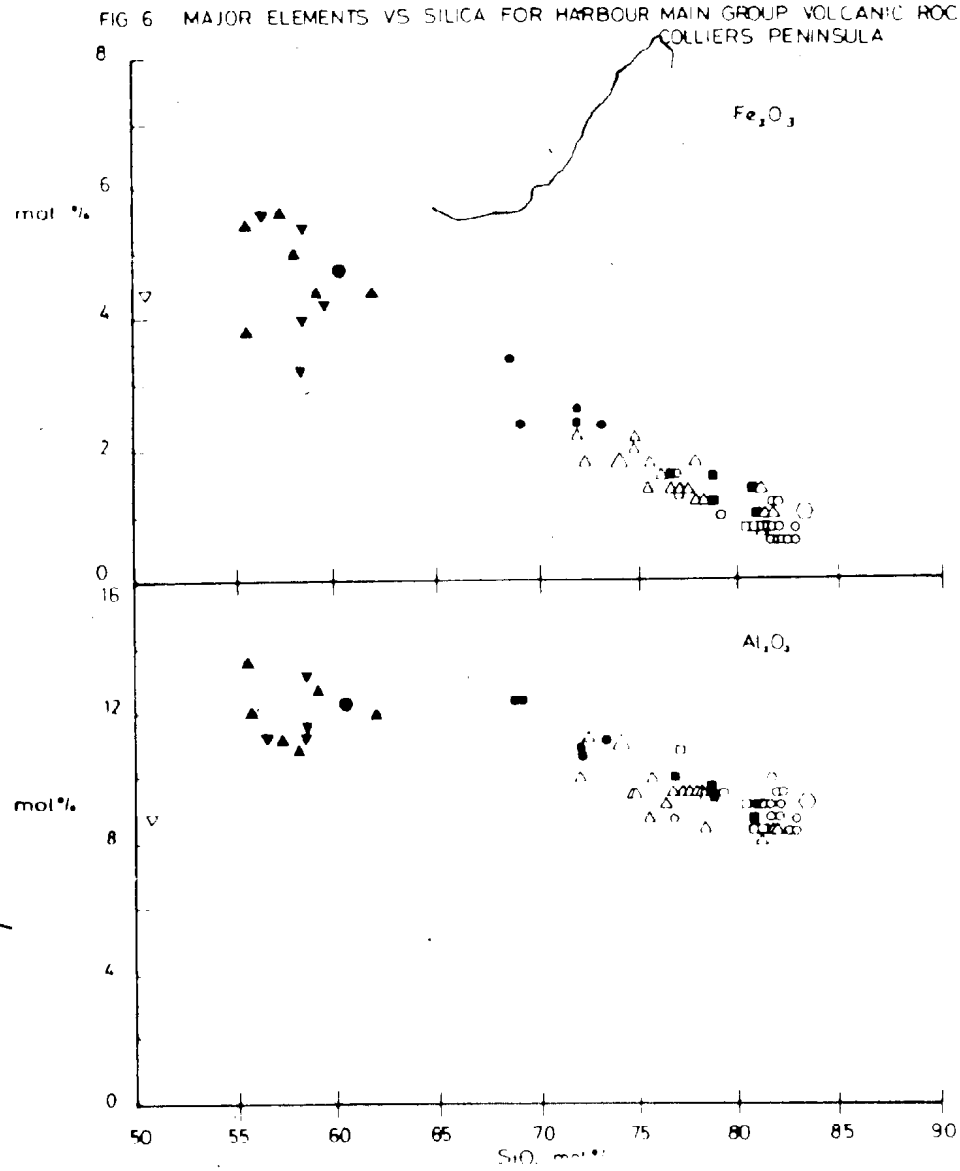

FIG 6 (cont.)

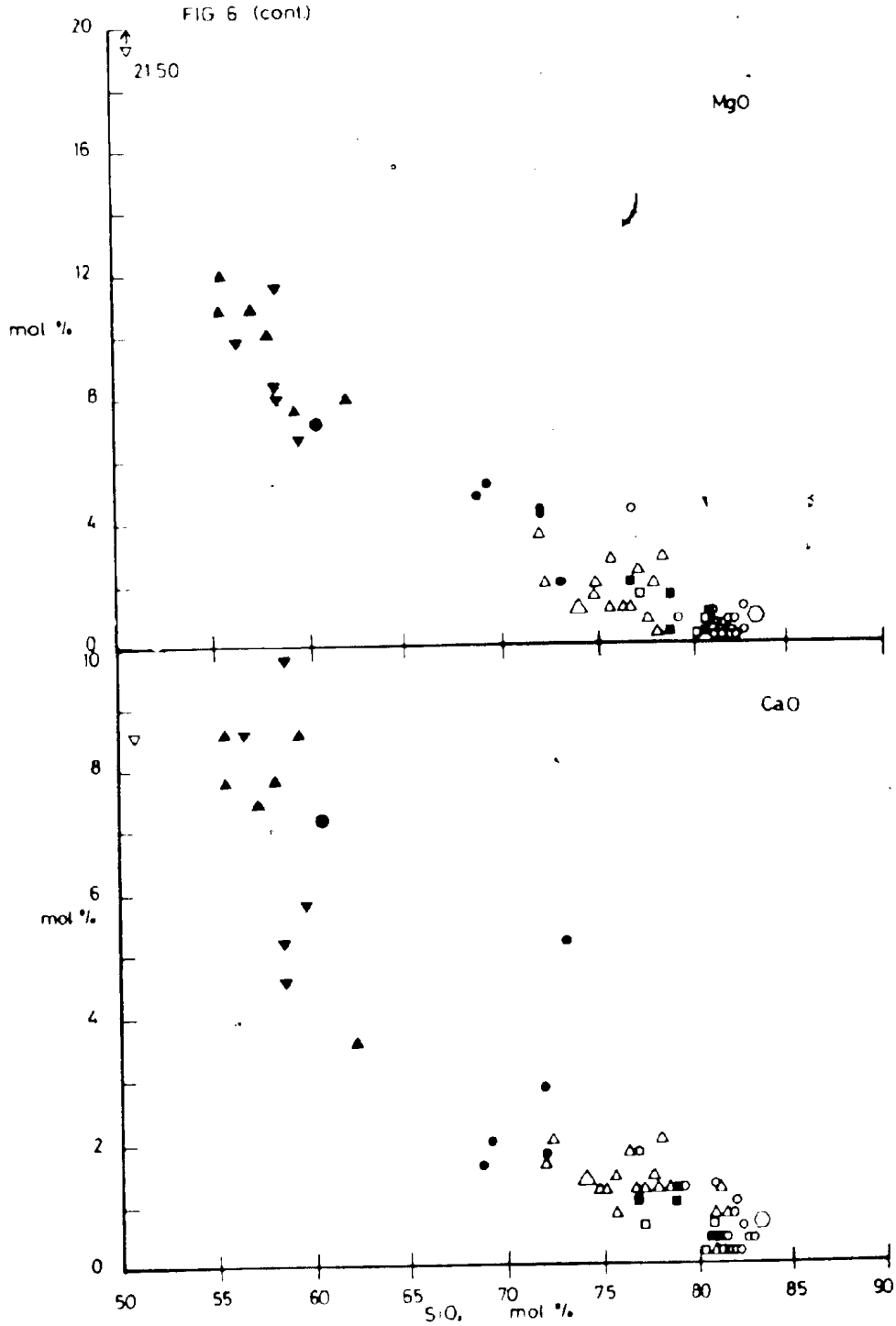
21.50
MgO
mol %
CaO
mol %
SiO_2 mol %
20
16
12
8
4
0
10
8
6
4
2
0
50
55
60
65
70
75
80
85
90

FIG 6 (cont.)

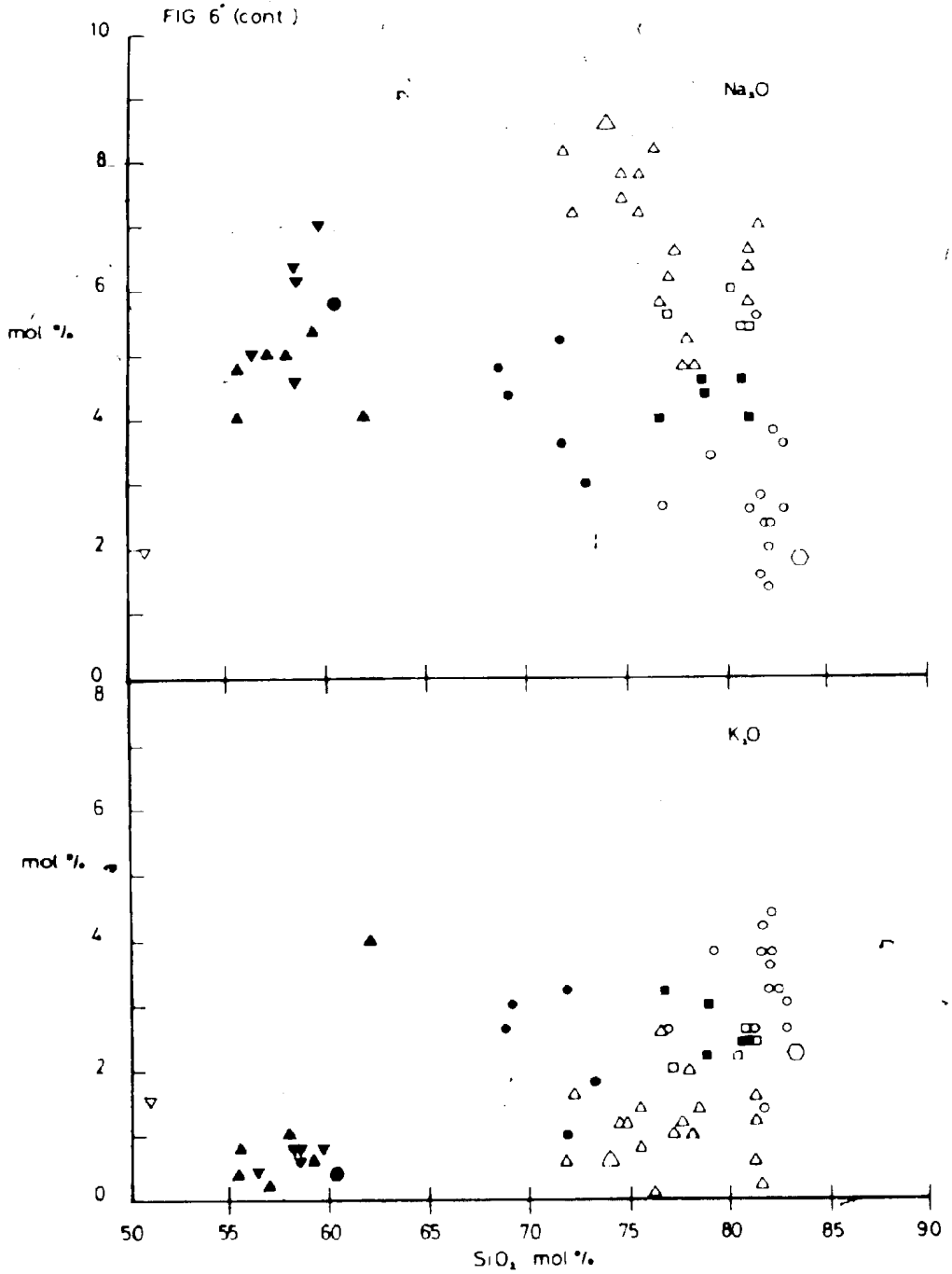

FIG 6 (cont.)

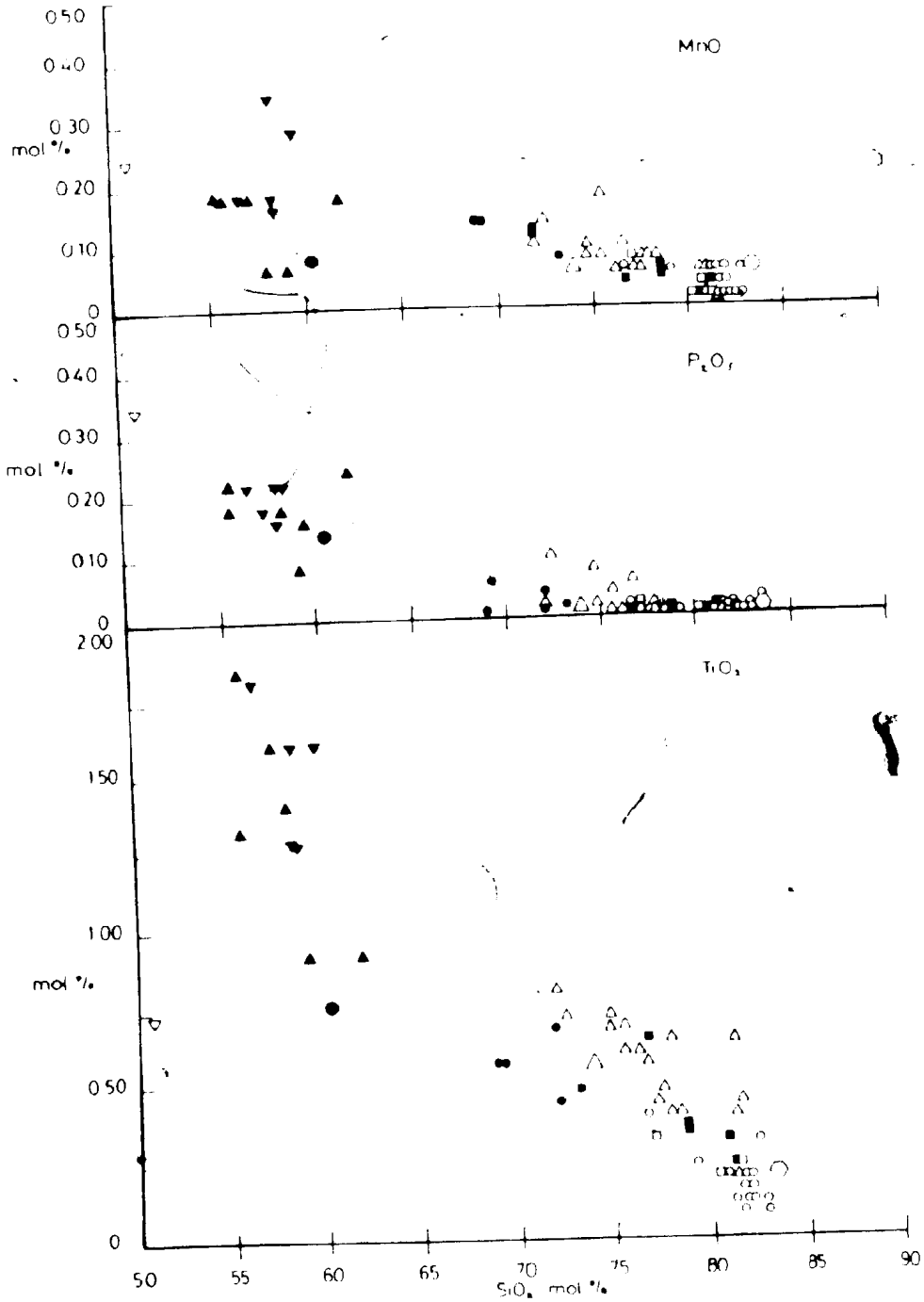
MnO
P_2O_5
TiO_2
mol %
0.50
0.40
0.30
0.20
0.10
0
2.00
1.50
1.00
50
55
60
65
70
75
80
85
90
SiO_2 mol %

FIG 6 (cont.)

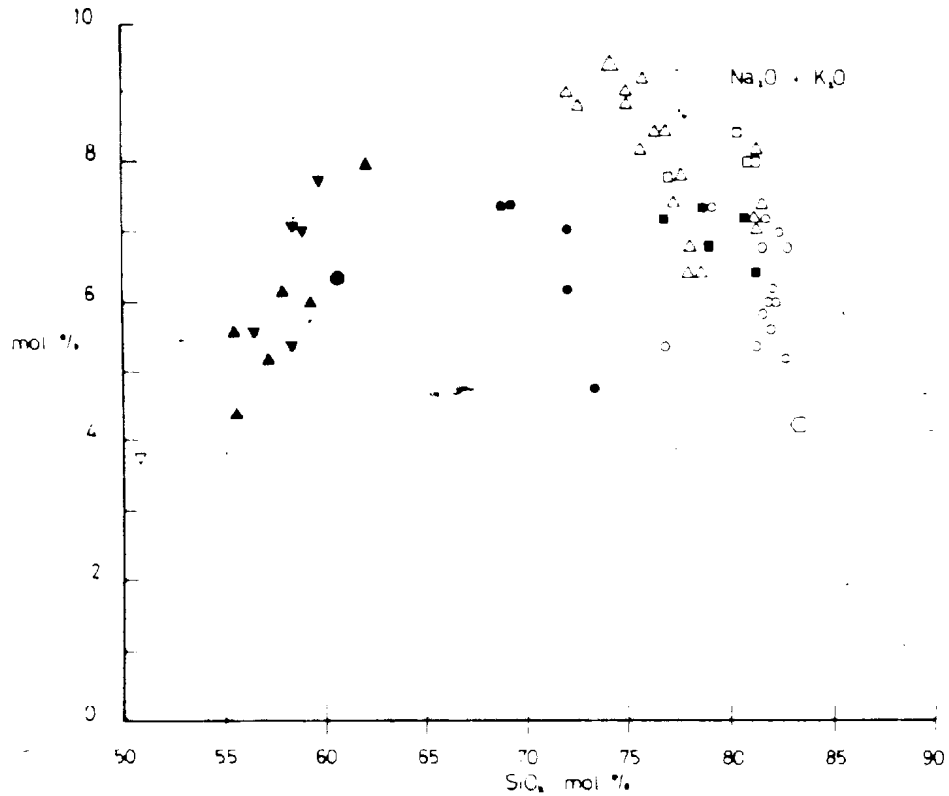

KEY

▲ Basalts ▼ Dykes ▽ Cumulate rock ■ Porphyrites

□ Rhyolite sill △ Finn Hill ash-flow sequence △ Dacite flow

□ Weavers Hill ash-flow sequence (biotite phenocrysts)

○ Weavers Hill ash-flow sequence ■ Bacon Cove ash-flow sequence

● Porphyritic intrusive (Western Block)

The analytical work was carried out using techniques similar to those described by Strong et al. (1973). The alkalies, MnO, and 20 whole-rock analyses (noted in table 7) were determined by atomic absorption spectrophotometry. All other elements were determined by X-ray fluorescence using a Phillips P.W. 1220-C computerised spectrometer. Values obtained for loss on ignition (L.O.I.) include H_2O+, H_2O-, and CO_2. Full analytical procedures are given in Appendix 3, and estimations of the precision and accuracy of the data are presented in tables 19-20.

Methods of bivariate statistical analysis were used to compute correlation matrices for major and trace elements (table 8). Table 9 contains average whole-rock compositions for the major petrographic/stratigraphic groupings of rock-types described earlier. The "average granite" and "average quartz-monzonite" of the Holyrood Plutonic Series (McCartney, 1967) are also included, and were compiled from data of Strong et al. (1973). Average compositions for the basaltic rocks are presented elsewhere (table 12). Tables 10-15 contain a compilation of average compositions of volcanic and plutonic rocks from different geologic environments, and are used for comparison purposes.

Difficulty is often encountered in presenting a large quantity of compositional data in a clear and meaningful manner. The use of appropriate geochemical variation diagrams are of great value and help to clarify compositional variability. Plots of the major oxides are given in figs. 6-12 and 17-19. Analyses with totals outside the range 98-102 wt. % oxides were omitted from the plots and calculation of average compositions. Since values for K_2O, Na_2O, MnO, and L.O.I.

were determined independently, these data are reliable.

Trace element abundances are plotted in figs. 13-16, and discussion of these data follows that for the major oxides of each rock-type. A guide to the theoretically predicted behaviour of trace elements determined in this study is provided in Appendix 4.

8.2.1. Rhyolitic Ignimbrites

Representative sampling of ignimbrites is fraught with difficulties since the very mechanism of ash-flow eruption provides an ideal opportunity for admixing of variable proportions of xenocrysts, xenoliths, and juvenile volcanic material. It may also promote crystal concentration due to gravitative settling or eolian differentiation of the fine ash fraction, thereby modifying original magmatic compositions (cf. Walker, 1972; Lipman, 1967; and section 2.3.). Individual cooling units may also record variations in magmatic composition; this is considered the case for a multiple flow cooling unit in the Finn Hill sequence (unit 59). However, this unit is severely altered in the area of most intense sampling and the validity of this suggestion must await consideration of the relative mobilities of oxide components during alteration (discussed below).

Careful choice of rock chips for analysis reduced the amount of xenolithic material to a minimum. Minor proportions of accessory rock fragments were probably the main source of contamination, though their effect would have been greatly reduced by dilution. Lithic lapilli of accidental origin, particularly basaltic fragments, would result in

more serious sampling error. Anomalously high concentrations of MgO among the major elements, and Ni, Cr, and Cu among the trace elements proved a reliable index to significant levels of contamination (cf. analyses GTN16, GTN231, and GTN34, table 7). Xenocrystic material was identified under the microscope (for example, GC6 and GC7).

Certain samples have been locally altered by metasomatic processes. Prior consideration of the chemical effects of the metasomatism will greatly reduce erroneous classification of magmatic trends and affinities (discussed later).

8.2.1.1. Chemical Effects of Alteration

The ideal platform for a study of chemical processes of alteration in volcanic assemblages of the Harbour Main Group is a precise knowledge of the composition of freshly erupted material. However, it is highly unlikely that rocks of such antiquity preserve totally "pristine" magmatic compositions. Alteration detected in this study is primarily a result of secondary hydrothermal reconstitution of glassy ignimbrites. The possible effects of earlier alteration cannot be distinguished; for example, extensive degassing of magmatic volatiles during eruption and their sustained mobility during initial cooling and devitrification of ash-flow sheets may result in alkali-exchange between aqueous pore fluids and reactive glass in the interior of cooling units (Friedman and Smith, 1958; Ross and Smith, 1961; Lipman, 1965; Noble *et al.*, 1967; Scott, 1966, 1971). Secondary hydration of volcanic glass also involves hydrolysis and cation-exchange reactions

(notably of Na^+ and K^+), and may lead to preferential leaching of alkalies in permeable and/or porous zones and modification of Fe_2O_3/FeO ratios (Friedman et al., 1966; Noble, 1965, 1967; Lipman, 1965). The course of hydrothermal alteration is largely controlled by the composition of the attendant fluids and their ability to differentiate during solution/solute interaction (Orville, 1963; Martin, 1969; Lofgren, 1971a). Several recent studies of alteration processes at low to moderate temperatures demarcate the nature of the compositional changes that take place in rhyolitic volcanic rocks.

Anderson (1968) pointed out the wide variability of K_2O/Na_2O ratios in Late Precambrian andesitic and rhyolitic rocks of the Yavapai Supergroup, central Arizona, in comparison with young obsidians from Mono Craters, Medicine Lake, Newberry, and Yellowstone. Most of the major elements showed a wide scatter apart from essentially constant Al_2O_3 and overall gain of H_2O+.

Lipman (1965) examined compositional differences between pairs of crystalline and hydrated rhyolitic glasses in Miocene to Recent volcanic rocks from southern Nevada. Apart from addition of CO_2 (now in calcium carbonate) and H_2O+, glassy samples showed significant modification of K_2O/Na_2O ratios relative to crystalline material. Densely welded crystallised tuffs and vitrophyres exhibited very little scatter of alkalies and preserved original magmatic K_2O/Na_2O variations. Loss of SiO_2 (several percent) and Na_2O (up to 0.5 wt. %) in glassy samples was directly proportional to surface area, and poorly welded zones were particularly susceptible to leaching. Part of the

Na_2O leached from the glass was replaced by K_2O during a period of K-metasomatism. No significance was attached to barely detectable variations of Al_2O_3, TiO_2, and MnO between crystallised and glassy rhyolites; however, slight modification of CaO, MgO, and total Fe were detected in some samples. Variable Fe_2O_3/FeO was attributed to conversion of magnetite crystallites in black vitrophyres to hematite in reddened crystallised horizons.

Scott (1966, 1971) recorded similar compositional heterogeneities in Tertiary ignimbrites of the Grant Range, east-central Nevada. He found that patterns produced by deuteric alteration and weathering formed distinct, direct and inverse relationships with density or the degree of welding of the ignimbrite. Ionic exchange between alkalies resulted in a negative slope on a K/Na plot (moles/kg rock) with a value close to -1 (Scott, 1971, fig. 9). A steep positive slope was obtained by preferential leaching of Na^+ relative to K^+. Least scatter was found in the abundances of Al_2O_3, MgO, and CaO. Moreover, Scott (1971, p. 109) remarked that "if ignimbrites without non-hydrated glasses are the subject of petrological study, the primary devitrification zones within thin (<100ft) highly welded units represent the best sampling choices.".

The most obvious effect of alteration in Harbour Main ignimbrites is secondary hydration, since natural rhyolitic glasses normally contain only a few tenths of a percent magmatic volatiles (Ross and Smith, 1955; Friedman et al., 1966). Relict perlitic fractures in ignimbrites with 0.5 wt. % L.O.I. or less, strongly suggest devitrification

FIG 7a QZ AB OR DIAGRAM FOR FELSIC VOLCANIC ROCKS

(C P W Norms)

(QZ + AB + OR > 80%)

Main Compositional Fields

- - Weavers Hill ash-flow sequence (biotite phenocryst)

Bacon Cove ash-flow sequence

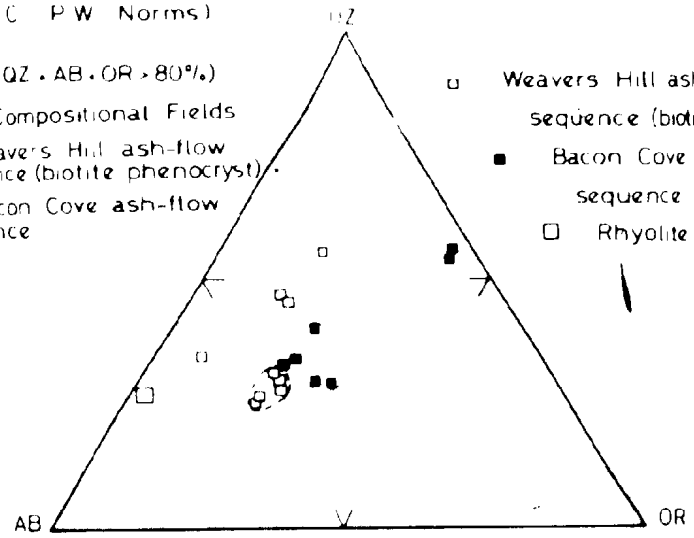

□ Weavers Hill ash-flow sequence (biotite phenocrysts)

■ Bacon Cove ash-flow sequence

□ Rhyolite flow

FIG 7b QZ AB OR DIAGRAM FOR FELSIC VOLCANIC ROCKS

(C I P W Norms)

(QZ + AB + OR > 80%)

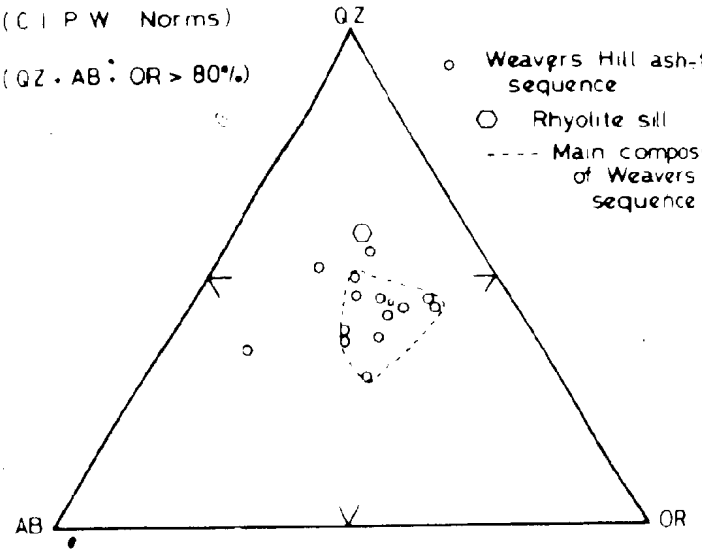

○ Weavers Hill ash-flow sequence

○ Rhyolite sill

- - - - Main compositional field of Weavers Hill ash-flow sequence

FIG 7c QZ AB OR DIAGRAM FOR FELSIC VOLCANIC ROCKS

(C I P W Norms)

(QZ + AB + OR > 80%)

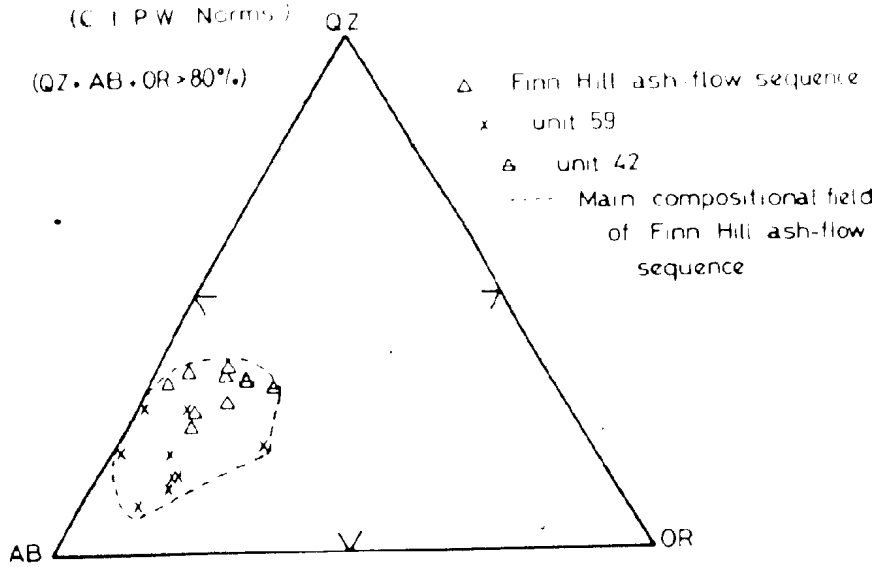

FIG 7d QZ AB OR DIAGRAM FOR MAIN COMPOSITIONAL FIELDS OF FELSIC VOLCANIC ROCKS

(C I P W Norms)

(QZ + AB + OR > 80%)

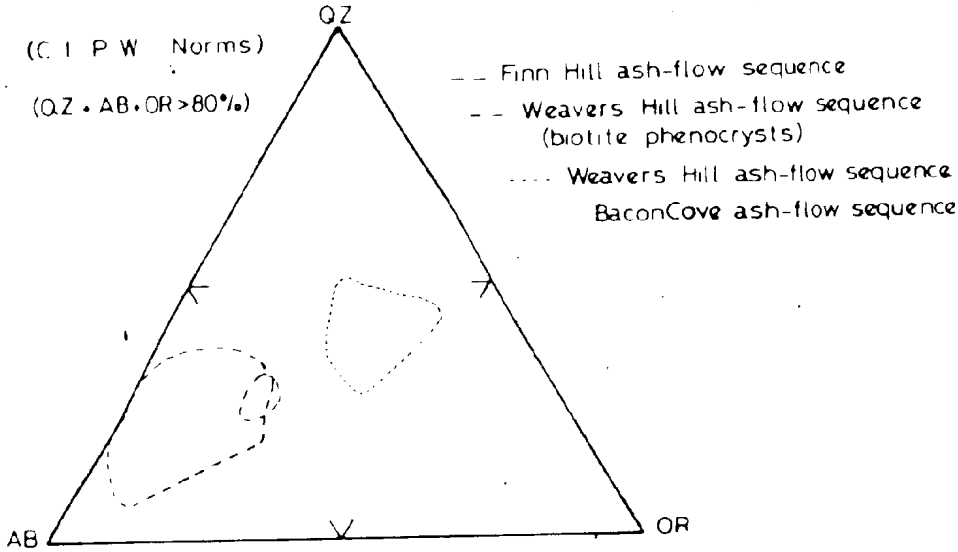

and dehydration of previously hydrated volcanic glass. Other textural features also support this conclusion (cf. section 3.4.).

Silicified and weathered samples were differentiated on the basis of anomalously high and low SiO_2/Al_2O_3 ratios, respectively (cf. GC34, GC36, GC32, GC47, and GC25).

The large number of analysed samples from each of the main ash-flow sequences greatly helped to clarify more complex chemical variations resulting from hydrothermal alteration. The compositions of rhyolitic volcanic rocks in the Harbour Main Group can be represented in a triangular plot of CIPW normative Qz-Ab-Or (figs. 7a-d). With the exception of the Finn Hill ash-flow sequence and a rhyolite sill (GC31), obviously altered samples with anomalous K_2O/Na_2O and/or Al_2O_3/SiO_2 ratios lie outside the compositional fields delineated in these plots. The limits of each of these compositional fields are natural boundaries consistent with chemical, mineralogical, and stratigraphic groupings of the ash-flow deposits.

The variability of K_2O/Na_2O ratios within an individual ash-flow sequence is a striking feature. Samples were collected chiefly from the central zones of ignimbrite cooling units, and the sampling interval was generally too large to detect internal variations. In the Bacon Cove ash-flow sequence, for example, specimens GC37a and GC37b from a vitric ash-flow tuff (unit 4) have K_2O/Na_2O ratios of 15.8 and 12.0, respectively. Such compositions are the result of extreme leaching of sodium with some addition of potassium by local hydrothermal fluids. Similar ratios were also identified as the

products of alkali metasomatism in rhyolitic ignimbrites by Scott (1966, p. 286) and Pichler and Zeil (1972, p. 204). Biotite-bearing ash-flow tuffs interbedded with porous volcanic breccias underlying the Weavers Hill sequence provide examples of extreme alteration involving leaching of alkalies and silicification (cf. table 7). Sample GC35 represents the densely welded interior of one such ignimbrite (unit 28) and plots within the narrow compositional field of other biotite-bearing ignimbrites at the top of the Weavers Hill sequence at James Cove (fig. 7a). GC36 represents the partly welded margin of the same cooling unit. Alteration of this type is pronounced where ignimbrites or lava flows (cf. GC32) are in contact with porous and/or permeable horizons in the pile (especially sediments), and commonly result in normative mineral compositions falling close to the Qz-Ab or Qz-Or joins. Ionic exchange and leaching of alkalies is also evident in specimens of the Weavers Hill sequence, notably GC24, GC47, P70-16, and GC45 (table 7 and fig. 7b), collected near the permeable margins of ignimbrite sheets. The main factors contributing to the greater spread of K_2O/Na_2O ratios in this sequence are the relatively high shard/crystal ratios, the abundance of porous pumice-lapilli, and the less densely welded nature of many of the cooling units. These factors would promote more extensive reaction between volcanic glass and percolating metasomatic fluids. In addition, increased amounts of potassium held in former glassy matrices may have served as a flux and promoted more intense remobilisation of other constituents. Lateral coherence of a potassium-rich bulk

chemistry together with the sodic nature of ignimbrites enveloping this sequence strongly suggest that alkali-exchange was predominantly internal and isochemical.

The Finn Hill ash-flow sequence exhibits a broad and continuous spectrum of K_2O/Na_2O values with no sharp distinction between unaltered and altered samples (except possibly P70-11). Consequently, the compositional field of this sequence encloses all ignimbrite analyses (fig. 7c). Samples that closely approach or may actually represent unaltered magmatic compositions are GC46a and GC46b (K_2O/Na_2O equals 0.48 and 0.67, respectively) from the crystal-rich basal zone of unit 42 at James Cove; and P70-11 (K_2O/Na_2O = 0.67) from the central part of unit 59 at Finn Hill. The combination of relatively high Na_2O and high K_2O clearly cannot be attributed to alkali-exchange processes. Remaining samples have K_2O/Na_2O ratios in the range 0.41 (P70-13; unit 43) to 0.02 (GTN22c; unit 59) and plot nearer the Qz-Ab join (fig. 7c). However, in view of the comparatively high Na_2O content of P70-13 and variability of K_2O/Na_2O at this one locality (compare GC49, GC50, GC17, and P70-13) the origin of the distribution of alkalies in this sample must remain uncertain. Any division between altered and unaltered samples, therefore, is necessarily arbitrary. Accordingly, samples with K_2O/Na_2O ratios greater than 0.41 in the Finn Hill ash-flow sequence are tentatively considered unaltered; whereas samples with K_2O/Na_2O less than 0.41 are regarded as altered.

Metasomatic alteration of Finn Hill ignimbrites involving introduction of Na chiefly at the expense of K, produces a rock closely

corresponding to "typical" analyses of "quartz-keratophyres" given, for example, by Turner and Verhoogen (1960, analysis 7, table 25), Joplin (1968, analysis 6, table XXVII), and Dickinson (1962, analysis 7, table 3). When plotted in fig. 7c, these rocks fall within the field of Finn Hill ash-flow tuffs close to analyses of unit 59 at Burkes Cove. However, other analyses of quartz-keratophyres have lower Na_2O and higher K_2O (cf. Turner and Verhoogen, 1960, analysis 6, table 25; Joplin, 1963, p. 112-137) and in certain cases there is no distinction between K_2O/Na_2O ratios in rocks regarded as keratophyres and in rocks termed "soda rhyolites" (cf. Joplin, ibid.). In addition, "potassic quartz-keratophyres" formed by alkali metasomatism are also known (Battey, 1955). Since the alteration processes that produce rocks of keratophyric chemistry have been locally operative in Harbour Main ignimbrites, the term "quartz-keratophyre" can be usefully retained to denote an altered rhyolitic rock affected by alkali metasomatism. Sodic quartz-keratophyres have $K_2O/Na_2O<0.41$ (the arbitrary boundary given above between altered and unaltered samples of the Finn Hill sequence); whereas GC37a and GC37b represent potassic quartz-keratophyres. Although keratophyres are commonly interbedded with marine sediments in a eugeosynclinal environment and are often thought of as characterising an orogenic tectonic setting (for example, Turner and Verhoogen, 1960, p. 258), it should be noted that keratophyres (and associated spilitic rocks) are also known from continental and epicontinental environments, particularly potassic variants (cf. Joplin, 1968, p. 150; Vallance, 1960). As

defined above, the term "quartz-keratophyre" has no specific tectonic implications and is consistent with modal definitions of keratophyric rocks given by Turner and Verhoogen (1960, p. 266-268) and Joplin (1968, p. 149-156).

8.2.1.2. Quantitative Aspects of Alkali Metasomatism

Some aspects of alkali metasomatism in rocks of keratophyric composition (as defined above) deserve further consideration.

Turner and Verhoogen (1960, p. 570) suggested that the course of alkali metasomatism is determined by the molecular ratio K_2O+Na_2O/Al_2O_3 in the parent rock and in the introduced fluid, and by ambient temperature and pressure conditions. Whereas this may be the case for a holocrystalline rock where alkali-exchange is rigorously controlled by the number of available K^+ and Na^+ sites in crystal lattices, this is not necessarily true for glassy volcanic rocks. Introduction of alkalies into glassy matrices undergoing hydrothermal reconstitution may involve displacement of other ions since ionic compatibility and substitution in strict stoichiometric proportions are not required. The course of alkali metasomatism, therefore, is more critically dependent upon the alkali chemistry of the fluid phase at a particular P and T, and the amount of excess Al_2O_3 in the rock capable of forming an alkalic mineral phase in the presence of alkali-bearing solutions.

Fixation of alkalies by excess alumina is a common phenomenon at elevated temperatures in the vicinity of granite-shale contacts and

during potash fenitisation (cf. Currie, 1971; Currie and Ferguson, 1971). During low temperature hydrothermal recrystallisation an alkali rhyolite ($K_2O+Na_2O/Al_2O_3<1$) cannot become peralkaline ($K_2O+Na_2O/Al_2O_3>1$) without the stability of subaluminous phases such as glaucophane or sodalite, or removal of alumina relative to alkalies. The latter is not a very likely alternative. Conversely, a peralkaline rhyolite cannot preserve its original alkali content under these conditions if breakdown of such magmatic minerals as aegirine, riebeckite, and arfvedsonite ensues. This may account for the apparent lack of strongly peralkalic comendites and pantellerites older than Tertiary.

Harbour Main ignimbrites are distinctly peraluminous with an average total alkali content of approximately 8 wt. %. Since the maximum grade of metamorphism is below the stability field of glaucophane assemblages, the highest possible combination of total alkalies and alumina is found in alkalic feldspar. In the extreme case, alkali-exchange in rocks with excess quartz relative to the alkali feldspar composition produces a rock composed essentially of albite-quartz or K-feldspar-quartz assemblages and molecular $K_2O+Na_2O/Al_2O_3 = 1$.

Consider the composition of unit 59 at Finn Hill (P70-11) and a series of 12 samples taken across two flow units of this ignimbrite at Burkes Cove (table 7). Average compositions for upper and lower flow units are given in table 9 (FHS-R and FHS-S, respectively). Although microprobe analysis reveals that the compositions of albite phenocrysts and crystals of K-feldspar (C88M, table 6) are of meta-

morphic origin, whole-rock composition of P70-11 appears little affected by alkali-exchange processes. Samples at Burkes Cove are quartz-keratophyres whose sodic composition is reflected to some extent by the high proportion of albite in the CIPW norm. However, the nature of the chemical reactions are more appropriately investigated in terms of molecular proportions. The observation that Al_2O_3 remains essentially constant during hydrothermal alteration provides an empirical basis for determining the relative gains and losses of oxide components (cf. Lipman, 1965; Anderson, 1968). If cation-exchange during the formation of quartz-keratophyre compositions was essentially limited to Na^+ and K^+, the molecular ratio K_2O+Na_2O/Al_2O_3 for the whole-rock should remain sensibly constant. This ratio for P70-11 equals approximately 0.85, while that for FHS-R and FHS-S is 0.91 and 0.90, respectively (impurities CaO, MgO, total Fe, MnO, TiO_2, P_2O_5 calculated out). This difference at most requires addition of approximately 0.9 mol. % total alkalies (presumably Na_2O) relative to Al_2O_3, and corresponding loss of an equivalent amount of other oxides, possibly MgO and CaO. In certain samples with very low K_2O/Na_2O ratios (for example, GTN11, GTN19, and GTN23i) MgO has locally been leached by sodic fluids. The mineralogy of unit 59 is essentially quartz, albite, and magnetite, and agrees remarkably well with high K_2O+Na_2O/Al_2O_3 ratios. Petrographically, therefore, the rock could be classified as an "albite-keratophyre". The low K_2O/Na_2O and high K_2O+Na_2O/Al_2O_3 ratios of other rhyolites from the Central and Eastern Blocks (Papezik, 1970,

Table 1, nos. 21-23) also suggest keratophyric compositions and a predominantly albite-quartz mineral assemblage.

Similar calculations were made for a potassic quartz-keratophyre (GC37a; unit 4) and an altered dacite flow (GC12). Assuming an original composition close to the average for the Bacon Cove ash-flow sequence (BCS-X, table 9), the keratophyre has molecular K_2O+Na_2O/Al_2O_3 equal to 0.63 while this ratio for BCS-X equals 0.72. Assuming constant alumina, leaching of approximately 2.4 mol. % Na_2O is required. An adjustment of this kind would result in GC37a (and GC37b) falling close to the main alkali-exchange curve for the Bacon Cove ash-flow sequence in fig. 8 (discussed below). Reciprocal exchange of Al_2O_3 and SiO_2 would not seriously affect these calculations (cf. Lipman, 1965, p. D11). Removal of small amounts of other oxide constituents (in this case CaO) may accompany such alteration. Analysis GC12 is a dacite with correspondingly lower silica and higher alumina, and an anomalously high alkali content (chiefly Na_2O). Molecular K_2O+Na_2O/Al_2O_3 equals 0.85 and reflects a predominantly albitic mineralogy. Introduction of sodium in excess of that probably required for complete removal of potassium proceeded in glassy matrices at the expense of MgO and CaO. Small pods of epidote-albite-chlorite assemblages in this flow indicate that migration of these elements was probably localised (cf. Smith, 1968; Reed and Morgan, 1971).

A K_2O vs. Na_2O plot of altered and unaltered samples is presented in fig. 8. The samples define a negative slope with intercepts of

FIG 8 Na_2O vs K_2O ASH-FLOW TUFFS AND FELSIC FLOWS

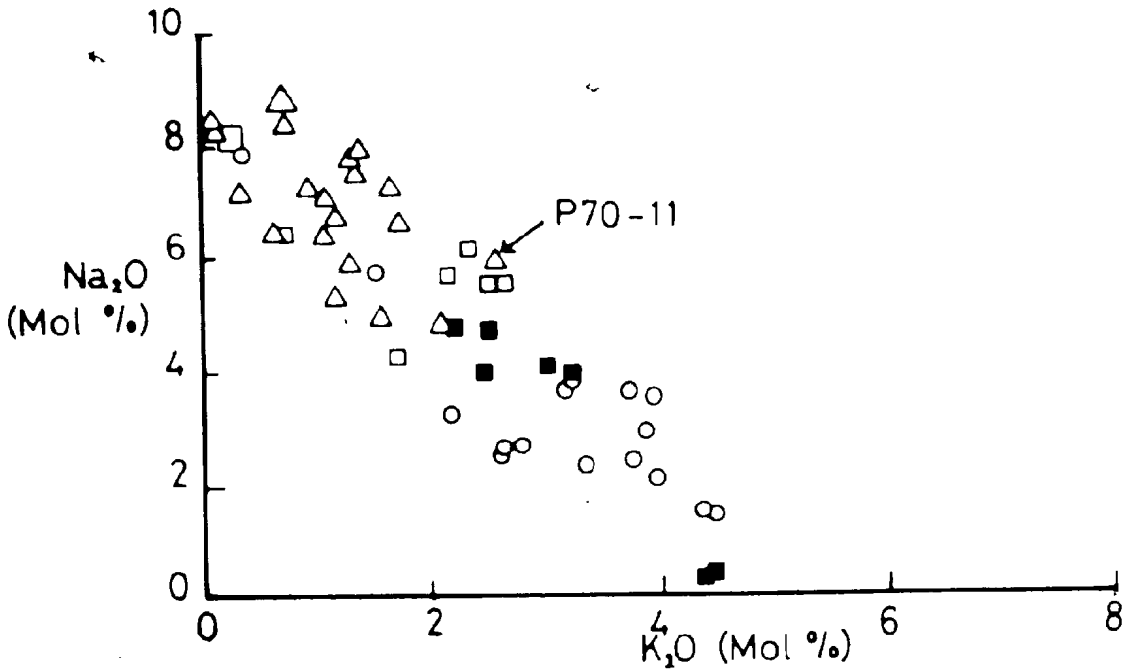

△ Finn Hill ash-flow sequence ○ Weavers Hill ash-flow sequence

□ Weavers Hill ash-flow sequence (biotite phenocrysts)

■ Bacon Cove ash-flow sequence □ Rhyolite flow △ Dacite flow

approximately 9.0 and 5.5 for Na_2O and K_2O, respectively. This slope is a function of a) original K_2O/Na_2O ratios in the silicate melt; b) the effects of alkali-exchange, local leaching or preferential addition of sodium or potassium by subsequent alteration processes; and c) minor removal or addition of other oxides, notably CaO and in certain cases MgO. Magmatic alkali variation is defined by the close grouping of points within each batch of differentiates, i.e. within each ash-flow sequence. The resultant slope for all these groups reflects the predominantly sodic chemistry of the population. Completely isochemical exchange of alkalies within each magma batch would displace whole-rock compositions toward the extremities of a -1 slope running through each predefined magmatic ratio. However, leaching of alkali elements causes points to move toward the origin along a positive slope determined by the proportional loss of Na_2O to K_2O. The increased scatter of Finn Hill and Weavers Hill ash-flow tuffs has been induced by superposition of such positive and negative slopes. In the case of the Finn Hill sequence, the limits of the exchange system are beyond the range of analysed samples. Although plots of this type purport to show variation between two elements, variable loss and gain of other major constituents have a significant effect (cf. Pearce, 1968). For example, addition of a small amount of sodium to a dacite (GC12) and concomitant loss of calcium and magnesium has displaced GC12 from the mean alkali-exchange trend for the Finn Hill ash-flow sequence (i.e., a -1 slope possibly running through P70-11) parallel to the ordinate in the direction of increasing Na_2O.

8.2.1.3. Magmatic Trends and Affinities

Major oxide abundances for Harbour Main volcanic rocks are plotted against SiO_2 in fig. 6. The plot is essentially a Harker variation diagram with oxide constituents expressed in terms of molecular percentages instead of the traditional wt. %. Though not all the deficiencies of Harker diagrams have been obviated (cf. Pearce, 1968), the trends undoubtedly have genetic significance in the broad sense. Linear to curved trends are well defined for Fe_2O_3 (total Fe), Al_2O_3, MgO, CaO, MnO, P_2O_5, and TiO_2; significant scatter is observed in trends for total alkalies, Na_2O, and K_2O. The relative strength of this coherence is evident from the correlation matrices in table 8. The significance of a distinct compositional gap with respect to silica will be discussed later.

The ignimbrites are rhyolitic in the broad sense, and characterised by high total alkalies, molecular $K_2O+Na_2O/Al_2O_3<1$, variable K_2O/Na_2O, low CaO, MgO, total Fe, MnO, TiO_2, and P_2O_5. Average compositions of the main chemical types are given in table 9.

Silica values for plotted samples range 64.08-76.00 wt. %. The lowest SiO_2 abundances are found in ignimbrites at the top of the Finn Hill sequence. Unit 58 (P70-9) has a SiO_2 content corresponding to dacite, but its relatively low K_2O/Na_2O ratio of 0.35 is transitional to sodic quartz-keratophyre as defined earlier. Microphenocrysts of augitic pyroxene are perfectly fresh, and this unit was classified as a sodic quartz-trachyte by Papezik (1970, table 1 and p. 1490). A distinctive layer of volcanic breccia in a similar ignimbrite (unit

59) at Burkes Cove serves to distinguish multiple flow relationships within a single cooling unit. Compositional variation between upper and lower flow units (cf. FHS-R and FHS-S, table 9) is marked by consistent differences in SiO_2, Al_2O_3, total Fe, and TiO_2; the latter three elements are relatively immobile under a variety of conditions of low-temperature alteration. The bulk composition of this ignimbrite is rhyodacitic, with a K_2O/Na_2O ratio corresponding to sodic quartz-keratophyre. At Finn Hill, the boundary between the flow units is gradational, and sample P70-11 from the middle of the cooling unit suggests that the transitional nature of the contact at this locality is accompanied by a gradation in composition. This unit lacks clinopyroxene, and the K_2O/Na_2O ratio of P70-11 is indicative of an unmodified sodic composition. With the exception of unit 42 (FHS-U, table 9) which has a K_2O/Na_2O ratio of 0.58, remaining ignimbrites in the Finn Hill sequence are sodic quartz-keratophyres. In comparison, the Weavers Hill ash-flow sequence is characterised by higher SiO_2 and K_2O, and lower Na_2O, MgO, total Fe, and TiO_2. The K_2O/Na_2O ratio for WHS-W (table 9) is approximately 1.52. Averages BCS-X and WHS-V (table 9) for the Bacon Cove sequence and biotite-bearing ignimbrites at the top of the Weavers Hill sequence at James Cove exhibit significant increase of total Fe, Na_2O, TiO_2, and MgO, and concomitant decrease of SiO_2 relative to WHS-W. This is correlated with the appearance of biotite and increased proportion of iron-oxide crystallites in the mode. The K_2O/Na_2O ratio bears an inverse relationship to the proportion of modal albite. Crystal

concentration in the Bacon Cove ash-flow sequence has produced unique compositional effects: average BCS-X bears a striking resemblance to the "average granite" and "average quartz-monzonite" of the Holyrood pluton (averages Y and Z, respectively, table 9). The tuffs, however, have higher total Fe and TiO_2, and lower CaO. Modal compositions generally differ only with respect to K-feldspar, which occurs as phenocrysts and in microperthitic intergrowth with sodic plagioclase in the granitoid rocks; the principal K-bearing phase in the tuffs is represented by alkalic feldspar, a product of the devitrification of glassy matrices.

The classification of Harbour Main volcanic rocks is more appropriately based on normative minerals and/or chemical composition, since the large proportion of devitrified glass and the albitic compositions of originally more calcic plagioclase render a strictly modal nomenclature useless.

A system of classification proposed by Baragar (1967) is reproduced in fig. 9. The transitional boundaries originally proposed are based on normative feldspar, and have been approximated by solid lines in the diagram. Although a dual nomenclature exists for each of the compositional fields, rhyolitic rocks of the Harbour Main Group are much more siliceous than typical trachytes or phonolites (cf. Irvine and Baragar, 1971, p. 546, analyses nos. 22 and 23) and fall in the fields of rhyolite and sodic rhyolite. However, it is evident from the position of altered rocks that part of the field of sodic rhyolite is also that of sodic quartz-keratophyre.

FIG 9 AN:AB:OR DIAGRAM FOR FELSIC VOLCANIC ROCKS
(C I P W Norms) (Baragar 1967)

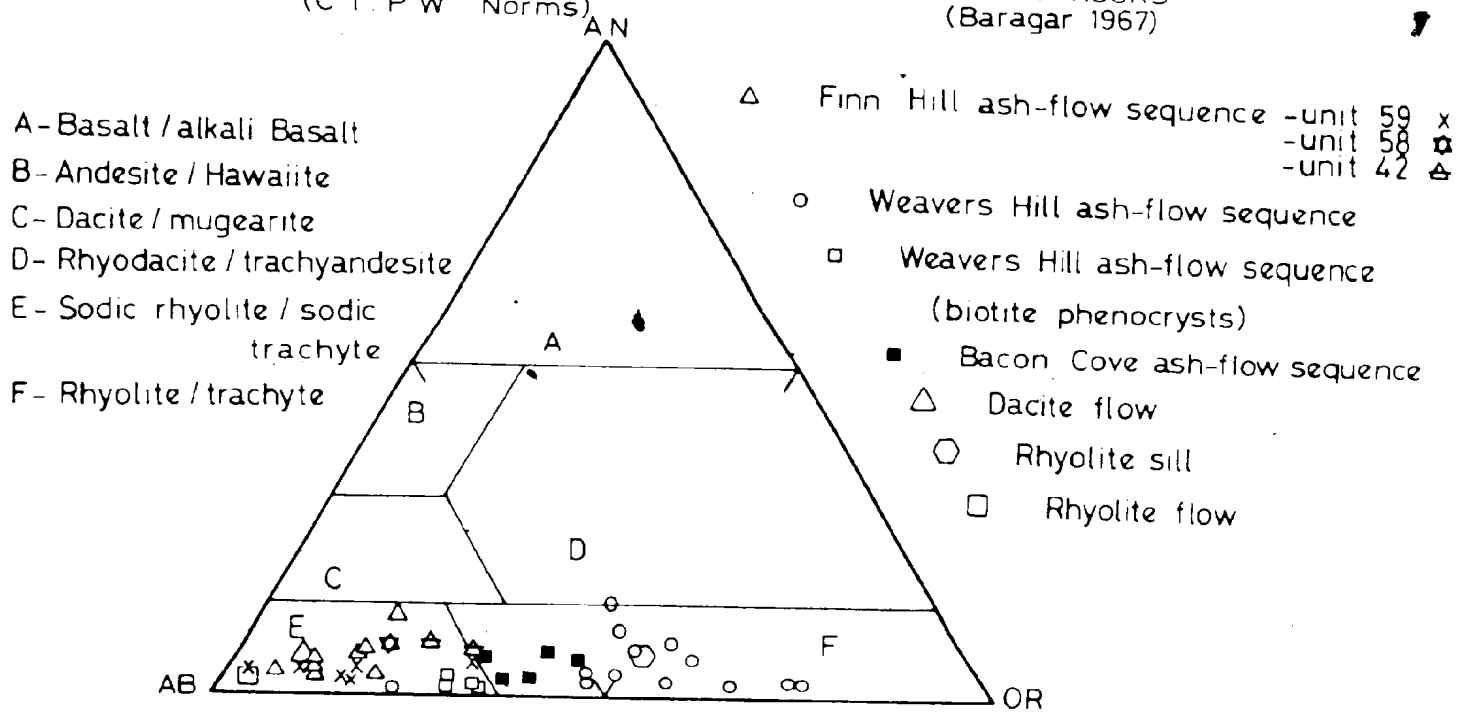

FIG 10a QZ OR AB+AN DIAGRAM CLASSIFICATION

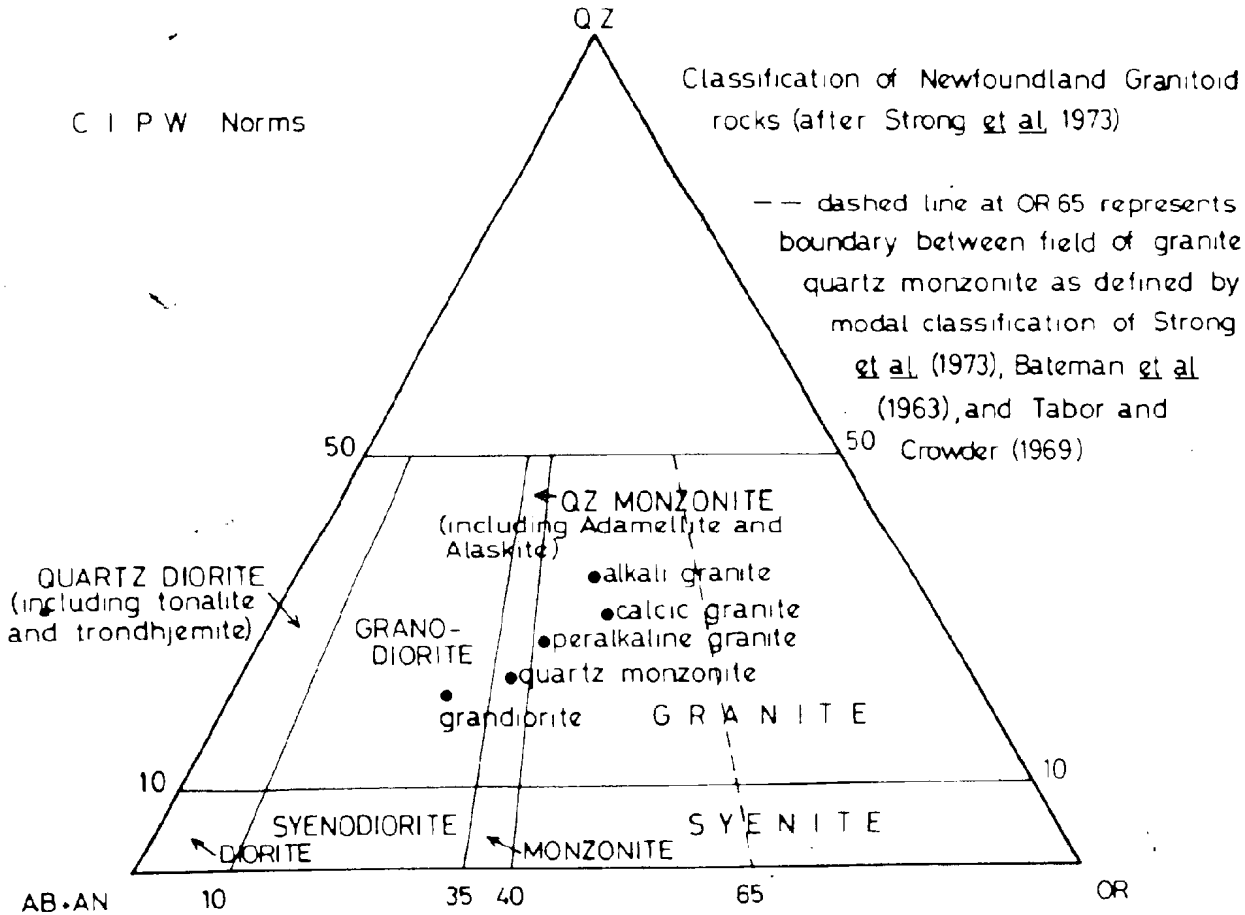

FIG 10b QZ : OR : AB + AN DIAGRAM FOR FELSIC VOLCANIC ROCKS

C.I.P.W Norms

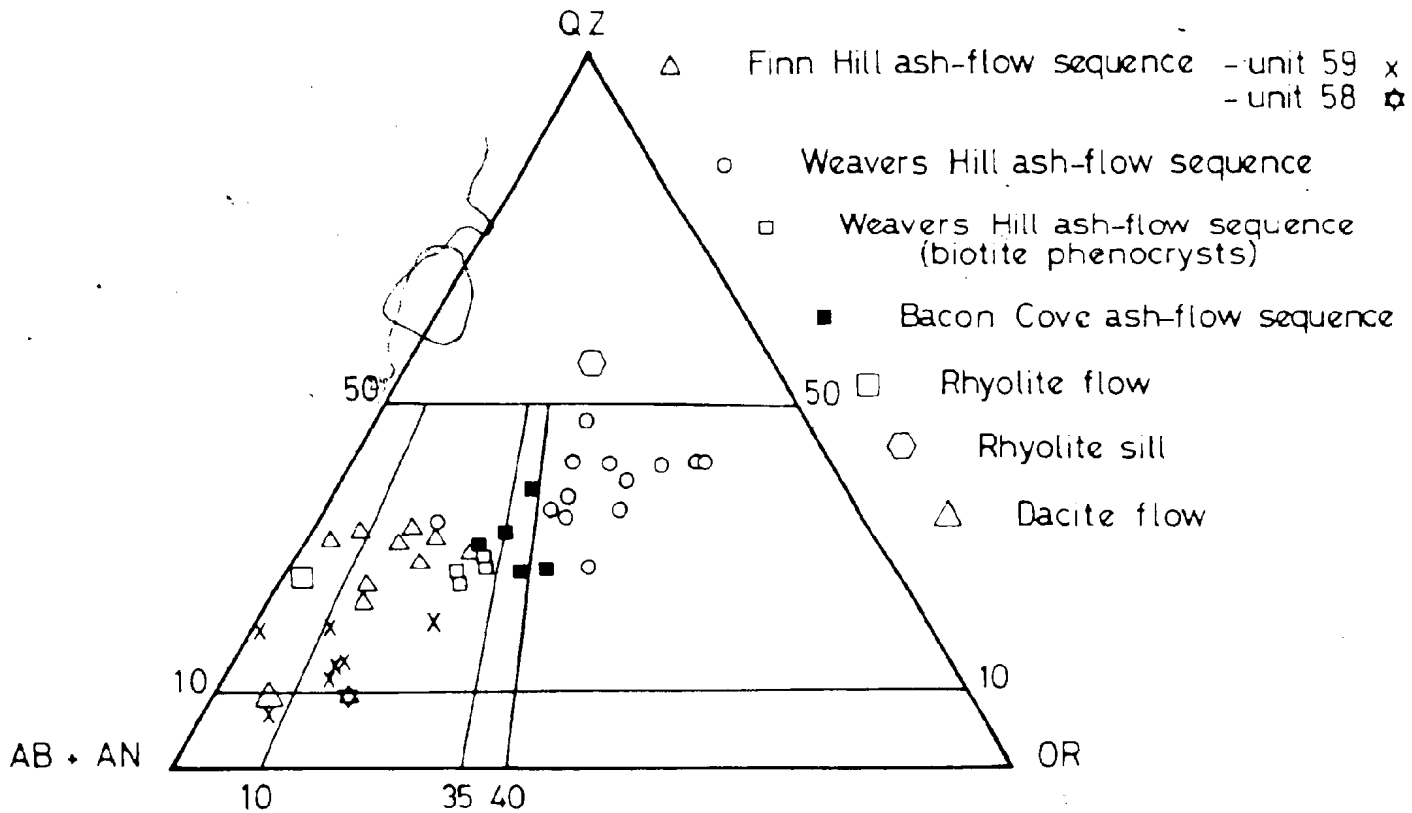

FIG 10c QZ OR AB + AN DIAGRAM FOR AVERAGE COMPOSITIONS OF ASH-FLOW TUFFS
(taken from table of averages)

C I P W Norms

R, S, P 70-11 Cooling unit 59, Finn Hill ash-flow sequence

T Cooling unit 58, Finn Hill ash-flow sequence

U Cooling unit 42, Finn Hill ash-flow sequence

V Weavers Hill ash-flow sequence (biotite phenocrysts)

W Weavers Hill ash-flow sequence

X Bacon Cove ash-flow sequence

Y Holyrood "Granite"

Z Holyrood QZ Monzonite

- - - basal flow unit (cooling unit 59 as analysed at Finn Hill (P 70-11) and Burkes Cove (R and S)

— — top (R) and basal (S) flow units (cooling unit 59)

----- approximate compositional range of Holyrood Pluton (Strong et al 1973)

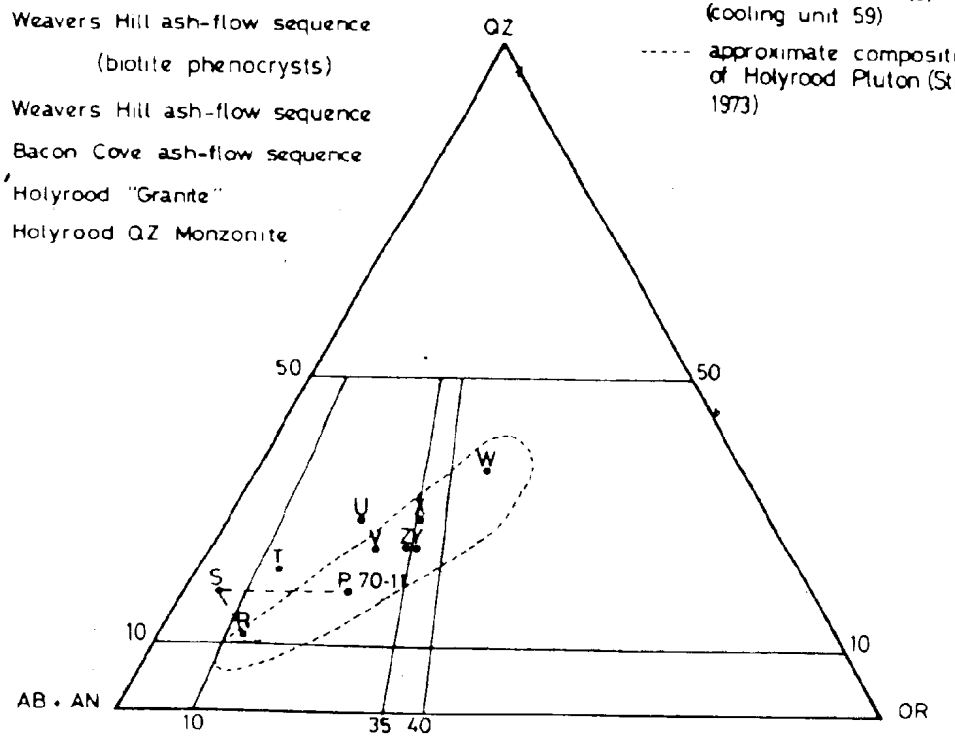

A geochemical study of granitoid rocks in eastern Newfoundland by Strong et al. (1973) provided an excellent opportunity to compare the compositional variability of Harbour Main ignimbrites and the Holyrood Plutonic Series. Classification of the granitoid rocks is based primarily on the averages of Nockolds (1954) expressed in terms of CIPW normative Qz-Or-Ab+An. The system of nomenclature and plots of Nockolds' averages are presented in fig. 10a. The essential difference between this and a modal classification is the location of the boundary between granite and quartz-monzonite, which is placed at approximately Or_{40} in the normative scheme and Or_{65} in the modal classification. The rhyolitic rocks plotted in fig. 10b straddle the fields of granite, quartz-monzonite, granodiorite, and quartz-diorite, and fall on a linear trend running from the Ab+An corner toward the normative composition $Qz_{50}Or_{50}$. Averages of the main chemical types of ignimbrite taken from table 9 are plotted in fig. 10c, and provide a better basis for discriminatory classification. Prefixes designating individual ash-flow sequences have been omitted for clarity. Apart from S, T, and U, ignimbrites fall within the compositional field of the Holyrood pluton. However, R, S, and T, have already been recognised as quartz-keratophyres, and are notably displaced from their "magmatic" counterpart P70-11. Granitic phases of the Holyrood Plutonic Series, represented by Y and Z, plot on the boundary of the quartz-monzonite-granodiorite fields close to averages X and V for biotite-bearing ignimbrites. Average U plots to the Qz-normative side of Holyrood granitoid rocks in the centre of the

granodiorite field. Weavers Hill ignimbrites, represented by W, plot in the field of granite close to Nockolds' average alkali granite.

The wide range of ignimbrite compositions and their close coherence with plutonic rocks intruding the Harbour Main Group provide for a very desirable classification, provided that a suitable volcanic nomenclature can be found. The generally accepted volcanic terminology corresponding to plutonic equivalents has been adopted (for example, Moorhouse, 1964). Accordingly, ignimbrites represented by W and X are strictly (alkali-) rhyolites and quartz-latites, respectively, while those corresponding to U, V, and P70-11 are rhyodacites. The proposed volcanic nomenclature is in accord with predicted and actual K_2O/Na_2O variation observed in such rock-types. High-alkali rhyolite is proposed as a useful blanketing term for describing the general nature of the rhyolitic suite.

Trace element data are plotted against SiO_2 (mol. %) in fig. 13. Rhyolitic rocks of the Harbour Main Group contain typically low Ni, Cr, Cu, more variable Sr, Zn, and Rb, highly variable Ba, and virtually constant Zr. Overall trends for Zr, Rb, and Ba define weak to strong positive slopes; Ni, Cr, Sr, Cu, and Zn lie on weak to moderate slopes inversely correlated with respect to SiO_2. The complete range of geochemical affinities is shown in the correlation matrices (table 8), which are strongly biased toward rhyolitic samples. The significance of K/Rb, Rb/Sr, and Ti/Zr ratios will be considered later.

K, Rb, and Ba exhibit a strong positive inter-element correlation (table 8) in the rhyolitic rocks analysed, as predicted by their

similar geochemical behaviour (Appendix 4). The Weavers Hill ash-flow sequence is the most differentiated chemical type with respect to these "incompatible" elements (cf. Harris, 1957). Rb attains approximately twice the average crustal abundance of 90 p.p.m. (Taylor, 1965), and Ba is strongly enriched (400-2097 p.p.m.) in the majority of the ash-flow sequences. Only in certain sodic quartz-keratophyres (for example, FHS-S and GC12) are Rb and Ba strongly depleted (<<90 and <<400 p.p.m., respectively) relative to Taylor's average crustal abundances.

It has been suggested that the Ba/Sr ratio is a critical index of fractionation and that Ba is not depleted in the magma until a relatively late stage of differentiation (Nockolds and Allen, 1953). Data from residual glasses and plagioclase phenocrysts of high-alkali ignimbrites in New Zealand support this conviction (Ewart et al., 1968; Ewart and Taylor, 1969). However, where biotite is an early precipitating phase, Ba-poor residual liquids may result (Jakes and Smith, 1970). In the rhyolitic compositions under investigation here, a marked increase in the abundance of Ba (and Rb) with increased differentiation factor, i.e. relative to SiO_2, strongly suggest that biotite was a relatively late phase to arrive on the liquidus in significant proportions (i.e. in quartz-latitic melts). Crystallisation of biotite was probably effectively controlled by water vapour pressures during late-stage differentiation.

The partitioning of Sr in volcanic liquids is largely controlled by the number of available Ca-sites in the plagioclase lattice (Taylor,

1965), which generally results in their similar depletion in residual liquids (cf. Ewart et al., 1968, fig. 6). Ewart and Taylor (1969) found that the maximum concentration of Sr in plagioclases representative of Taupo rhyolites occurs in the range An_{40} to An_{55}. The distribution coefficients for partitioning of Ba and Sr between plagioclase phenocrysts and residual liquids in these rhyolites indicate that fractional crystallisation of a plagioclase of this composition would deplete Sr relative to Ba (Ewart and Taylor, ibid., table 4). The trend for Ba relative to Sr observed in Harbour Main ignimbrites could likewise be produced by crystallisation and removal of andesine from early differentiating silicate liquids. This conclusion is in accord with the late appearance of biotite as previously indicated.

Sr exhibits only a weak positive correlation with Ca (table 8), and stronger correlations are observed with Mn, Zr, Cu, Zn, Cr, and Ni, of which Zr, Ni, Cr, and possibly Zn appear least affected by alteration processes. Depletion of Sr in some quartz-keratophyres (for example, GC32, GC37a and GC37b) and porous volcanic breccias (for example, WHT) can possibly be correlated with removal of Ca.

Zr generally behaves as an excluded element during fractionation and is known to concentrate in residual liquids (Taylor, 1965). However, the abundance of Zr in Harbour Main ignimbrites is remarkably uniform and averages approximately 178 p.p.m. This appears to demand steady removal of Zr relative to Rb and Ba, possibly by its incorporation into zircon or possibly an iron-titanium oxide. The presence of

zircon in the Bacon Cove sequence indicates that Zr had reached levels of saturation in these quartz-latitic liquids. Tiny crystals of zircon occurring free in the matrix or enclosed within biotite phenocrysts suggest that depletion of Zr in the latest differentiates (for example, the Weavers Hill ash-flow sequence) was accomplished by zircon and/or biotite fractionation. It is pertinent to note that the highest concentration of Zr is found in a rhyodacitic ignimbrite (FHS-U, table 9) at the base of the Finn Hill ash-flow sequence, and that Zr is clearly depleted in biotite-bearing ignimbrites, especially quartz-latites (cf. also Holyrood "granite", Y, table 9).

A moderately strong positive correlation exists between Cu and Zn, and between these elements and Sr, Zr, and Mn. The abundance of Zn is consistent with the range of average granite and granodiorite compositions (40-60 p.p.m.) given by Taylor (1965, table 21); Cu abundances are somewhat lower than expected, except for an anomalously high value in GTN34 which represents a mineralised rock fragment. A strong negative correlation of Zn with SiO_2 is weakened by the conspicuously divergent trend of the Finn Hill ash-flow sequence (cf. fig. 13).

Cr and Ni exhibit a strong overall positive coherence and have uniformly low abundances in rhyolitic rocks. Anomalously high values distinguished samples contaminated by basaltic xenoliths.

In comparison with selected analyses of rhyolitic rocks from continental regions (table 10, nos. 1-5), Harbour Main ignimbrites are enriched in total Fe, MgO, and TiO_2, with slightly higher Al_2O_3

TABLE 10. Major and Trace Element Compositions of Rhyolitic Ignimbrites, Flows, and Granitoid Rocks Used for Comparison with Harbour Main Ignimbrites (analyses in weight percent are recalculated to 100% on a volatile-free basis).

Source	1	2a	3	4	5	6	7	8
No. of Analyses	(2)	(5)	(25)	(17)	(10)	(6)	(n.d.p.)	(n.d.p.)
(Wt. %)								
SiO_2	73.36	77.03	75.00	74.80	76.54	75.47	71.33	67.57
Al_2O_3	14.06	12.22	13.41	13.73	12.71	13.50	14.73	15.86
Fe_2O_3	0.45	0.59	0.89	1.27	0.99	0.40(2)	–	–
FeO	1.55	1.10	0.93	0.61	0.56	0.97(2)	3.25	3.82
CaO	1.30	0.51	1.61	1.55	0.79	0.61	2.00	3.60
Na_2O	4.50	3.36	4.29	3.76	3.63	4.32	3.55	3.88
K_2O	4.15	5.05	3.21	3.65	4.32	4.02	4.19	3.10
MgO	0.26	0.14	0.28	0.30	0.22	0.39	0.55	1.58
MnO	0.09	n.d.p.	0.05	0.05	0.03	0.07	n.d.p.	n.d.p.
TiO_2	0.22	n.d.p.	0.28	0.23	0.14	0.22	0.40	0.58
P_2O_5	0.06	n.d.p.	0.05	0.05	0.07	0.03	n.d.p.	n.d.p.

TABLE 10 (Cont'd.)

Source (p.p.m.)	1	2b	(c)	5	6	7	8
Rb	140	171(9)	108	194(128-231)*	122(99-160)*	145	110
Sr	70	8(4)	125	67(14-199)*	62(31-117)*	285	440
Ba	920	253(9)	870	n.d.p.	543(162-887)*	600	500
Zr	280	249(9)	160	n.d.p.	220(142-293)*	180	140
Cu	16	n.d.p.	6	6	n.d.p.	10	25
Zn	n.d.p.	n.d.p.	n.d.p.	n.d.p.	n.d.p.	n.d.p.	n.d.p.
Cr	2	n.d.p.	1.7	n.d.p.	n.d.p.	10	30
Ni	<4	n.d.p.	n.d.p.	n.d.p.	n.d.p.	4	15
K/Rb	n.d.p.	n.d.p.	250	293(181-342)*	270(201-321)*	240	230
Rb/Sr	2.00	21.37	0.86	2.90	1.97	0.51	0.25
Ba/Sr	13.14	31.63	6.96	-	8.76	2.11	1.14

*Range of values

n.d.p. = no data presented in source reference

†Total iron given as FeO

(c) = Average of 3-4

TABLE 10 (Cont'd.)

1. North obsidian flow, Newberry Volcano (Higgins, 1973; major elements: Table 5, nos. 52-53; trace elements: Table 8, no. 52 only).

2a. Rhyolitic glasses from Yellowstone (Anderson, 1968, Table 1, no. 3).

2b. Residual glasses from Yellowstone (Leeman, unpublished data).

3. Rhyolitic lavas of the Taupo Volcanic Zone (Ewart et al., 1968, Table 2, no. 1).

4. Ignimbrites of the Taupo Volcanic Zone (Ewart et al., 1968, Table 2; trace elements (Table 3, no. 35) represent average for 3-4).

5. Late Paleozoic-Mesozoic ignimbrites of N. Chile (Pichler and Zeil, 1972; major elements: Table 1; trace elements: Table 2; nos. 1-3, 5, 8-12, 14).

6. Granitic phase of high-K diorite, Yeoval Complex, New South Wales (Gulson, 1972, Table 4).

7. "Average Granite" (Taylor, 1968, Table 3).

8. "Average Granodiorite" (Taylor, 1968, Table 3).

and correspondingly lower SiO_2. However, trace elements, K_2O, Na_2O, and CaO provide a better basis for examining compositional differences.

The K_2O/Na_2O ratio of rhyolitic glasses from Yellowstone (nos. 2a and 2b, table 10) approximates that for the Weavers Hill ash-flow sequence (WHS-W, table 9); however, Zr is concentrated and Ba and Sr strongly depleted in Yellowstone rocks relative to WHS-W. This is probably due to a celsian variety of the anorthoclase-sanidine series appearing on the liquidus of Yellowstone residual glasses (Leeman, pers. comm., 1974). The K_2O/Na_2O ratio of Bacon Cove ash-flow tuffs (BCS-X, table 9) is the same as that for young obsidians from Newberry and ignimbrites from New Zealand (nos. 1 and 4, table 10); but total alkalies and CaO are dissimilar, and in this respect BCS-X is close to Andean ignimbrites (no. 5, table 10). However, enrichment of Ba and Sr in Bacon Cove quartz-latites distinguishes these rocks from both the Andean and Newberry suites. The granitic phase of a composite pluton, the Yeoval Complex of New South Wales (no. 6, table 10), compares well with BCS-X; Zr is relatively enriched and Ba and Sr depleted in the former, though Ba/Sr ratios are very similar. The close similarity between the Bacon Cove ash-flow sequence and Holyrood "granite" has already been recognised (compare no. 6 in table 10, with Z in table 9).

Rhyodacites of the Finn Hill sequence (FHS-U and P70-11, table 9) are markedly more sodic than the average granite of Taylor (1968), and more siliceous and less calcic than his average granodiorite (cf. nos. 7 and 8, table 10). FHS-U contains markedly higher Zr and Ba/Sr

ratios are likewise distinctive. The distinction between Taylor's granite and granodiorite is considerably greater than that between granite and quartz-monzonite facies in the Holyrood pluton, and apart from essentially K_2O, Ba, and Zr, FHS-U is closer in composition to the quartz-monzonite and Taylor's granite.

8.2.2. Porphyrites

The chemistry of a suite of exclusively hypabyssal rocks from the Colliers Peninsula, referred to earlier as "porphyrites", has not been described previously from the Harbour Main Group. Papezik (1970, p. 1492 and table 7, P70-8) presented an analysis of one of these rocks but related it to feldsparphyric sills of basaltic composition that intrude the Eastern and Western Blocks (cf. P70-4, table 7; and Papezik, 1970, table 1, nos. 6, 17, and 19). He explained the comparatively high SiO_2 content by contamination with quartz xenocrysts detected under the microscope. However, the porphyrites form a coherent suite of high-level sills distinct in composition, mineralogy, and timing from basaltic lavas and intrusions to the west.

Representative sampling of these rocks is indeed a severe problem since they commonly contain a diverse population of xenocrysts and xenoliths incorporated in an intrusion breccia at chilled contacts, and a high proportion of their total surface area is occupied by a "mixed" rock of this type. However, extraneous material is of strictly local origin and exhibits little or no reaction with its host.

FIG 11 AN:AB:OR DIAGRAM (Baragar 1967)
(C.I.P.W. Norms)

A- Basalt/alkali Basalt
B- Andesite / Hawaiite
C- Dacite / mugearite
D- Rhyodacite / trachyandesite
E- Sodic rhyolite / sodic trachyte
F- Rhyolite / trachyte

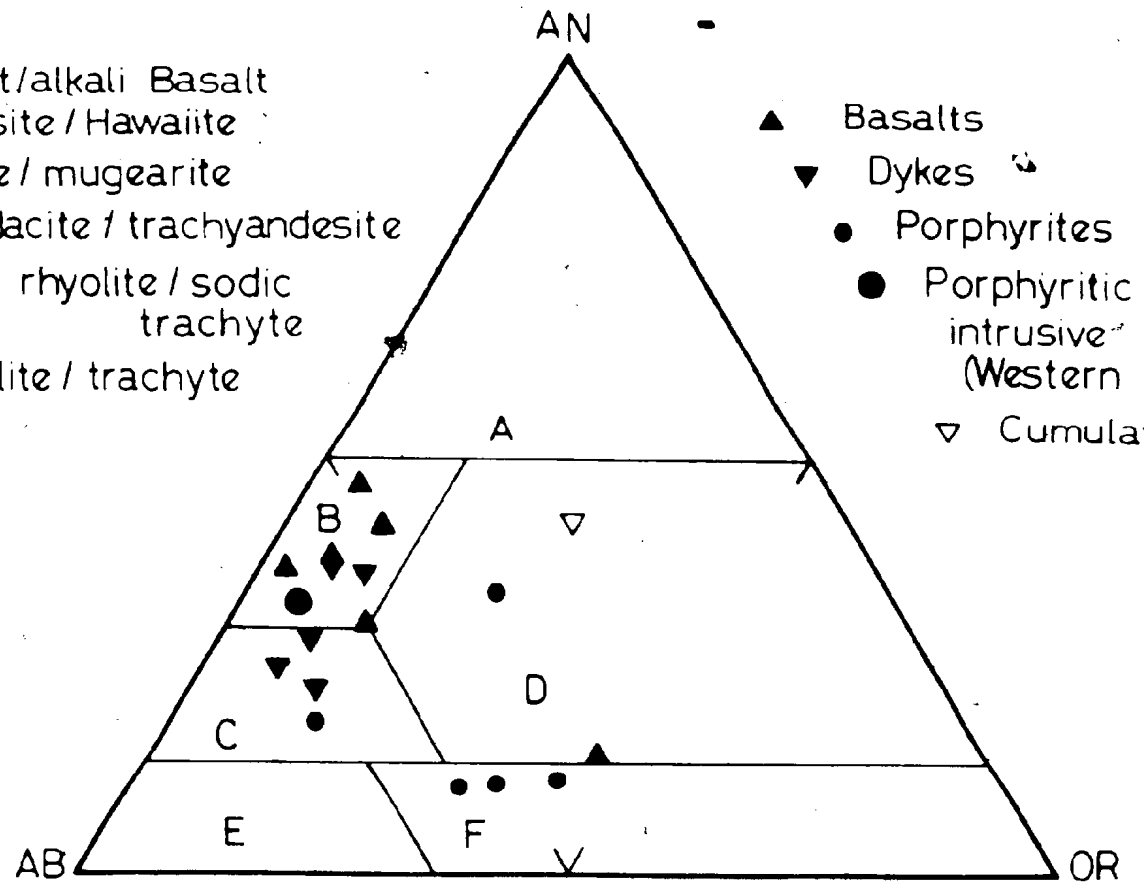

▲ Basalts
▼ Dykes
● Porphyrites
● Porphyritic intrusive (Western Block)
▽ Cumulate rock

FIG 12 TOTAL ALKALIES vs ALUMINA (after Kuno 1960)

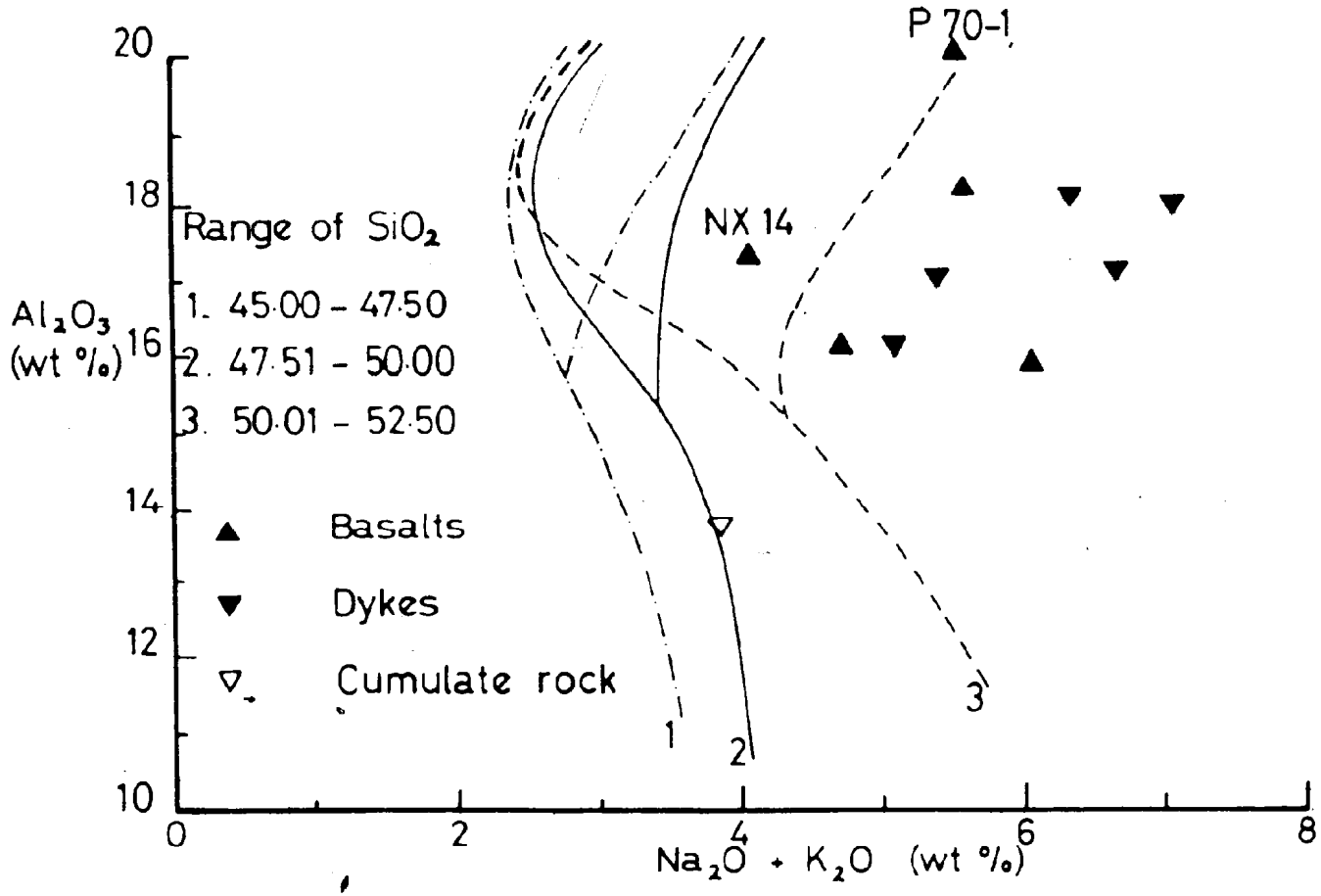

FIG 13 TRACE ELEMENTS VS SILICA FOR HARBOUR MAIN GROUP VOLCANIC ROCKS. COLLIERS PENINSULA

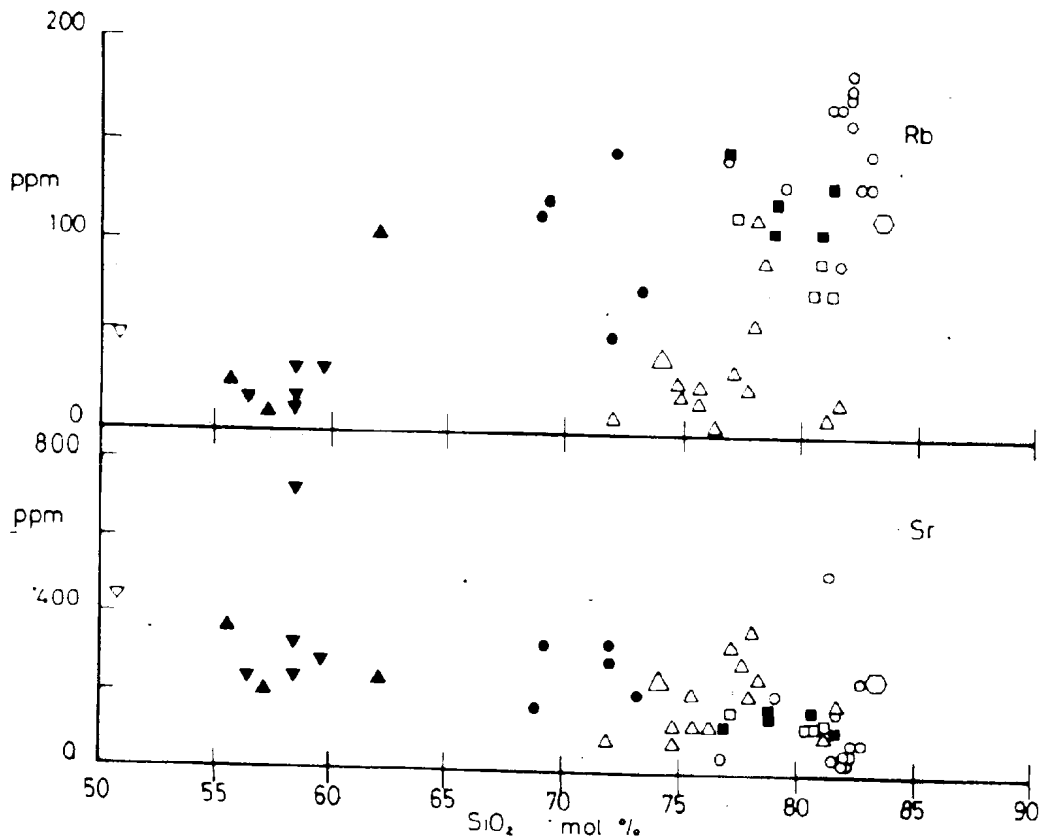

(Key as for major elements)

FIG 13 (cont.)

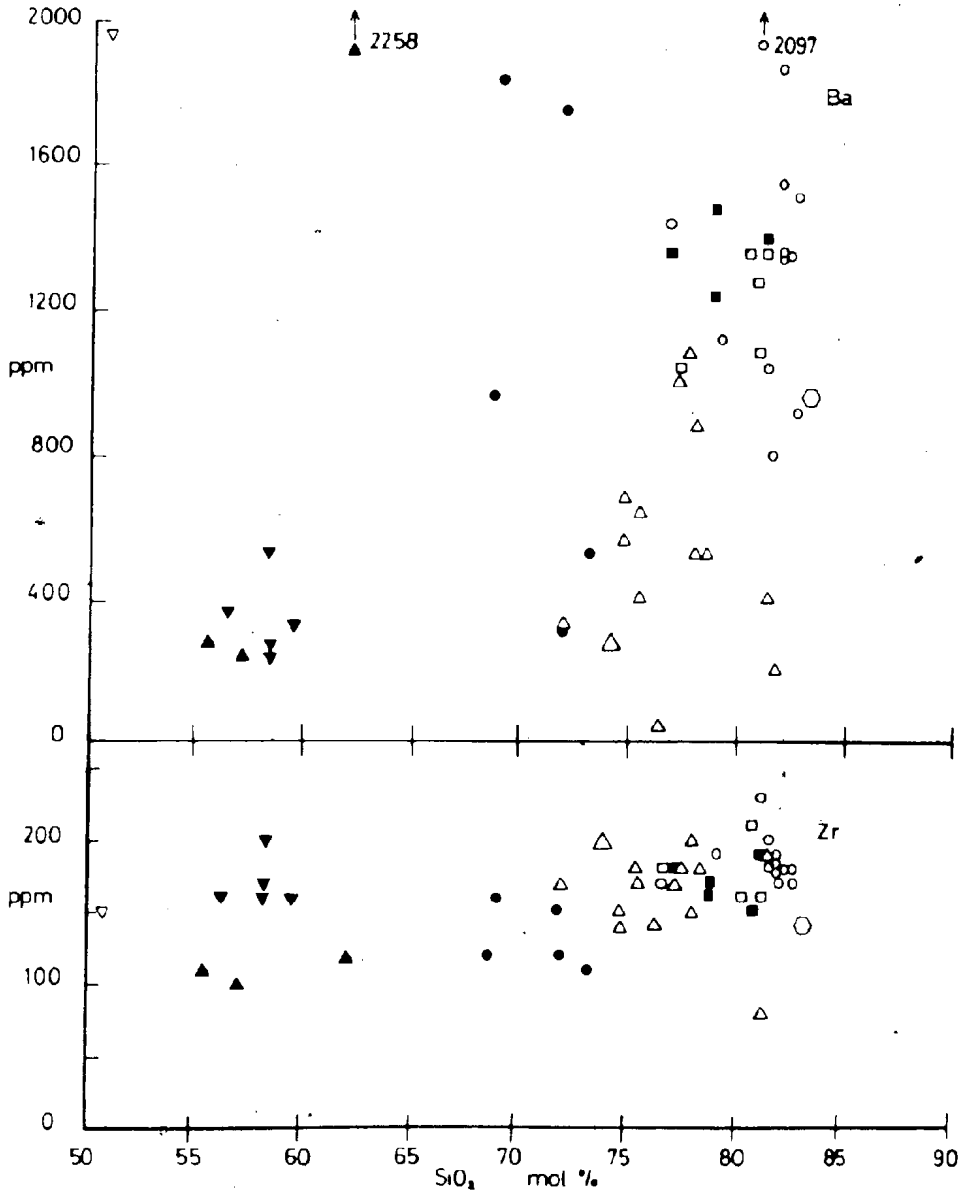

(Key as for major elements)

FIG 13 (cont.)

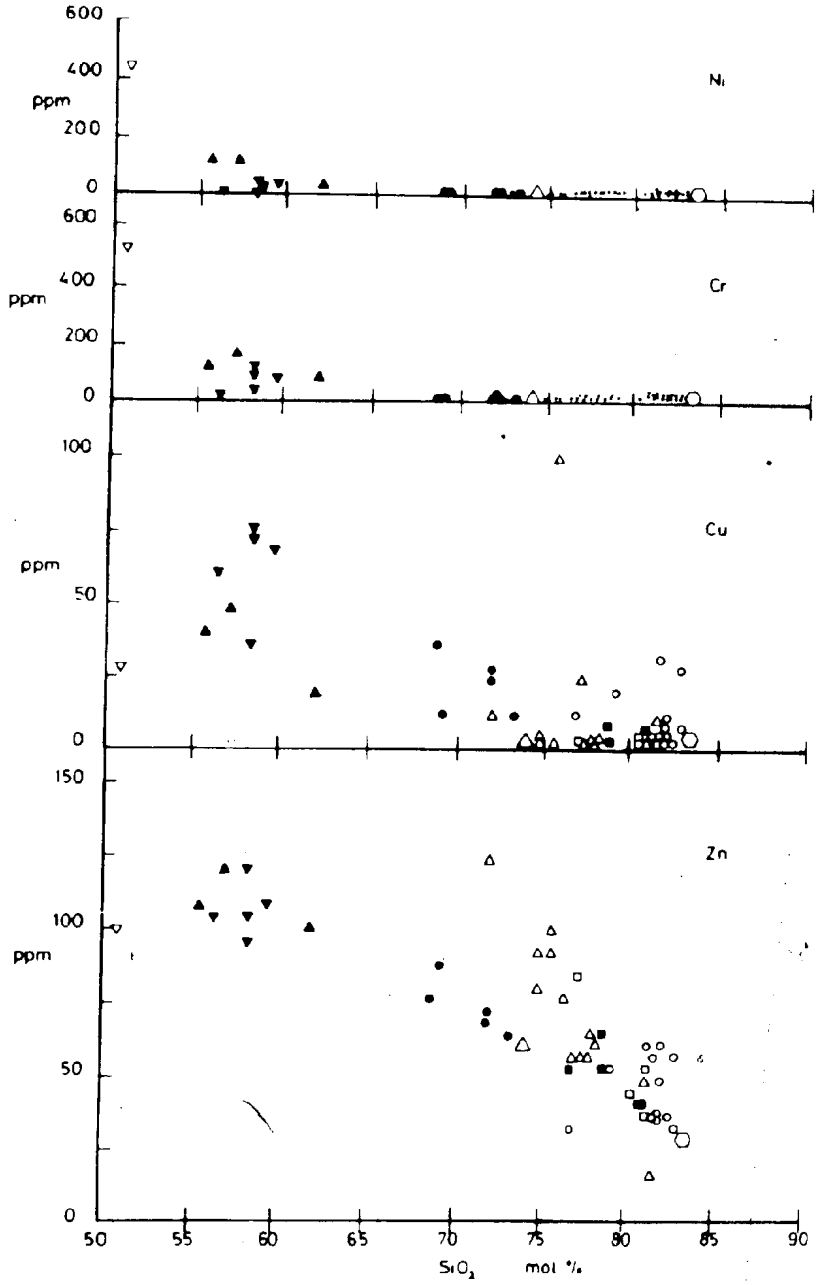

(Key as for major elements)

Of the 10 analyses presented in table 7, 5 are contaminated or otherwise altered. In general, porphyrites are markedly Qz-Hy normative with a small amount of corundum but no olivine appearing in the norm. Leucocratic types are most common and have higher normative Qz and Ab (GC8, GC10, and GC41); more melanocratic types have less Qz and more Hy (GC40 and GC51). An average composition for the entire porphyrite suite is given in table 9 (POR-Q).

The porphyrites occupy a critical position in the variation diagrams examined earlier (figs. 6 and 13) since they fall within a distinct hiatus in SiO_2 which separates basaltic and rhyolitic extrusive rocks of the Harbour Main Group. However, the porphyrites plot near dacitic to rhyodacitic ignimbrites of the Finn Hill sequence and a dacite flow (GC12), and a significant "silica gap" is still apparent. Considered as a group, porphyrites fall on the main trends for total Fe, Al_2O_3, CaO, MgO, MnO, and P_2O_5 (fig. 6). Compared with low-silica ignimbrites and flows, however, porphyrites exhibit low TiO_2 and total alkalies, particularly Na_2O, and high K_2O. The main differences in respect of trace elements are relatively low Zr and appreciable scatter of Ba and Rb (fig. 13). K_2O and Na_2O are no more variable than expected when sampling highly porphyritic rocks with large phenocrysts; Ba and Rb would be even more sensitive.

Elements most likely to be affected by alteration are the alkalies and corresponding alkali-group trace elements, CaO, and Sr. Weathering does not appear to deplete CaO and Sr but rather increase their respective abundances in the whole-rock analysis

(for example, GC25). Hydrothermal alteration of sample GC8 has resulted in a low MgO content and somewhat higher CaO compared with other porphyrites. This sample contains minor epidote in the groundmass and a relatively high L.O.I. reflects loss of CO_2 combined as $CaCO_3$. A significant amount of Ca has also been lost from pyroxene sites in GC51 which are represented by chlorite pseudomorphs. Although CaO appears somewhat low for rocks of this silica content, Sr is only anomalously low in this one sample. It is evident that mild leaching of Ca, and to a lesser extent Sr, has not appreciably affected K_2O/Na_2O ratios, since more extreme values are produced where alkali-exchange can be demonstrated (for example, sodic quartz-keratophyres of the Finn Hill sequence). This observation is in conflict with the suggestion of Hughes (1972a, 1972b) that alteration in Harbour Main rock-types can be detected solely on the basis of variations in K_2O and Na_2O. Although such parameters could possibly identify keratophyric compositions in rhyolitic rocks with originally low CaO and high total alkalies, they cannot differentiate removal of CaO in rocks of intermediate and basaltic compositions. Although rocks altered in this manner would not necessarily be termed "spilites" (depending upon the definition employed) they would nevertheless plot in the centre of the "igneous spectrum" allegedly reserved for rocks with unaltered magmatic compositions (cf. Hughes, 1972a, fig. 1). The possible bulk loss of CaO from an individual sample is probably only significant for porphyrites and basaltic rocks with their considerable contents of lime. It should be noted that low CaO is a coherent and

distinctly magmatic feature of both rhyolitic and granitoid rocks in the Harbour Main Group.

An important petrological characteristic of the porphyrites is their general similarity to calc-alkaline or orogenic andesites, especially their SiO_2 and high Al_2O_3 contents. Using the normative classification of Baragar (1967), porphyrites occupy the fields of rhyolite/trachyte, rhyodacite/trachyandesite, and dacite/mugearite (fig. 11). Porphyrites are generally more Or- and less An-normative than andesite/hawaiite. GC10, GC40, and GC51 are less siliceous than typical rhyolite and slight adjustment for their anomalously low An would place all porphyrites except GC41 in the compositional field of rhyodacite/trachyandesite. Further distinction in this normative plot is not possible without a prior independent classification between the alkali and calc-alkali volcanic series. It is worth noting at this stage that a porphyritic sill on the eastern shore of Colliers Bay falls in the field of hawaiite/mugearite compositions with the majority of basalts and dykes (cf. P70-4, table 7).

Better discrimination can be attained by comparing the "average porphyrite" (POR-Q(b), table 9/ no. 1, table 11) with a carefully selected group of andesitic rocks of very different environments and compositions (cf. table 11). The definition of "andesite" given by Taylor (1968, table 1) is synonymous with orogenic andesite, and he used the term andesite to denote a member of the calc-alkaline volcanic series chemically distinct from intermediate rocks of the alkalic and tholeiitic suites. The relevant compositional data and

TABLE 11. Major and Trace Element Compositions of Andesitic Lavas and Plutonic Rocks Used for Comparison with Intermediate Intrusive Rocks ("Porphyrites") of the Harbour Main Group (analyses in weight percent are recalculated to 100% on a volatile-free basis).

Source	1	2	3	4	5	6	7	8	9
No. of Analyses	(5)	(n.d.p.)	(1)	(1)	(1)	(89)	(29)	(13)	(6)
(Wt. %)									
SiO_2	62.93	60.00	59.61	59.80	59.66	59.39	59.12	59.13	60.61
Al_2O_3	17.65	17.31	17.24	17.43	16.52	17.50	17.57	17.47	16.67
Fe_2O_3	6.44*	-	3.94	2.55	2.99	3.01	3.24	3.36	2.60(2)
FeO	-	6.14†	2.60	2.73	3.35	4.01	3.51	2.59	4.52(2)
CaO	2.28	7.08	7.16	5.94	5.70	7.22	6.31	5.23	5.80
Na_2O	3.91	3.70	3.84	4.41	3.71	3.28	3.85	4.66	3.01
K_2O	3.38	1.61	1.28	2.05	2.72	1.29	2.01	3.67	2.93
MgO	2.55	3.45	3.28	3.96	4.22	3.19	3.31	2.20	2.92
MnO	0.13	n.d.p.	0.15	0.09	0.09	0.12	0.10	0.13	0.19
TiO_2	0.67	0.71	0.70	0.76	0.78	0.82	0.80	1.12	0.60
P_2O_5	0.06	n.d.p.	0.20	0.28	0.26	0.17	0.18	0.44	0.15

TABLE 11 (Cont'd.)

Source	1	2	3	4	5	6	7	8	9
(p.p.m.)				(a)					
Rb	105(55-150)‡	31(19-44)‡		30					100(89-109)‡
Sr	275(188-354)‡	385(215-570)‡		385					467(316-536)‡
Ba	1094(339-1857)‡	270(180-400)‡		270		n.d.p.	n.d.p.	n.d.p.	671(565-759)‡
Zr	138(119-165)‡	110(90-170)‡		110					123(112-136)‡
Cu	24(13-39)‡	54(25-150)‡		n.d.p.					n.d.p.
Zn	75(66-89)‡	n.d.p.		n.d.p.					n.d.p.
Cr	28(25-32)‡	56(19-100)‡		25					13(1)
Ni	9(4-14)‡	18(5-38)‡		18					6(1)
K/Rb	254(228-268)‡	430		430					239(205-264)‡
Rb/Sr	0.38	0.08		0.08					0.21
Ba/Sr	3.98	0.70		0.70					1.44

*Total iron given as Fe_2O_3

+Total iron given as FeO

‡Range of values

n.d.p. = no data presented in source reference

(a) = Average trace element abundances in andesite at 58 wt. % SiO_2 (Jakes and White, 1972, Table 2B).

TABLE 11 (Cont'd.)

1. Average Harbour Main "Porphyrite" (Table 9, no. POR-Q).
2. "Average Andesite" (Taylor, 1968, Table 3).
3. Calc-alkaline low-K andesite (Jakes and White, 1972; major elements: Table 2A, no. 6; trace elements: Table 2B).
4. Calc-alkaline andesite (Jakes and White, 1972; major elements: Table 2A, no. 7; trace elements: Table 2B).
5. Calc-alkaline high-K andesite (Jakes and White, 1972; major elements: Table 2A, no. 8; trace elements: Table 2B).
6. Calcic andesites from island arcs (McBirney, 1969, Table 2).
7. Calc-alkaline andesites from continental margins (McBirney, 1969, Table 2).
8. Alkali-calcic andesites from continental interior regions (McBirney, 1969, Table 2).
9. High-K diorite, Yeoval Complex, New South Wales (Gulson, 1972, Table 3).

distinctions drawn by him will not be repeated here (cf. Taylor, ibid., table 2). However, Taylor's "average andesite" (no. 2, table 11) has slightly less SiO_2, and distinctly lower K_2O, Rb, Ba, and Zr, and higher CaO, MgO, Sr, Cu, Cr, and Ni than POR-Q (no. 1, table 11). The calc-alkaline suite can be subdivided on the basis of variations in SiO_2 and K_2O into low-Si/high-Si and low-K/high-K variants (Taylor and White, 1966; Taylor et al., 1969; Jakes and White, 1972). Differences between typical high-K and low-K calc-alkaline andesites from island arcs in the western Pacific are given in table 11 (nos. 3-5). Even high-K andesites of island arc environments are significantly lower in total alkalies, notably K_2O, and SiO_2, and contain more CaO and MgO than the average porphyrite. Trace element abundances are the same as Taylor's average andesite apart from Cr which is lower.

Following the classification of various groups of andesites given by Peacock (1931), McBirney (1969) presented a collection of average analyses for calcic, calc-alkaline, and alkali-calcic andesites from island arcs, continental margins, and continental interior regions, respectively (table 11, nos. 6-8). On the basis of major oxides, the same dissimilarities are apparent between the average porphyrite and various island arc andesites given by Jakes and White (1972) as between porphyrite and the calcic and calc-alkaline andesites of McBirney (1969). Ignoring lime, and minor differences in silica, Harbour Main porphyrite bears a distinct resemblance to alkali-calcic andesites of continental interiors, particularly with respect to K_2O;

however, TiO_2 is distinctly lower, total alkalies slightly lower, and MgO between that for continental margin and interior types of andesite. Similarities noted previously with granitic differentiates of the Yeoval Complex, New South Wales, can be extended to Harbour Main porphyrites. A rock described as high-K diorite by Gulson (1972) is also intermediate in composition between McBirney's continental andesites though somewhat lower in Al_2O_3; TiO_2 is remarkably similar to average porphyrite.

8.2.3. Basaltic Rocks

The lower part of a predominantly basaltic lava sequence at the top of the Harbour Main Group has been analysed previously by Papezik (1970, table 1). The basalts and a sill are distinctly feldsparphyric types with locally trachytic texture (P70-1, -2, -3, -4, table 7). A further 4 analyses of feldsparphyric lavas (NX12 and NX15), olivine basalt (NX14), and a picritic sill (NX17) in the lower and middle parts of the sequence are presented together with analytical data for 8 diabase dykes that intrude the map area (cf. table 7, fig. 4, and geological map).

Rock samples chosen for analysis were generally dark grey in colour, though greenish grey (for example, GC2 and NX17) and reddish grey (P70-2) rocks were included locally. Use of the term "cumulate" to describe NX17 in the variation diagrams (figs. 6 and 13) simply indicates its accumulative origin (defined below) and does not denote a cumulate texture. Compositional differences between samples reflect

local variations in the basaltic pile that are not necessarily representative of the entire sequence of lavas and intrusions.

Basaltic rocks of the Harbour Main Group pose a considerable problem of nomenclature and classification (cf. Papezik, 1970; and Hughes, 1972a). Certain chemical and mineralogical features are commonly attributed to the liquid line of descent of the alkali-olivine basalt series, particularly hawaiites and mugearites (Papezik, 1970). However, such distinctly sodic compositions, especially the diabase dykes, and the development of secondary mineral assemblages also point to a group of rocks known collectively as "spilites" which are commonly found in close association with keratophyric rocks (cf. Turner and Verhoogen, 1960, p. 257-272; and Joplin, 1968, p. 18 and p. 149-156). Before proceeding with the chemical features of Harbour Main basalts, some petrographic and compositional characteristics of typical spilite require clarification.

Hypotheses advanced to account for the origin of spilite, often in reference to the so-called "spilite problem", have been reviewed in depth by Turner and Verhoogen (1960), Vallance (1960), and Amstutz (1968). The currently popular belief as to the origin of spilite is probably that expressed by Vallance (1969) who regards all spilites as a product of the "hydrous degradation of basalt", i.e. secondary alteration of a basaltic rock at low P and T conditions involving hydrolysis or hydrogen ion metasomatism (Hemley and Jones, 1964). A suitable petrographic definition for spilite has been given by Vallance (1969, p. 38) who states that "mineral associations found in spilites

are those typically attributed to the greenschist or prehnite-pumpellyite facies of metamorphism ..... Spilites might well represent adjustments under PT conditions ranging across those of diagenesis/zeolite facies to greenschist facies". This clearly allows for the variety of secondary mineral assemblages found in the basalts and so does not exclude the possible occurrence of spilite in the Harbour Main Group (cf. also Vallance, 1969, table 2 for spilitic mineral associations). The definition of spilite proposed by Cann (1969, p. 1) is not generally applicable to the Harbour Main Group since the vast majority of mineral assemblages investigated so far are demonstrably sub-greenschist. However, such petrographic characteristics by themselves are not sufficiently stringent to detect chemical readjustment of basaltic compositions.

The chemical attributes of spilite are a particularly perplexing problem. According to Turner and Verhoogen (1960, p. 267) spilites are characterised by low CaO/Na_2O ratios (approximately 1.5 using wt. %) while common basalts of tholeiitic and alkaline affinities exhibit high CaO/Na_2O (usually 3-5). However, it should be noted that hawaiites and mugearites are also typified by relatively low CaO/Na_2O (cf. Irvine and Baragar, 1971, p. 546, nos. 18 and 19).

Vallance (1969, fig. 1) compiled a series of frequency distribution curves for oxide variation between typical basalt and spilite. According to these plots, spilites exhibit overall gain of H_2O+ and CO_2, generally higher but extremely variable Na_2O, low CaO (5.5-6.0 wt. %), and slightly lower K_2O and MgO relative to the average basalt

of Manson (1968); arithmetic means and modes of both sample populations are comparatively close for SiO_2, Al_2O_3, MnO, TiO_2, and P_2O_5. However, Vallance's estimates of relative gains and losses (his sample population contains some 2200 analyses) can only be used as a guide to the general effects of spilitisation processes operating in an open system (compare Smith, 1968; and Reed and Morgan, 1971). The complete transformation of basalt to spilite, therefore, requires a locally open system, and must ultimately depend upon the composition of the reagents, physiochemical conditions, parameters such as porosity and permeability, and various kinetic variables.

The effects of spilitic alteration on trace elements are comparatively poorly documented; however, Cann (1970) noted that Rb, and to a lesser extent Sr, were susceptible to leaching during incipient greenschist metamorphism and ocean-floor weathering of Carlsberg Ridge basalts.

From the above, and inspection of the scatter in chemical variation diagrams (figs. 6 and 13), it appears that the most useful chemical criteria with which to distinguish possible spilitic alteration of Harbour Main basalts are an anomalous distribution of alkalies, CaO, Rb, Ba, and possibly MgO and Sr relative to the basalt composition as given, for example, by Manson (1968) and Prinz (1968). As in the case of the quartz-keratophyres, the processes of spilitisation are not unique to any particular tectonic environment and K-rich continental "spilites" are known (cf. Vallance, 1960, p. 12; Joplin, 1968, p. 149-150).

In common with Harbour Main ignimbrites and porphyrites, the basalts have undergone appreciable secondary hydration; L.O.I. values range 2.38-5.41 and most of this represents H_2O+. The effects of hydration on the chemical analyses and normative compositions (if any) are unknown. Analyses have been recalculated free of volatiles (plotted samples only) in order to provide a better basis for comparison (cf. table 7).

The basaltic suite as a whole is characterised by uniformly high Al_2O_3 and low but variable TiO_2. Total Fe, MgO, MnO, Cu, and Zr exhibit significant variation with respect to SiO_2; CaO and Na_2O (hence total alkalies) are highly variable (cf. figs. 6 and 13). Variations of MgO are proportionate to the amount of modal olivine.

A diabasic sill (NX17) plots in the field of accumulative rocks in an AFM diagram (Nockolds and Allen, 1953). In view of its high proportion of modal (>25%) and normative (34.48%) olivine, NX17 is a picrite, according to the definition of Wilkinson (1968a) and Irvine and Baragar (1971). Abundances of Cr and Ni are in excess of the maximum concentrations (550 and 350, respectively) found in basaltic liquids (Prinz, 1968) and clearly point to an accumulative origin for the olivine, the chief recipient of these trace elements. The anomalous K_2O/Na_2O ratio of this rock is the result of introduction of K_2O (and Ba); chiefly in the form of alkalic feldspar in recrystallised basaltic glass. Calcium in this rock appears to have been fixed by epidote; the occurrence of this Ca-Al silicate ends abruptly at the contact with surrounding lavas.

Diabase dykes are substantially altered due to their location in permeable fault-zones and locally porous volcaniclastic rocks. GC13, GC26, and H165 have anomalously low CaO/Na_2O when compared to the basalts, and exhibit K_2O/Na_2O ratios appropriate to those of typical spilite given by Turner and Verhoogen (1960, table 25, nos. 1-4), and Vallance (1969, table 3). K_2O/Na_2O ratios in remaining dykes range from little altered (if at all) to strongly modified: GC31t (Na_2O and K_2O only) represents the intensely altered glassy margin of a dyke with a more holocrystalline interior (GC31u). GC2 contains abundant epidote in the matrix and consequently CaO and Sr are anomalously high, revoking its classification as a typical spilite, but nevertheless intimately associated with spilitisation processes (cf. Smith, 1968). Except for strong leaching of Sr and possibly Zr in GC31t, there is no distinct relationship between removal of Ca and low Sr in spilitised dykes. However, leaching of K_2O may have affected Rb and Ba.

The effects of spilitisation on the normative compositions of GC13, GC26, and H165 is considerable, though much easier to detect than to adjust for quantitatively. Variable addition of Na_2O to these rocks creates more potential albite in the norm. In rocks of low silica content, excess Ab relative to Qz may be converted to Ne according to the empirical relationship: 5Ab = 3Ne + 2Qz (cf. Poldervaart, 1964). Consequently, the appearance of strongly nepheline-normative compositions in these feldsparphyric dykes (for example, H165) is almost certainly a product of spilitisation. Re-

moval of such bias in the CIPW calculation favours a shift toward a more Ol-Hy-normative composition, though small amounts of Ne could quite possibly be retained in the norm. Vallance (1969) also noted conversion of Ol-Hy-normative basalts of the Carlsberg Ridge to Ne-normative spilites (cf. Cann and Vine, 1966).

Apart from the variable effects of oxidation and hydration, the only basaltic lavas that appear in any way altered are NX15, NX12, and P70-2. Excessive K_2O in NX15 is due to contamination by K-feldspar which occupies amygdales in the upper part of this flow; CaO is notably low. The K_2O/Na_2O ratios of NX12 and P70-2 are similar to those of partially spilitised dykes, yet there is no detectable leaching of CaO, MgO, or Sr. CaO/Na_2O ratios in all the lavas are relatively low (1.31-1.92) when compared with averages for various basalts listed by Manson (1968); however, this is a coherent feature and cannot be attributed to spilitisation.

In general, Ne-normative compositions in these lavas appear to have a different origin than those of the dykes: the degree of post-extrusion oxidation, usually expressed by the Fe_2O_3/FeO ratio, may seriously shift normative parameters toward an anomalous appearance of Qz or Ne (cf. Chayes, 1966). However, oxidation alone, though severe in the case of P70-2, poses no more of a threat to the accurate representation of Precambrian basalts in the norm than it does to their modern extrusive equivalents. Fe_2O_3/FeO ratios determined by Papezik (1970) for Harbour Main basalts of feldsparphyric type, range from 1.92 to 17.73 (calculated in wt. %) and a basaltic sill

has a value of 0.85. A statistical average for young basalts is 0.4 according to Chayes (1966), but even an adjustment of this magnitude would leave a considerable amount of Fe_2O_3 in P70-2. Coombs (1963) chose 1.5 wt. % Fe_2O_3 as an upper limit, and Irvine and Baragar (1971) suggested that an appropriate adjustment was given by the formula $\%Fe_2O_3 = 1.5 + \%TiO_2$. Papezik (1970, table III) allowed for 2.0% Fe_2O_3, recalculating the remainder as FeO and thereby producing small amounts of Ne (0.6-1.4%) in the (cation) norm. In view of the relatively low TiO_2 contents of Harbour Main basaltic rocks, the above calculations closely approximate the recommendations of Coombs (1963) and Irvine and Baragar (1971). Taking total Fe as FeO increases the amount of CIPW normative Ne in these lavas by approximately 1.0% (P70-1, -2, -3, table 7). This in turn reduces the amount of hypersthene in the norm, and may prevent its appearance altogether. However, the very fact that small adjustments of this kind are crucial to the appearance of normative Ne brings out a fundamental chemical characteristic of these basalts.

Additional inferences concerning specific magmatic heritage can be made on the basis of relict mineral compositions, particularly pyroxenes (cf. Vallance, 1969a). Whereas predominantly feldsparphyric basalts with little groundmass olivine and pyroxene are slightly Ne-normative, lavas with appreciable olivine in the groundmass (NX12), or groundmass olivine accompanied by olivine phenocrysts (NX14), are Ol-Hy-normative with somewhat higher ΣFeO/MgO ratios. The lack of a textural relationship between groundmass olivine and pyroxene, combined

with the predominant lack of Ca-poor pyroxene in lavas and intrusives alike, emphatically point to an alkalic affinity for these basalts (cf. Kuno, 1960; Wilkinson, 1968a; Best and Brimhall, in press).

Trace element abundances are consistently within the range for the "average basalt" given by Prinz (1968, table II). Zr in dykes is close to or greater than Prinz's arithmetic mean for Ne-normative basalts (164 p.p.m.), while Zr in the more olivine-rich basalts is close to his average for Ol-normative alkali basalts (118 p.p.m.). Average Sr for the basaltic suite is generally lower than that for either Ne-normative or Ol-normative types of basalt, and Rb intermediate between the two.

Evidently, the difficulties experienced in finding a definitive classification for basaltic rocks of the Harbour Main Group are inherently magmatic. Testing the high-alumina nature of the entire basaltic suite against Kuno's (1960) classification of "island arc" high-alumina basalts (fig. 12), the rocks are predominantly of alkali-olivine basalt kindred (altered samples demonstrably so) with two samples falling in the high-alumina field; NX14, however, has too low a silica content to be defined strictly as "high-alumina basalt". An alkalies-silica diagram (fig. 18) clearly distinguishes the suite as alkaline rather than "subalkaline" (cf. Wilkinson, 1968a); yet when compared with Hawaiian alkali-olivine basalts, which provide the critical boundary in this plot (Macdonald and Katsura, 1964), Harbour Main rocks are distinctly more aluminous and contain less

titania. Although Irvine and Baragar (1971) decided to adjust this boundary slightly (cf. fig. 18), they noted that it was generally unsuitable for their lavas with Opx in the norm (Coppermine River lavas).

A classification based on normative parameters is obviously more desirable since more use is made of the complete chemical analysis. Following the normative scheme of Baragar (1967) and Irvine and Baragar (1971), K_2O/Na_2O ratios define the Harbour Main suite as a derivative of the sodic alkali-olivine basalt series (fig. 11). Apart from spilitised dykes which fall in the field of mugearite, and NX15 which plots as a "trachyandesite", samples occupy the field of hawaiite, a seemingly appropriate appellation in view of their relatively low CaO/Na_2O ratios and correspondingly low normative An contents. According to this classification, therefore, no true alkali-olivine basalts (normative An>50) are represented among analysed samples.

A widely accepted normative classification of basaltic rocks has been proposed by Yoder and Tilley (1962). Although the exact locus of the "critical plane of silica saturation" is in some doubt (cf. Poldervaart, 1964; and Irvine and Baragar, 1971), this scheme can be used effectively provided that Fe_2O_3/FeO ratios have been previously evaluated. From the preceding discussion concerning the normative status of Harbour Main basaltic rocks, it is apparent that the lavas, at least, straddle the boundary between Ne-normative and Ol- and Hy-normative compositions. In Yoder and Tilley's classification,

the appropriate name for basaltic lavas with Ol and Hy in the norm is "olivine tholeiite". Although olivine-bearing basalts of the Harbour Main Group lack Qz and Ne in the norm, their close association in time and space with weakly Ne-normative basalts together with their alkalic affinity, places them in a group of "weakly alkaline" or "transitional" basalts of alkalic character as opposed to those of tholeiitic character (cf. Coombs, 1963; and Wilkinson, 1968b).

Although basaltic rocks of the Harbour Main Group cannot be conveniently bracketed as distinctly tholeiitic or alkalic (cf. Chayes, 1966, for a quantitative approach to this problem), their rather unique magmatic signature provides an independent basis for assessing the tectonic environment of Harbour Main volcanism. Transitional basalts of alkalic character are often associated with low-K tholeiitic rocks in continental regions and mid-oceanic environments characterised by high heat flow and extensional tectonism (Leeman and Rogers, 1970; Bass, 1972; Gass, 1970; Mohr, 1971; Best and Brimhall, in press). The continental setting of Harbour Main basalts promotes an analogy with Late Cenozoic basaltic volcanism in and around the periphery of the Basin-Range province.

A statistical method, taken from Ragland _et al_. (1968), for comparing chemical similarities between various basalts, was employed by Leeman and Rogers (1970) to test the interdependence of specific magma type and tectonic regime. This method is particularly advantageous since a) it provides for a rigorous and simple quantitative

comparison between basalts; b) it utilises the complete chemical analysis, thereby incorporating elements such as titanium, rarely included in normative classification schemes but nevertheless an important petrogenetic indicator; c) it allows mobile elements in Harbour Main basalts, such as the alkalies and calcium, to be judged independently of relatively immobile elements such as Al_2O_3, TiO_2, total Fe, and MgO.

Accordingly, the following quantities were calculated after Ragland *et al*. (1968):

1) the sum, for all oxides, of the quantity:

$$\frac{(\%X-\%HM)^2}{\%HM}$$

2) the sum, for all oxides, of the quantity:

$$\frac{|\%X-\%HM|}{\%HM}$$

where %X is the abundance of an oxide in the comparison basalt, and %HM is the abundance of an oxide in the Harbour Main basalt. In the case of comparisons made here, these quantities were calculated twice: A = K_2O and Na_2O computed independently; B = K_2O and Na_2O combined as total alkalies. Each calculation, therefore, yields two values (A and B) which permit a rank ordering of the various comparison basalts. The respective sums of these rank orders provide a comparison number: the lowest sum corresponds to the basalt that is most similar to the Harbour Main basalt; the highest sum denotes the least similar basalt. The Harbour Main basalts used for comparison are an olivine basalt

TABLE 12. Major Element Compositions of Basalts Used for Comparison with Harbour Main Basaltic Rocks (analyses in weight percent and recalculated to 100% on a volatile-free basis).

Source	SiO_2	Al_2O_3	*FeO	CaO	Na_2O	K_2O	MgO	MnO	TiO_2	P_2O_5	(a)
1	50.80	18.79	8.98	6.63	4.64	1.39	6.31	0.13	1.95	0.38	2
2	49.38	18.28	11.52	7.15	3.71	0.56	7.15	0.19	1.59	0.47	1
3	46.94	14.80	12.18	10.45	2.95	0.85	8.28	0.14	3.04	0.37	28
4	49.18	16.69	11.31	7.88	4.48	1.62	4.76	0.18	3.20	0.70	33
5	52.24	16.76	10.07	6.34	5.24	2.02	3.58	0.21	2.59	0.94	13
6	48.25	15.07	11.17	11.35	3.39	0.73	6.70	0.19	2.78	0.37	3
7	51.49	15.48	10.29	8.68	3.23	0.97	7.13	-	1.75	-	107
8	51.10	15.31	10.18	7.61	3.80	1.76	7.18	-	2.19	-	20
9	51.23	16.95	9.85	8.01	3.59	1.59	6.08	-	1.84	-	18
10	49.50	15.40	9.80	9.70	3.60	1.50	7.60	-	1.80	-	36
11	50.45	15.29	11.96	7.50	4.36	1.93	6.18	-	2.33	-	6
12	48.61	17.45	10.58	10.35	3.33	0.54	7.19	0.15	1.45	0.35	5
13	51.43	16.07	11.80	8.80	3.43	1.06	5.04	0.19	1.81	0.37	4
14	49.91	17.44	8.67	10.95	3.10	1.01	7.00	0.13	1.47	0.32	7

TABLE 12 (Cont'd.)

Source	SiO_2	Al_2O_3	*FeO	CaO	Na_2O	K_2O	MgO	MnO	TiO_2	P_2O_5	(a)
15	49.37	17.58	9.43	10.27	3.10	0.91	7.18	0.15	1.65	0.36	5
16	49.69	17.93	9.79	10.02	2.91	0.73	6.99	0.14	1.54	0.26	21
17	50.54	17.70	9.82	10.57	2.77	0.40	7.44	-	0.76	-	11
18	48.60	15.71	9.98	10.54	2.88	1.14	9.41	-	1.74	-	7
19	52.01	16.30	12.07	6.24	4.63	2.01	3.62	-	2.42	0.70	8
20	47.32	15.77	13.49	9.55	3.52	1.21	4.72	0.20	3.72	0.50	7
21	52.38	17.20	10.32	6.94	4.93	2.41	2.61	0.20	2.31	0.70	6
22	49.23	16.73	10.04	9.12	3.67	1.50	6.23	0.15	2.52	0.81	3
23	50.74	17.27	9.78	8.15	4.30	1.99	4.07	0.15	2.55	1.00	2
24	51.08	16.12	10.55	6.78	4.75	2.55	4.16	0.17	2.52	1.32	1
25	51.97	16.34	10.38	8.06	4.35	1.17	5.63	0.19	1.59	0.32	225
26	49.67	16.39	10.11	10.95	3.05	0.18	7.70	0.20	1.67	0.08	6
27	50.24	15.77	9.51	8.12	4.59	0.06	9.55	0.26	1.83	0.07	1
28	52.35	15.12	9.52	7.14	5.95	0.04	8.19	0.27	1.93	0.05	1

*Total iron given as FeO
(a) No. of analyses involved in calculating the average

TABLE 12 (Cont'd.)

1. Harbour Main feldsparphyric basalt (Average of P70-1, P70-3, Table 7).
2. Harbour Main olivine-bearing basalt (NX-14, Table 7).
3. Hawaiian alkali-olivine basalt (MacDonald and Katsura, 1964, Table 10, no. 4).
4. Hawaiian hawaiite (MacDonald and Katsura, 1964, Table 10, no. 5).
5. Hawaiian mugearite (MacDonald and Katsura, 1964, Table 10, no. 6).
6. Low-magnesia alkalic basalt, Galapagos Islands (McBirney and Williams, 1969, Table 4, no. 5).
7. Grand Wash basalt, western margin of Colorado Plateau (Best et al., 1969, col. 1, p. 13).
8. K-variant of Grand Wash basalt, western margin of Colorado Plateau (Best et al., 1969, col. 2, p. 13).
9. Craigs Ranch basalt, western margin of Colorado Plateau (Best et al., 1969, col. 6, p. 13).
10. Basin-Range alkali-olivine basalt (Leeman and Rogers, 1970, Table 5, no. 13).
11. Sodic-hawaiite, Colorado Plateau-Basin-Range transition zone (Best and Brimhall, in press, Table 4).
12. Beaver Ridge 1 lavas, Black Rock Desert, Utah (Hoover, 1974, Table A-3).
13. Beaver Ridge 2 lavas, Black Rock Desert, Utah (Hoover, 1974, Table A-5).
14. Pavant 1 lavas, Black Rock Desert, Utah (Hoover, 1974, Table A-6).
15. Pavant 2 lavas, Black Rock Desert, Utah (Hoover, 1974, Table A-7).
16. High-alumina basalt, Cascade Range and Oregon Plateaus (Waters, 1962, Table 5).
17. High-alumina basalt, Japan (Kuno, 1960, Table 6).

TABLE 12 (Cont'd.)

18. Alkali-olivine basalt, Japan (Kuno, 1960, Table 6).

19. Mugearite, Scotland (Walker, 1952, Table 3).

20. Hawaiite, Reunion Island (Upton and Wadsworth, 1972, Table 6, no. 2B).

21. Mugearite, Reunion Island (Upton and Wadsworth, 1972, Table 6, no. 3B).

22. Alkali-olivine basalt, Nandewar Volcano, New South Wales (Abbott, 1969, Table 3, nos. 1-3).

23. Hawaiite, Nandewar Volcano, New South Wales (Abbott, 1969, Table 3, nos. 4-5).

24. Mugearite, Nandewar Volcano, New South Wales (Abbott, 1969, Table 3, no. 6).

25. Average spilite (Vallance, 1969, Table 1).

26. Average "fresh" basalt, Carlsberg Ridge (Cann, 1969, Table 3, no. 7).

27. Incompletely spilitised diabase, Carlsberg Ridge (Cann, 1969, Table 1, no. 2).

28. Spilite, Carlsberg Ridge (Cann, 1969, Table 1, no. 1).

TABLE 13. Rank Order of Basalts Used for Comparison with Feldsparphyric Basalts, Harbour Main Group (Table 12, no. 1).

Comparison Basalt	Source (Table 12)	$\Sigma(\%X-\%HM)^2 / \%HM$ Value A*	Rank	Value B†	Rank	$\Sigma\lvert\%X-\%HM\rvert / \%HM$ Value A*	Rank	Value B†	Rank	Sum of Rank Orders A*	Sum of Rank Orders B†
Craigs Ranch Basalt	9	1.32	2	1.18	2	1.36	1	0.99	1	3	3
Average spilite (Vallance)	25	1.10	1	1.09	1	1.65	2	1.43	8	3	9
Grand Wash Basalt (K-variant)	8	1.84	3	1.63	3	1.67	3	1.22	3	6	6
Sodic-hawaiite	11	2.55	5	2.33	6	1.81	4	1.36	5	9	11
Grand Wash Basalt	7	2.59	6	2.59	8	1.97	8	1.37	6	14	14
Pavant 2 lavas	15	2.99	10	2.99	12	1.87	6	1.19	2	16	14
Nandewar alkalic basalt	22	2.20	4	2.11	5	2.51	13	2.22	16	17	21
Beaver Ridge 2 lavas	13	2.68	8	2.68	10	2.06	9	1.56	11	17	21
Basin-Range alkalic basalt	10	3.15	13	3.05	14	1.83	5	1.53	10	18	24
Oregon high-Al_2O_3 basalt	16	3.03	11	3.02	13	2.23	10	1.38	7	21	20
Hawaiian hawaiite	4	2.64	7	2.60	9	2.90	14	2.71	20	21	29
Pavant 1 lavas	15	3.76	15	3.75	18	1.89	7	1.29	4	22	22

TABLE 13 (Cont'd.)

Comparison Basalt	Source (Table 12)	$\frac{\Sigma(\%X-\%HM)^2}{\%HM}$ Value A*	Rank	Value B†	Rank	$\frac{\Sigma\lvert\%X-\%HM\rvert}{\%HM}$ Value A*	Rank	Value B†	Rank	Sum of Rank Orders A*	B†
Beaver Ridge 1 lavas	12	3.71	15	3.59	17	2.38	11	1.48	9	26	26
Nandewar hawaiite	23	2.82	9	2.55	7	3.35	20	2.85	21	29	28
Hawaiian mugearite	5	3.04	12	2.93	11	3.74	22	3.15	22	34	33
Japanese alkalic basalt	18	5.67	22	5.63	22	2.46	12	1.90	12	34	34
Reunion mugearite	21	3.71	16	3.23	15	3.26	19	2.46	17	35	33
Scottish mugearite	19	3.79	17	3.57	16	3.06	18	2.61	18	35	34
Japanese high-Al_2O_3 basalt	17	5.26	20	5.16	20	3.05	17	1.93	13	37	33
Galapagos low-magnesia basalt	6	5.81	23	5.77	23	2.92	15	2.18	14	38	37
Carlsberg Ridge spilite	28	3.51	14	1.83	4	3.87	25	2.62	19	39	23
Hawaiian alkalic basalt	3	6.53	24	6.53	24	2.95	16	2.20	15	40	39
Spilitised diabase	27	4.18	18	3.23	15	3.81	23	2.85	21	41	36
Carlsberg Ridge basalt	26	5.51	21	5.21	21	3.83	24	2.62	19	45	40

TABLE 13 (Cont'd.)

Comparison Basalt	Source (Table 12)	$\frac{\Sigma(\%X-\%HM)^2}{\%HM}$ Value A*	Rank	Value B†	Rank	$\frac{\Sigma\lvert\%X-\%HM\rvert}{\%HM}$ Value A*	Rank	Value B†	Rank	Sum of Rank Orders A*	B†
Nandewar mugearite	24	4.87	19	4.16	19	4.62	26	3.76	24	45	43
Reunion hawaiite	20	6.65	25	6.64	25	3.56	21	3.19	23	46	48

*A = K_2O and Na_2O computed independently

†B = computation with K_2O and Na_2O combined as total alkalies

TABLE 14. Rank Order of Basalts Used for Comparison with Olivine Basalt, Harbour Main Group (Table 12, no. 2).

Comparison Basalt	Source (Table 12)	$\frac{\Sigma(\%X-\%HM)^2}{\%HM}$ Value A*	Rank	Value B†	Rank	$\frac{\Sigma\lvert\%X-\%HM\rvert}{\%HM}$ Value A*	Rank	Value B†	Rank	Sum of Rank Orders A*	B†
Grand Wash Basalt	7	1.57	1	1.21	2	1.69	2	0.83	1	3	3
Beaver Ridge 1 lavas	12	1.65	2	1.65	7	1.29	1	1.15	9	3	16
Oregon high-Al_2O_3 basalt	16	1.76	4	1.63	6	1.86	3	1.34	10	7	16
Average spilite (Vallance)	25	1.70	3	1.29	3	2.17	6	0.91	3	9	6
Beaver Ridge 2 lavas	13	1.88	5	1.43	4	2.03	5	1.06	5	10	9
Pavant 2 lavas	15	2.12	6	1.82	8	1.93	4	1.14	8	10	16
Craigs Ranch basalt	9	2.82	8	1.12	1	2.77	11	0.90	2	19	3
Pavant 1 lavas	14	3.31	10	2.85	14	2.53	9	1.57	11	19	25
Carlsberg Ridge basalt	26	3.14	9	3.01	15	2.63	10	1.77	12	19	27
Japanese high-Al_2O_3 basalt	17	3.37	12	3.37	16	2.49	8	1.95	16	20	32
Spilitised diabase	27	2.71	7	2.08	11	3.30	15	2.17	20	22	31
Galapagos low-MgO basalt	6	4.09	16	4.01	21	2.23	7	1.84	13	23	34

TABLE 14 (Cont'd.)

Comparison Basalt	Source (Table 12)	$\frac{\Sigma(\%X-\%HM)^2}{\%HM}$ Value A*	Rank	Value B†	Rank	$\frac{\Sigma\lvert\%X-\%HM\rvert}{\%HM}$ Value A*	Rank	Value B†	Rank	Sum of Rank Orders A*	B†
Basin-Range alkalic basalt	10	3.47	13	2.05	10	2.78	12	1.07	6	25	16
Grand Wash basalt (K-variant)	8	3.74	15	1.56	5	3.14	14	0.97	4	29	9
Nandewar alkalic basalt	22	3.36	11	1.97	9	3.83	19	2.14	19	30	28
Carlsberg Ridge spilite	28	3.54	14	2.40	13	3.61	16	2.08	17	30	30
Hawaiian alkalic basalt	3	4.19	17	3.93	19	3.0[illegible]	13	2.30	21	30	40
Japanese alkalic basalt	18	4.41	18	3.64	18	3.14	14	1.88	14	32	32
Sodic-hawaiite	11	4.70	19	2.19	12	3.71	18	1.09	7	37	19
Reunion hawaiite	20	6.02	21	5.30	23	3.69	17	2.48	22	38	45
Hawaiian hawaiite	4	4.93	20	3.54	17	4.20	20	2.10	18	40	35
Scottish mugearite	19	6.82	23	4.15	22	4.73	21	1.89	15	44	37
Nandewar hawaiite	23	6.75	22	3.96	20	5.46	22	2.75	24	44	44
Hawaiian mugearite	5	7.90	24	5.56	24	5.64	24	2.61	23	48	47

TABLE 14 (Cont'd.)

Comparison Basalt	Source (Table 12)	$\Sigma\frac{(\%X-\%HM)^2}{\%HM}$ Value A*	Rank	Value B†	Rank	$\Sigma\frac{\lvert\%X-\%HM\rvert}{\%HM}$ Value A*	Rank	Value B†	Rank	Sum of Rank Orders A*	B†
Reunion mugearite	21	10.21	25	5.91	26	5.52	23	1.88	14	48	40
Nandewar mugearite	24	11.11	26	5.90	25	7.04	25	3.21	25	51	50

*A = K_2O and Na_2O computed independently

†B = computation with K_2O and Na_2O combined as total alkalies

(NX14) and the average of two feldsparphyric basalts (P70-1 and P70-3). These basalts and a group of 26 comparison basalts of high-alumina, transitional, and alkalic affinities from oceanic island and continental occurrences are presented in table 12. Also included in the comparison are spilites from the Carlsberg Ridge (Cann, 1969) and Vallance's (1969) average "continental" spilite. All comparisons were made with total Fe combined as FeO and analyses recalculated volatile-free. The results of these calculations for feldsparphyric and olivine basalts of the Harbour Main Group are given in tables 13 and 14, respectively. Comparison basalts are arranged in ascending order of A, the sum of the rank orders; the most similar basalt with respect to A (not necessarily B) is the lowest number at the top of each table; the least similar basalt is placed at the bottom.

The strongest influence on the rank ordering of comparison basalts in tables 13 and 14 is exerted by TiO_2 and the alkalies, particularly K_2O. All other factors being equal, continental basalts with their comparatively low concentrations of TiO_2 are statistically preferred over relatively high-TiO_2 basalts from oceanic islands. It is interesting to note that continental margin basalts from Scotland (Walker, 1952) and the Nandewar Mountains (Abbott, 1969) group with the latter.

The feldsparphyric variety of Harbour Main basalt (cf. table 13; rank order A) shows a very close similarity to hawaiites of the western Grand Canyon region (Best and Brimhall, 1970, in press); to high-alumina transitional lavas of the Black Rock Desert (Hoover, 1974);

and to the average spilite of Vallance (1969). The plateau hawaiites described by Best and Brimhall (in press) are characterised by a) low normative An (andesine); b) normative Ne<5%; and c) normative Hy commonly <5% but as great as 14% in some samples. These characteristics aptly fit the range of normative compositions found in Harbour Main basalts. Late segregation veins of Na-hawaiite/mugearite composition occur locally within Grand Canyon lavas (cf. table 12, no. 11). Discrimination between these various basalts is based predominantly on the variation of K_2O, as exemplified by the statistical choice of the K-rich variant of Grand Wash basalt over the K-poor type. The close similarity of Vallance's (1969) average spilite to Harbour Main feldsparphyric basalt, and consequently late Cenozoic hawaiites and transitional basalts, carries with it an interesting corollary. Several authors have tried to explain the spilite composition by the derivation of this unusual rock-type from an alkali-olivine basaltic magma via differentiation of a mugearite (cf. for example, Turner and Verhoogen, 1960, p. 270 and table 26, no. 2). Joplin (1968, p. 156) also noted that "these rocks (spilites) have a composition fairly close to a mugearite or basalt", and included mugearite in her "spilite suite" together with a picrite basalt (cf. Joplin, ibid., table XXVII, nos. 1-3). In compiling his average, Vallance (1969) was especially careful to reject pillowed spilites, which were included elsewhere (cf. Vallance, ibid., table 1). Since the incorporation of large numbers of analyses in his average spilite must necessarily induce a chemical compromise, it appears that Vallance's

average "continental" spilite may well represent rocks of hawaiite/mugearite heritage rather than reflect their present state of alteration. Carlsberg Ridge spilites (Cann, 1969) are ranked low in the list, but it is important to note [illegible] typical spilite is preferred over "fresh" basalt.

The effect of combining total alkalies when two analyses are compared in this manner reduces their influence on the rank ordering, so that differences in other oxides become more pronounced (compare ranks A and B, table 13). Consider, for example, the rank ordering of high-alumina basalts of the Cascades and Oregon plateaus (Waters, 1962) and Hawaiian hawaiite (Macdonald and Katsura, 1964) in table 13. Although both are equally dissimilar to Harbour Main basalt, according to the order of rank given by A, the affinity of the Oregon basalt, according to rank order B, is markedly improved over that of Hawaiian hawaiite (and other basalts above) which is relegated due to its higher concentration of TiO_2, MgO, and FeO.

In the comparisons made using Harbour Main olivine basalt (table 14), the preference for continental basalts of transitional and mildly alkaline compositions is again striking. Critical differences with respect to K_2O (rank order A) is evident by the relegation of Craigs Ranch and Grand Wash (K-variant) basalts and improved status of Beaver Ridge 1 and Oregon high-alumina basalt types. When differences are evaluated on the basis of rank B these roles are dramatically reversed; CaO and FeO make up the critical difference in these analyses. An important feature of this comparison in relation to earlier observations

concerning feldsparphyric basalt, is the reduced preference for "fresh" Carlsberg Ridge basalt as opposed to spilite. This demonstrates statistically the direction of spilitisation processes with respect to normative compositions and confirms previous observations made by Vallance (1969) concerning conversion of Ol- and Hy-normative basalt to Ne-normative spilite.

Using the statistical methods outlined above, it can be shown explicitly that Harbour Main basalts exhibit strong chemical similarities with transitional to mildly alkalic basalts of Late Cenozoic age presently located at the margins of the Basin-Range province. This conclusion can be extended to cover the altered basaltic rocks of the Harbour Main Group since they share identical chemical traits with respect to immobile components (TiO_2, total Fe, Al_2O_3, and MgO), and are closely associated with the basalts in time and space. On a worldwide scale, the average Basin-Range alkalic basalt (which includes rock-types such as basanite and alkali-olivine basalt (s.s.) not yet recognised in the Harbour Main Group) (Leeman, pers. comm., 1974) shows definite chemical ties with continental alkalic basalts of similar tectonic environments (Leeman and Rogers, 1970; Best and Brimhall, in press). The analyses of comparison basalts used by Leeman and Rogers (1970) are presented in identical fashion to analyses in table 12 enabling them to be compared directly with Harbour Main basalts (cf. Leeman and Rogers, ibid., comparison basalts listed in table 5; results given in table 6).

Although it can be demonstrated on the basis of the chemical evidence presented above and the structural data presented earlier

(chapter VI) that Harbour Main volcanism was concurrent with a period of extensional tectonism, the products of this volcanic activity are not necessarily genetically related. The petrologic evolution of the Harbour Main volcanic suite is examined below.

8.2.4. Magmatic Evolution of the Harbour Main Volcanic Suite

Certain major and trace element variation diagrams are currently used to examine the origin and differentiation mechanisms of a suite of closely associated volcanic rocks. The application of these diagrams to the Harbour Main volcanic suite meets with varying success.

The K/Rb ratio is considered to be an important indicator of differentiation within igneous rock series (Taylor, 1965; Taubeneck, 1965; Prinz, 1968). In general, K/Rb decreases in response to progressive differentiation of a silicate melt (Butler *et al.*, 1962; Jakes and White, 1970). A K/Rb plot (fig. 14) of Harbour Main volcanic rocks records an overall decrease in K/Rb with increasing differentiation factor (i.e. SiO_2). Plotted analyses form a trend subparallel to the "main trend" (300-150) of Shaw (1968) which he defines as the predicted path for a differentiating silicate liquid. However, anomalously high K/Rb ratios in sodic quartz-keratophyres are due to greater loss of Rb relative to K during hydrothermal alteration. Furthermore, K/Rb ratios for ignimbrites are somewhat higher than expected for rocks with such a high content of alkalies. Removal of altered samples, therefore, produces a trend that exhibits approximately constant K/Rb with increase

FIG 14 K/Rb RATIOS FOR HARBOUR MAIN GROUP VOLCANIC ROCKS, COLLIERS PENINSULA

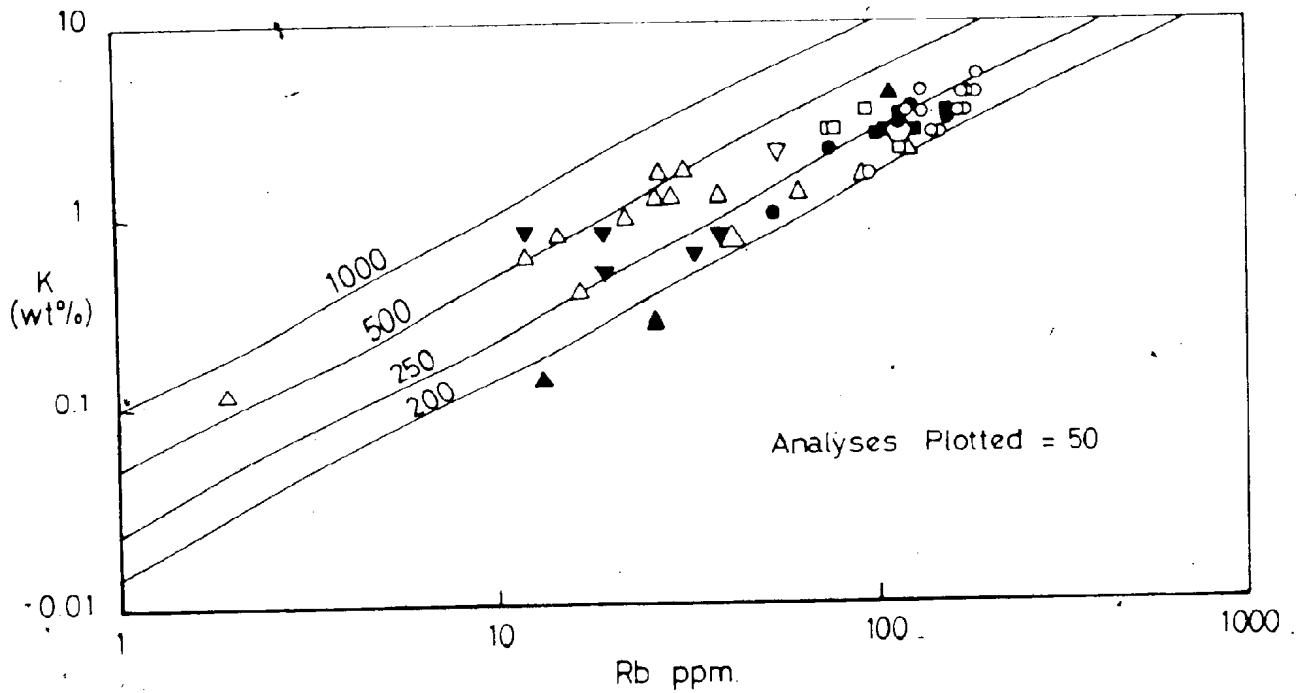

▲ Basalts ▼ Dykes ▽ Cumulate rock ● Porphyrites
⬡ Rhyolite sill △ Finn Hill ash-flow sequence △ Dacite flow
□ Weavers Hill ash-flow sequence (biotite phenocrysts)
○ Weavers Hill ash-flow sequence ■ Bacon Cove ash-flow sequence

FIG 15. Rb / Sr RATIOS FOR HARBOUR MAIN GROUP VOLCANIC ROCKS, COLLIERS PENINSULA

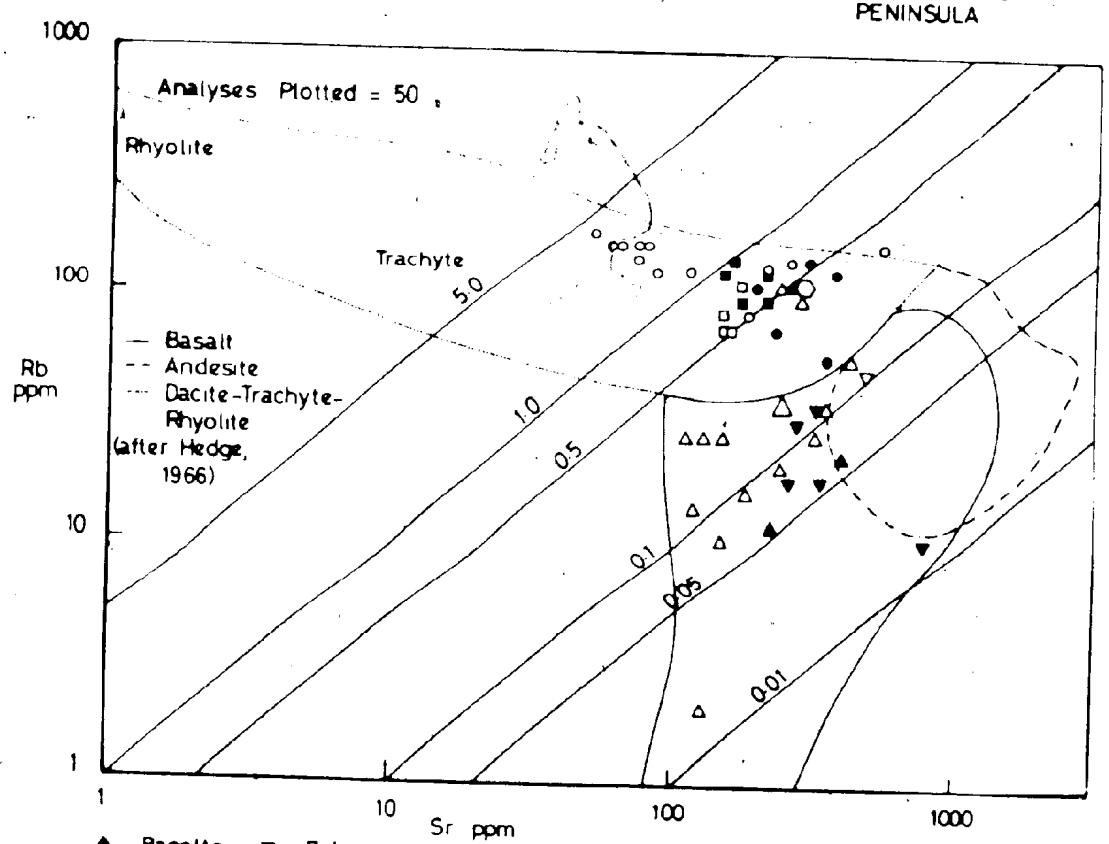

▲ Basalts ▼ Dykes ▽ Cumulate rock ● Porphyrites
○ Rhyolite sill △ Finn Hill ash-flow sequence △ Dacite flow
□ Weavers Hill ash-flow sequence (biotite phenocrysts)
○ Weavers Hill ash-flow sequence ■ Bacon Cove ash-flow sequence

of SiO_2. This indicates that basaltic and rhyolitic rocks of the Harbour Main Group cannot be related by any known mechanism of differentiation from a melt. The range of K/Rb values within the intermediate and rhyolitic rocks shows appreciable overlap (cf. table 9).

A Rb/Sr plot appears to be more informative (fig. 15). The majority of plotted samples fall in the fields of basalt and rhyolite-trachyte-dacite constructed by Hedge (1966). Ignimbrites of the Bacon Cove and Weavers Hill ash-flow sequences have Rb/Sr ranging 0.35-4.20. Sodic quartz-keratophyres of the Finn Hill sequence, basalts (except NX15), and diabase dykes, form a separate group with Rb/Sr ranging 0.05-0.18 (apart from GTN29 and GC2 which have lower values). Porphyrites group demonstrably with the ignimbrites (Rb/Sr = 0.17-0.60). The overall trend is subparallel to that described for differentiated rocks of the Sierra Nevada Batholith (Kistler et al., 1971). However, Harbour Main basaltic rocks have notably higher Rb/Sr ratios than mafic fractions of the Sierra Nevada intrusion. The occurrence of high-alkali ignimbrites within the dacite field of Hedge (1966) reflects a comparatively short period of differentiation prior to their eruption and emplacement.

Critical relationships between and within rhyolitic and intermediate rocks are distinguished by Rb/Sr and Ba/Sr ratios (cf. table 9). Since K-feldspar does not appear on the liquidus in volcanic rocks of the Harbour Main Group, and partition coefficients show

FIG 16 Ti / Zr RATIOS FOR HARBOUR MAIN GROUP VOLCANIC ROCKS, COLLIERS PENINSULA

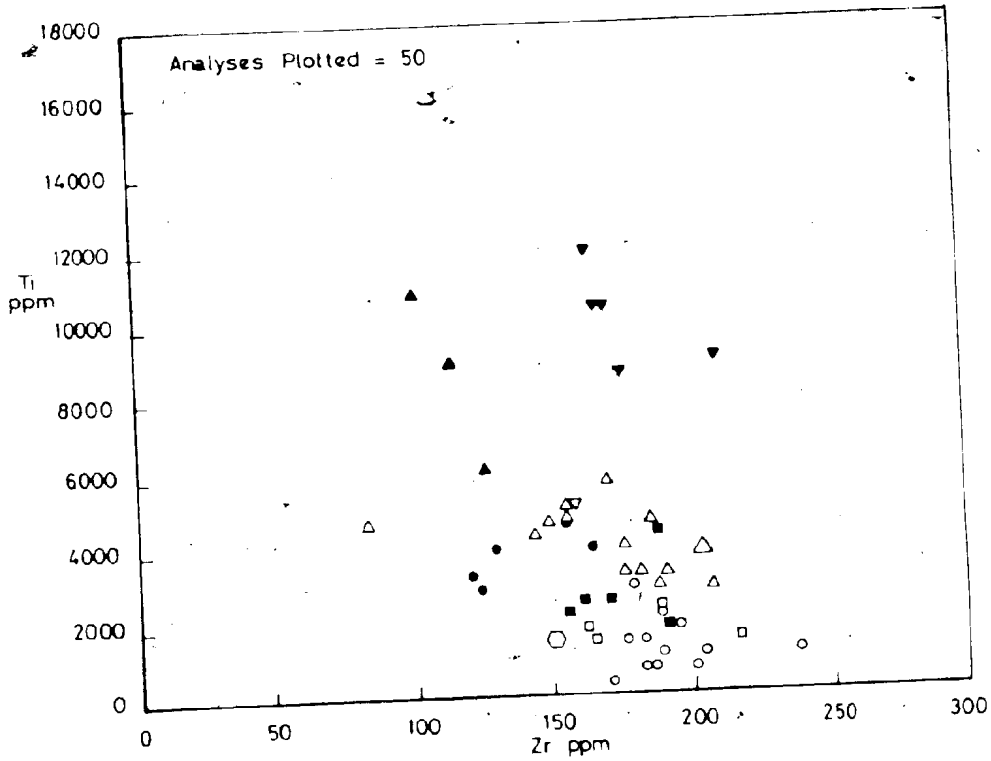

▲ Basalts ▼ Dykes ▽ Cumulate rock ● Porphyrites
○ Rhyolite sill △ Finn Hill ash-flow sequence △ Dacite flow
□ Weavers Hill ash-flow sequence (biotite phenocrysts)
○ Weavers Hill ash-flow sequence ■ Bacon Cove ash-flow sequence

FIG 17 ALKALI - LIME INDEX FOR HARBOUR MAIN GROUP VOLCANIC ROCKS, COLLIERS PENINSULA (after Peacock 1931)

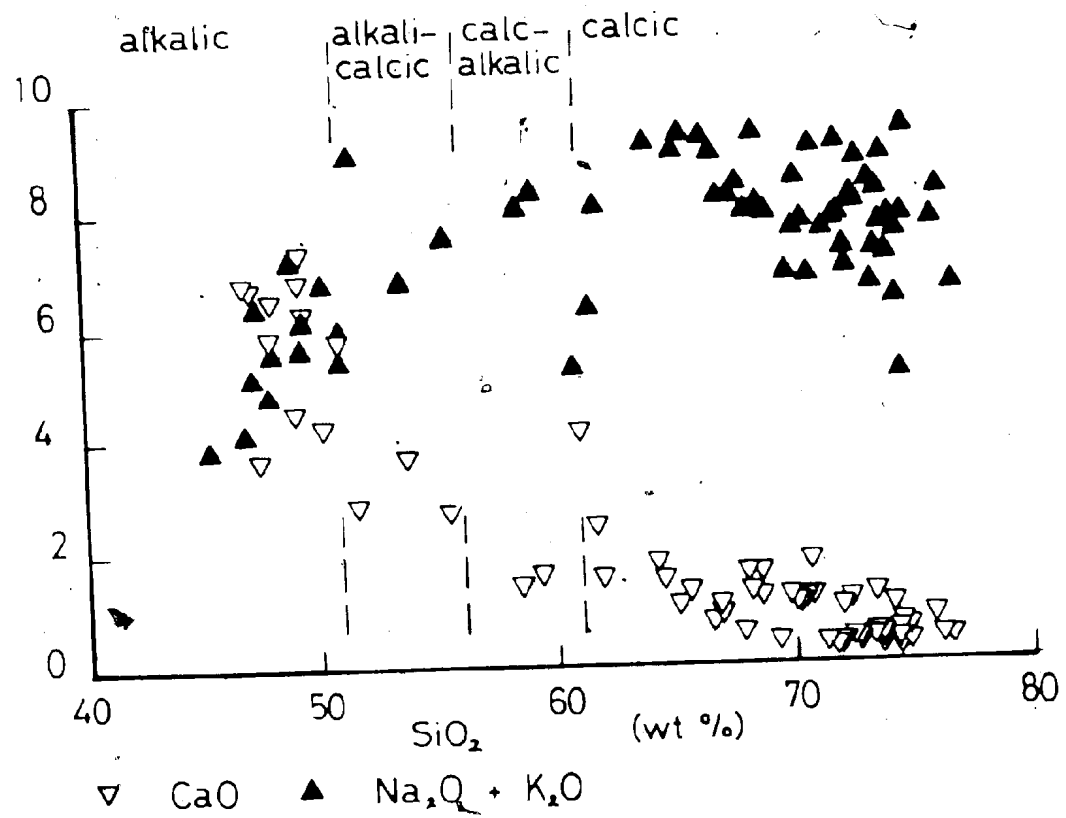

that Ba enters biotite preferentially over Rb or K (Philpotts and Schnetzler, 1972), Ba is only effectively depleted at a late stage by the onset of a significant amount of biotite crystallisation, while Sr is strongly partitioned into plagioclase. Consequently, Rb/Sr and Ba/Sr ratios increase during differentiation. The order of differentiation in ignimbrites and granitoid rocks is systematic with respect to both these parameters and given strictly by the sequence (from least evolved to most evolved): U-(Z)-V-X-W-(Y) (cf. table 9). In the granitoid rocks, K-feldspar joins plagioclase and biotite on the liquidus, resulting in marked depletion of Ba and Sr in Holyrood "granite" (Y) relative to "quartz-monzonite" (X, table 9). Note that there is no correlation between the age of emplacement and degree of differentiation. On the basis of relatively high K_2O, Ba, Rb, and Ba/Sr, the porphyrites (with considerably less silica) are markedly more differentiated than rhyodacitic ignimbrites (FHS-U, table 9). This strongly indicates that they cannot be related to the ignimbrites simply by fractional crystallisation.

The application of discriminant analysis using Zr, Ti, and Y, has lead to the use of a Ti/Zr plot for distinguishing specific basaltic parentage (Pearce and Cann, 1971). These elements are particularly useful in Harbour Main basaltic rocks since they are apparently invariant during secondary alteration processes. A Ti/Zr plot (fig. 16) adequately distinguishes between high-Zr dykes and low-Zr basalts; the dykes are comparatively more differentiated than the basalts and cannot have served as feeders for these particular flows. The chemistry

FIG 18 TOTAL ALKALIES vs SILICA. (after Macdonald and Katsura, 1964)

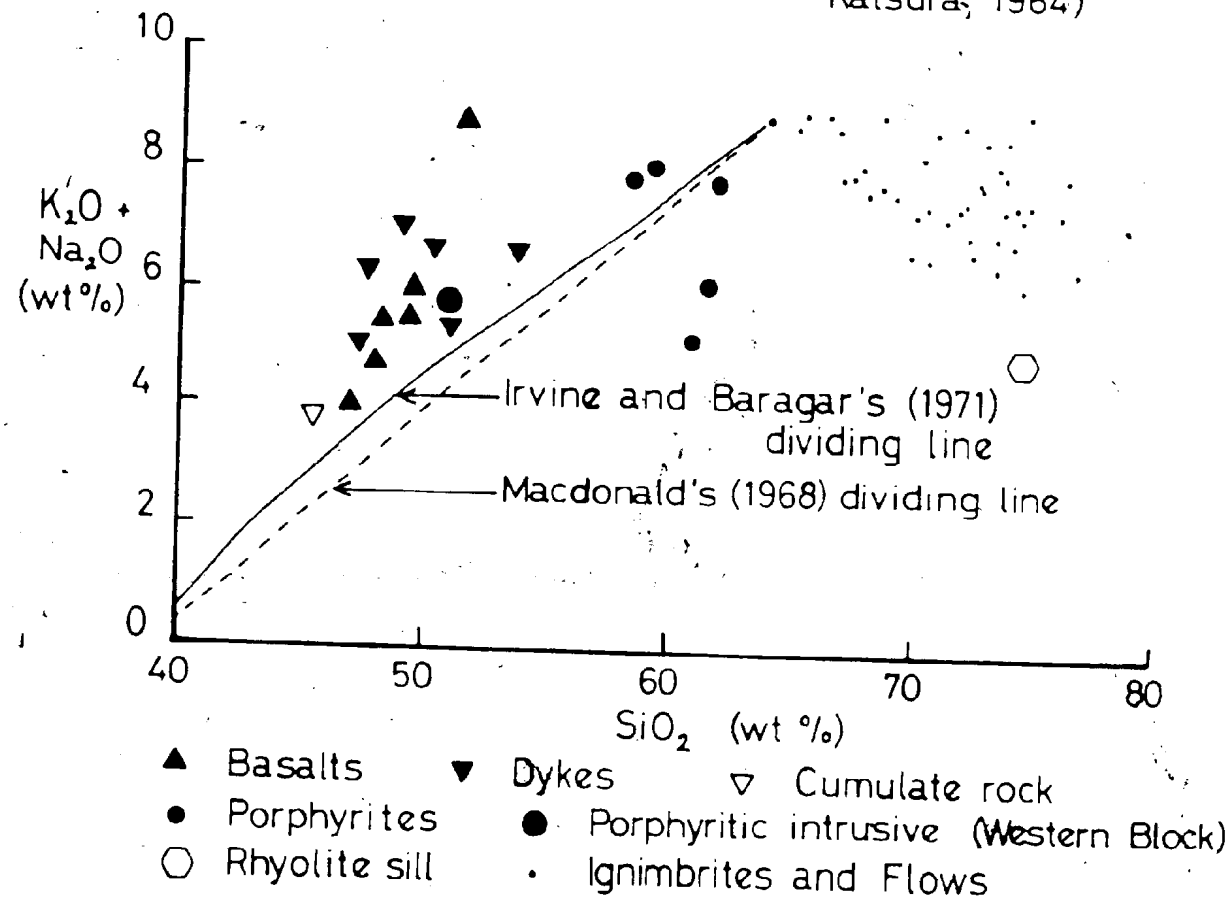

FIG 19 A F M DIAGRAM FOR HARBOUR MAIN GROUP VOLCANIC ROCKS, COLLIERS PENINSULA

(after Nockolds and Allen 1953)

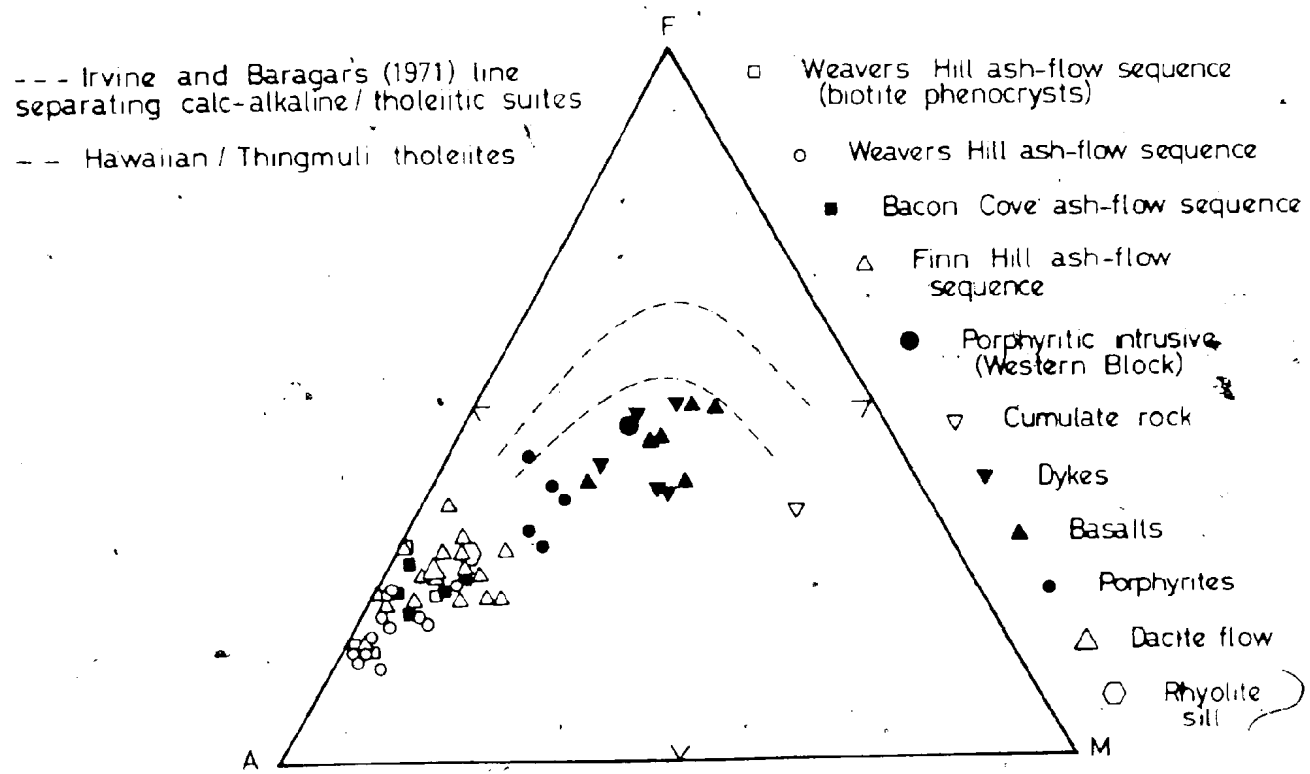

A = $Na_2O + K_2O$, F = Total iron as FeO, M = MgO

of the basaltic rocks is quite compatible with their derivation from a common parent with the composition of alkali-olivine basalt. Crystallisation and removal of varying proportions of olivine, clinopyroxene, and plagioclase could very simply relate picrite to olivine basalt to feldsparphyric basalt. The details of the fractionation history of these rocks require further work.

The alkali-lime index (Peacock, 1931) for the suite is approximately 51 (fig. 17; compare Papezik, 1970, fig. 6), i.e. located on the boundary between the alkalic and alkali-calcic rock series. This diagram, however, assumes, but does not prove, that intermediate and rhyolitic rocks are related to the basaltic rocks.

The merits of an alkalies-silica diagram (fig. 18) have already been discussed in their application to basaltic members of the suite. Although porphyrites straddle the boundary between alkaline and subalkaline rocks in this plot, discrimination between rock series was not intended for these levels of silica saturation (Macdonald and Katsura, 1964).

An AFM diagram (fig. 19) reveals a moderate degree of iron enrichment for plotted analyses, clearly distinct from typical tholeiitic suites of Hawaii and Thingmuli described by Irvine and Baragar (1971, fig. 2a). The trend of Harbour Main volcanic rocks exhibits slightly more iron enrichment than that for the general Cascades, but is indistinguishable from trends given for calc-alkaline rocks of the Aleutians and the alkaline suite of Gough Island (cf. Irvine and Baragar, 1971, figs. 2f and 2d).

FIG 20 DISTRIBUTION OF CHEMICAL ANALYSES AND ESTIMATED ABUNDANCES OF VOLCANIC ROCK-TYPES IN VARIOUS ENVIRONMENTS

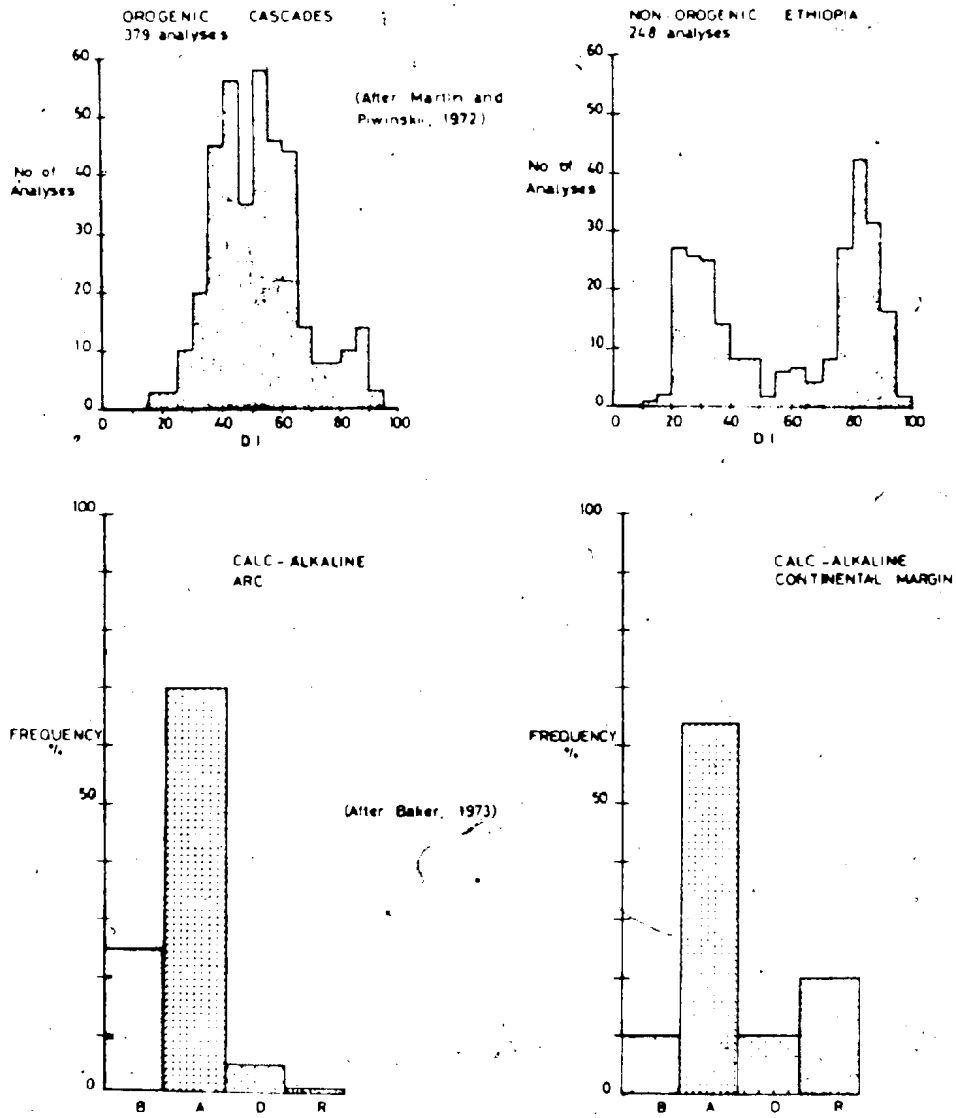

D I Differentiation Index = normative Ne + Lc + Ks + Ab + Or + Q (Thornton and Tuttle 1960)
B Basalt A Andesite D Dacite R Rhyolite
calc-alkaline arc based on Lesser Antilles
continental margin based on Western U.S.A., New Zealand and Andes

The most distinctive feature of the Harker diagrams presented earlier (figs. 6 and 13) is the hiatus in SiO_2 extending from approximately 60.44 to 68.97 mol. % SiO_2 (58.40-50.91 wt. %), if an altered basalt (NX15) is ignored. The map area occupies a critical transition zone between predominantly rhyolitic and predominantly basaltic volcanism in the Harbour Main Group and the complete range of rock-types are represented in the variation diagrams. Furthermore, this bimodality is so characteristic of recently emplaced volcanic suites in extensional tectonic environments that it cannot be attributed to sampling problems (cf. Chayes, 1963). Martin and Piwinskii (1972) demonstrated that a bimodal association is characteristic of "non-orogenic" as opposed to "orogenic" rock suites; and that orogenic rock suites are characterised by a maximum on a frequency vs. differentiation index plot, and non-orogenic by two maxima (fig. 20). Similar plots for calc-alkaline island arc and calc-alkaline continental margin (orogenic) rock series both exhibit a single maximum, though the relative proportions of rhyolite are different in each case (fig. 20). The nature of Harbour Main volcanism, therefore, is completely consistent with concurrent major block-faulting and attenuation of continental lithosphere.

The petrogenetic conclusions can be summarised as follows:

1) Ignimbrites of the Harbour Main Group were derived by fractional crystallisation of parental silicate melt(s).

a) Plagioclase was obtained on the liquidus in early differentiates, thereby significantly depleting residual liquids (late differentiates)

~~in Ba and~~ Sr, and consequently increasing Ba/Sr and Rb/Sr ratios in later salic fractions.

b) Relatively late-stage crystallisation of biotite in quartz-latitic liquids (Bacon Cove ash-flow sequence) removed Ti, Fe, Mg, and juvenile H_2O from residual liquids enriched in Si and K (Weavers Hill ash-flow sequence).

c) The compositions of rhyolitic and granitoid rocks of the Harbour Main Group are very similar; the predominance of plagioclase in the ignimbrites, and plagioclase coexisting with potash feldspar in the plutonic rocks, suggests that volcanic liquids had not cooled enough to impinge upon the two-feldspar boundary surface (Carmichael, 1963) in spite of their low CaO contents.

d) Rb/Sr ratios for silicic volcanic and plutonic rocks of the Harbour Main Group fall in the dacite field of Hedge (1966) and indicate relatively weak differentiation of the original silicate melt.

2) Porphyrites form a group of high-alkali intermediate intrusions, similar to continental interior "andesites", and chemically distinct from the basalts or ignimbrites; relatively high K_2O, Rb, and Ba, and low Sr contents suggests that K-feldspar did not appear on the liquidus of early differentiates, and that the ignimbrites did not differentiate by fractional crystallisation of a porphyrite melt.

3) Harbour Main basaltic rocks are "transitional" to "mildly alkaline" types, characterised by low Ti and high Al, and possibly related by fractional crystallisation of olivine, clinpyroxene, and plagio-

clase; K/Rb ratios are inconsistent with the view that intermediate and rhyolitic volcanic rocks of the Harbour Main Group differentiated from a basaltic magma.

4) The chemistry of the basaltic rocks and bimodality of the Harbour Main volcanic suite are characteristics of an extensional tectonic environment.

CHAPTER IX

GENERAL CONCLUSIONS AND A TENTATIVE MODEL FOR LATE PRECAMBRIAN MAGMATISM AND TECTONISM ON AVALON

Conclusions concerning the nature and timing of Harbour Main volcanic activity (sections 2.3. and 2.4.), structural events (sections 6.3. and 6.4.), alteration and metamorphism (sections 7.3. and 7.4.), and the interpretation of the chemical data (sections 8.1.1., 8.1.2., and 8.2.4.) are entirely consistent with the concept of an ensialic setting for Late Precambrian magmatism and tectonism on the Avalon Peninsula. These new data require revision and refinement of previous interpretations of Avalon geology. In particular, the following points are emphasised:

1) Neither the structural data, nor mode of alteration and metamorphism, can provide a definitive fingerprint of the specific tectonic setting of magmatism on Avalon. It should be noted that the Late Precambrian "Avalonian Orogeny" is a complex tectonic episode involving intense faulting and large-scale folding with no clear relationship to a plate tectonic event.
2) The bimodal association and chemical composition of the volcanic rocks of the Harbour Main Group are inconsistent with the view of Hughes (1970) and Hughes and Brueckner (1971) that Late Precambrian igneous and tectonic activity is characteristic of an island arc environment. However, the facies concept,

applied by them to resolve the geologic evolution of the Avalon, is potentially a very powerful tool when used in conjunction with the appropriate geochemical data.

3) The bimodal association and chemical data are compatible with the suggestions of Papezik (1970, 1972b), Strong et al. (1974), and Strong (1974), that Harbour Main volcanism was broadly concurrent with major block-faulting of the Basin Range type. However, the style of volcanism is not necessarily "post-orogenic" (Papezik, 1970, p. 1495) since evidence for an orogeny immediately preceding Harbour Main volcanism is lacking.

4) It has been shown that a large population of representative samples is advantageous to the recognition of specific magmatic parentage in variably altered and metamorphosed rocks of the Harbour Main Group. To designate the volcanic rocks as a "spilite/keratophyre" province (Hughes, 1972a), however defined, simply obscures the fundamental nature of the magmatism.

5) Data for the lithophile elements (K, Rb, Ba, and Zr) are strongly indicative of separate origins for the ignimbrites, porphyrites, and basaltic rocks of the Harbour Main Group.

6) The anomalously low Rb/Sr whole-rock age (568±29 m.y.) given by Fairbairn et al. (1966) for Harbour Main volcanic rocks may have resulted from a small and variable amount of Rb diffusion (possibly involving Ba and K) into the rocks during later deformation. Hydrothermal alteration and metamorphism to prehnite-pumpellyite grade are interpreted as Precambrian events (compare Hughes and Malpas, 1971).

The concept of the intra- or epicontinental regional setting of Harbour Main volcanism and plutonism is supported by the following lines of evidence:

1) Appreciable amounts of garnet and muscovite detritus in Late Precambrian (Cabot Group) and Cambro-Ordovician (Bell Island Group) clastic sequences are presumably derived from an uplifted source region consisting of leucocratic garnetiferous granites or gneissic basement hidden beneath the present continental shelf to the east and northeast of the Avalon Peninsula (Kennedy and McGonigal, 1972; Papezik, 1973; Poole, 1973).

2) Initial $^{87}Sr/^{86}Sr$ ratios (0.7054 ± 0.0020) given by Fairbairn *et al.* (1966) for Harbour Main volcanic rocks near Holyrood are intermediate between upper mantle and old crustal material, and indicate that subsialic lower crust and upper mantle were involved in magma genesis.

3) The common association of granitic batholiths and voluminous silicic volcanic rocks of broadly similar composition in regions of continental crust. For example, the western two-thirds of the Aleutian chain, developed on oceanic crust, contains predominantly andesitic rocks with very small amounts of trondhjemite and rhyolite; in the eastern one-third, however, where the volcanic rocks have penetrated sialic crust, stocks of quartz-diorite and quartz-monzonite are common (Gilluly, 1971).

4) The Avalon is part of a much more extensive Late Precambrian terrane (Zone H of Williams et al., 1972) about 500 miles (805 km) across, that extends southwards through eastern Massachusetts possibly as far as Florida (cf. Williams and Stevens, in press). The presence of continental basement east of Zone H (i.e. in Zone I of Williams et al., ibid.) has been postulated by Schenk (1971) during a study of Lower Paleozoic metasediments of the Meguma Group, Nova Scotia. It is of interest to note that the Meguma Group is intruded by granites dated as approximately 415-350 m.y. (Cormier and Smith, 1973, using Rb/Sr whole-rock isochron methods) and very similar in composition to the Holyrood Plutonic Series (607 ± 11 m.y. according to Frith and Poole, 1972), which probably represents the last magmatic event on Avalon; in addition, granites similar in age and composition to the Holyrood rocks are found in Cape Breton Island (Cormier, 1972). This can be taken as evidence of repeated fusion of the lower crust.

A recent model for the plate-tectonic setting of eastern Newfoundland has been proposed by Strong et al. (1974) and Strong (1974). These authors suggested that a long-lived (250 m.y.) subduction zone dipping eastward beneath the continental margin would explain an eastward increase of K_2O in the granitoid rocks along with the metallogenic zoning in eastern Newfoundland, and drew an analogy with a Cordilleran-type continental margin. Furthermore, they noted that Avalon plutonic rocks marked a sharp discontinuity in the K_2O trend (cf. Strong et al.,

1974, fig. 3), and following Lipman et al. (1972) tentatively postulated that it marked a second east-dipping subduction zone beneath the Avalon. However, the products of Hadrynian volcanism in the Harbour Main Group do not resemble orogenic andesites or form a unimodal distribution of rock-types (Martin and Piwinskii, 1972), features typically associated with a consuming plate margin. The effects of gross thermal instabilities created in the upper mantle during subduction of a "cold" slab of oceanic lithosphere are entirely speculative, but in some indirect way could conceivably lead to magma generation in adjacent continental regions.

Late Precambrian volcanism on Avalon, as typified by the magmatic evolution of the Harbour Main Group, can be accommodated within the present plate-tectonic framework outlined by Strong et al. (1974) and Strong (1974). In view of the new data presented above, a tentative model is proposed:

Stage 1: Intersection of the melting curve for lower continental crust by the geotherm gave rise to partial melting of subsialic material. Episodic silicic volcanism ensued. Volcanic activity was characterised by voluminous fissure eruptions of high-alkali ignimbrites and emplacement of Holyrood-type granitoid batholiths. Hydrothermal alteration and block-faulting were initiated at this stage. Volcanogenic material eroded from fault-scarps was reworked and incorporated in clastic deposits interbedded with the ignimbrites.

Stage 2: Sustained partial melting of less refractory lower crustal material, possibly involving the residuum after extraction of ignimbrite melts, produced the porphyrites, a discrete suite of high-level intrusive rocks of continental "andesitic" character. Metasomatic alteration and block-faulting continued.

Stage 3: Partial melting of a peridotitic upper mantle source region (Green and Ringwood, 1967; O'Hara, 1965) followed by extensive outpourings of high-alumina, low-titania plateau basalts of transitional to mildly alkaline compositions. Analogous basaltic volcanism of Late Cenozoic age in the Basin-Range province suggests that the Colliers section is located at the margins of a "palaeotensional" environment and probably proximal to a region of older Precambrian basement. Lavas were extruded into an environment of continental rifting and distension. Prehnite-pumpellyite facies metamorphism probably took place when regional geothermal gradients were lowered and may have persisted throughout Late Precambrian folding.

Implicit to this model is the subsequent modification of "primitive" magmas by varying degrees of fractional crystallisation. The bulk chemical attributes of the lower crustal source region prior to melting is probably best approximated by an andesitic composition (Green and Lambert, 1965; Ringwood and Green, 1966). Using such a

TABLE 15. Selected Estimates of the Average Composition of the Continental Crust

(analyses in weight percent are recalculated to 100% on a volatile-free basis)

Source	1	2a
(Wt. %)		
SiO_2	56.15	66.07
Al_2O_3	15.63	16.08
Fe_2O_3	2.43	1.42
FeO	7.70	3.14
CaO	7.76	3.44
Na_2O	3.00	3.95
K_2O	0.68	2.90
MgO	5.24	2.22
MnO	0.18	0.08
TiO_2	1.01	0.54
P_2O_5	0.22	0.16
Total:	100.00	100.00
(p.p.m.)		2b
Ba	194	1070
Sr	214	340
Zr	160	400
Cu	84	14
Zn	98	-
Cr	199	99
Ni	89	23

TABLE 15 (Cont'd.)

---

1. Weighted salic and mafic fractions of average Archean volcanic rock (Baragar and Goodwin, 1969, table IV, p. 138).

2a. Average major oxide composition of Canadian Shield - Archean and Proterozoic (Fahrig and Eade, 1968, table 1, no. 12).

2b. Average trace element composition of Canadian Shield - Archean and Proterozoic (Shaw *et al.*, 1967).

hypothetical composition, Presnall and Bateman (1973) demonstrated that the broad compositional field of the Sierra Nevada Batholith could be produced by processes involving partial to complete fusion of the lower crust combined with subsequent fractional crystallisation. Inspection of a normative Qz-Or-Ab+An plot for the Sierran rocks (Presnall and Bateman, ibid., fig. 2) reveals a trend similar to that for the Holyrood Plutonic Series (fig. 10c), allowing a parallel argument to be advanced for the origin of Holyrood granitoid and Harbour Main volcanic rocks. The strength of such a model, however, is more critically evaluated by comparing the relative abundances of trace elements in the assumed parental material and successive daughter products with the predicted behaviour of these elements during fractionation processes (cf. Taylor, 1965, 1968; Tauson, 1965). A crude comparison between the weighted averages of salic and mafic fractions of Archean volcanic rocks (table 15, no. 1) and averages of Holyrood and Harbour Main rocks (table 9) brings out significant differences (note especially K, Ba, Cr, and Ni). Comparing these rock-types with an estimate of oxide and trace element concentrations in Proterozoic and Archean rocks of the Canadian Shield (table 15, no. 2) it is apparent that Stages 1 and 2 in the above model could successfully accomplish the observed "crustal differentiation" (note Ba and K) with only minor contributions from Stage 3 (note Cr and Ni).

Although such a crude model as that presented above may not stand the test of time, it may nevertheless persuade other authors

to omit the omnipresent dotted subduction zone beneath the Avalon in future plate-tectonic reconstructions.

BIBLIOGRAPHY

Abbott, M. J. 1969. Petrology of the Nandewar Volcano, N.S.W., Australia. Contrib. Mineral. and Petrol., v. 20, p. 115-134.

Amstutz, G. C. 1968. Spilites and spilitic rocks. In Basalts: The Poldervaart Treatise on Rocks of Basaltic Composition. Editors, Hess, H. H., and Poldervaart, A., Interscience, New York, v. 2, p. 737-753.

Anderson, C. A. 1968. Metamorphosed Precambrian silicic volcanic rocks in central Arizona. In Studies in Volcanology. Editors, Coats, R. R., Hay, R. L., and Anderson, C. A., Geol. Soc. Amer. Mem. 112, 678 p.

Anderson, J. E. Jr. 1969. Development of snowflake texture in a welded tuff, Davis Mountains, Texas. Geol. Soc. Amer. Bull., v. 80, p. 2075-2080.

Anderson, J. E. Jr. 1970a. Snowflake texture not diagnostic of devitrified ash-flow tuffs: Reply. Geol. Soc. Amer. Bull., v. 81, p. 2529-2530.

Anderson, J. E. Jr. 1970b. Recognition and time distribution of texturally altered welded tuff. Geol. Soc. Amer. Bull., v. 81, p. 287-291.

Anderson, M. M., and Misra, S. B. 1968. Fossils found in the Precambrian Conception Group of southeastern Newfoundland. Nature, v. 220, p. 680-681.

Anderson, T., and Flett, J. S. 1903. Report on the eruptions of the Soufrière in St. Vincent, and on a visit to Montagne Pelée in Martinique, Pt. 1. Phil. Trans., Royal Soc. London, ser. A, v. 200, p. 353-553.

Bailey, D. K. 1964. Crustal warping -- a possible tectonic control of alkaline magmatism. J. Geophys. Res., v. 69, p. 1103-1111.

Bailey, D. K., and Macdonald, R. 1970. Petrochemical variations among mildly peralkaline (comendite) obsidians from the oceans and continents. Contrib. Mineral. and Petrol., v. 28, p. 340-351.

BIBLIOGRAPHY (Cont'd.)

Baker, P. E. 1973. Volcanism at destructive plate margins. J. Earth Sci., v. 8, p. 183-195.

Baragar, W. R. A. 1967. Unpublished report to the Volcanology Sub-Committee, Assoc. Committee of Geodosy and Geophysics, National Research Council of Canada. (Incorporated in Irvine and Baragar, 1971).

Baragar, W. R. A., and Goodwin, A. M. 1969. Andesites and Archean volcanism of the Canadian Shield. In Proceedings of the Andesite Conference. Editor, McBirney, A. R., Oregon Dept. Geol. Min. Ind. Bull. 65, p. 121-142.

Barning, K. 1965. Petrology of the northwestern part of the Holyrood granite batholith. M. Sc. Thesis (unpublished), Memorial University of Newfoundland, St. John's, Newfoundland.

Bass, M. N. 1972. Occurrences of transitional abyssal basalt. Lithos, v. 5, p. 57-67.

Bateman, P. C., Clark, L. D., Huber, N. K., Moore, J. G., and Rinehart, C. D. 1963. The Sierra Nevada batholith -- A synthesis of recent work across the central part. U. S. Geol. Surv. Prof. Paper 414D, p. D1-D46.

Battey, M. H. 1955. Alkali metasomatism and the petrology of some keratophyres. Geol. Mag., v. 92, p. 104-126.

Beavon, R. V., Fitch, F. J., and Rast, N. 1961. Nomenclature and diagnostic character of ignimbrites, with special reference to Snowdonia. L'pool. Manchr. geol. J., v. 2, p. 600-610.

Best, M. G., and Brimhall, W. H. 1970. Late Cenozoic basalt types in the western Grand Canyon region. In The western Grand Canyon district: Guidebook to the Geology of Utah. Editors, Hamblin, W. K., and Best, M. G., v. 23, p. 56-74.

Best, M. G., and Brimhall, W. H. (in press). Late Cenozoic alkalic basaltic magmas in the western Colorado Plateaus and the Basin and Range Transition Zone, U. S. A., and their bearing on mantle dynamics. Geol. Soc. Amer. Bull., v. 84.

Best, M. G., Brimhall, W. H., and Hamblin, W. K. 1969. Late Cenozoic basalts on the Colorado Plateaus, Utah and Arizona. Research Rept. 69-1, Geol. Dept., Brigham Young University.

BIBLIOGRAPHY (Cont'd.)

Bordet, P., Marinelli, G., Mittempergher, M., and Tazieff, H. 1963. Contribution à l'étude volcanologique du Katmai et de la Vallée des Dix Mille Fumées. Soc. Belg. Geol. Mem., ser. in octavo, p. 1-114.

Boulton, W. S. 1904. The igneous rocks of Pontesford Hill, Shropshire. J. Geol. Soc. London, v. 60, p. 450-486.

Bowen, N. L. 1913. The melting phenomena of the plagioclase feldspars. Amer. J. Sci., v. 35, p. 577-599.

Boyd, F. R. 1961. Welded tuffs and flows in the rhyolite plateau of Yellowstone Park, Wyoming. Geol. Soc. Amer. Bull., v. 72, p. 387-426.

Boyd, F. R., and Kennedy, G. C. 1951. Some experiments and calculations relating to the origin of welded tuffs. Abstracts Amer. Geophys. Union Trans., v. 32, p. 327-328.

Brown, M. C. 1962. Discussion -- nuées ardentes and fluidization. Amer. J. Sci., v. 260, p. 467-470.

Browne, P. R. L., and Ellis, A. J. 1970. The Ohaki-Broadlands hydrothermal area, New Zealand: mineralogy and related geochemistry. Amer. J. Sci., v. 269, p. 97-131.

Brueckner, W. D. 1969. Geology of eastern part of Avalon Peninsula, Newfoundland -- a summary. Amer. Assoc. Petrol. Geol. Mem. 12, p. 130-138.

Brueckner, W. D., and Anderson, M. M. 1971. Late Precambrian glacial deposits in southeastern Newfoundland -- a preliminary note. Geol. Assoc. Can., Proc., v. 24, p. 95-102.

Buddington, A. F. 1916. Pyrophyllitization, pinitization, and silicification of rocks around Conception Bay, Newfoundland. J. Geol., v. 24, p. 130-152.

Buddington, A. F. 1919. Pre-Cambrian Rocks of Southeast Newfoundland. J. Geol., v. 27, p. 449-479.

Butler, J. R., Bowden, P., and Smith, A. Z. 1962. K/Rb ratios in the evolution of the younger granites of northern Nigeria. Geochim. et Cosmochim. Acta, v. 26, p. 89-100.

BIBLIOGRAPHY (Cont'd.)

Cann, J. R. 1969. Spilites from the Carlsberg Ridge, Indian Ocean. J. Petrology, v. 10, p. 1-19.

Cann, J. R. 1970. Rb, Sr, Y, Zr, and Nb in some ocean floor basaltic rocks. Earth Planet. Sci. Letters, v. 10, p. 7-11.

Cann, J. R., and Vine, F. J. 1966. An area on the crest of the Carlsberg Ridge: petrology and magnetic survey. Phil. Trans. Royal Soc. London, series A, v. 259, p. 198-217.

Carmichael, I. S. E. 1960. The feldspar phenocrysts of some Tertiary acid glasses. Mineral. Mag., v. 34, p. 107-125.

Carmichael, I. S. E. 1963. The crystallisation of feldspar in volcanic acid liquids. J. Geol. Soc. London, v. 119, p. 95-131.

Chayes, F. 1963. Relative abundance of intermediate members of the oceanic basalt-trachyte association. J. Geophys. Res., v. 68, p. 1519-1534.

Chayes, F. 1966. Alkaline and subalkaline basalts. Amer. J. Sci., v. 264, p. 128-145.

Cook, E. F. 1962. Ignimbrite bibliography and review. Idaho Bur. Mines Geol. Inform. Circ. 13, p. 1-64.

Cook, E. F. 1966. Editor. Tufflavas and Ignimbrites. American Elsevier Publishing Co., Inc., New York, p. 1-212.

Coombs, D. S. 1960. Lower grade mineral facies in New Zealand. Proc. 21st I. G. C., Copenhagen, Norden, part 13, p. 339-351.

Coombs, D. S. 1963. Trends and affinities of basaltic magmas and pyroxenes as illustrated on the diopside-olivine-silica diagram. Amer. Mineral. Soc. Special Paper 1, p. 227-250.

Coombs, D. S., and Wilkinson, J. F. G. 1969. Lineages and fractionation trends in undersaturated volcanic rocks from the East Otago volcanic province (New Zealand) and related rocks. J. Petrology, v. 10, p. 440-501.

Coombs, D. S., Horodyski, R. J., and Naylor, R. S. 1970. Occurrence of prehnite-pumpellyite facies metamorphism in northern Maine. Amer. J. Sci., v. 268, p. 142-156.

Cormier, R. F. 1972. Radiometric ages of granitic rocks, Cape Breton Island, Nova Scotia. Can. J. Earth Sci., v. 9, p. 1074-1086.

BIBLIOGRAPHY (Cont'd.)

Cormier, R. F., and Smith, T. E. 1973. Radiometric ages of granitic rocks, southwestern Nova Scotia. Can. J. Earth Sci., v. 10, p. 1201-1210.

Currie, K. L. 1971. A study of potash fenitization around the Brent Crater, Ontario -- a Paleozoic alkaline complex. Can. J. Earth Sci., v. 8, p. 481-497.

Currie, K. L., and Ferguson, J. 1971. A study of fenitization around the alkaline carbonatite complex at Callander Bay, Ontario, Canada. Can. J. Earth Sci., v. 8, p. 498-517.

Deer, W. A., Howie, R. A., and Zussman, J. 1963. Rock-forming Minerals: Volume 4. Framework Silicates. Longmans, London, 435 p.

Deer, W. A., Howie, R. A., and Zussman, J. 1966. An Introduction to the Rock-forming Minerals. Longmans, London, 528 p.

Dewey, J. F., and Bird, J. M. 1970. Mountain belts and the new global tectonics. J. Geophys. Res., v. 75, p. 2625-2647.

Dickinson, W. R. 1962. Metasomatic quartz keratophyre in central Oregon. Amer. J. Sci., v. 260, p. 249-266.

Dickinson, W. R., and Hatherton, T. 1967. Andesitic volcanism and seismicity around the Pacific. Science, v. 157, p. 801-803.

Dixon, W. J., and Massey, F. J. Jr. 1957. Introduction to Statistical Analysis. McGraw-Hill Inc., New York, 488 p.

Ekren, E. B. 1968. Geologic setting of Nevada Test Site and Nellis Air Force Range. Geol. Soc. Amer. Mem. 110, p. 11-19.

Elston, W. E., and Smith, E. I. 1970. Determination of flow direction of rhyolitic ash-flow tuffs from fluidal textures. Geol. Soc. Amer. Bull., v. 81, p. 3393-3406.

Ewart, A., and Taylor, S. R. 1969. Trace element geochemistry of the rhyolitic volcanic rocks, central North Island, New Zealand. Phenocryst data. Contrib. Mineral. and Petrol., v. 22, p. 127-146.

Ewart, A., Taylor, S. R., and Capp, A. C. 1968. Trace and minor element geochemistry of the rhyolitic volcanic rocks, central North Island, New Zealand: total rock and residual liquid data. Contrib. Mineral. and Petrol., v. 18, p. 76-104.

BIBLIOGRAPHY (Cont'd.)

Fahrig, W. F., and Eade, K. E. 1968. The chemical evolution of the Canadian Shield. Can. J. Earth Sci., v. 5, p. 1247-1252.

Fairbairn, H. W., Bottino, M. L., Pinson, W. H. Jr., and Hurley, P. M. 1966. Whole-rock age and initial $^{87}Sr/^{86}Sr$ of volcanics underlying fossiliferous Lower Cambrian in the Atlantic Provinces of Canada. Can. J. Earth Sci., v. 3, p. 509-521.

Fenner, C. N. 1923. The origin and mode of emplacement of the great tuff deposit in the Valley of Ten Thousand Smokes. Natl. Geogr. Soc., Contrib. Tech. Papers, Katmai Ser., no. 1, 74 p.

Fenner, C. N. 1948. Incandescent tuff flows in southern Peru. Geol. Soc. Amer. Bull., v. 59, p. 879-893.

Fiske, R. S. 1963. Subaqueous pyroclastic flows in the Ohanapekosh Formation, Washington. Geol. Soc. Amer. Bull., v. 74, p. 391-406.

Fiske, R. S. 1969. Recognition and significance of pumice in marine pyroclastic rocks. Geol. Soc. Amer. Bull., v. 80, p. 1-8.

Fiske, R. S., and Matsuda, T. 1964. Submarine equivalents of ash-flows in the Tokiwa Formation, Japan. Amer. J. Sci., v. 262, p. 76-106.

Fiske, R. S., Hopson, C. A., and Waters, A. C. 1963. Geology of Mount Rainier National Park, Washington. U. S. Geol. Surv. Prof. Paper 444, p. 1-93.

Fisher, R. V. 1958. Definition of volcanic breccia. Geol. Soc. Amer. Bull., v. 69, p. 1071-1073.

Fisher, R. V. 1960. Classification of volcanic breccias. Geol. Soc. Amer. Bull., v. 71, p. 973-982.

Fisher, R. V. 1961. Proposed classification of volcaniclastic sediments and rocks. Geol. Soc. Amer. Bull., v. 72, p. 1409-1414.

Fisher, R. V. 1966. Mechanism of deposition from pyroclastic flows. Amer. J. Sci., v. 264, p. 350-363.

Flinn, D. 1956. On the deformation of the Funzie conglomerate, Fetlar, Shetland. J. Geol., v. 64, p. 480-505.

Flinn, D. 1962. On folding during three-dimensional progressive deformation. J. Geol. Soc. London, v. 118, p. 385-433.

BIBLIOGRAPHY (Cont'd.)

Francis, E. H., and Howells, M. F. 1973. Transgressive welded ash-flow tuffs among the Ordovician sediments of N. E. Snowdonia, N. Wales. J. Geol. Soc. London, v. 129, p. 621-641.

Friedman, I. I., and Smith, R. L. 1958. The deuterium content of water in some volcanic glasses. Geochim. et Cosmochim. Acta, v. 15, p. 218-228.

Friedman, I. I., Smith, R. L., and Long, W. D. 1966. Hydration of natural glass and formation of perlite. Geol. Soc. Amer. Bull., v. 77, p. 323-328.

Frith, R. A., and Poole, W. H. 1972. Late Precambrian rocks of eastern Avalon Peninsula, Newfoundland -- A volcanic island complex: Discussion. Can. J. Earth Sci., v. 9, p. 1058-1059.

Fritsch, W. 1966. Zum Einteilungsprinzip der Gesteine nache dem Umwandlungsgrad mit besonderer Berucksichtigung der Anchimetamorphose. N. Jb. Miner. Abh., v. 105, p. 111-132.

Gass, I. G. 1970. The evolution of volcanism in the junction area of the Red Sea, Gulf of Aden, and the Ethiopian rifts. Phil. Trans. Royal Soc. London, series A, v. 267, p. 369-381.

Gay, N. C. 1968. Pure shear and simple shear deformation of inhomogeneous viscous liquids. 1. Theory. Tectonophysics, v. 5, p. 211-234.

Gay, N. C. 1969. The analysis of strain in the Barberton Mountain Land, Eastern Transvaal, using deformed pebbles. J. Geol., v. 77, p. 377-396.

Gedney, L., Matteson, C., and Forbes, R. B. 1970. Seismic refraction profiles of the ash flow in the Valley of Ten Thousand Smokes, Katmai National Monument, Alaska. J. Geophys. Res., v. 75, p. 2619-2624.

Gibson, I. L. 1970. A pantelleritic welded ash-flow tuff from the Ethiopian rift valley. Contrib. Mineral. and Petrol., v. 28, p. 89-111.

Gibson, I. L., and Tazieff, H. 1967. Additional theory of origin of fiamme in ignimbrites. Nature, v. 215, p. 1473-1474.

Gorshkov, G. S. 1959. Gigantic eruption of the volcano Bezymianny. Bull. Volcanol., ser. 2, v. 20, p. 77-109.

BIBLIOGRAPHY (Cont'd.)

Green, D. H., and Lambert, I. B. 1965. Experimental crystallization of anhydrous granite at high pressures and temperatures. J. Geophys. Res., v. 70, p. 5259-5268.

Green, D. H., and Ringwood, A. E. 1967. The genesis of basalt magmas. Contrib. Mineral. and Petrol., v. 15, p. 103-190.

Gulson, B. L. 1972. The high-K diorites and associated rocks of the Yeoval Diorite Complex, N. S. W. Contrib. Mineral. and Petrol., v. 35, p. 173-192.

Harris, P. G. 1957. Zone refining and the origin of potassic basalts. Geochim. et Cosmochim. Acta, v. 12, p. 195-208.

Hay, R. L. 1959. Formation of the crystal-rich glowing avalanche deposits of St. Vincent, B. W. I. J. Geol., v. 67, p. 540-562.

Hedge, C. E. 1966. Variations in radiogenic strontium found in volcanic rocks. J. Geophys. Res., v. 71, p. 6119-6120.

Helgeson, H. C. 1970. Description and interpretation of phase relations in geochemical processes involving aqueous solutions. Amer. J. Sci., v. 268, p. 415-438.

Heier, K. S., and Taylor, S. R. 1959a. The distribution of Li, Na, K, Rb, Cs, Pb, and Tl in southern Norwegian pre-Cambrian alkali feldspars. Geochim. et Cosmochim. Acta, v. 15, p. 284-304.

Heier, K. S., and Taylor, S. R. 1959b. Distribution of Ca, Sr, and Ba in southern Norwegian pre-Cambrian alkali feldspars. Geochim. et Cosmochim. Acta, v. 17, p. 286-304.

Hemley, J. J., and Jones, W. R. 1964. Chemical aspects of hydrothermal alteration with emphasis on hydrogen metasomatism. Econ. Geol., v. 59, p. 538-569.

Henderson, E. P. 1960. Surficial deposits, St. John's, Newfoundland. Geol. Surv, Can., Map 35-1959.

Higgins, M. W. 1973. Petrology of Newberry Volcano, Central Oregon. Geol. Soc. Amer. Bull., v. 84, p. 455-488.

Hjelmquist, S. 1955. On the occurrence of ignimbrite in the Pre-Cambrian. Sveriges Geol. Undersökning, Arsbok 49, Ser. C, p. 1-12.

BIBLIOGRAPHY (Cont'd.)

Hoover, J. D. 1974. Periodic Quaternary volcanism in the Black Rock Desert, Utah. Brigham Young University Geology Studies, v. 21, p. 3-72.

Howell, B. F. 1925. The faunas of the Cambrian Paradoxides beds at Manuels, Newfoundland. Bull. Am. Paleo., v. 11, p. 1-140.

Howley, J. P., and Murray, A. 1918. Reports of Progress, 1881-1909. Geol. Surv. Newfoundland.

Hughes, C. J. 1970. The Late Precambrian Avalonian orogeny in Avalon, southeast Newfoundland. Amer. J. Sci., v. 269, p. 183-190.

Hughes, C. J. 1971. Anatomy of a granophyre intrusion. Lithos, v. 4, p. 403-415.

Hughes, C. J. 1972a. Late Precambrian volcanic rocks of Avalon, Newfoundland -- a spilite/keratophyre province: recognition and implications. Can. J. Earth Sci., v. 10, p. 272-282.

Hughes, C. J. 1972b. Spilites, keratophyres, and the igneous spectrum. Geol. Mag., (in press).

Hughes, C. J., and Brueckner, W. D. 1971. Late Precambrian rocks of eastern Avalon Peninsula, Newfoundland -- a volcanic island complex. Can. J. Earth Sci., v. 8, p. 899-915.

Hughes, C. J., and Malpas, J. G. 1971. Metasomatism in the Late Precambrian Bull Arm Formation in Southeastern Newfoundland. Geol. Assoc. Can., Proc., v. 24, p. 85-93.

Hutchinson, R. D. 1953. Geology of Harbour Grace map-area, Newfoundland. Geol. Surv. Can., Mem. 275.

Hutchinson, R. D. 1954. Harbour Grace, Newfoundland. Geol. Surv. Can., Map 1035A.

Irvine, T. N., and Baragar, W. R. A. 1971. A guide to the chemical classification of the common volcanic rocks. Can. J. Earth Sci., v. 8, p. 523-548.

Jakes, P., and Smith, I. E. 1970. High potassium calc-alkaline rocks from Cape Nelson, eastern Papua. Contrib. Mineral. and Petrol., v. 28, p. 259-271.

Jakes, P., and White, A. R. J. 1970. K/Rb ratios of some rocks from island arcs. Geochim. et Cosmochim. Acta, v. 34, p. 849-856.

BIBLIOGRAPHY (Cont'd.)

Jakes, P., and White, A. R. J. 1972. Major and trace element variations in volcanic rocks from orogenic areas. Geol. Soc. Amer. Bull., v. 83, p. 29-46.

Jenness, S. E. 1960. Late Pleistocene glaciation of eastern Newfoundland. Geol. Soc. Amer. Bull., v. 71, p. 161-180.

Jenness, S. E. 1963. Terra Nova and Bonavista map-area, Newfoundland. Geol. Surv. Can., Mem. 327.

Jenks, W. F., and Goldich, S. S. 1956. Rhyolitic tuff flows in southern Peru. J. Geol., v. 64, p. 156-172.

Jolly, W. T. 1970. Zeolite and prehnite-pumpellyite facies in south-central Puerto Rico. Contrib. Mineral. and Petrol., v. 27, p. 204-224.

Joplin, G. A. 1963. Chemical analyses of Australian rocks, Part I: Igneous and metamorphic. Austr. Bur. Mineral Resources, Geol. Geophys. Bull., v. 65.

Joplin, G. A. 1968. A Petrography of Australian Igneous Rocks. American Elsevier Publ. Co., Inc., New York, 214 p.

Jukes, J. B. 1843. General report of the Geological Survey of Newfoundland, during the years 1839 and 1840. London, England, John Murray, v. I and II, 160 p.

Kennedy, M. J., and McGonigal, M. H. 1972. The Gander Lake and Davidsville Groups of northeastern Newfoundland: new data and geotectonic implications. Can. J. Earth Sci., v. 9, p. 452-459.

King, A. F. 1972. Late Precambrian molasse of the Avalon Platform, Newfoundland (Abs.). Geol. Soc. Amer., 7th Ann. Meeting, Northeastern section, Abstracts, p. 26.

Kistler, R. W., Evernden, J. F., and Shaw, H. R. 1971. Sierra Nevada Plutonic cycle: Part I, Origin of composite granitic batholiths. Geol. Soc. Amer. Bull., v. 82, p. 853-868.

Korzhinskii, D. S. 1959. Physiochemical basis of the analysis of the paragenesis of minerals. Chapman and Hall, London, 142 p.

Kuno, H. 1959. Origin of Cenozoic petrographic provinces of Japan and surrounding area. Bull. Volcanol., ser. 2, v. 20, p. 37-76.

BIBLIOGRAPHY (Cont'd.)

Kuno, H. 1960. High-alumina basalt. J. Petrology, v. 1, p. 121-145.

Kuno, H. 1964. Sorting of pumice and lithic fragments as a key to eruptive and emplacement mechanism. Jap. J. Geol. Geogr., v. 35, p. 223-238.

Lacroix, A. 1904. La Montagne Pelée et ses éruptions. Masson et Cie, Paris, 662 p.

Langmhyr, F. J., and Paus, P. E. 1968. The analysis of inorganic siliceous materials by atomic absorption spectrophotometry and the hydrofluoric acid decomposition technique. Part 1: the analysis of silicate rocks. Anal. Chim. Acta, v. 43, p. 397-408.

Leeman, W. P., and Rogers, J. J. W. 1970. Late Cenozoic alkali-olivine basalts of the Basin-Range province, U. S. A. Contrib. Mineral. and Petrol., v. 25, p. 1-24.

Levi, B. 1969. Burial metamorphism of a Cretaceous volcanic sequence west of Santiago, Chile. Contrib. Mineral. and Petrol., v. 24, p. 30-49.

Lilley, H. D. 1966. Late Precambrian and Appalachian tectonics in the light of submarine exploration on the Great Bank of Newfoundland and in the Gulf of St. Lawrence. Preliminary views. Amer. J. Sci., v. 264, p. 569-574.

Liou, J. G. 1971. Synthesis and stability relations of prehnite, $Ca_2Al_2Si_3O_{10}(OH)_2$. Amer. Mineral., v. 56, p. 507-531.

Lipman, P. W. 1965. Chemical comparison of glassy and crystalline volcanic rocks. U. S. Geol. Surv. Bull. 1201D, p. D1-D24.

Lipman, P. W. 1967. Mineral and chemical variations within an ash-flow sheet from Aso Caldera, southwestern Japan. Contrib. Mineral. and Petrol., v. 16, p. 300-327.

Lipman, P. W., Christiansen, R. L., and Van Alstine, R. E. 1969. Retention of alkalis by calc-alkaline rhyolites during crystallisation and hydration. Am. Mineral., v. 54, p. 286-291.

Lipman, P. W., Prostka, H. J., and Christiansen, R. L. 1972. Cenozoic volcanism and plate-tectonic evolution of the western United States. Phil. Trans. Royal Soc. London, series A, v. 271, p. 217-248.

BIBLIOGRAPHY (Cont'd.)

Lofgren, G. 1971a. Experimentally produced devitrification textures in natural rhyolite glass. Geol. Soc. Amer. Bull., v. 82, p. 111-124.

Lofgren, G. 1971b. Spherulitic textures in glassy and crystalline rocks. J. Geophys. Res., v. 76, p. 5635-5648.

Luedke, R. G., and Burbank, W. S. 1961. Central vent ash-flow eruption, western San Juan Mountains, Colorado. U. S. Geol. Surv. Prof. Paper 424D, p. 94-96.

Macdonald, G. A. 1972. Volcanoes. Prentice-Hall Inc., New Jersey, 510 p.

Macdonald, G. A., and Alcarez, A. 1956. Nuées ardentes of the 1948-1953 eruption of Hibok-Hibok. Bull. Volcanol., ser. 2, v. 18, p. 169-178.

Macdonald, G. A., and Katsura, T. 1964. Chemical composition of Hawaiian lavas. J. Petrology, v. 5, p. 82-133.

Malpas, J. G. 1972. The Petrochemistry of the Bull Arm Formation near Rantem Station, southeast Newfoundland. M. Sc. Thesis (unpublished), Memorial University of Newfoundland, St. John's, Newfoundland. 95 p.

Mansfield, G. R., and Ross, C. S. 1935. Welded rhyolitic tuffs in southeastern Idaho. Amer. Geophys. Union Trans., 16th Ann. Meeting, part 1, p. 308-321.

Manson, V. 1968. Geochemistry of basaltic rocks: major elements. In Basalts: The Poldervaart Treatise on Rocks of Basaltic Composition. Editors, Hess, H. H., and Poldervaart, A., New York, Interscience, v. 1, p. 215-269.

Marshall, P. 1935. Acid rocks of the Taupo Rotorua volcanic district. Royal Soc. New Zealand, Trans., v. 64, p. 328-366.

Marshall, R. R. 1961. Devitrification of natural glass. Geol. Soc. Amer. Bull., v. 72, p. 1493-1520.

Martin, R. F. 1969. The hydrothermal synthesis of low albite. Contrib. Mineral. and Petrol., v. 23, p. 323-339.

Martin, R. F., and Piwinskii, A. J. 1972. Magmatism and tectonic settings. J. Geophys. Res., v. 77, p. 4966-4975.

BIBLIOGRAPHY (Cont'd.)

McBirney, A. R. 1968. Second additional theory of the origin of fiamme in ignimbrites. Nature, v. 217, p. 938.

McBirney, A. R. 1969. Andesitic and rhyolitic volcanism of orogenic basalts. In The Earth's Crust and Upper Mantle. Editor, Hart, P. J., Amer. Geophys. Union Monograph 13, p. 501-507.

McBirney, A. R., and Williams, Howel. 1969. Geology and petrology of the Galapagos Islands. Geol. Soc. Amer. Mem. 118, 197 p.

McCartney, W. D. 1954. Holyrood, Newfoundland. Geol. Surv. Can., Prelim. Map 54-3.

McCartney, W. D. 1967. Whitbourne map-area, Newfoundland. Geol. Surv. Can., Mem. 341.

McCartney, W. D. 1969. Geology of Avalon Peninsula, southeast Newfoundland. Amer. Assoc. Petrol. Geol., Mem. 12, p. 115-129.

McCartney, W. D., Poole, W. H., Wanless, R. K., Williams, H., and Loveridge, W. D. 1966. Rb/Sr age and geological setting of the Holyrood granite, southeast Newfoundland. Can. J. Earth Sci., v. 3, p. 947-957.

McTaggart, K. C. 1960. The mobility of nuées ardentes. Amer. J. Sci., v. 258, p. 369-382.

Misra, S. B. 1969. Late Precambrian (?) fossils from southeastern Newfoundland. Geol. Soc. Amer. Bull., v. 80, p. 2133-2140.

Mohr, P. A. 1971. Ethiopian Rift and Plateaus: some volcanic petrochemical differences. J. Geophys. Res., v. 76, p. 1967-1985.

Moore, J. G., and Melson, W. G. 1969. Nuées ardentes of the 1968 eruption of Mayon Volcano, Philippines. Bull. Volcanol., v. 33, p. 600-620.

Moorhouse, W. W. 1964. The study of rocks in thin section. Harper and Row Publishers Inc., New York, 514 p.

Muffler, L. J. P., and White, D. E. 1969. Active metamorphism of upper Cenozoic sediments in the Salton Sea geothermal field and the Salton Trough, Southeastern California. Geol. Soc. Amer. Bull., v. 80, p. 157-182.

BIBLIOGRAPHY (Cont'd.)

Murai, I. 1961. A study of the textural characteristics of pyroclastic flow deposits in Japan. Bull. Earthq. Res. Inst. Tokyo Univ., v. 39, p. 133-254.

Murray, A., and Howley, J. P. 1881. Map of the Peninsula of Avalon. Geol. Surv. Newfoundland.

Mutti, E. 1965. Submarine flood tuffs (ignimbrites) associated with turbidites in Oligocene deposits of Rhode Island (Greece). Sedimentology, v. 5, p. 265-288.

Neumann, H. 1949. Notes on the mineralogy and geochemistry of zinc. Mineral. Mag., v. 28, p. 575-581.

Noble, D. C. 1965. Ground-water leaching of sodium from quickly cooled volcanic rocks (Abs.). Amer. Mineral., v. 50, p. 289.

Noble, D. C., Smith, V. C., and Peck, L. C. 1967. Loss of halogens from crystallised and glassy silicic volcanic rocks. Geochim. et Cosmochim. Acta, v. 31, p. 215-223.

Nockolds, S. R. 1954. Average chemical composition of some igneous rocks. Geol. Soc. Amer. Bull., v. 65, p. 1007-1032.

Nockolds, S. R., and Allen, R. 1953. The geochemistry of some igneous rock series. Geochim. et Cosmochim. Acta, v. 4, p. 105-142.

Nockolds, S. R., and Allen, R. 1954. The geochemistry of some igneous rock series: Part II. Geochim. et Cosmochim. Acta, v. 5, p. 245-285.

Nockolds, S. R., and Mitchell, R. L. 1948. The geochemistry of some Caledonian plutonic rocks: A study in the relationship between the major and trace elements of igneous rocks and their minerals. Trans. Royal Soc. Edinburgh, v. 61, p. 533-575.

Norton, W. H. 1917. Studies for students: a classification of breccias. J. Geol., v. 25, p. 160-194.

O'Hara, M. J. 1965. Primary magmas and the origin of basalts. Scott. J. Geol., v. 1, p. 19-40.

Ono, K. 1966. Glass lens in welded tuffs (Abs.). Jap. Volcanol. Soc. Bull., v. 11, p. 47-48.

Orville, P. M. 1963. Alkali ion exchange between vapor and feldspar phases. Amer. J. Sci., v. 261, p. 201-237.

BIBLIOGRAPHY (Cont'd.)

Otalora, G. 1964. Zeolites and related minerals in Cretaceous rocks of east-central Puerto Rico. Amer. J. Sci., v. 262, p. 726-734.

Papezik, V. S. 1969. Late Precambrian ignimbrites on the Avalon Peninsula, Newfoundland. Can. J. Earth Sci., v. 6, p. 1405-1414.

Papezik, V. S. 1970. Petrochemistry of volcanic rocks of the Harbour Main Group, Avalon Peninsula, Newfoundland. Can. J. Earth Sci., v. 7, p. 1485-1498.

Papezik, V. S. 1972a. Burial Metamorphism of Late Precambrian sediments near St. John's, Newfoundland. Can. J. Earth Sci., v. 9, p. 1568-1572.

Papezik, V. S. 1972b. Late Precambrian ignimbrites in eastern Newfoundland and their tectonic significance. Proc. 24th I. G. C., Montreal, Quebec, section 1, p. 147-152.

Papezik, V. S. 1973. Detrital garnet and muscovite in Late Precambrian sandstone near St. John's, Newfoundland, and their significance. Can. J. Earth Sci., v. 10, p. 430-432.

Parsons, W. H. 1969. Criteria for the recognition of volcanic breccias: review. Geol. Soc. Amer. Mem. 115, p. 263-304.

Peacock, M. A. 1931. Classification of igneous rock series. J. Geol., v. 39, p. 54-67.

Pearce, J. A., and Cann, J. R. 1971. Ophiolite origin investigated by discriminant analysis using Ti, Zr, and Y. Earth and Planet. Sci. Letters, v. 12, p. 339-349.

Pearce, T. H. 1968. A contribution to the theory of variation diagrams. Contrib. Mineral. and Petrol., v. 19, p. 142-157.

Peterson, D. W. 1970. Ash-flow deposits -- their character, origin, and significance. J. Geol. Educ., v. 18, p. 66-76.

Philpotts, J. A., and Schnetzler, C. C. 1972. Large trace cation partitioning in igneous processes. Proc. 24th I. G. C., Montreal, Quebec, section 10, p. 51-59.

Pichler, H., and Zeil, W. 1972. Paleozoic and Mesozoic ignimbrites of northern Chile. N. Jb. Miner. Abh., v. 116, p. 196-207.

BIBLIOGRAPHY (Cont'd.)

Poldervaart, A. 1964. Chemical classification of alkali basalts and tholeiites. Geol. Soc. Amer. Bull., v. 75, p. 229-232.

Poole, W. H. 1967. Tectonic evolution of Appalachian region of Canada. Geol. Assoc. Can. Special Paper 4, p. 9-51.

Poole, W. H. 1973. Detrital garnet and muscovite in Late Precambrian sandstone near St. John's, Newfoundland, and their significance: Discussion. Can. J. Earth Sci., v. 10, p. 1697-1698.

Presnall, D. C., and Bateman, P. C. 1973. Fusion relations in the system $NaAlSi_3O_8$-$CaAl_2Si_2O_8$-$KAlSi_3O_8$-SiO_2-H_2O and generation of granitic magmas in the Sierra Nevada Batholith. Geol. Soc. Amer. Bull., v. 84, p. 3181-3202.

Prinz, M. 1968. Geochemistry of basaltic rocks: trace elements. In Basalts: The Poldervaart Treatise on Rocks of Basaltic Composition. Editors, Hess, H. H., and Poldervaart, A., Interscience, New York, v. 1, p. 271-323.

Ragland, P. C., Rogers, J. J. W., and Justus, P. S. 1968. Origin and Differentiation of Triassic Dolerite Magmas, North Carolina, USA. Contrib. Mineral. and Petrol., v. 20, p. 57-80.

Reed, J. C., and Morgan, B. A. 1971. Chemical alteration and spilitization of the Catoctin greenstones, Shenandoah National Park, Virginia. J. Geol., v. 79, p. 526-548.

Ringwood, A. E., and Green, D. H. 1966. Petrologic nature of the stable continental crust. In The Earth beneath the continents. Editors, Steinhart, J. S., and Smith, T. J. Amer. Geophys. Union Monograph 10, p. 611-619.

Rittman, A. 1962. Volcanoes and their activity. Interscience Publ., John Wiley and Sons, New York, 305 p.

Roberts, B., and Siddans, A. W. B. 1971. Fabric studies in the Llwyd Mawr Ignimbrite, Caernarvonshire, North Wales. Tectonophysics, v. 12, p. 283-306.

Rogers, J. 1967. Chronology of tectonic movements in the Appalachian region of eastern North America. Amer. J. Sci., v. 265, p. 408-427.

Rogers, J. 1968. The eastern edge of the North American continent during the Cambrian and Early Ordovician. In Studies of Appalachian geology, Northern and Maritime. Editors, Zen, E-an, White, W. S., Hadley, J. B., and Thompson, J. B. Jr., Interscience, New York, 475 p.

BIBLIOGRAPHY (Cont'd.)

Rose, E. R. 1952. Torbay map-area, Newfoundland. Geol. Surv. Can., Mem. 265.

Rose, H. J., Adler, I., and Flanagan, F. J. 1962. Use of La_2O_3 as a heavy absorber in the X-ray fluorescence analysis of silicate rocks. U. S. Geol. Surv. Prof. Paper 450B, 80 p.

Ross, C. S., and Smith, R. L. 1955. Water and other volatiles in volcanic glasses. Amer. Mineral., v. 40, p. 1071-1089.

Ross, C. S., and Smith, R. L. 1961. Ash-flow tuffs: their origin, geologic relations and identification. U. S. Geol. Surv. Prof. Paper 366, 81 p.

Rucklidge, J. C. 1967. A computer program for processing microprobe data. J. Geol., v. 75, p. 126.

Schenk, P. E. 1971. Southeastern Atlantic Canada, northwestern Africa, and continental drift. Can. J. Earth Sci., v. 8, p. 1218-1251.

Schmincke, H.-U. 1967. Fused tuff and peperites in south-central Washington. Geol. Soc. Amer. Bull., v. 78, p. 319-330.

Schmincke, H.-U., and Swanson, D. A. 1967. Laminar viscous flowage structures in welded ash-flow tuffs, Gran Canaria, Canary Islands. J. Geol., v. 25, p. 641-663.

Schrijver, K. 1973. Composition of garnet in anorthosite-charnockite suites: bias and precision in electron-probe microanalysis. Can. J. Earth Sci., v. 10, p. 1257-1266.

Schwartz, G. M. 1958. Alteration of biotite under mesothermal conditions. Econ. Geol., vol. 53, p. 164.

Scott, R. B. 1966. Origin of chemical variations within ignimbrite cooling units. Amer. J. Sci., v. 264, p. 273-288.

Scott, R. B. 1971. Alkali exchange during devitrification and hydration of glasses in ignimbrite cooling units. J. Geol., v. 79, p. 100-110.

Seki, Y. 1965. Prehnite in low-grade metamorphism. Sci. Rep. Saitama Univ., Urawa, Japan, v. 5, ser. B, p. 29-43.

Shaw, D. M. 1968. A review of K/Rb fractionation trends by covariance analysis. Geochim. et Cosmochim. Acta, v. 32, p. 573-603.

BIBLIOGRAPHY (Cont'd.)

Shaw, D. M., Reilly, G. A., Muysson, J. R., Pattenden, G. E., and Campbell, F. E. 1967. An estimate of the chemical composition of the Canadian Precambrian Shield. Can. J. Earth Sci., v. 5, p. 829-853.

Shaw, H. R. 1963. Obsidian-H_2O viscosities at 1000 and 2000 bars in the temperature range 700°-900°C. Geophys. Res., v. 68, p. 6337-6343.

Shaw, H. R. 1965. Comments on viscosity, crystal settling, and convection in granitic magmas. Amer. J. Sci., v. 263, p. 120-152.

Sibree, J. O. 1934. The viscosity of froth. Faraday Soc. Trans., v. 30, p. 325-331.

Smith, R. E. 1968. Redistribution of major elements in the alteration of some basic lavas during burial metamorphism. J. Petrology, v. 9, p. 191-219.

Smith, R. E. 1969. Zones of progressive regional burial metamorphism in part of the Tasman Geosyncline, Eastern Australia. J. Petrology, v. 10, p. 144-163.

Smith, R. L. 1960. Ash flows. Geol. Soc. Amer. Bull., v. 71, p. 795-842.

Smith, R. L. 1960a. Zones and zonal variations in welded ash flows. U. S. Geol. Surv. Prof. Paper 354F, p. 149-159.

Smith, R. L., and Bailey, R. A. 1966. The Bandelier Tuff: a study of ash-flow eruption cycles from zoned magma chambers. Bull. Volcanol., ser. 2, v. 29, p. 83-104.

Smith, R. L., Friedman, I. I., and Long, W. D. 1958. Welded tuffs: expt. 1. Amer. Geophys. Union Trans., v. 39, p. 352-353.

Sparks, R. S. J., Self, S., and Walker, G. P. L. 1973. Products of ignimbrite eruptions. Geology, v. 1, p. 115-118.

Steiner, A. 1963. The rocks penetrated by drillholes in the Waiotapu Thermal Area, and their hydrothermal alteration. New Zealand Dept. Sci. Ind. Research Bull. 155, p. 26-34.

Streckeisen, A. L. 1967. Classification and nomenclature of igneous rocks. N. Jb. Miner. Abh., v. 107, p. 144-214.

BIBLIOGRAPHY (Cont'd.)

Strong, D. F. 1974. Plate tectonic setting of Appalachian-Caledonian mineral deposits as indicated by Newfoundland examples. SME Trans., v. 255, p. 121-128.

Strong, D. F., Dickson, W. L., and O'Driscoll, C. F. 1973. Geochemistry of eastern Newfoundland granitoid rocks. Newfoundland Mineral Resources Div., interim report, 121 p.

Strong, D. F., Dickson, W. L., O'Driscoll, C. F., Kean, B. F., and Stevens, R. K. 1974. Geochemical evidence for east-dipping Appalachian subduction in Newfoundland. Nature, v. 248, p. 37-39.

Surdam, R. C. 1969. Electron-probe study of prehnite and pumpellyite from the Karmutsen Group, Vancouver Island, British Columbia. Amer. Mineral., v. 54, p. 256-266.

Surdam, R. C. 1973. Low-grade metamorphism of tuffaceous rocks in the Karmutsen Group, Vancouver Island, British Columbia. Geol. Soc. Amer. Bull., v. 84, p. 1911-1922.

Tabor, R. W., and Crowder, D. F. 1969. On batholiths and volcanoes -- Intrusion and eruption of Late Cenozoic magmas in the Glacier Peak area, North Cascades, Washington. U. S. Geol. Surv. Prof. Paper 604, 67 p.

Taubeneck, W. H. 1965. An appraisal of some potassium-rubidium ratios in igneous rocks. J. Geophys. Res., v. 70, p. 475-478.

Tauson, L. V. 1965. Factors in the distribution of the trace elements during the crystallisation of magmas. In Physics and Chemistry of the Earth. Editors, Ahrens, L. H., Press, F., Runcorn, S. K., and Urey, H. C., v. 6, p. 215-249.

Taylor, G. A. 1958. The 1951 eruption of Mount Lamington, Papua. Austr. Bur. Mineral Resources, Geol. Geophys. Bull., v. 38, p. 1-117.

Taylor, S. R. 1965. The application of trace element data to problems in petrology. In Physics and Chemistry of the Earth. Editors, Ahrens, L. H., Press, F., Runcorn, S. K., Urey, H. C., v. 6, p. 133-213.

Taylor, S. R. 1968. Geochemistry of Andesites. Proc. Int. Symposium. Origin and Distribution of the Elements. Editor, Ahrens, L. H., section 5, p. 559-583.

BIBLIOGRAPHY (Cont'd.)

Taylor, S. R., and White, A. J. R. 1966. Trace element abundances in andesites. Bull. Volcanol., series 2, v. 29, p. 177-194.

Taylor, S. R., Capp, A. C., Graham, A. L., and Blake, D. H. 1969. Trace element abundances in andesites. II. Saipan, Bougainville, and Fiji. Contrib. Mineral. and Petrol., v. 23, p. 1-26.

Tazieff, H. 1969. Mechanism of ignimbrite eruption. In Mechanism of Igneous Intrusion. Editors, Newall, G., and Rast, N., p. 157-164.

Thieme, J. G. 1970. The Geology of the Mansa Area: explanation of Degree Sheet 1128, parts of N. W. Quarter and N. E. Quarter. Rep. Geol. Surv. Zambia.

Thornton, C. P., and Tuttle, O. F. 1960. Chemistry of igneous rocks, 1, Differentiation index. Amer. J. Sci., v. 258, p. 664-684.

Turner, F. J., and Verhoogen, J. 1960. Igneous and Metamorphic Petrology. McGraw-Hill, Inc., New York, 694 p.

Tuttle, O. F. 1952. Origin of the contrasting mineralogy of extrusive and plutonic salic rocks. J. Geol., v. 60, p. 107-124.

Tuttle, O. F., and Bowen, N. L. 1958. Origin of granite in the light of experimental studies in the system $NaAlSi_3O_8$-$KAlSi_3O_8$-SiO_2-H_2O. Geol. Soc. Amer. Mem. 74, 153 p.

Upton, B. G. J., and Wadsworth, W. J. 1972. Aspects of magmatic evolution on Réunion Island. Phil. Trans. Royal Soc. London, series A, v. 271, p. 105-130.

Vallance, T. G. 1960. Concerning spilites. Proc. of the Linnean Soc. of New South Wales, v. 85, p. 8-52.

Vallance, T. G. 1969. Spilites again: some consequences of the degradation of basalts. Proc. of the Linnean Soc. of New South Wales, v. 94, p. 8-55.

Vallance, T. G. 1969a. Recognition of specific magmatic character in some Paleozoic mafic lavas in New South Wales. Geol. Soc. Austr., Special Publication 2, p. 163-167.

Van Bemmelen, R. W. 1949. The geology of Indonesia, v. 1A, General Geology of Indonesia and adjacent archipelagos. Govt. Printing Office, The Hague, 732 p.

BIBLIOGRAPHY (Cont'd.)

Verhoogen, J. 1951. Mechanics of ash formation. Amer. J. Sci., v. 249, p. 729-739.

Walcott, C. D. 1899. Pre-Cambrian Fossiliferous Formations. Geol. Soc. Amer. Bull., v. 10, p. 199-224.

Walker, F. 1952. Mugearites and oligoclase basalts. Geol. Mag., v. 89, p. 337-345.

Walker, G. P. L. 1972. Crystal concentration in ignimbrites. Contrib. Mineral. and Petrol., v. 36, p. 135-146.

Waters, A. C. 1962. Basalt magma types and their tectonic associations: Pacific Northwest of the United States. In The Crust of the Pacific Basin. Editors, Macdonald, G. A., and Kuno, H., Amer. Geophys. Union Monograph 6, p. 158-170.

Wentworth, C. K., and Williams, Howel. 1932. The classification and terminology of the pyroclastic rocks. Nat. Research Council, Rept. Comm. Sedimentation, Bull., v. 89, p. 19-53.

White, D. E., and Sigvaldason, G. D. 1963. Epidote in hot spring systems, and depth of formation of propylitic epidote in epithermal ore deposits. U. S. Geol. Surv. Prof. Paper 450E, p. E80-E84.

Wilkinson, J. F. G. 1968a. The petrography of basaltic rocks. In Basalts: The Poldervaart Treatise on Rocks of Basaltic Composition. Editors, Hess, H. H., and Poldervaart, A., Interscience, New York, v. 1, p. 163-214.

Wilkinson, J. F. G. 1968b. Analcimes from some potassic igneous rocks and aspects of analcime-rich igneous assemblages. Contrib. Mineral. and Petrol., v. 18, p. 252-269.

Williams, Harold. 1964. The Appalachians in northwestern Newfoundland -- a two-sided symmetrical system. Amer. J. Sci., v. 262, p. 1137-1158.

Williams, Harold. 1967. Island of Newfoundland. Geol. Surv. Can., Map 1231A.

Williams, Harold, Kennedy, M. J., and Neale, E. R. W. 1972. The Appalachian Structural Province. In Variations in Tectonic Styles in Canada. Editors, Price, R. A., and Douglas, R. J. W., Geol. Assoc. Can. Special Paper, 11, p. 181-261.

BIBLIOGRAPHY (Cont'd.)

Williams, Harold, and Stevens, R. K. (in press). The ancient continental margin of eastern North America.

Williams, Howel. 1942. The geology of Crater Lake National Park, Oregon, with a reconnaissance of the Cascade Range southward to Mount Shasta. Carnegie Inst. Washington Pub. 540, 162 p.

Wright, A. E., and Bowes, D. R. 1963. Classification of volcanic breccias: a discussion. Geol. Soc. Amer. Bull., v. 74, p. 79-86.

Yoder, H. S., and Tilley, C. E. 1962. Origin of basalt magmas: an experimental study of natural and synthetic rock systems. J. Petrology, v. 3, p. 342-532.

Zen, E-an. 1961. The zeolite facies: An interpretation. Amer. J. Sci., v. 259, p. 401-409.

APPENDIX 1 WHOLE ROCK(mol %)

SAMPLE	FE	TI	[illegible]	SI	CA	[illegible]	MG	AL	FEO	NA	[illegible]
GTN23E	2.10	0.71	0.[illegible]	76.60	1.28	1.33	2.35	9.94	0.0	7.82	0.09
GTN23D	1.80	0.70	0.10	75.77	0.92	1.90	1.36	10.92	0.0	7.93	0.08
GTN23A	2.24	0.75	0.10	74.99	1.20	1.34	1.81	9.86	0.0	7.51	0.10
GTN23C	2.26	0.82	0.02	72.12	1.74	0.78	3.67	10.15	0.0	8.38	0.12
GTN22I	1.35	0.64	0.0	76.88	1.01	2.11	1.23	9.36	0.0	8.35	0.07
GTN34	1.47	0.61	0.0	75.76	1.02	0.36	3.18	9.10	0.0	7.27	0.18
GTN 11	1.18	0.07	0.0	81.06	0.86	0.36	3.0	8.54	0.0	7.16	0.01
GTN19	1.08	0.67	0.010	81.28	1.32	0.64	3.0	8.15	0.0	6.83	0.06
GTN1A1	1.91	0.66	0.01	78.28	2.03	1.19	0.86	9.02	0.0	5.53	0.08
P78.11	1.01	0.68	0.06	76.77	1.35	3.68	1.20	9.97	0.0	5.98	0.11
P78-9	1.98	0.76	0.10	72.30	2.08	1.69	2.38	11.27	0.0	7.24	0.15
P78-11	0.91	0.22	0.06	81.10	0.21	1.77	0.40	8.63	0.0	6.61	0.03
P78-14	1.06	0.43	0.03	81.08	0.82	1.31	0.91	8.68	0.0	5.89	0.06
GC 49	1.56	0.39	0.0	77.09	1.58	1.21	1.19	9.79	0.0	6.72	0.06
GC52	1.57	0.46	0.0	77.93	1.32	1.94	2.40	9.66	0.0	6.36	0.06
GC86A	1.20	0.42	0.0	78.[illegible]7	1.37	1.58	3.10	8.88	0.0	6.97	0.08
GC86B	1.08	0.33	0.0	78.10	1.25	2.13	2.10	9.72	0.0	6.81	0.06
GC17	1.08	0.09	0.0	82.83	0.47	3.16	0.67	8.59	0.0	3.69	0.03
GC16	0.72	0.35	0.0	82.24	0.63	3.20	0.33	8.83	0.0	3.83	0.02
GC15	1.03	0.45	0.01	78.92	1.91	2.66	0.55	9.07	0.0	3.76	0.04
GC14	0.73	0.15	0.[illegible]	82.17	1.15	3.13	0.99	9.42	0.0	3.71	0.03
GC8B	0.83	0.13	0.0	82.12	0.88	3.74	0.47	9.34	0.0	3.46	0.03
P78-12	0.77	0.11	0.00	81.53	0.57	3.88	0.58	9.51	0.0	3.98	0.00
GC 23	0.91	0.16	0.0	81.28	1.38	2.79	1.16	9.53	0.0	3.75	0.04
GC22	0.85	0.13	0.0	82.97	0.85	2.85	1.33	8.87	0.0	3.68	0.04
GC29	0.99	0.18	0.0	81.63	0.28	1.54	0.40	9.15	0.0	5.74	0.03
GC28A	1.25	0.24	0.0	81.84	0.31	0.99	0.30	9.04	0.0	1.55	0.07
GC28B	1.25	0.24	0.0	81.78	0.38	0.36	0.30	10.01	0.0	1.68	0.04
H 157	0.83	0.17	0.0	81.90	0.51	3.97	0.99	9.78	0.0	3.14	0.03
CAT 1	1.08	0.27	0.0	79.92	1.53	3.91	1.03	9.93	0.0	3.54	0.07

Cont.

GC35	0.48	3.21	0.0	48.74	0.45	2.64	0.81	8.04	0.0	5.55	0.45
GC44	3.85	3.26	0.0	41.36	0.38	2.53	0.53	8.76	0.0	5.51	0.42
GC 18	1.08	0.36	0.0	77.11	0.62	2.18	1.70	10.86	0.0	5.49	0.08
GC19	0.49	0.22	0.0	84.35	0.33	2.36	0.15	9.07	0.0	4.49	0.03
NX 1	1.34	0.34	0.0	78.65	1.08	2.21	1.63	9.02	0.0	3.76	0.04
GC38	1.03	3.33	0.0	80.87	0.51	2.51	3.55	9.05	0.0	0.73	0.02
GC42	1.50	0.27	0.0	81.40	0.65	2.08	1.41	9.30	0.0	0.80	0.05
GC39A	1.72	0.47	0.21	78.99	1.07	3.22	2.23	10.73	0.0	0.81	0.05
GC39H	1.68	0.17	0.01	78.41	1.26	3.03	0.53	9.74	0.0	0.40	0.07
GCA	2.52	3.50	0.03	73.31	5.20	1.88	2.38	11.31	0.0	3.12	0.08
GC10	2.50	0.70	0.02	72.04	1.91	3.36	4.46	11.18	0.0	3.72	0.12
GC40	2.50	0.50	0.06	69.35	2.41	3.86	5.20	12.50	0.0	0.52	0.10
GC41	2.61	0.47	0.00	71.85	2.46	1.12	4.47	11.14	0.0	5.22	0.12
GC51	3.47	0.68	0.0	68.97	1.78	3.71	0.93	12.08	0.0	0.80	0.10
P70-19	3.85	1.04	0.13	60.90	5.58	0.96	7.20	11.13	0.0	5.92	0.10
P70-4	4.40	0.77	0.10	60.44	7.31	0.53	7.50	12.08	0.0	5.87	0.09
P70-8	4.46	1.62	0.11	60.88	4.72	3.25	5.70	11.85	0.0	4.62	0.15
P70-17	3.11	0.82	0.10	60.10	5.00	0.25	12.67	11.55	0.0	4.27	0.05
H165	4.23	1.62	0.17	59.79	5.82	0.83	7.13	13.22	0.0	7.10	0.20
GC2	3.22	1.32	0.23	58.31	11.00	0.88	0.32	11.52	0.0	0.04	0.17
GC11	5.03	1.83	0.23	56.38	8.60	0.56	10.15	11.31	0.0	5.24	0.10
GC13	5.57	1.62	0.18	58.07	0.79	0.00	0.53	13.32	0.0	4.51	0.35
GC20	4.17	1.29	0.28	58.38	5.23	0.81	11.85	11.79	0.0	4.27	0.10
NX12	5.69	1.64	0.18	57.92	7.47	0.28	11.17	11.30	0.0	5.13	0.18
NX14	5.42	1.30	0.22	55.62	0.42	0.00	12.00	12.10	0.0	0.95	0.18
NX 15	0.50	0.95	0.25	61.06	3.63	0.13	0.04	12.20	0.0	0.04	0.10
P70-1	3.80	1.86	0.10	55.63	7.96	0.86	10.80	13.72	0.0	0.88	0.18
P70-2	0.62	0.04	0.00	50.02	8.65	0.62	7.22	12.93	0.0	5.55	0.07
P70-3	5.06	1.32	0.17	57.92	7.09	1.12	10.11	11.93	0.0	5.17	0.26
NX17	4.59	0.70	0.15	58.93	0.71	1.76	21.59	9.12	0.0	2.87	0.20
GC31	1.15	0.21	0.0	83.23	0.66	2.23	1.17	9.33	0.0	1.99	0.07
GC12	1.81	0.57	0.0	73.93	1.48	0.76	1.02	11.24	0.0	0.76	0.27

APPENDIX 2 FELDSPARS(mol %)

SAMPL	FE	TI	P	SI	CA	K	MG	AL	FEO	NA	MN	SSS
M00M-1M	0.0	0.0	0.0	0.0	2.07	0.69	0.0	0.0	0.0	97.24	0.0	100.00
M00M-1C	0.0	0.0	0.0	0.0	3.07	1.02	0.0	0.0	0.0	95.90	0.0	100.00
M00M-2M	0.0	0.0	0.0	0.0	1.38	1.38	0.0	0.0	0.0	97.24	0.0	100.00
M00M-2C	0.0	0.0	0.0	0.0	2.30	0.67	0.0	0.0	0.0	96.97	0.0	100.00
M00M-3M	0.0	0.0	0.0	0.0	1.37	1.02	0.0	0.0	0.0	97.61	0.0	100.00
M00M-3C	0.0	0.0	0.0	0.0	1.67	0.67	0.0	0.0	0.0	97.66	0.0	100.00
M100M-1M	0.0	0.0	0.0	0.0	1.39	1.39	0.0	0.0	0.0	97.22	0.0	100.00
M100M-1C	0.0	0.0	0.0	0.0	1.36	1.02	0.0	0.0	0.0	97.62	0.0	100.00
M100M-2M	0.0	0.0	0.0	0.0	1.34	1.00	0.0	0.0	0.0	96.98	0.0	100.00
M100M-2C	0.0	0.0	0.0	0.0	1.35	1.35	0.0	0.0	0.0	97.31	0.0	100.00
M170M-1M	0.0	0.0	0.0	0.0	2.03	1.01	0.0	0.0	0.0	96.96	0.0	100.00
M170M-1C	0.0	0.0	0.0	0.0	1.70	1.02	0.0	0.0	0.0	97.28	0.0	100.00
M170M-2M	0.0	0.0	0.0	0.0	1.68	1.01	0.0	0.0	0.0	97.31	0.0	100.00
M170M-2C	0.0	0.0	0.0	0.0	1.70	0.68	0.0	0.0	0.0	97.62	0.0	100.00
M170M-3M	0.0	0.0	0.0	0.0	1.37	1.02	0.0	0.0	0.0	97.61	0.0	100.00
M105M-1M	0.0	0.0	0.0	0.0	2.30	0.68	0.0	0.0	0.0	96.96	0.0	100.00
M105M-1C	0.0	0.0	0.0	0.0	1.98	0.99	0.0	0.0	0.0	97.03	0.0	100.00
M105M-2M	0.0	0.0	0.0	0.0	2.65	2.32	0.0	0.0	0.0	95.03	0.0	100.00
M105M-2C	0.0	0.0	0.0	0.0	1.01	0.34	0.0	0.0	0.0	98.66	0.0	100.00
M105M-3M	0.0	0.0	0.0	0.0	2.05	0.68	0.0	0.0	0.0	97.27	0.0	100.00
M105M3C1	0.0	0.0	0.0	0.0	1.01	0.67	0.0	0.0	0.0	98.32	0.0	100.00
M105M3C2	0.0	0.0	0.0	0.0	0.34	0.0	0.0	0.0	0.0	99.66	0.0	100.00
M01M-1M	0.0	0.0	0.0	0.0	2.79	0.70	0.0	0.0	0.0	96.52	0.0	100.00
M01M-1M	0.0	0.0	0.0	0.0	2.79	0.70	0.0	0.0	0.0	96.52	0.0	100.00
M01M-1C	0.0	0.0	0.0	0.0	1.71	1.02	0.0	0.0	0.0	97.27	0.0	100.00
M01M-2M	0.0	0.0	0.0	0.0	2.39	1.37	0.0	0.0	0.0	96.25	0.0	100.00
M01M-2C	0.0	0.0	0.0	0.0	2.41	0.69	0.0	0.0	0.0	96.91	0.0	100.00
L00M-1M	0.0	0.0	0.0	0.0	4.93	1.06	0.0	0.0	0.0	94.01	0.0	100.00
L00M-1C	0.0	0.0	0.0	0.0	4.93	0.35	0.0	0.0	0.0	94.72	0.0	100.00
L00M-1X	0.0	0.0	0.0	0.0	0.0	96.80	0.0	0.0	0.0	3.20	0.0	100.00

Cont.

C88M-2C	0.0	0.0	0.0	0.0	4.07	0.34	0.0	0.0	0.0	95.59	0.0	100.00
C88M-3M	0.0	0.0	0.0	0.0	4.42	2.38	0.0	0.0	0.0	93.20	0.0	100.00
C88M-3C	0.0	0.0	0.0	0.0	3.37	1.68	0.0	0.0	0.0	94.95	0.0	100.00
C88M-1M	0.0	0.0	0.0	0.0	3.68	1.34	0.0	0.0	0.0	94.98	0.0	100.00
C88M-1C	0.0	0.0	0.0	0.0	5.05	1.35	0.0	0.0	0.0	93.60	0.0	100.00
C88M-2M	0.0	0.0	0.0	0.0	3.07	2.05	0.0	0.0	0.0	94.88	0.0	100.00
C88M-2C	0.0	0.0	0.0	0.0	8.41	11.33	0.0	0.0	0.0	88.26	0.0	100.00
C63M-1M	0.0	0.0	0.0	0.0	1.34	0.67	0.0	0.0	0.0	97.99	0.0	100.00
C63M-1C	0.0	0.0	0.0	0.0	1.33	0.66	0.0	0.0	0.0	98.01	0.0	100.00
C63M-1CC	0.0	0.0	0.0	0.0	0.00	0.33	0.0	0.0	0.0	99.68	0.0	100.00
C63M-2M	0.0	0.0	0.0	0.0	1.33	1.00	0.0	0.0	0.0	97.67	0.0	100.00
C63M-2C	0.0	0.0	0.0	0.0	1.32	0.99	0.0	0.0	0.0	97.69	0.0	100.00
C63M-3M	0.0	0.0	0.0	0.0	1.65	1.32	0.0	0.0	0.0	97.03	0.0	100.00
C63M-3C	0.0	0.0	0.0	0.0	1.31	0.98	0.0	0.0	0.0	97.70	0.0	100.00
GC20M-1M	0.0	0.0	0.0	0.0	0.34	0.68	0.0	0.0	0.0	98.98	0.0	100.00
GC20M1CC	0.0	0.0	0.0	0.0	4.76	18.73	0.0	0.0	0.0	76.51	0.0	100.00
GC20M2CC	0.0	0.0	0.0	0.0	0.34	0.68	0.0	0.0	0.0	98.97	0.0	100.00
GC20M2CT	0.0	0.0	0.0	0.0	7.79	14.29	0.0	0.0	0.0	77.92	0.0	100.00
C29M-1M	0.0	0.0	0.0	0.0	1.68	1.34	0.0	0.0	0.0	96.98	0.0	100.00
C29M-2C	0.0	0.0	0.0	0.0	2.04	1.36	0.0	0.0	0.0	96.60	0.0	100.00
C29M-3M	0.0	0.0	0.0	0.0	1.97	1.64	0.0	0.0	0.0	96.38	0.0	100.00
C29M-3C	0.0	0.0	0.0	0.0	1.91	15.92	0.0	0.0	0.0	82.17	0.0	100.00
C29M1AB1	0.0	0.0	0.0	0.0	2.00	12.00	0.0	0.0	0.0	86.00	0.0	100.00
C29M-1M	0.0	0.0	0.0	0.0	0.29	83.62	0.0	0.0	0.0	16.09	0.0	100.00
C29M1AB2	0.0	0.0	0.0	0.0	1.37	0.68	0.0	0.0	0.0	97.95	0.0	100.00
M188M-1M	0.0	0.0	0.0	0.0	2.41	1.03	0.0	0.0	0.0	96.55	0.0	100.00
M188M-1C	0.0	0.0	0.0	0.0	1.69	0.68	0.0	0.0	0.0	97.69	0.0	100.00
M188M-2M	0.0	0.0	0.0	0.0	2.41	1.03	0.0	0.0	0.0	96.56	0.0	100.00
M188M-2C	0.0	0.0	0.0	0.0	1.71	1.02	0.0	0.0	0.0	97.27	0.0	100.00
M188M-3M	0.0	0.0	0.0	0.0	1.34	0.67	0.0	0.0	0.0	97.99	0.0	100.00
M188M-3C	0.0	0.0	0.0	0.0	1.02	1.02	0.0	0.0	0.0	97.97	0.0	100.00
M188M-1A	0.0	0.0	0.0	0.0	0.0	88.51	0.0	0.0	0.0	11.49	0.0	100.00

Cont.

M163M-1R	0.0	0.0	0.0	0.0	2.19	0.36	0.0	0.0	0.0	97.45	0.0	100.00
M163M-1L	0.0	0.0	0.0	0.0	1.09	0.36	0.0	0.0	0.0	98.55	0.0	100.00
M163M-2R	0.0	0.0	0.0	0.0	3.10	0.70	0.0	0.0	0.0	96.14	0.0	100.00
M163M-2L	0.0	0.0	0.0	0.0	0.34	0.0	0.0	0.0	0.0	99.66	0.0	100.00
M163M-3R	0.0	0.0	0.0	0.0	2.87	2.87	0.0	0.0	0.0	94.27	0.0	100.00
M163M-3L	0.0	0.0	0.0	0.0	2.65	0.32	0.0	0.0	0.0	96.84	0.0	100.00
GC1M1R	0.0	0.0	0.0	0.0	6.12	1.02	0.0	0.0	0.0	92.86	0.0	100.00
GC1M-1L	0.0	0.0	0.0	0.0	6.71	1.01	0.0	0.0	0.0	92.28	0.0	100.00
GC1M-2R	0.0	0.0	0.0	0.0	5.70	0.68	0.0	0.0	0.0	93.54	0.0	100.00
GC1M-2L	0.0	0.0	0.0	0.0	6.80	0.68	0.0	0.0	0.0	92.52	0.0	100.00
M157M-1R	0.0	0.0	0.0	0.0	2.50	0.66	0.0	0.0	0.0	97.84	0.0	100.00
M157M-1L	0.0	0.0	0.0	0.0	2.76	1.03	0.0	0.0	0.0	96.21	0.0	100.00
M157M-2L	0.0	0.0	0.0	0.0	3.01	0.67	0.0	0.0	0.0	96.33	0.0	100.00
M157M-3L	0.0	0.0	0.0	0.0	2.99	1.00	0.0	0.0	0.0	96.01	0.0	100.00
P/140M2R	0.0	0.0	0.0	0.0	2.34	2.68	0.0	0.0	0.0	94.98	0.0	100.00
P/140M2L	0.0	0.0	0.0	0.0	1.66	1.33	0.0	0.0	0.0	97.01	0.0	100.00
P/140M3R	0.0	0.0	0.0	0.0	2.02	1.01	0.0	0.0	0.0	96.97	0.0	100.00
P/140M3L	0.0	0.0	0.0	0.0	2.03	1.01	0.0	0.0	0.0	96.96	0.0	100.00
NX1M-1R	0.0	0.0	0.0	0.0	2.41	1.03	0.0	0.0	0.0	96.56	0.0	100.00
NX1M-1L	0.0	0.0	0.0	0.0	1.36	0.0	0.0	0.0	0.0	98.64	0.0	100.00
NX1M-2R	0.0	0.0	0.0	0.0	1.71	0.34	0.0	0.0	0.0	97.95	0.0	100.00
NX1M-2L	0.0	0.0	0.0	0.0	1.01	0.34	0.0	0.0	0.0	98.65	0.0	100.00
NX1M-3R	0.0	0.0	0.0	0.0	2.05	0.68	0.0	0.0	0.0	97.26	0.0	100.00
NX1M-3L	0.0	0.0	0.0	0.0	1.71	0.0	0.0	0.0	0.0	98.29	0.0	100.00
LB5M-1R	0.0	0.0	0.0	0.0	11.76	16.67	0.0	0.0	0.0	71.57	0.0	100.00
LB5M-1L	0.0	0.0	0.0	0.0	5.69	3.68	0.0	0.0	0.0	90.64	0.0	100.00
LB5M-2R	0.0	0.0	0.0	0.0	46.78	3.39	0.0	0.0	0.0	49.83	0.0	100.00
LB5M-2L	0.0	0.0	0.0	0.0	48.99	2.03	0.0	0.0	0.0	48.99	0.0	100.00
LB8M-1R	0.0	0.0	0.0	0.0	6.08	0.68	0.0	0.0	0.0	93.24	0.0	100.00
LB8M-1L	0.0	0.0	0.0	0.0	5.03	0.34	0.0	0.0	0.0	94.63	0.0	100.00
LB8M-2R	0.0	0.0	0.0	0.0	4.75	0.68	0.0	0.0	0.0	94.58	0.0	100.00

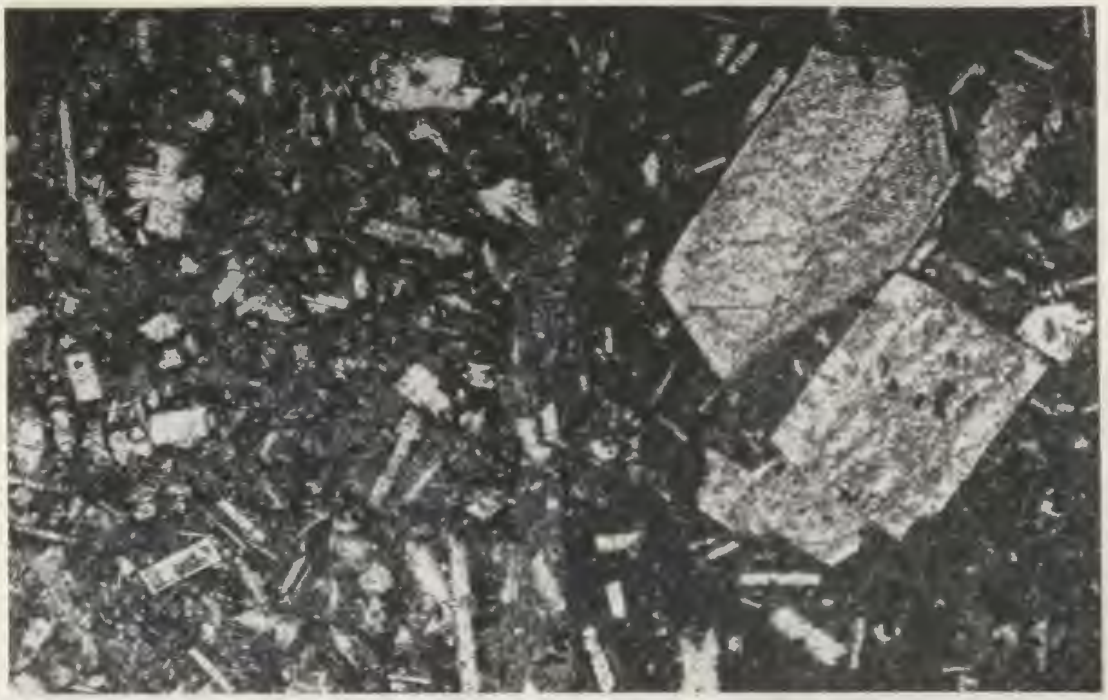

Photomicrograph 47. Sharp contact between successive intrusive phases of a multiple dyke. Note marginal chill and thin clear rim surrounding turbid cores of albite phenocrysts. Plane-polarized light; field of view approx. 12mm across. Analysis H165; map ref. 3490,5965.

Photomicrograph 48. Olivine diabase containing subhedral olivine phenocrysts (upper right and lower left) replaced by iron-oxide (black), iddingsite (grey), and colourless to pale green serpentine (white) set in a groundmass of clinopyroxene (greyish white with high relief) and clouded albite. The clear white recrystallised areas with low relief are albite. Plane-polarized light; field of view approx. 12mm across. Analysis NX17; cf. fig. 4.

TABLE 16. "Classical" Analyses of McGill Feldspar Standards
(In Weight Percent)

Oxide Wt. %	Oligoclase 161	Albite 37	Orthoclase 35
SiO_2	62.57	68.00	64.05
TiO_2	0.00	0.00	0.00
Al_2O_3	22.76	19.80	17.17
Fe_2O_3	0.51	0.09	1.31
FeO	0.00	-	-
MnO	0.00	-	-
MgO	0.09	0.04	0.07
CaO	4.43	0.22	0.00
Na_2O	8.44	11.42	1.62
K_2O	0.75	0.32	15.36
BaO	0.05	-	0.03
H_2O+	0.27	0.03	0.52
H_2O-	0.01	-	0.18
Total:	99.88	99.90	100.31

Analyst: C. O. Ingamells

TABLE 17. Electron-Probe Sequence of Measurements per Analytical Run

Set No.	No. of Measurements*	Description	Target
1	8	peak	Albite 37
2	8	peak	Oligoclase 161
3	12	peak	unknown, Phenocryst 1 Rim
4	12	peak	unknown, Phenocryst 1 Core
5	8	peak	Oligoclase 161
6	8	peak	Albite 37
7	12	peak	unknown, Phenocryst 2 Rim
8	12	peak	unknown, Phenocryst 2 Core
9	8	peak	Albite 37
10	8	peak	Oligoclase 161
11	12	peak	unknown, Phenocryst 2 Rim
12	12	peak	unknown, Phenocryst 3 Core
13	8	peak	Oligoclase 161
14	8	peak	Albite 37
15	6	background	Albite 37
16	12	background	unknown, Phenocryst 1,2, or 3
17	6	background	Oligoclase 161
		(if K-feldspar detected)	
18	8	peak	Orthoclase 35
19	12	peak	unknown, K-spar patch Phenocryst 1
20	8	peak	Orthoclase 35
21	6	background	Orthoclase 35
22	6	background	K-feldspar patch

*The term measurement denotes the number of pulses received by a scalar during a period of 10 seconds.

APPENDIX 3 (Cont'd.)

The feldspar standards used were selected from the McGill collection of standards so as to approach the composition and physical state of the unknown species; a complete chemical analysis of each of these standards is presented in table 16. For more detailed information on the specifications and uses of the McGill microprobe the reader is referred to the McGill University Microprobe Handbook and the analytical work of Schrijver (1973).

A minimum of 2 phenocrysts were selected from each specimen i.e. thin section, and Mercator grid coordinates noted prior to evacuation of the column. After a vacuum had been established, the spectrometers were manually adjusted to the desired wave-lengths using the chosen standards.

X-ray peak intensities i.e. concentrations, of Na, K, Ca, and Si in each unknown (feldspar phenocryst) were measured directly; Al was determined from stoichiometry.

Each phenocryst was analysed by recording a fixed number of measurements of X-ray peak and background intensities on both standards and unknowns (cf. table 17). Two measurements were carried out on each phenocryst by analysing "spots" distributed around the margins (rim analyses) and within the centre (core analyses) of each grain. The electron beam was optically refocused at each "spot".

Upon completion of the analysis of a thin section the vacuum was broken and the next section inserted in the microanalyser. Subsequently, vacuum was reestablished and the spectrometers were set anew.

TABLE 18

Precision of Electron-Probe Analyses

Specimen No. C88M
Phenocryst 1 Core and Rim Analyses

	1st Determination		2nd Determination		Difference (wt. %)	
	1 Rim	1 Core	1 Rim	1 Core	1 Rim	1 Core
SiO_2	67.63	67.72	67.40	67.58	0.23	0.14
Al_2O_3	19.01	18.96	19.23	19.17	0.22	0.21
CaO	0.98	1.00	1.08	1.04	0.10	0.04
Na_2O	10.35	10.41	10.19	10.23	0.16	0.18
K_2O	0.19	0.03	0.12	0.07	0.07	0.04
Total:	98.16	98.13	98.02	98.09		

APPENDIX 3 (Cont'd.)

An impression of the precision of the electron microprobe work can be gained from table 18. The accuracy of the analyses is unknown; but considered to lie within the range of analyses given by Ingamells (table 16), Deer *et al.*, 1963, p. 45, no. 4 (Orthoclase 35), Deer *et al.*, 1966, p. 324, no. 1 (Albite 37), and Horska (McGill University) (Oligoclase 161, Hawk Mica Mine, Bakersville, N. Carolina).

The data thus obtained, punched on paper tape and cards, were processed through computer program EMPADR VII (Rucklidge, 1967) at the McGill Computer Centre. This program (McGill revised 4-spectrometer version) corrects the peak intensities for dead time, background, drift, atomic number, absorption, and fluorescence, and converts corrected peak intensities to oxide weight percentages (the results of these calculations have been presented in table 6). A fixed stoichiometry provision in the program allows unanalysed elements to be included in the unknowns in fixed stoichiometric ratios in terms of analysed elements. The stoichiometry assumed in the calculation of element concentrations is given by the formula:

$$Al = 1\ (Na,K) + 2\ Ca$$

A.3.2. Whole-Rock Analytical Methods

A.3.2.1. Sample Preparation

All the samples were crushed according to the following procedure:

APPENDIX 3 (Cont'd.)

1) Each sample was broken into chips using a small sledge hammer on a thick plywood board. A slab was saved for sectioning.

2) A clean, representative sample of chips was crushed to 1-2 cm. or smaller pieces in a steel jaw crusher.

3) A representative sample of these pieces was crushed in a tungsten-carbide Seibtechnik swing mill for three to four minutes producing a rock powder of -100 mesh, as determined by random sieving checks.

4) The powder was put into 4 oz. jars and dried overnight in an oven at 110°C.

A.3.2.2. Major and Trace Element Analysis

Seven major and eight trace elements were determined by X-ray fluorescence analysis of discs pressed from the rock powder using a Phillips 1220-C computerised spectrometer. Approximately 1/3 of the samples were analysed by a method modified from that of Rose *et al.* (1962). The sample discs were prepared in the following manner:

1) 1.5 g of rock powder was thoroughly mixed with two to three drops of N-30-88 Mowiol binding agent until the colour was uniform.

2) Using a boric acid backing, this powder was pressed into a disc for one minute at 15 tons per square inch.

The major elements determined using fused powders were prepared by the following method:

APPENDIX 3 (Cont'd.)

1) 0.7500 g of rock powder + 0.7500 g of La_2O_3 + 6.00 g of $Li_2B_4O_7$ were carefully weighed out, mixed together, and put in a graphite crucible.

2) A dozen crucibles at a time were put in a muffle furnace pre-heated to 1,000°C and left to fuse for 30-35 minutes.

3) After fusion the resulting glass beads were allowed to cool for 1 minute and put in clean glass jars.

4) The weight of each bead was readjusted to exactly 7.5000 g with dried $Li_2B_4O_7$, compensating for weight lost during fusion and thus giving an exact dilution.

5) Each bead plus the $Li_2B_4O_7$ was placed in a tungsten-carbide ball mill vial, cracked with a steel cylinder, and then crushed in the ball mill to -100 mesh.

6) The powder was then put in bottles and dried overnight at 110°C.

7) The sample discs were then prepared as outlined above.

K_2O, Na_2O, and MnO were analysed using a Perkin Elmer 303 Atomic Absorption Spectrometer using a method similar to Langmhyr and Paus (1968). The solutions were prepared by the following method:

1) 0.2000 g of powder was mixed with 5 ml of concentrated HF and heated on a steam bath for 20 minutes until completely dissolved.

2) Each sample was diluted with 50 ml of saturated boric acid and made up to 200 ml with distilled water.

APPENDIX 3 (Cont'd.)

3) Analyses were done by comparison with international rock standards.

A.3.2.3. Loss on Ignition

Loss on ignition was calculated by measuring a known amount of powder into a porcelain crucible, heating at 1050°C for two hours, weighing again and expressing the difference in percent. It is assumed that the loss on ignition represents predominantly H_2O+, H_2O-, and CO_2.

A.3.2.4. Precision and Accuracy

The precision and accuracy of major and trace element analyses are shown in table 19 and 20.

TABLE 19

(a) Precision of Major Element Analyses

Element	FUSED SAMPLE (CD-371)				UNFUSED SAMPLE (LD-75)			
	Range (%)	Mean	S.Dev.	No. Stds.	Range (%)	Mean	S.Dev.	No. Stds.
SiO_2	10.70	76.58	1.94	41	6.90	76.21	1.91	13
TiO_2	0.10	0.17	0.03	41	0.02	0.03	0.01	13
Al_2O_3	1.40	12.28	0.36	41	1.37	14.13	0.35	13
Fe_2O_3	0.34	1.15	0.08	41	0.57	1.45	0.20	13
MgO	5.80	0.30	0.94	41	1.66	0.91	0.45	13
CaO	0.76	0.87	0.10	41	0.24	1.11	0.08	13
P_2O_5	0.01	0.005	0.002	41	0.10	0.04	0.09	13

(b) Precision of Trace Element Analyses

(from 9 independent discs of LD-75).

Element	Range	Mean	S. Dev.
Zr	33	68	10
Sr	21	138	9
Rb	8	106	3
Zn	9	37	3
Cu	16	4	6
Ba	197	755	74

TABLE 20

(a) Accuracy of Major Element Analysis as Determined by Fit of Standards to Calibration Curve

Element	FUSED SAMPLES			UNFUSED SAMPLES		
	Range (%)	S.Dev.	No.Stds.	Range (%)	S.Dev.	No.Stds.
SiO_2	38.50	0.67	21	23.30	1.63	10
TiO_2	4.59	0.03	23	1.08	0.06	9
Al_2O_3	23.35	0.37	23	4.20	0.67	11
Fe_2O_3	27.83	0.16	20	7.50	0.20	9
MgO	49.70	0.89	18	3.33	0.27	7
CaO	13.63	0.10	21	7.70	0.55	8
P_2O_5	1.90	0.09	18	-	-	-

(b) Accuracy of Major Element Analysis as Determined by Comparison of 24 samples Analysed by X-ray Fluorescence and Atomic Absorption

Element	Range (%)	S. Dev.
SiO_2	7.74	0.99
TiO_2	0.71	0.02
Al_2O_3	7.40	0.30
Fe_2O_3	5.06	0.10
MgO	0.34	0.05
CaO	0.55	0.05
P_2O_5	0.23	0.04

TABLE 20 (Cont'd.)

(c) Accuracy of Trace Element Analysis by Fit of Standards to Calibration Curve

Element	Range (p.p.m.)	S. Dev.	No. Stds.
Zr	490	13	16
Sr	784	18	19
Rb	245	6	23
Zn	161	12	24
Cu	108	5	23
Ba	1,803	33	18

APPENDIX 4

Theoretical Predictions of Trace Element Behaviour

(after Taylor, 1965)

		Rb^+	K^+
Rubidium	Ionic radii	1.47	1.33

Rb^+ exhibits a well-marked overall coherence with K^+. Electronegativities and ionization potentials of both elements are very similar, and the only significant difference is one of size. This difference usually becomes effective during large-scale igneous processes of fractionation with the result that Rb^+ is concentrated relative to K^+ in rasidual liquids, though it does not form a separate phase. Rb^+ commonly enters the K^+ positions in feldspars and K-micas. The K/Rb ratio provides a guide to the degree of differentiation of successive silicate melts.

		Sr^{2+}	Ca^{2+}
Strontium	Ionic radii	1.18	0.99

Sr^{2+} is intermediate in size between Ca^{2+} and K^+ but prefers eight- or ten-fold coordination with oxygen. Sr^{2+} may be expected to enter Ca^{2+} positions in plagioclase, apatite, and sphene. The Ca^{2+} positions in pyroxenes are too small and the K^+ positions in micas too large. Ca/Sr ratios may be expected to increase during fractionation.

APPENDIX 4 (Cont'd.)

		Ba^{2+}
Barium	Ionic radius	1.34

Ba^{2+} substitutes only for K^+ among the common cations. It is nearly identical in size to K^+ but the Ba-O bond is slightly more covalent. Ba^{2+} enters K-feldspars more readily than biotite (Nockolds and Mitchell, 1948). Although Ba^{2+} competes with Sr^{2+} for feldspar lattice sites, fractionation trends for pegmatitic feldspars indicate that Ba/Sr ratios decrease during differentiation (Heier and Taylor, 1959b).

		Zr^{4+}	Ti^{4+}
Zirconium	Ionic radii	0.79	0.68

Zr^{4+} is known to concentrate in the liquid phase during fractionation and commonly forms a separate phase (zircon) in salic differentiates. It may be expected to substitute for Ti^{4+} in early crystallising fractions, and may accompany that element in substituting for Fe^{3+}.

		Cu^{2+}	Cu^{+}	Fe^{2+}	Na^{+}
Copper	Ionic radii	0.72	0.96	0.75	0.97

Among the major elements Cu^{2+} is similar in size to Fe^{2+}, and Cu^{+} close to Na^{+}. The Cu-O bond is more covalent than either Na-O or Fe-O bonds and implies that both Cu/Na and Cu/Fe ratios will decrease during fractionation. Copper may be expected in most of the common rock-forming minerals; and where concentration is high may form a separate sulphide phase.

APPENDIX 4 (Cont'd.)

		Zn^{2+}
Zinc	Ionic radius	0.74

Present knowledge of the geochemical behaviour of Zn^{2+} in silicate melts is incomplete. Zn^{2+} is very nearly the same size as Fe^{2+} and the Zn-O bond is more covalent than the Fe-O bond. It may be expected to enter late Fe^{2+} positions and result in an increase in the Zn/Fe ratio. Neumann (1949) noted that Zn^{2+} commonly occurred in four-fold coordination instead of its geometrically predicted six-fold coordination.

		Cr^{3+}	Fe^{3+}
Chromium	Ionic radii	0.63	0.64

Cr^{3+} is almost identical in size to Fe^{3+} but forms a more ionic bond with oxygen, leading to its preferential entry into Fe^{3+} lattice sites and consequent depletion at an early stage of differentiating basaltic magmas. It is commonly concentrated in pyroxene and magnetite relative to olivine and ilmenite. The Ni/Cr ratio is not a good index of fractionation since it varies appreciably with the mode and may exhibit a wide range of variation in accumulate rocks.

		Ni^{2+}	Mg^{2+}
Nickel	Ionic radii	0.69	0.66

Ni^{2+} is intermediate in size between Mg^{2+} and Fe^{2+} and appears to enter early Fe^{2+} rather than Mg^{2+} positions. In basaltic rocks, Ni^{2+} (and Co^{2+}) is strongly partitioned into olivine.

Plate 1. Dark green collapsed pumice-lapilli defining a nearly vertical foliation, Weavers Hill ash-flow sequence (map ref. 3460,5915).

Plate 2. James Cove, Colliers Bay, viewed from the west. Note porphyrite sill (foreground) and barren ridge formed by unit 40 (middle distance).

Plate 3. Strike ridges of Finn Hill sequence ignimbrites, 0.25 mile (0.4km) northeast of Finn Hill, viewed from the northwest. Weavers Hill in the background.

Plate 4. Xenolith of feldsparphyric basalt in eutaxitic welded tuff, unit 59, Finn Hill.

Plate 5. Eutaxitic fiamme in unit 59 at Finn Hill. Note frayed extremities of fiamme and included crystals.

Plate 6. Ryans Head and Burkes Cove looking east toward Campbell Hill and Enchanted Pond. Steep cliffs formed by laharic breccias; the point to the north is formed by unit 59.

Plate 7. Eutaxitic fiamme, unit 59, Burkes Cove.

Plate 8. Slump structure in welding at the base of a xenolithic layer in the central part of unit 59, Burkes Cove.

Plate 9. Eastern rhyolite sill (white) intruded by porphyrite (dark grey) and cut by numerous high-angle faults.

Plate 10. Large porphyrite intrusion (barren ground) near Kitchuses, viewed from the east. Note contact between porphyrite (grey cliffs) and volcanogenic sandstones (dark brown cliffs) in foreground.

Plate 11. Xenolith of quartz-monzonite in porphyrite at James Cove. Note dark brown rim due to subaerial weathering of this cobble prior to inclusion.

Plate 12. Autobrecciated porphyrite at Old Schoolhouse Point (map ref. 3460,6040). Epidotised angular blocks set in an unaltered igneous matrix.

Plate 13. Brecciated porphyrite intruding reddish siltstones near Old Schoolhouse Point (map ref. 3470,6040). Contorted laminae in siltstone are barely visible.

Plate 14. Mudball horizon intercalated with thinly bedded argillaceous siltstones, north of Ryans Head (map ref. 3365,5965).

Plate 15. Poorly consolidated cobble conglomerate overlying channeled sandstone and dipping steeply to the west (right). Viewed from the north (map ref. 3555,6235).

Plate 16. Fine-grained volcanic breccias, sandstones, and siltstones of the Harbour Main Group dipping steeply west near Ryans Head (map ref. 3380,5980).

Plate 17. Folded Conception siltstones 0.5mile (0.8km) north of Bacon Cove, Gasters Bay.

Plate 18. Angular unconformity between steeply dipping Conception siltstones and flat-lying Cambrian limestone at Bacon Cove (map ref. 3660,6120). Note the uneven nature of the Precambrian regolith.

Plate 19. Gently plunging synform in thinly-bedded sandstones and siltstones of the Harbour Main Group, Colliers Bay (map ref. 3560,6280).

Plate 20. Tight syncline in fault slice of Conception siltstones emplaced within coarse-grained clastic rocks of the Harbour Main Group. Note sheared southern limb (left).

Plate 21. Loose block of red- and green-altered tuff, north-northwest slopes of Campbell Hill. Note sharp contact at centre-right and more diffuse boundary to the left.

Plate 22. Green altered volcanic breccias containing unaltered clasts of rhyolite (white). Campbell Hill in the background littered with erratics (viewed looking northwest).

Photomicrograph 1. Granophyre xenolith enclosed in base of unit 3. Crossed nicols; field of view approx. 6.1mm across. Specimen H25.

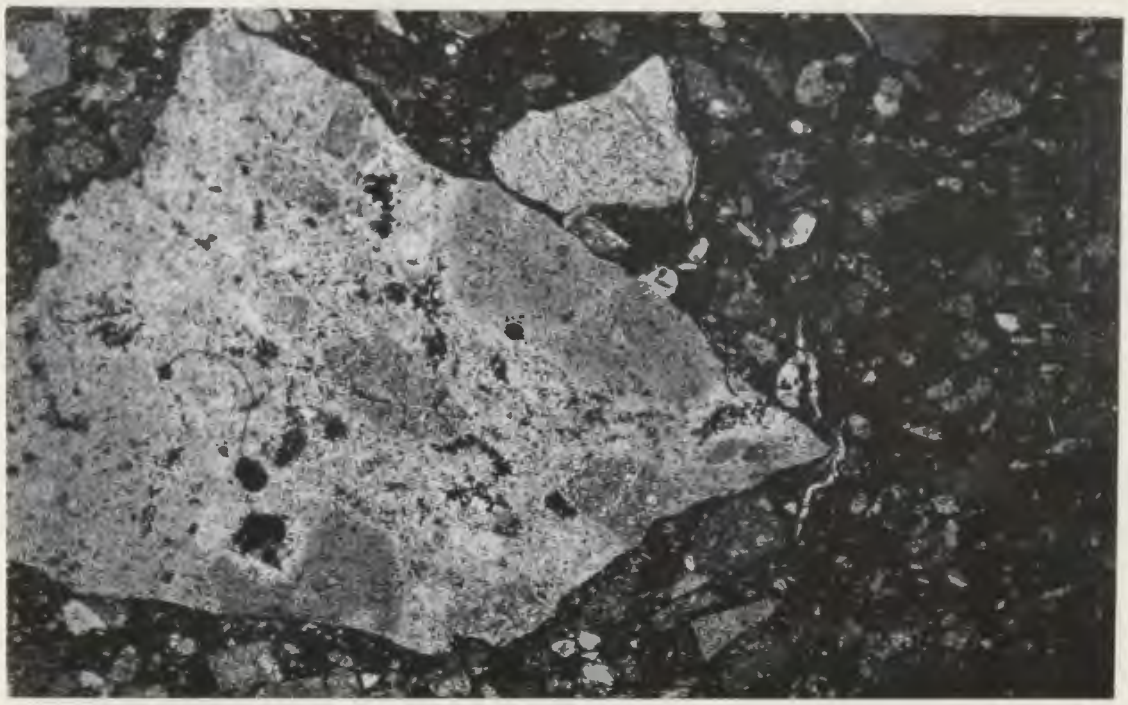

Photomicrograph 2. Pink to pale green mottled fragment of recrystallised tuff in volcanic breccia. Dark areas are hematitic; pale grey areas have been leached of hematite. Plane-polarized light; field of view approx. 4.8mm across. Specimen C117; map ref. 3255,5775.

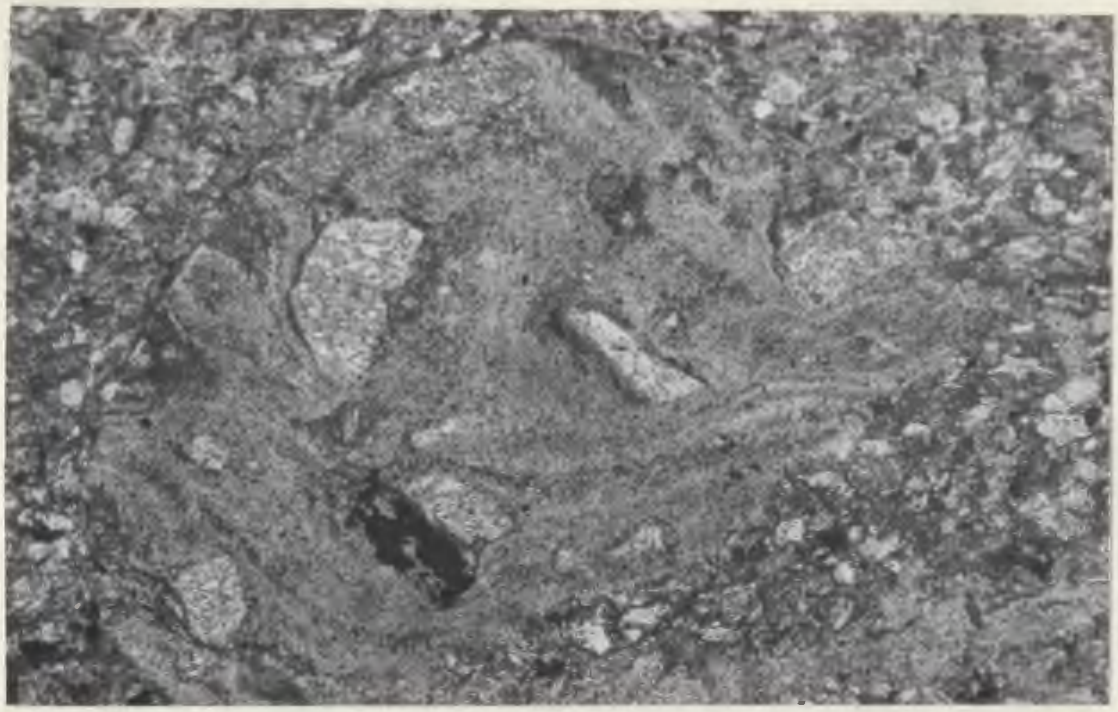

Photomicrograph 3. Fragment of flow-banded rhyolite in Conception greywacke. Note oxidised biotite phenocryst (largely black), and mottled phenocrysts of albite (white) partly replaced by potassium feldspar (grey). Crossed nicols; field of view approx. 12mm across. Specimen C1; map ref. 3635,5895.

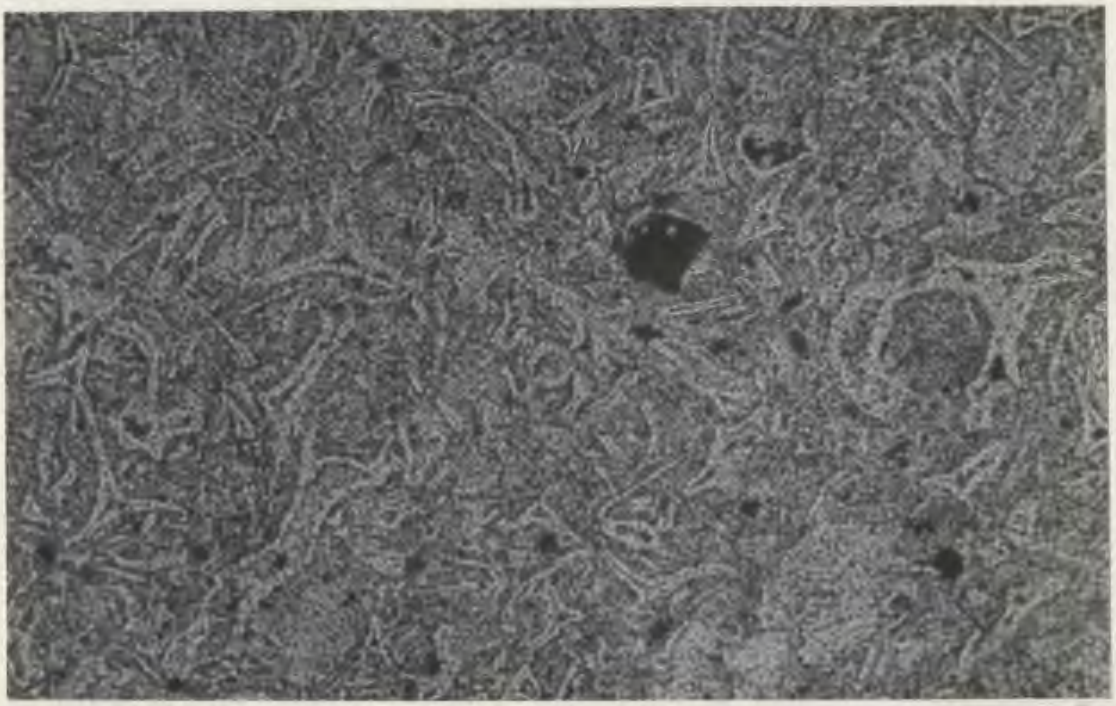

Photomicrograph 4. Tricuspate, cuspate, and rod-like shards exhibiting open vitroclastic texture and replaced by alkali feldspar, quartz, and sericite. Plane-polarized light; field of view approx. 12mm across. Specimen H8; top of unit 11.

Photomicrograph 5. Altered, densely welded crystal-vitric tuff enclosing devitrified platy shards, possibly of accidental origin. Plane-polarized light; field of view approx. 7.5mm across. Specimen H93; 18ft (5.5m) above base of unit 11.

Photomicrograph 6. Densely welded vitric tuff. Cuspate and rod-like shard boundaries are transgressed by finely fibrous alkalic feldspar dusted with hematite. Plane-polarized light; field of view approx. 2.6mm across. Specimen NX6; middle of unit 4; analyses 37a and 37b.

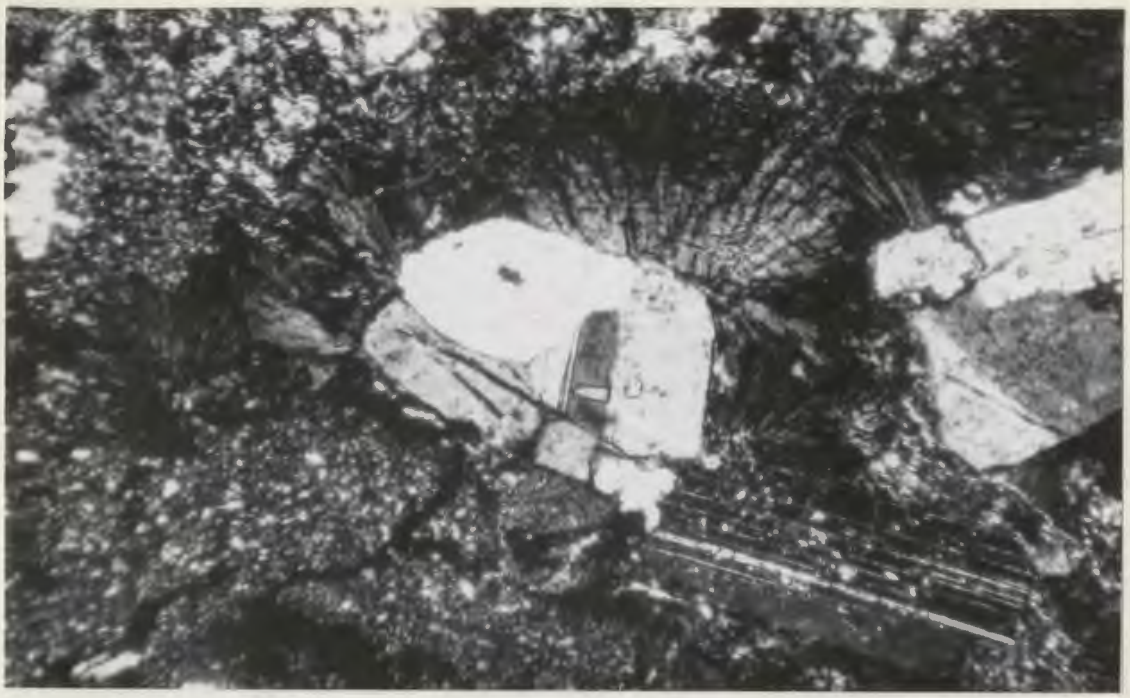

Photomicrograph 7. Microspherulitic alkalic feldspar in the matrix of a sillar, nucleated preferentially along crystal boundaries. Note fine lamellar twinning in albite phenocrysts. Crossed nicols; field of view approx. 6.1mm across. Middle of unit 6; analyses GC38 and NX1.

Photomicrograph 8. Euhedral paramorph of alpha-quartz after beta-quartz in ignimbrite. Note faint cleavage oriented roughly north-south. Crossed nicols; field of view approx. 6.1mm across. Specimen H93; 18ft (5.5m) above base of unit 11.

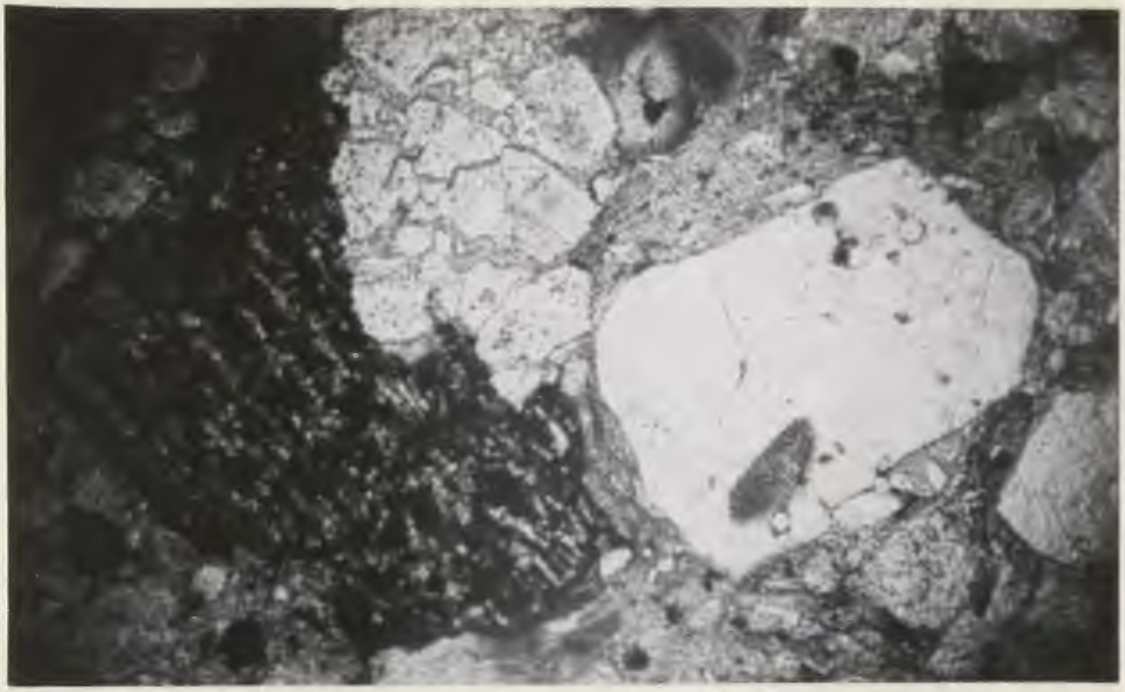

Photomicrograph 9. Partially resorbed quartz and oxidised biotite phenocrysts in sillar. Plane-polarized light; field of view approx. 7.5mm across. Base of unit 6; analyses GC38 and NX1.

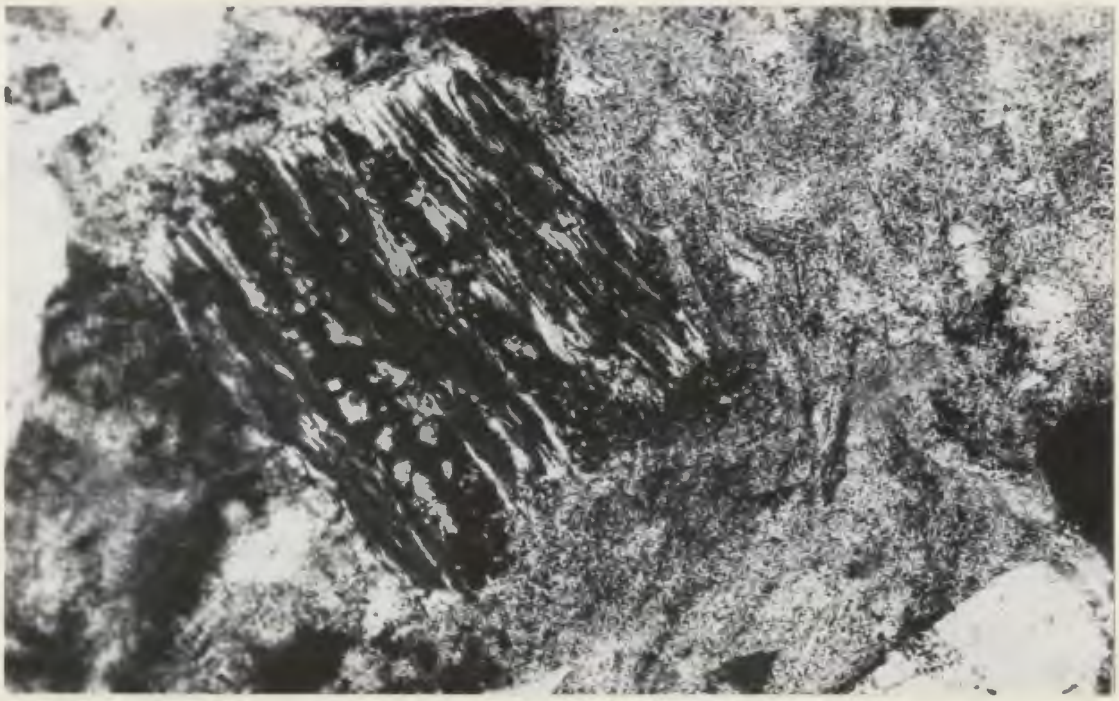

Photomicrograph 10. Biotite phenocryst altered to magnetite (black), leucoxene (dark grey), alkalic feldspar (irregular intergrowths with magnetite toward right of crystal), and muscovite (white linear areas oriented northwest-southeast). Plane-polarized light; field of view is approx. 3mm across. Specimen H60; vitric tuff in north; map ref. 3585,6180.

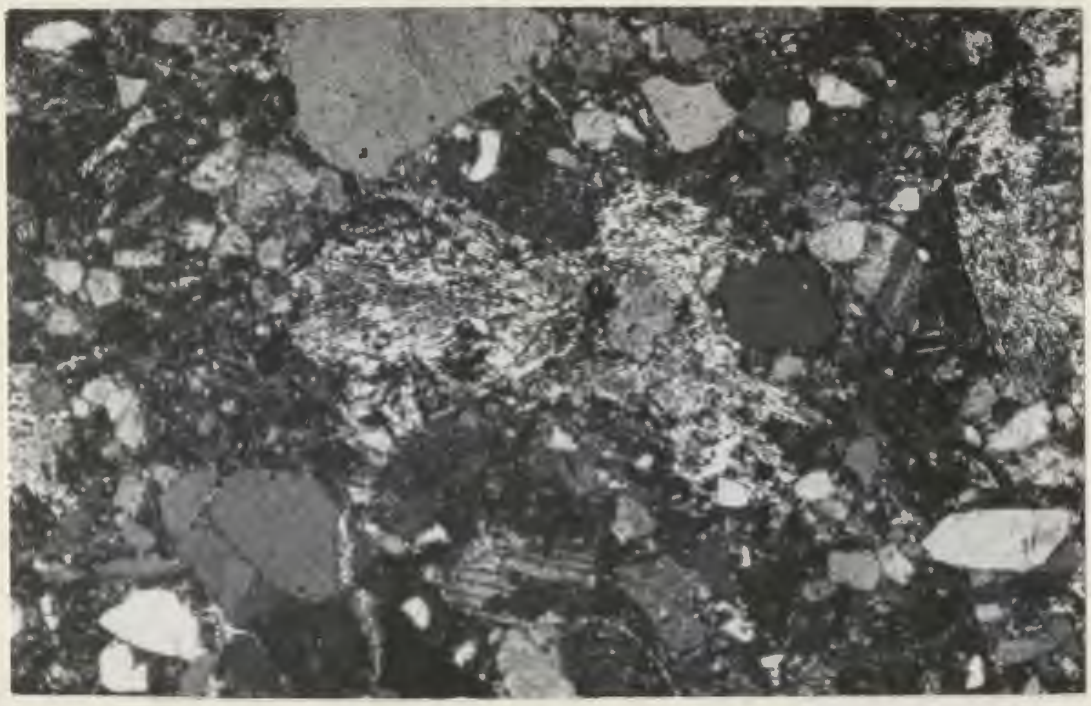

Photomicrograph 11. Deformed biotite phenocrysts altered to magnetite (black), leucoxene (dark grey), alkalic feldspar (light grey), and muscovite (white). Crossed nicols; field of view approx. 6.1mm across. Specimen H30; base of unit 3; analyses 39a and 39b.

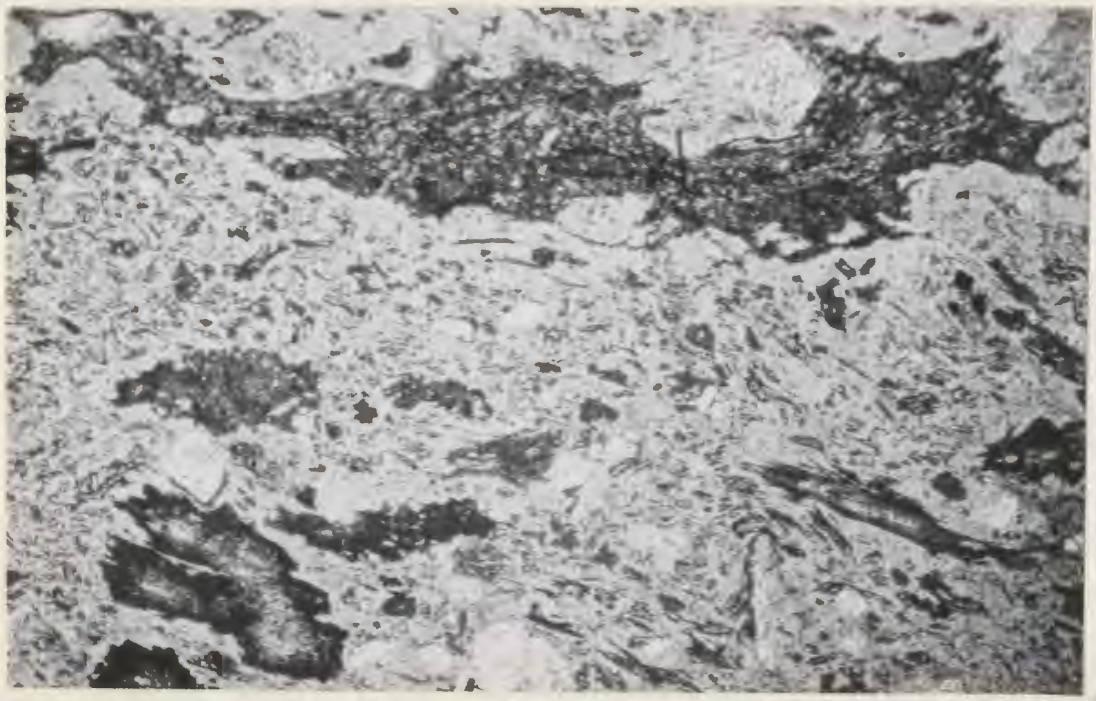

Photomicrograph 12. Ragged, comminuted pumice coated with hematite and set in a bleached vitroclastic matrix. Note the marked orientation with little evidence of welding. Plane-polarized light; field of view approx. 30mm across. Specimen H170; near base of unit 38.

Photomicrograph 13. Delicate cuspate, platy, and rod-like shards set in a finely comminuted, hematitic matrix. Plane-polarized light; field of view approx. 7.5mm across. Specimen H126; top of unit 20.

Photomicrograph 14. Eutaxitic pumice-lapilli exhibiting delicately frayed extremities and recrystallisation to alkalic feldspar and quartz. Bleached vitroclastic matrix. Plane-polarized light; field of view approx. 30mm across. Specimen H168; upper-middle part of unit 36.

Photomicrograph 15. Same specimen as photomicrograph 14. Plane-polarized light; field of view approx. 7.5mm across.

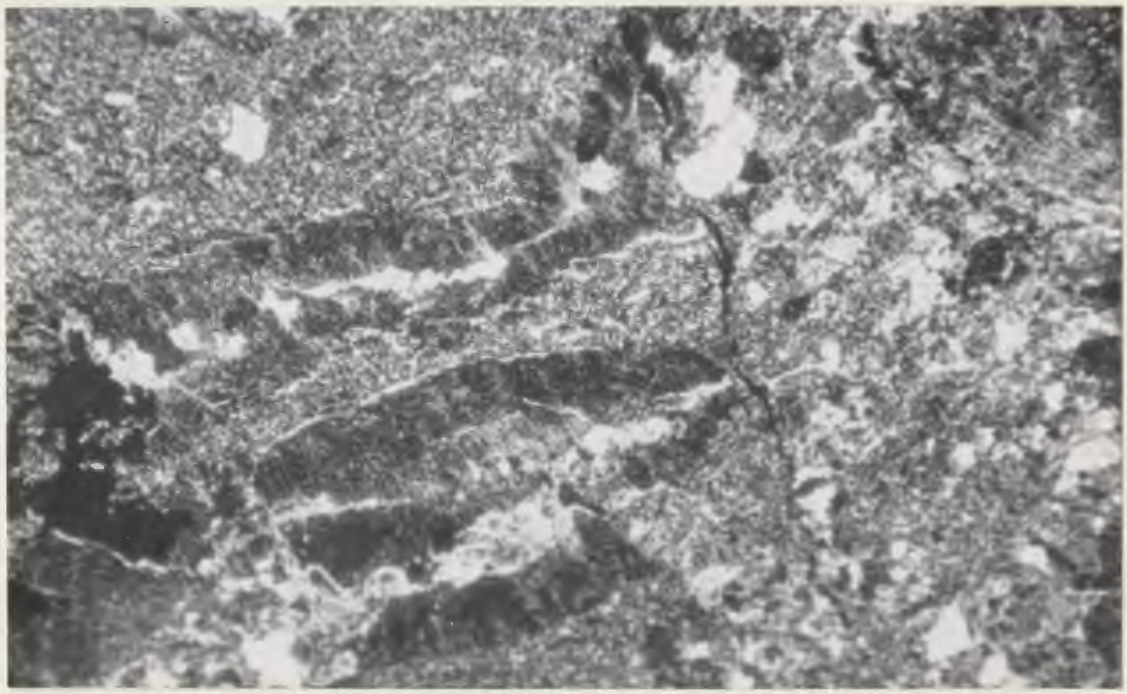

Photomicrograph 16. Collapsed pumice-lapilli exhibiting fibres of quartz and alkalic feldspar in axiolitic intergrowth. Crossed nicols; field of view approx. 12mm across. Specimen H170; unit 29; analysis CWT.

Photomicrograph 17. Pumice fragment exhibiting concentric layers of chiefly alkalic feldspar with fine axiolitic structure coated with opaque dust and partly replaced by sericite. Minute crystals of albite have served as a site for nucleation and growth. Plane-polarized light; field of view approx. 12mm across. Base of unit 38.

Photomicrograph 18. Non-welded vitroclastic texture in basal zone of unit 26. Note serial size of shards and pumice, and drawn out pumice-lapillus (left-centre). Plane-polarized light; field of view approx. 30mm across. Analysis GC24.

Photomicrograph 19. Dense welding in central part of dark brown fiamme-bearing ignimbrite. Plane-polarized light; field of view approx. 12mm across. Specimen C87; unit 58; analysis P70-9.

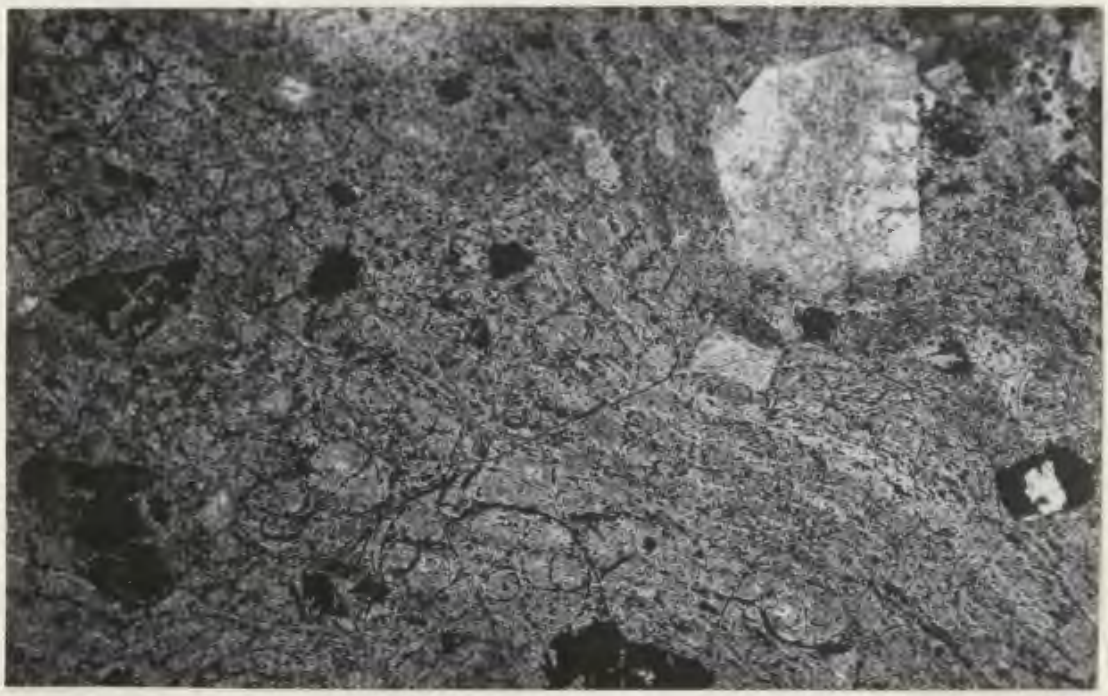

Photomicrograph 20. Perlite cracks in devitrified densely welded ignimbrite. Plane-polarized light; field of view approx. 12mm across. Specimen C85; unit 58.

Photomicrograph 21. Same specimen as photomicrograph 20. Perlite cracks developed preferentially in fiamme, emphasising their glassy origin. Plane-polarized light; field of view approx. 12mm across.

Photomicrograph 22. Same specimen as photomicrograph 20. Welding wraps around lithophysal cavities infilled with quartz (white), bladed crystals of yellow pleochroic epidote (dark grey with high relief), and minor chlorite (pale grey with lower relief). Note clinopyroxene microphenocryst (lower left). Light-coloured area at upper left is an irregular vein of albite. Plane-polarized light; field of view approx. 7.5mm across.

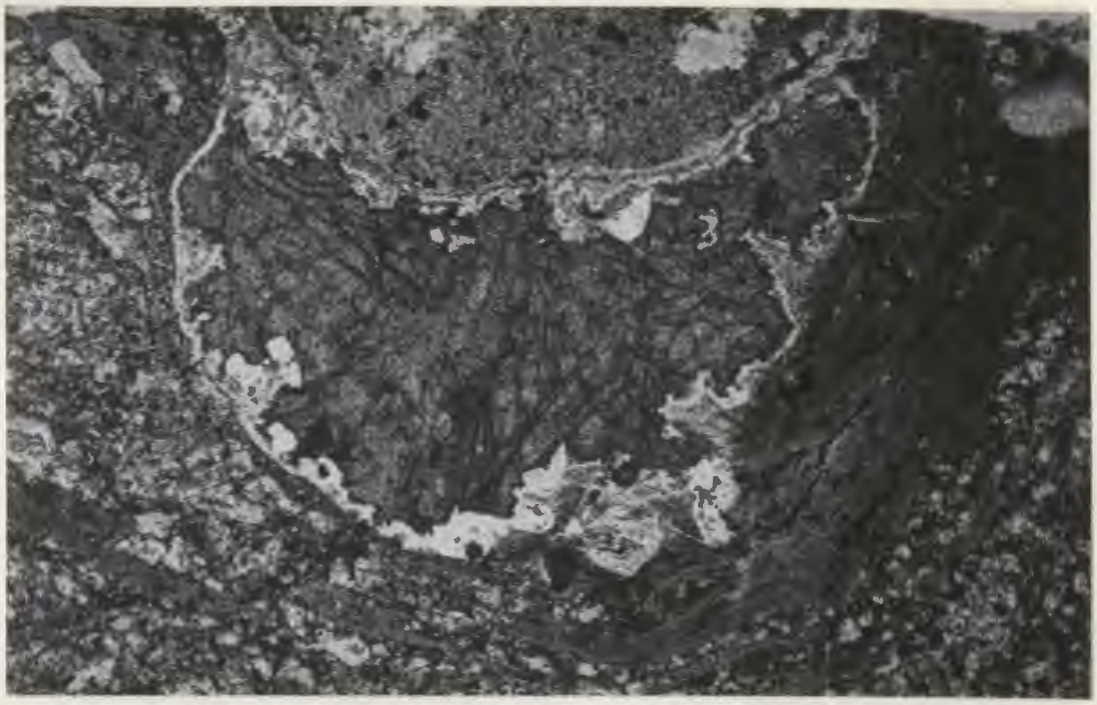

Photomicrograph 23. Same specimen as photomicrograph 20. Crystallisation products impinging on a rock fragment (top centre). Note curving habit of shard foliation and bladed habit of epidote. Crossed nicols; field of view approx. 12mm across.

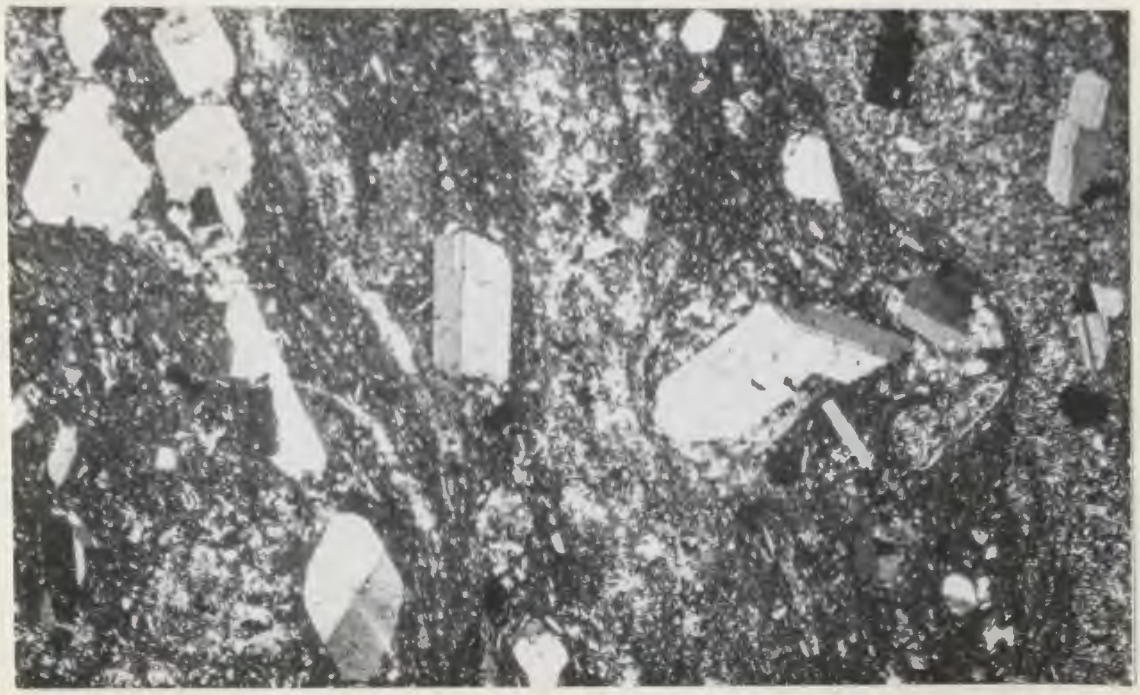

Photomicrograph 24. Intensely recrystallised fiamme-bearing ignimbrite. Shard outlines are not discernible and fiamme (coarsely devitrified to albitic feldspar) locally simulate flow lines. Note Carlsbad twinning in clear albite phenocrysts. Crossed nicols; field of view approx. 30mm across. Lower flow unit of cooling unit 59; analysis GTN34.

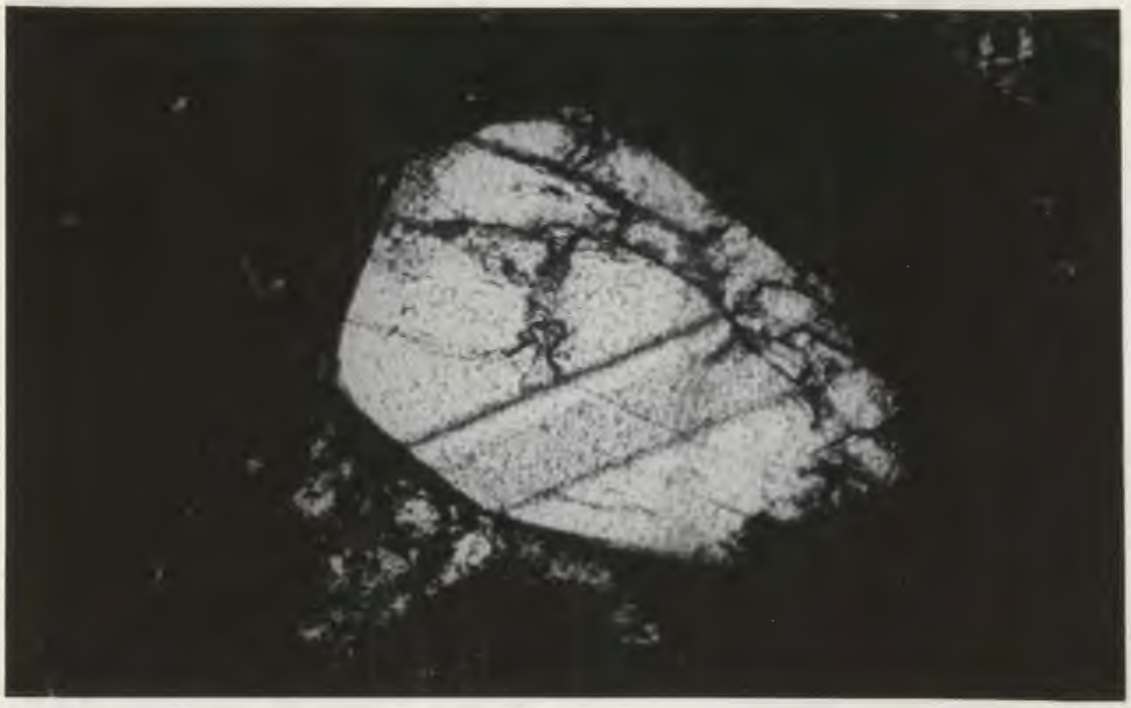

Photomicrograph 25. Lamellar twinning in clinopyroxene microphenocryst. Crossed nicols; field of view approx. 3mm across. Specimen C87; unit 58.

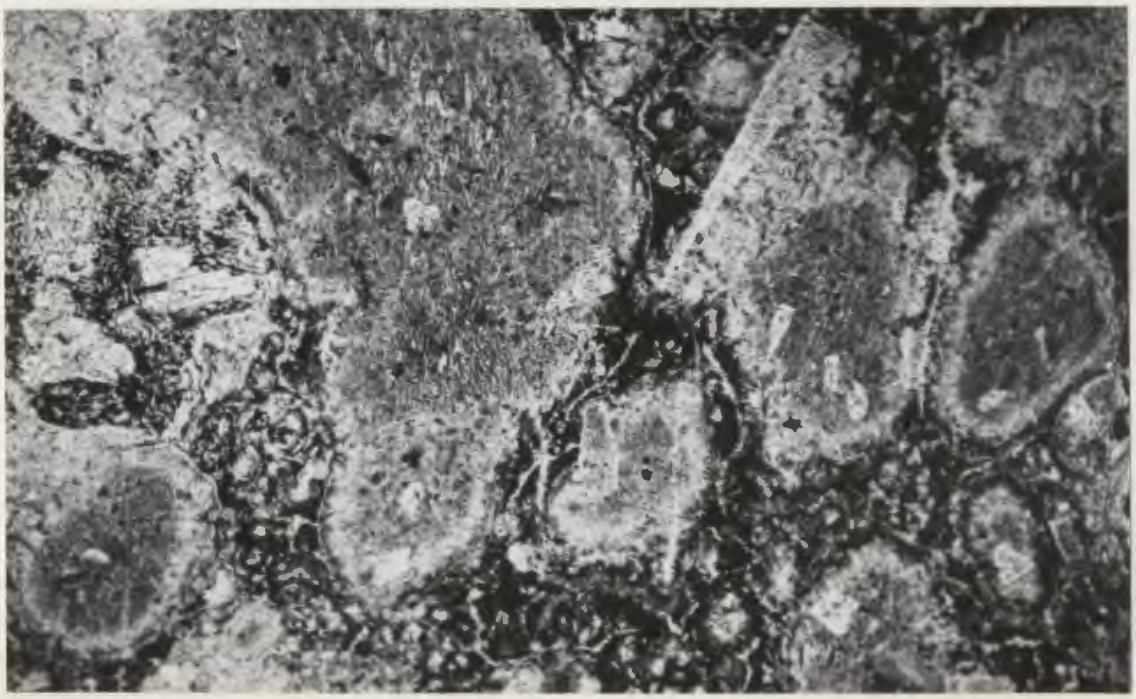

Photomicrograph 26. Irregular recrystallisation destroying densely welded textures in ignimbrite. The grey areas preserving the shard foliation are dark red to pink due to hematite dust. Plane-polarized light; field of view approx. 30mm across. Specimen C75; base of unit 55.

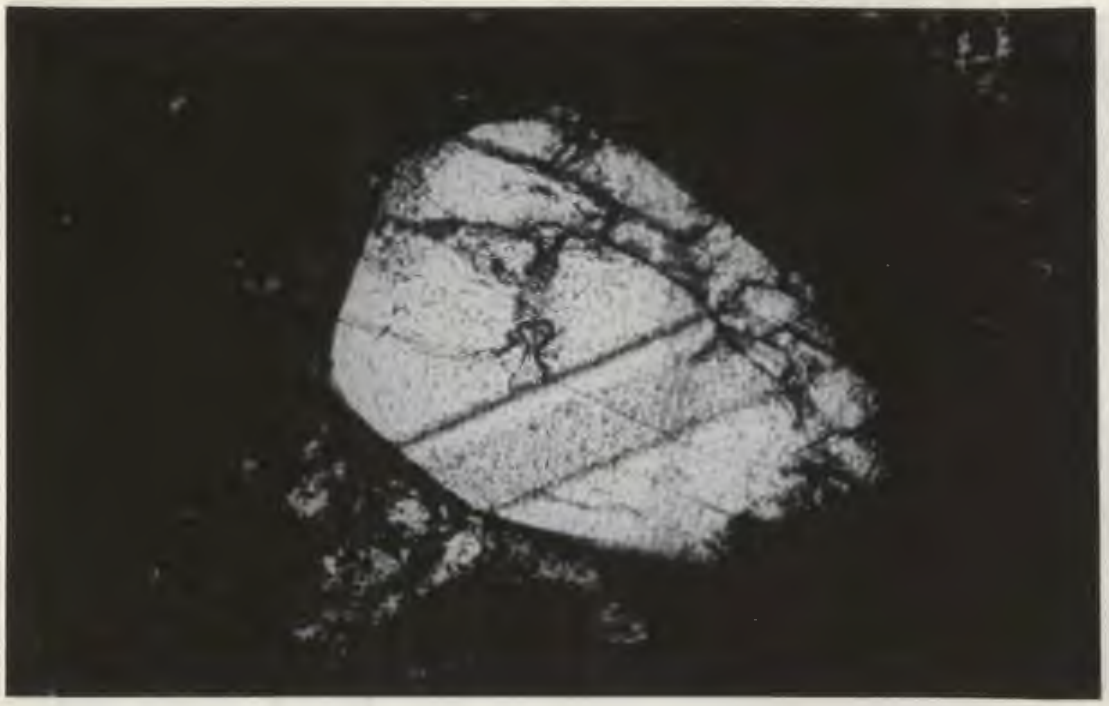

Photomicrograph 25. Lamellar twinning in clinopyroxene microphenocryst. Crossed nicols; field of view approx. 3mm across. Specimen C87; unit 58.

Photomicrograph 26. Irregular recrystallisation destroying densely welded textures in ignimbrite. The grey areas preserving the shard foliation are dark red to pink due to hematite dust. Plane-polarized light; field of view approx. 30mm across. Specimen C75; base of unit 55.

Photomicrograph 29. Same specimen as photomicrograph 27. Thin curvilinear "canals" of minor alkalic feldspar in a quartz base grade outwards into an axiolitic zone rich in iron ore, which in turn is surrounded by a zone practically devoid of opaque material. Plane-polarized light; field of view approx. 12mm across.

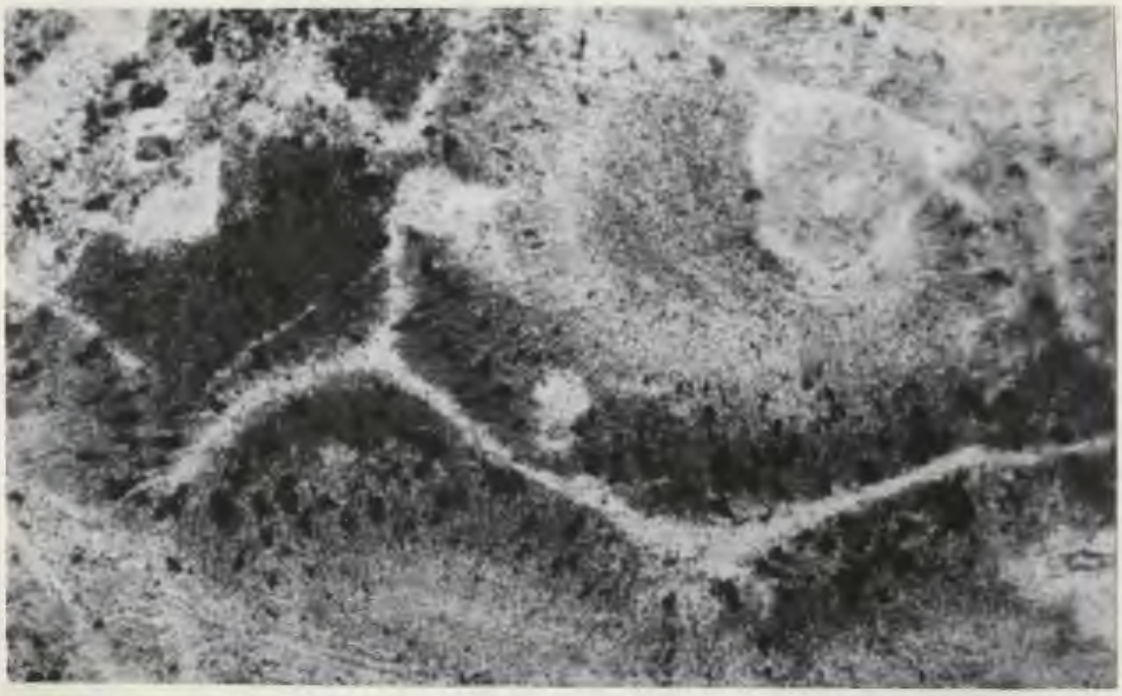

Photomicrograph 30. Same specimen as photomicrograph 27. Microspherulitic quartz (white with low relief), alkali feldspar (grey with higher birefringence), granular magnetite and relict shards (lower left). Plane-polarized light; field of view approx. 3mm across.

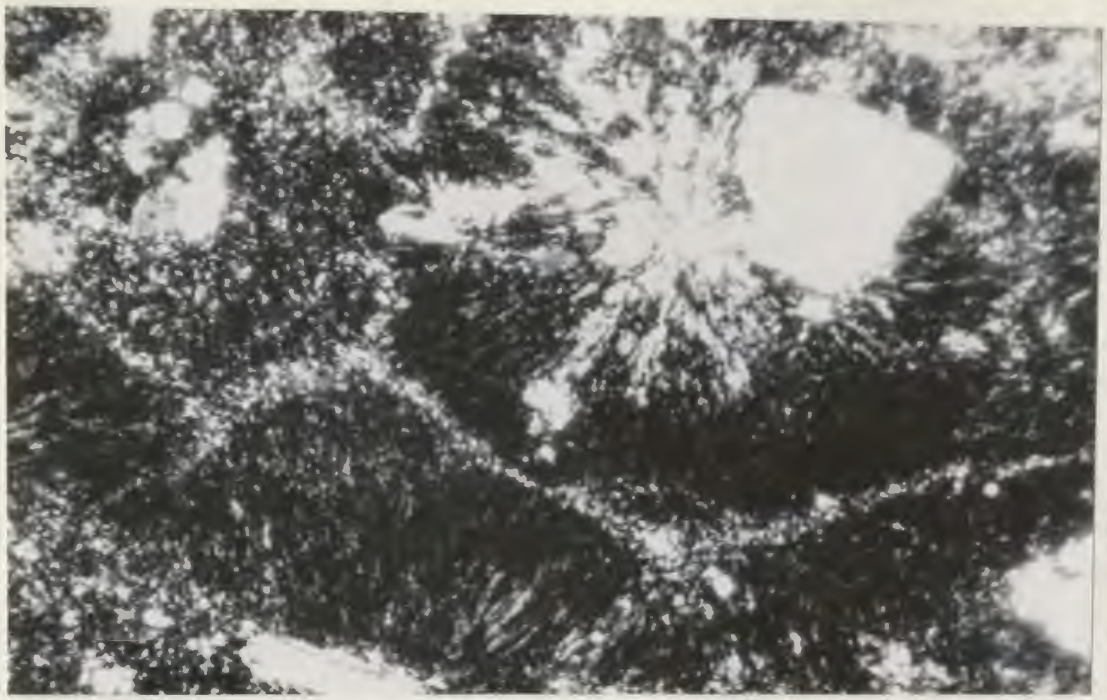

Photomicrograph 31. Same specimen as photomicrograph 27. Crossed nicols. Note micropoikilitic quartz (white) concentrated near centre of spherulite.

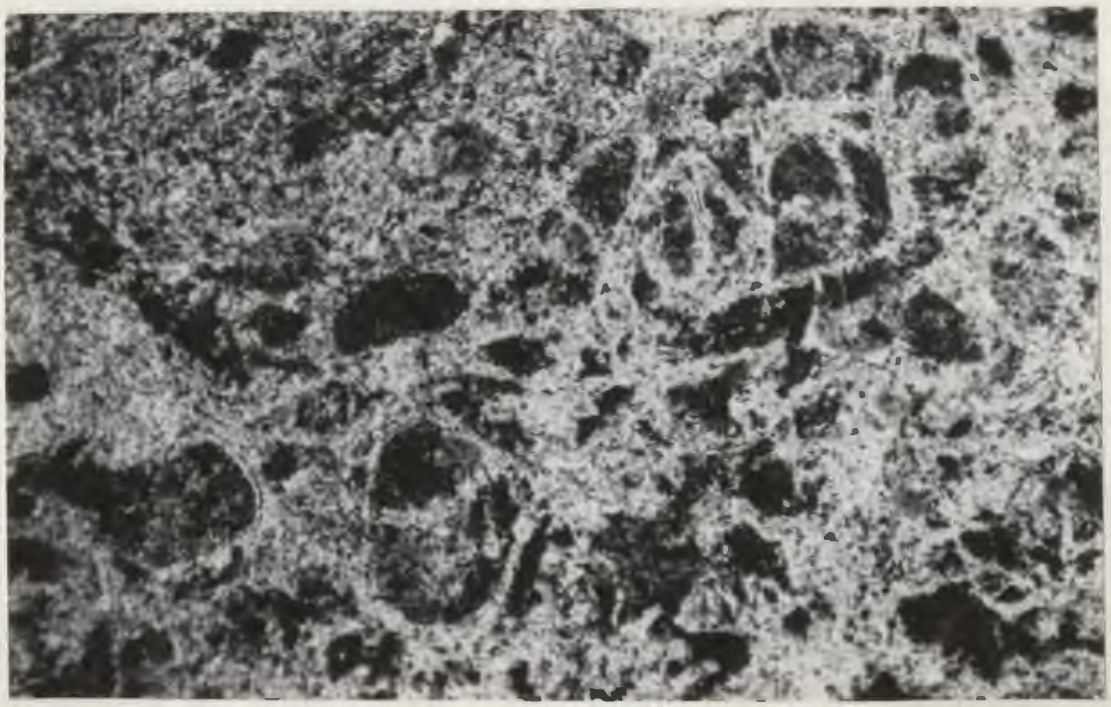

Photomicrograph 32. Well-developed perlitic cracks in recrystallised welded tuff. Sites of bleached areas are localised along the cracks. Plane-polarized light; field of view approx. 4.8mm across. Specimen C91; base of unit 59.

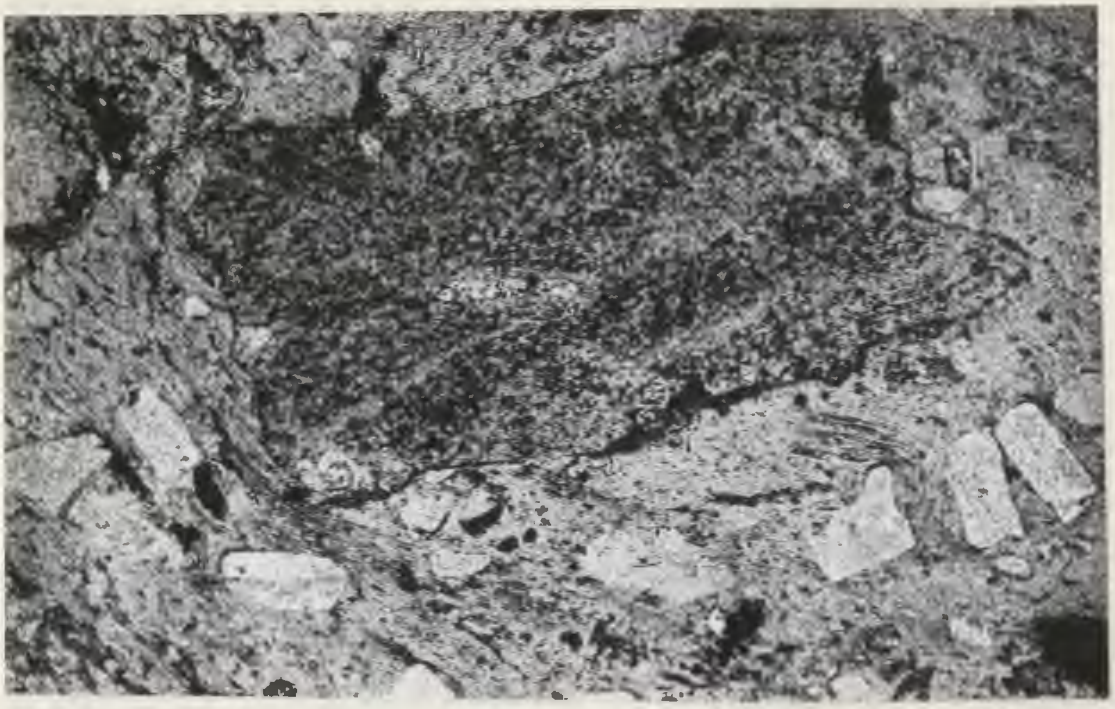

Photomicrograph 33. Incipient development of microspherulitic alkali feldspar and granophyric quartz in devitrified tuff fragment. Plane-polarized light; field of view approx. 30mm across. Specimen H183; top of unit 41.

Photomicrograph 34. Same specimen as photomicrograph 33. Typical development of "bird's-eye" devitrification textures in welded tuff. Note bleached areas with discernible shards (far right and lower left). Plane-polarized light; field of view approx. 30mm across.

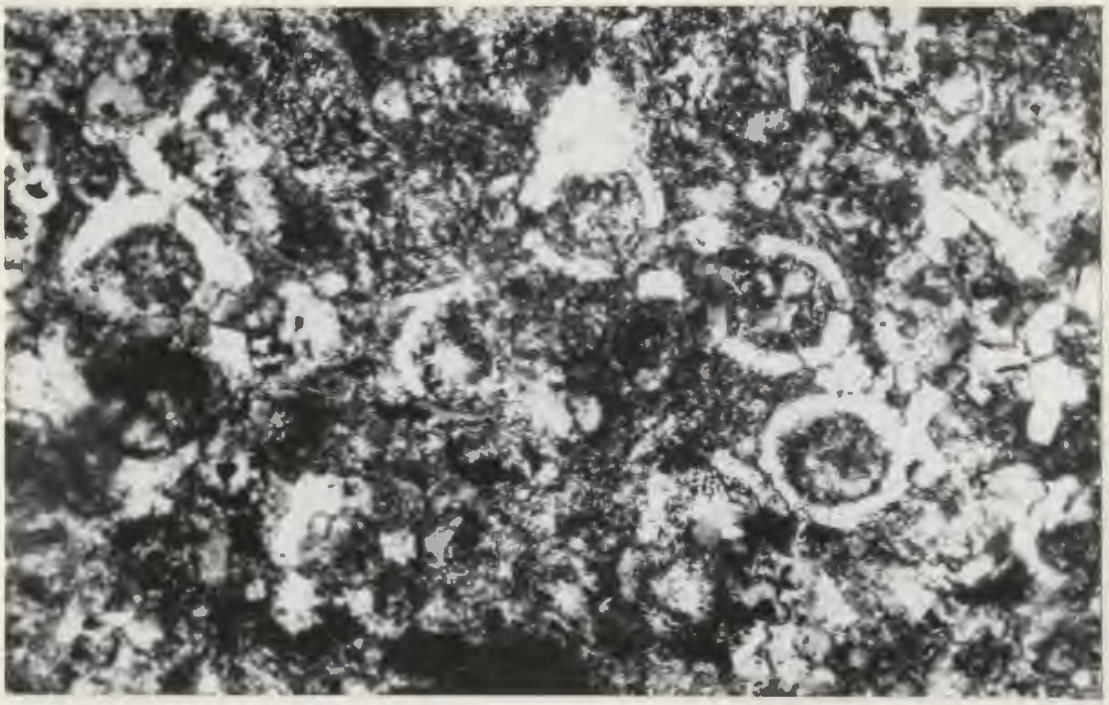

Photomicrograph 35. Same specimen as photomicrograph 33. "Bird's-eye" devitrification involving granophyric quartz (clear white rims) and microspherulitic alkali feldspar with chloritic material and iron-oxide. Crossed nicols; field of view approx. 2.3mm across.

Photomicrograph 36. Fairly sharp contact between microspherulitic devitrification textures (quartz, alkalic feldspar, opaques) and bleached cryptocrystalline zone in which shard outlines are barely visible. Plane-polarized light; field of view approx. 18.8mm across. Collected 6ft (1.8m) below top of unit 43; analysis GC49.

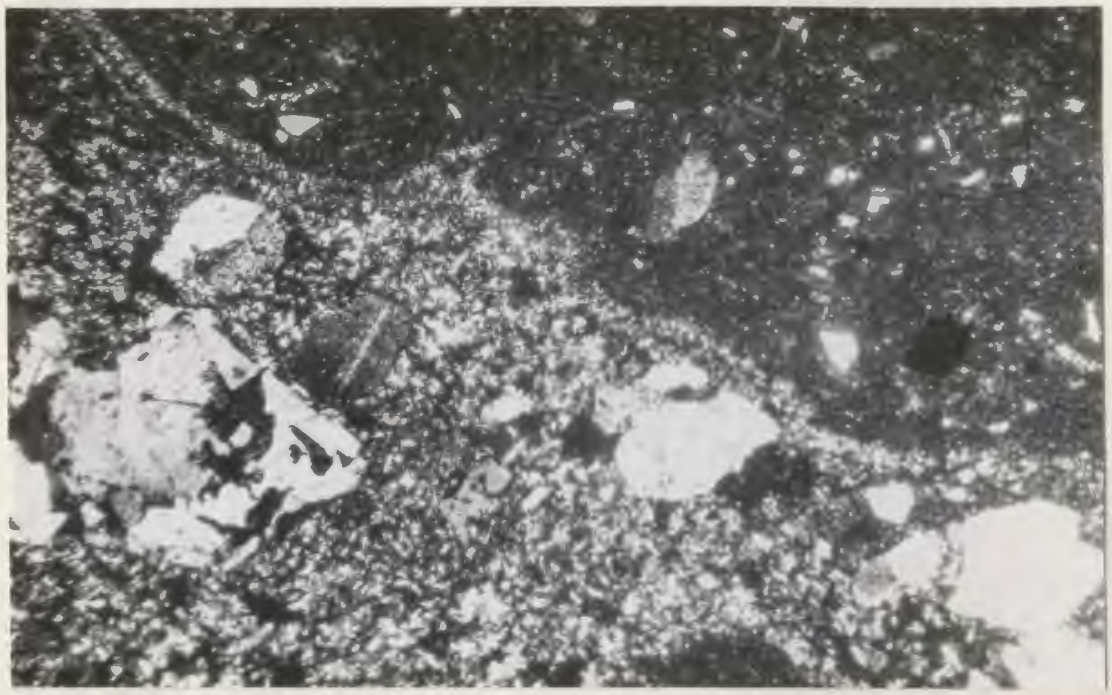

Photomicrograph 37. Same specimen as photomicrograph 36. Crossed nicols.

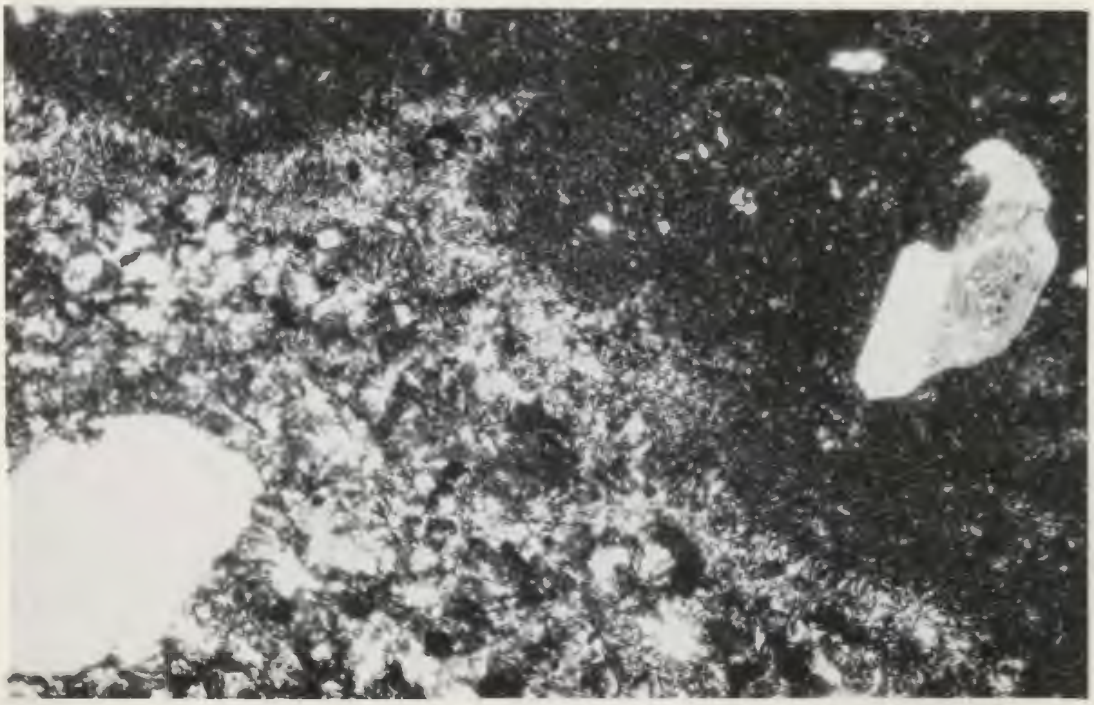

Photomicrograph 38. Same specimen as photomicrograph 36. Crossed nicols; field of view approx. 7.5mm across. Note the finely crystalline zone separating coarse and cryptocrystalline devitrification products.

Photomicrograph 39. Amphibole microphenocrysts in dacite oriented subparallel to the flow banding. Plane-polarized light; field of view approx. 7.5mm across. Analysis GC12; map ref. 3460,6040.

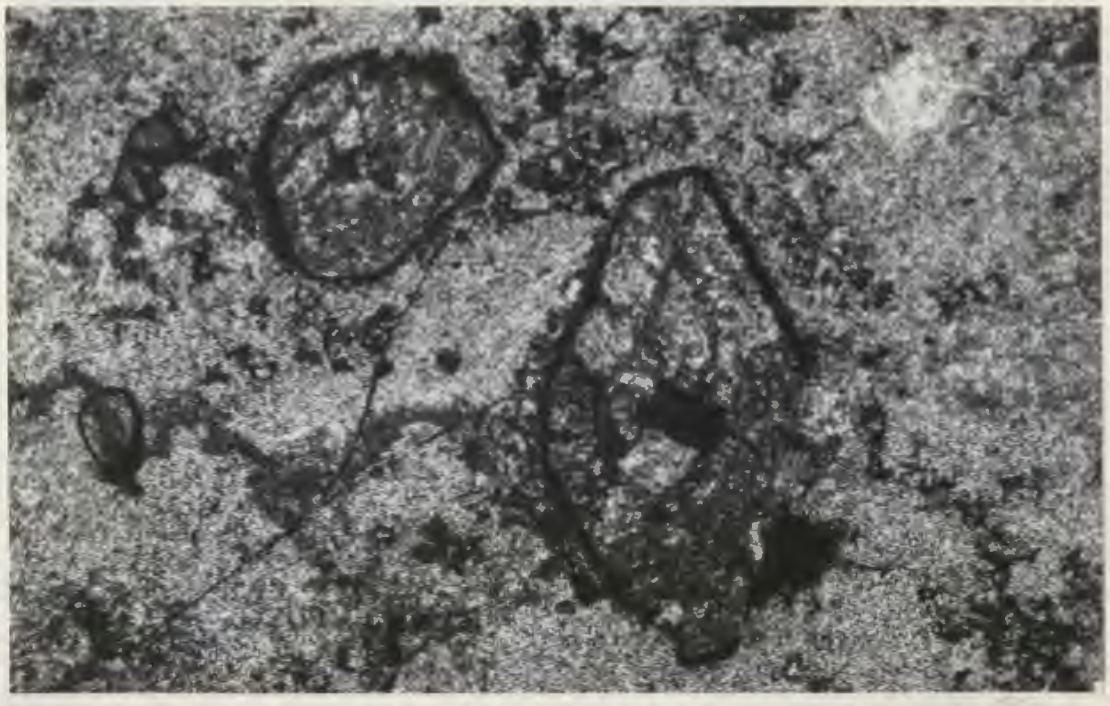

Photomicrograph 40. Subhedral amphiboles in dacite replaced by alkalic feldspar, chlorite, and clay minerals. Note amphibole cross-sections and relict cleavage. Plane-polarized light; field of view approx. 3.8mm across. Analysis GC12.

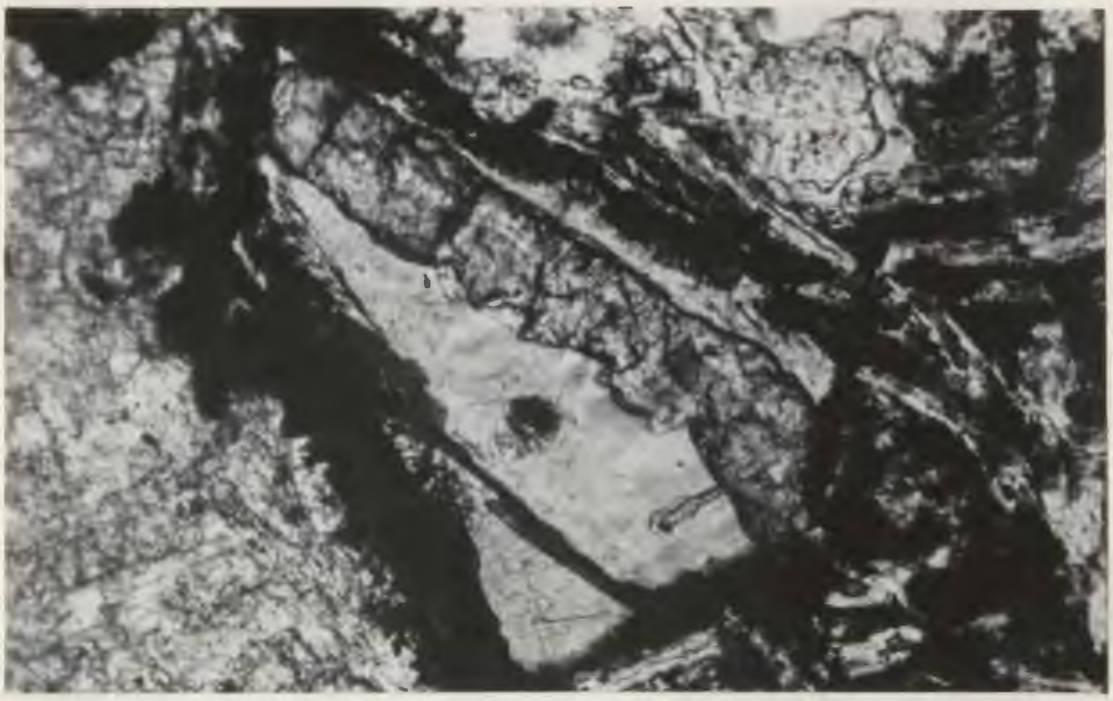

Photomicrograph 41. Groundmass olivine in mafic lava flow exhibiting a core of fresh olivine (high relief) partly replaced by yellow pleochroic serpentine (pale grey) rimmed by iron-oxide (black). Plane-polarized light; field of view approx. 1.5mm across. Analysis NX12; cf. fig. 4.

Photomicrograph 42. Olivine phenocrysts and microphenocrysts in mafic lava flow replaced by iron-oxide (black), iddingsite (grey) and a thin rim of serpentine (white). Plane-polarized light; field of view approx. 3mm across. Analysis NX14; cf. fig. 4.

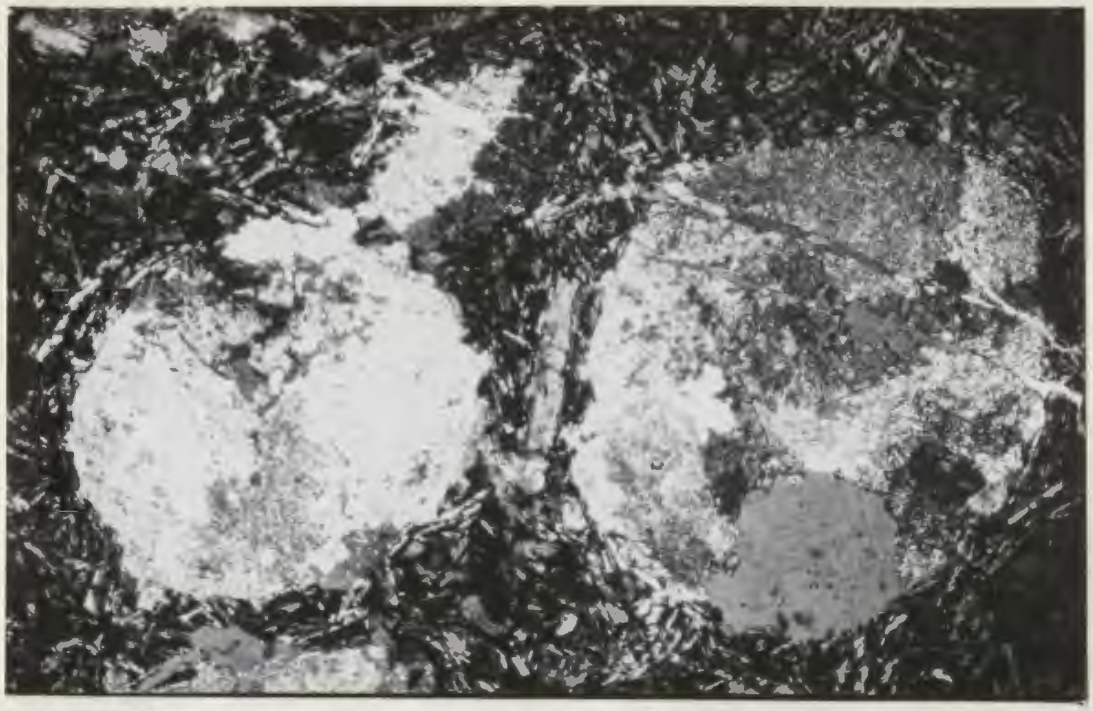

Photomicrograph 43. Amygdaloidal top of mafic lava flow. Amygdales infilled with prehnite (grey to white) and minor albite. Crossed nicols; field of view approx. 30mm across. Analysis NX12 (flow interior); cf. fig. 4.

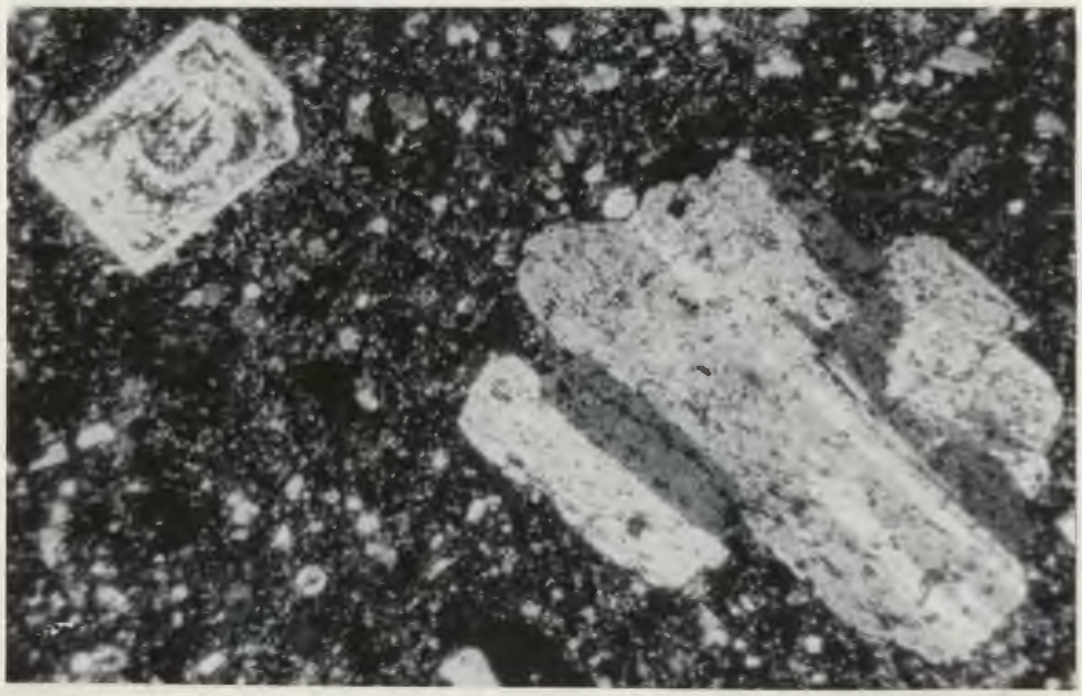

Photomicrograph 44. Subhedral phenocrysts of albite enclosing tiny inclusions of chlorite (original glass) and exhibiting zonal replacement by epidote (upper left) which possibly represent areas of calcium enrichment in a former compositionally zoned phenocryst. Crossed nicols; field of view approx. 11.9mm across. Specimen GC10; Old Schoolhouse Point.

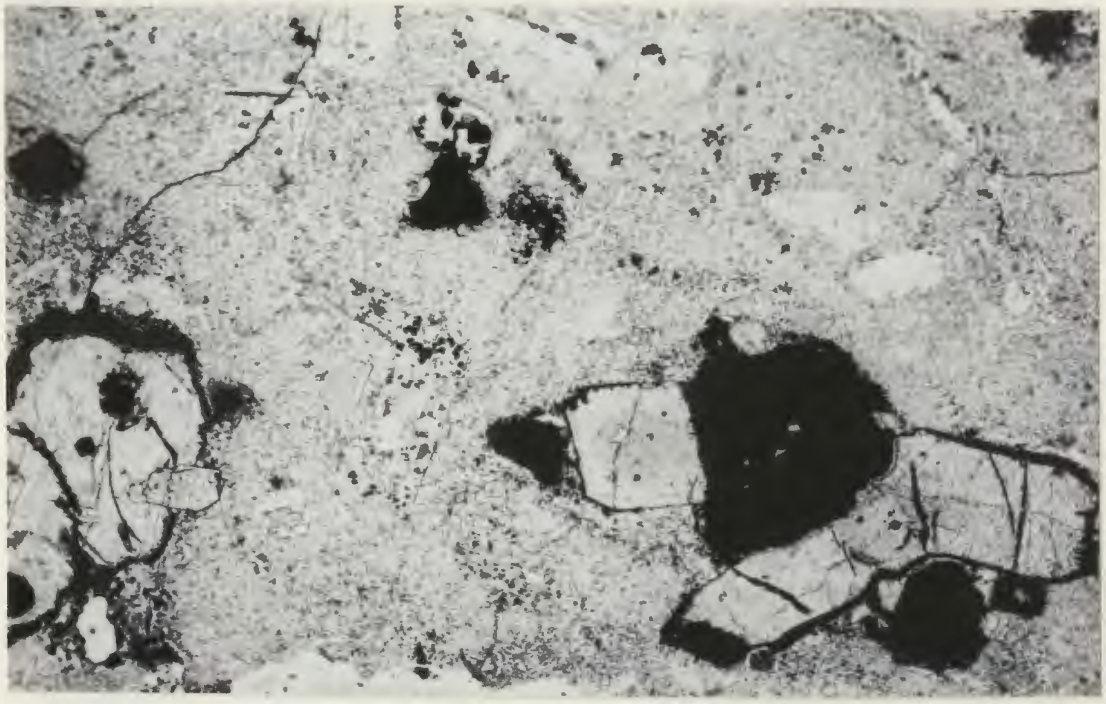

Photomicrograph 45. Glomeroporphyritic intergrowth of chlorite (pale grey) pseudomorphous after pyroxene, magnetite (black), and subhedral apatite (pale grey; mottled high relief). Plane-polarized light; field of view approx. 12mm across. Specimen GC51; 3350,5870.

Photomicrograph 46. Feldsparphyric dyke with hyalophitic texture. Slightly turbid albite laths exhibit fretted margins, and interstitial glass has been completely replaced by chlorite, and minor calcite and epidote. Plane-polarized light; field of view approx. 6.1mm across. Specimen H215; map ref. 3380,5980.

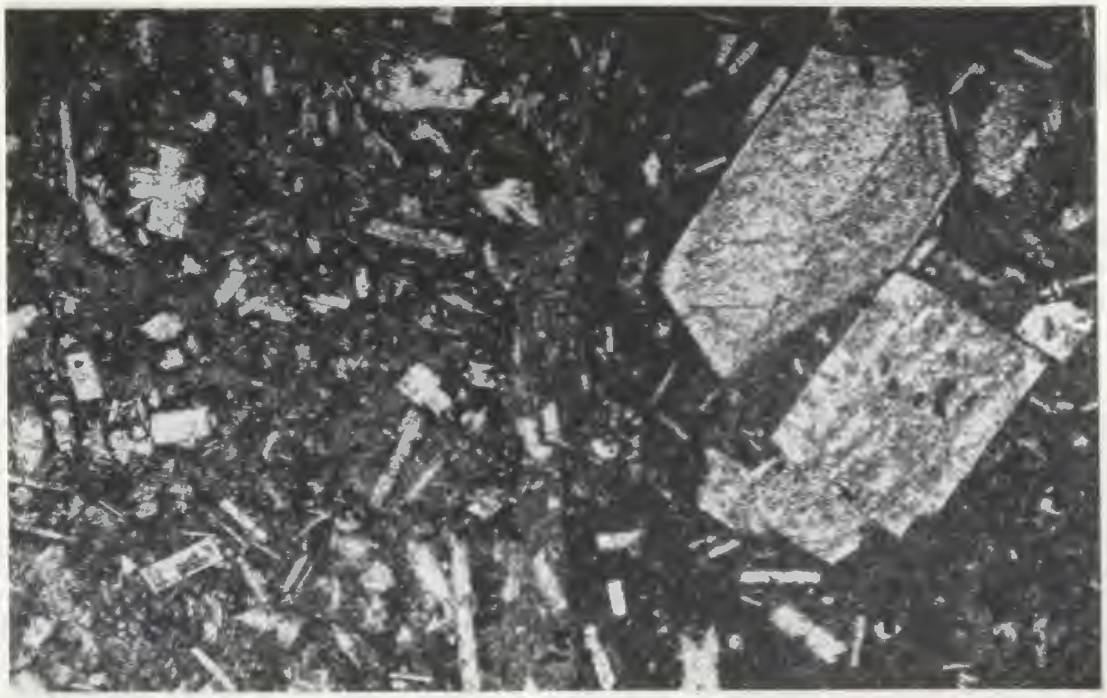

Photomicrograph 47. Sharp contact between successive intrusive phases of a multiple dyke. Note marginal chill and thin clear rim surrounding turbid cores of albite phenocrysts. Plane-polarized light; field of view approx. 12mm across. Analysis H165; map ref. 3490,5965.

Photomicrograph 48. Olivine diabase containing subhedral olivine phenocrysts (upper right and lower left) replaced by iron-oxide (black), iddingsite (grey), and colourless to pale green serpentine (white) set in a groundmass of clinopyroxene (greyish white with high relief) and clouded albite. The clear white recrystallised areas with low relief are albite. Plane-polarized light; field of view approx. 12mm across. Analysis NX17; cf. fig. 4.

Photomicrograph 49. Green biotite phenocryst in sericitised and bleached welded tuff. Plane-polarized light; field of view approx. 6.1mm across. Specimen H82; map ref. 3410,5735.

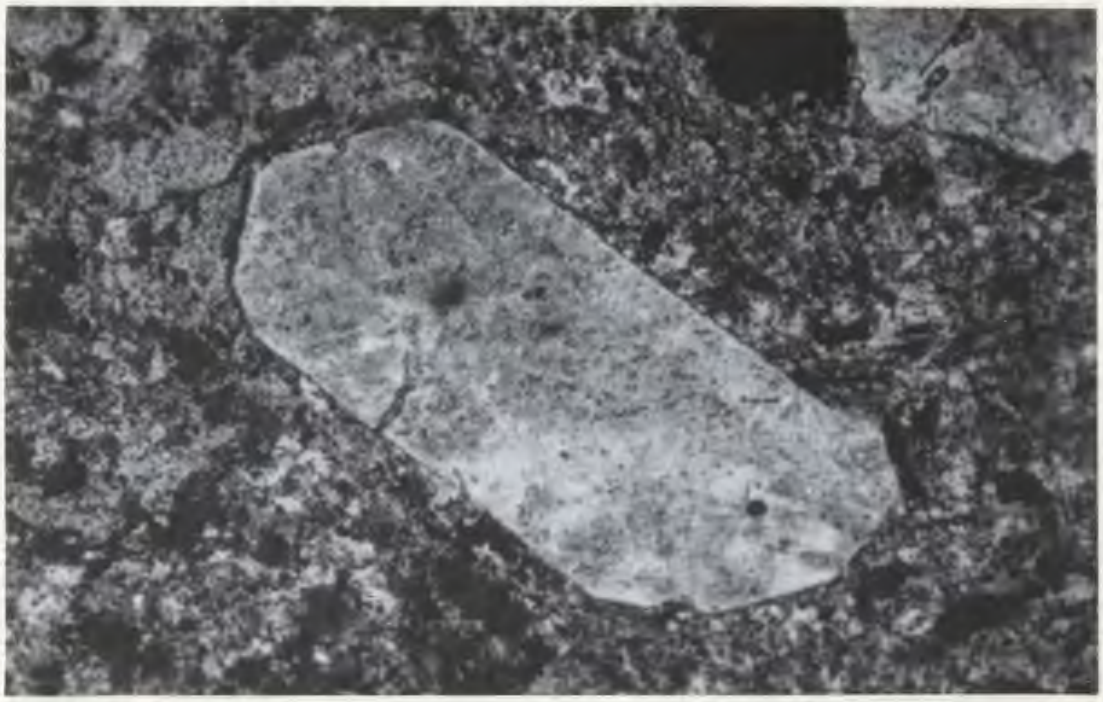

Photomicrograph 50. Albite phenocryst dusted with hematite showing alteration to sericite and clay minerals. Note clear areas in the core and thin clear rim. Plane-polarized light; field of view approx. 4.8mm across. Specimen C100; top of unit 58.

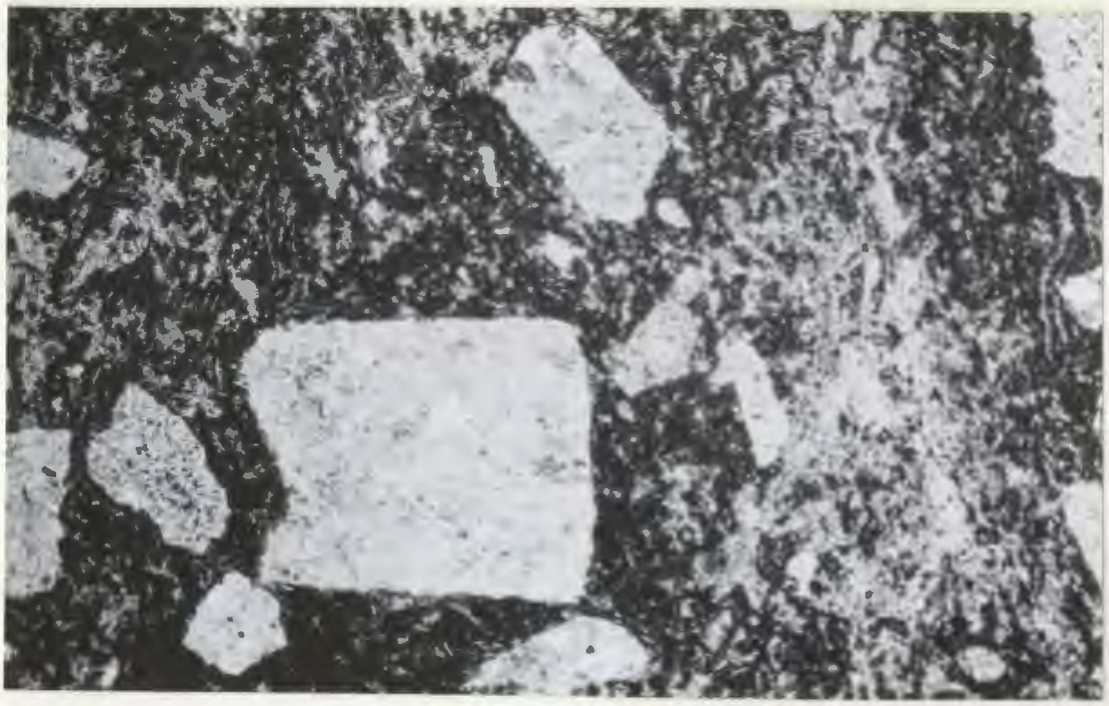

Photomicrograph 51. Epidotised shards in welded tuff. Rod-like shards replaced by epidote (dark to pale grey) curving around turbid albite phenocrysts. Plane-polarized light; field of view approx. 6.1mm across. Specimen H198; top of unit 60.

Photomicrograph 52. Intense recrystallisation of dacite to a fine-grained assemblage of "mossy" epidote (pale to dark grey), quartz, and albite (both white). Note relict feldspar phenocryst (right-centre). Plane-polarized light; field of view approx. 6.1mm across. Specimen H162; map ref. 3460,6040.

Photomicrograph 53. Incipient welding in sericitised crystal-lithic tuff. Anhedral phenocrysts are albite. Plane-polarized light; field of view approx. 6.1mm across. Specimen H173; top of unit 40; analysis GC43.

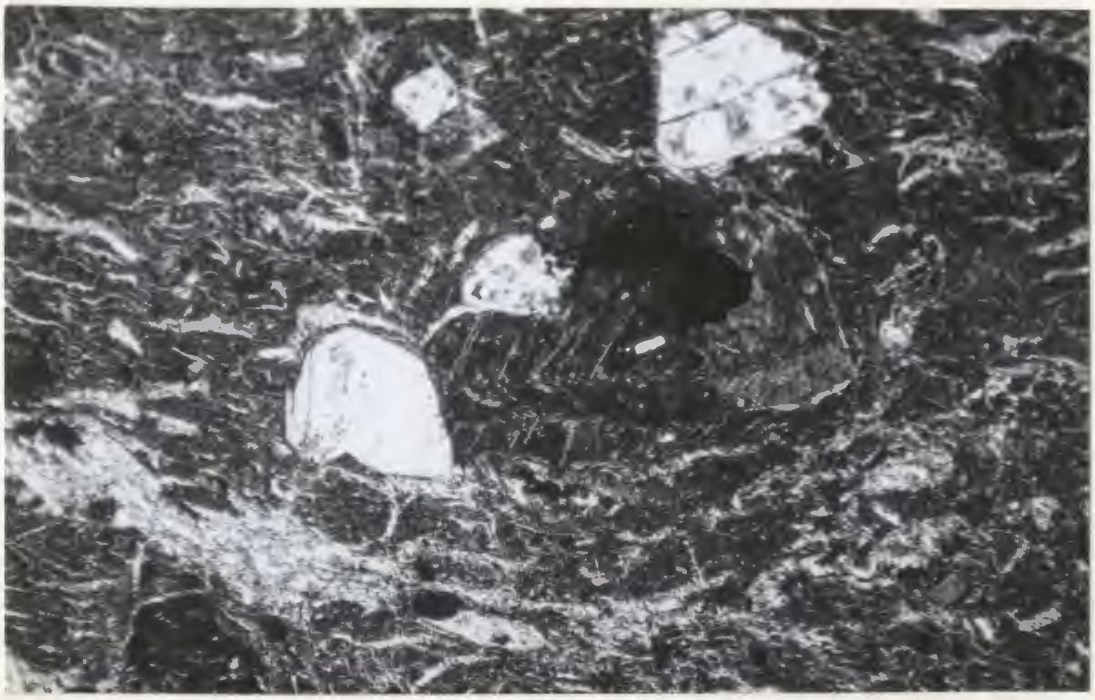

Photomicrograph 54. Same specimen as photomicrograph 53. Light-coloured areas replacing shard matrix are predominantly sericite. Crossed nicols.

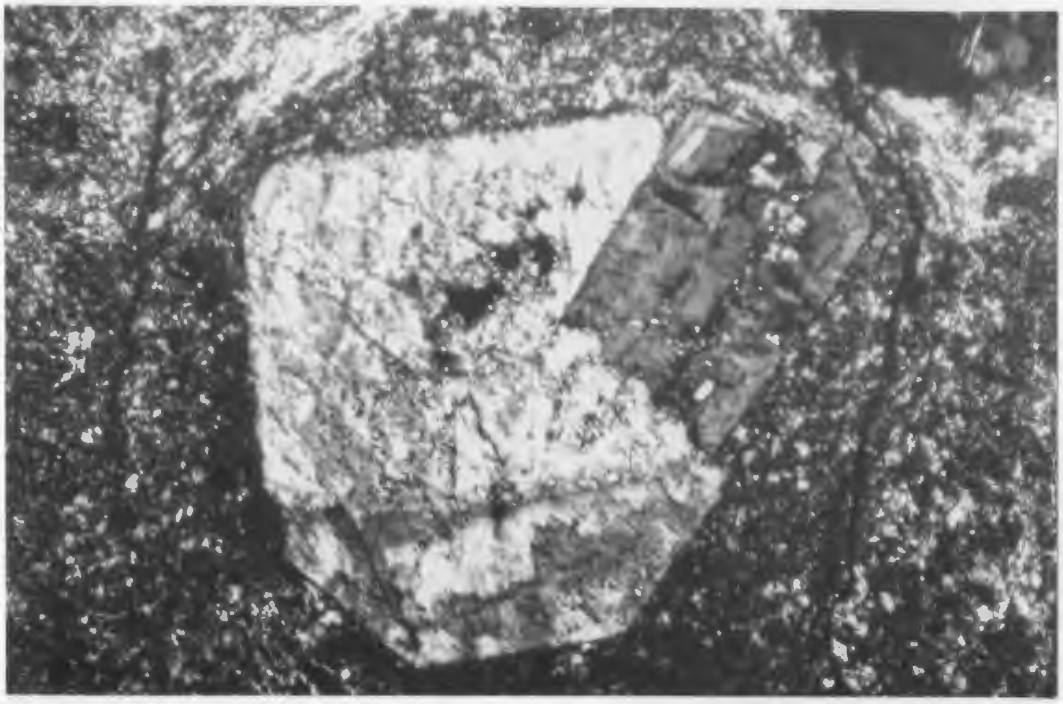

Photomicrograph 55. Mottled albite glomerocryst exhibiting patchy replacement by potassium feldspar and minor sericite. Crossed nicols; field of view approx. 6.1mm across. Specimen H96; middle of unit 15.

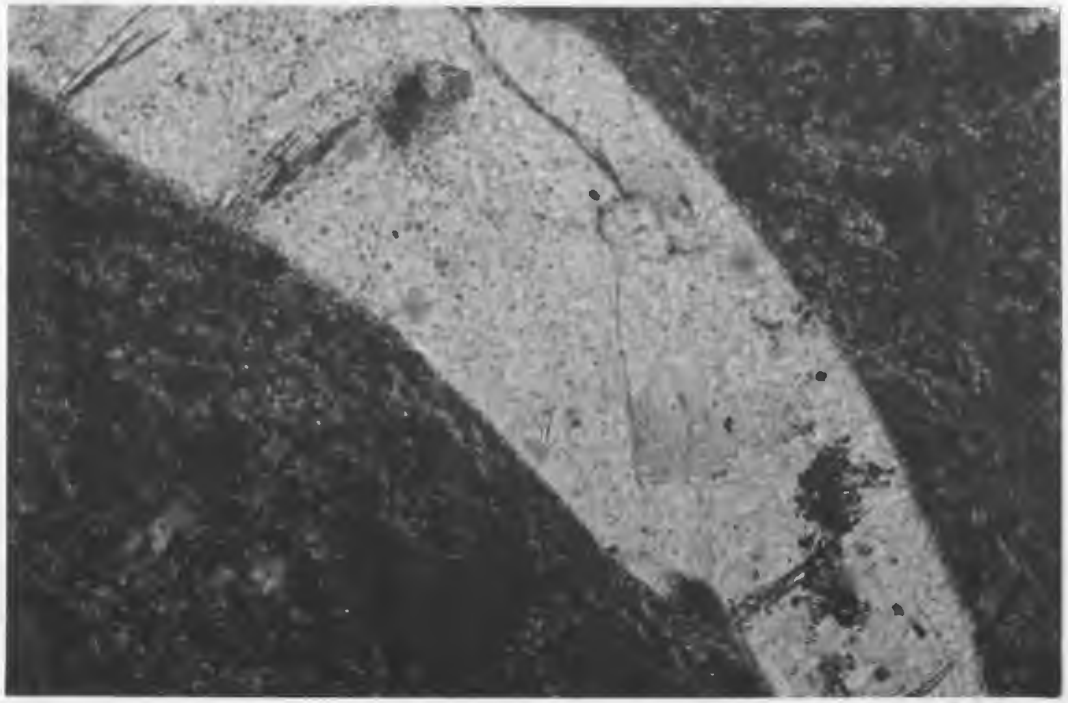

Photomicrograph 56. K-feldspar (darker grey with lower relief) spreading from fractures and partly replacing resorbed albite phenocryst. Crossed nicols; field of view approx. 3mm across. Specimen H120; central zone of welding in unit 23.

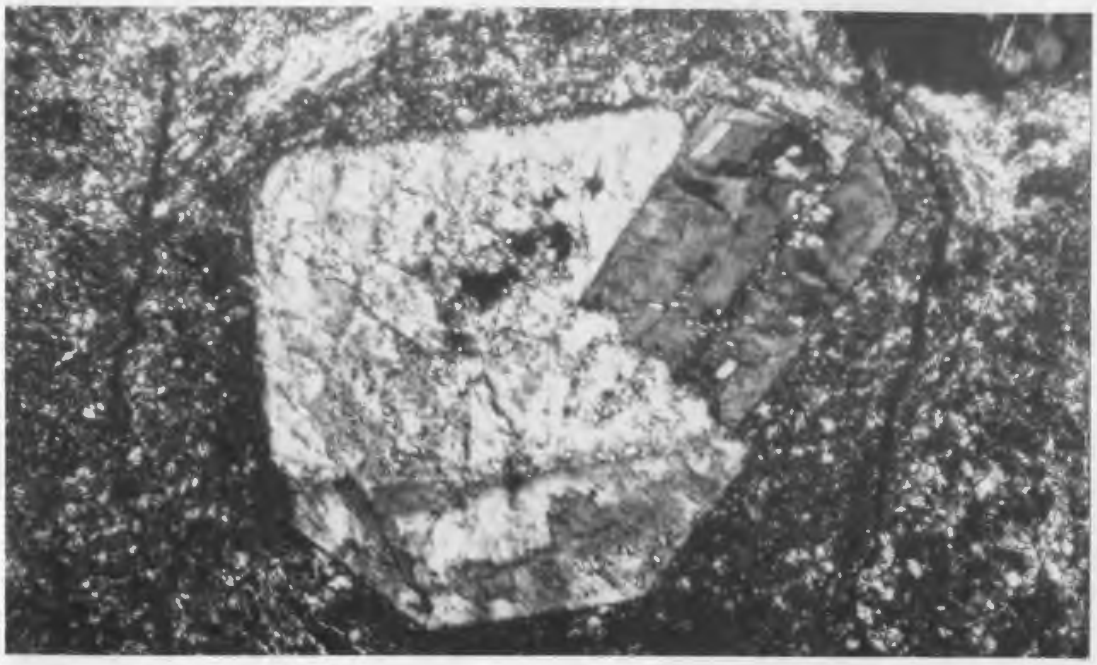

Photomicrograph 55. Mottled albite glomerocryst exhibiting patchy replacement by potassium feldspar and minor sericite. Crossed nicols; field of view approx. 6.1mm across. Specimen H96; middle of unit 15.

Photomicrograph 56. K-feldspar (darker grey with lower relief) spreading from fractures and partly replacing resorbed albite phenocryst. Crossed nicols; field of view approx. 3mm across. Specimen H120; central zone of welding in unit 23.

Photomicrograph 59. "Tuffisite" pipe transecting welded tuff and carrying rotated fragments and crystals. Plane-polarized light; field of view approx. 30mm across. Specimen C91; base of unit 59.

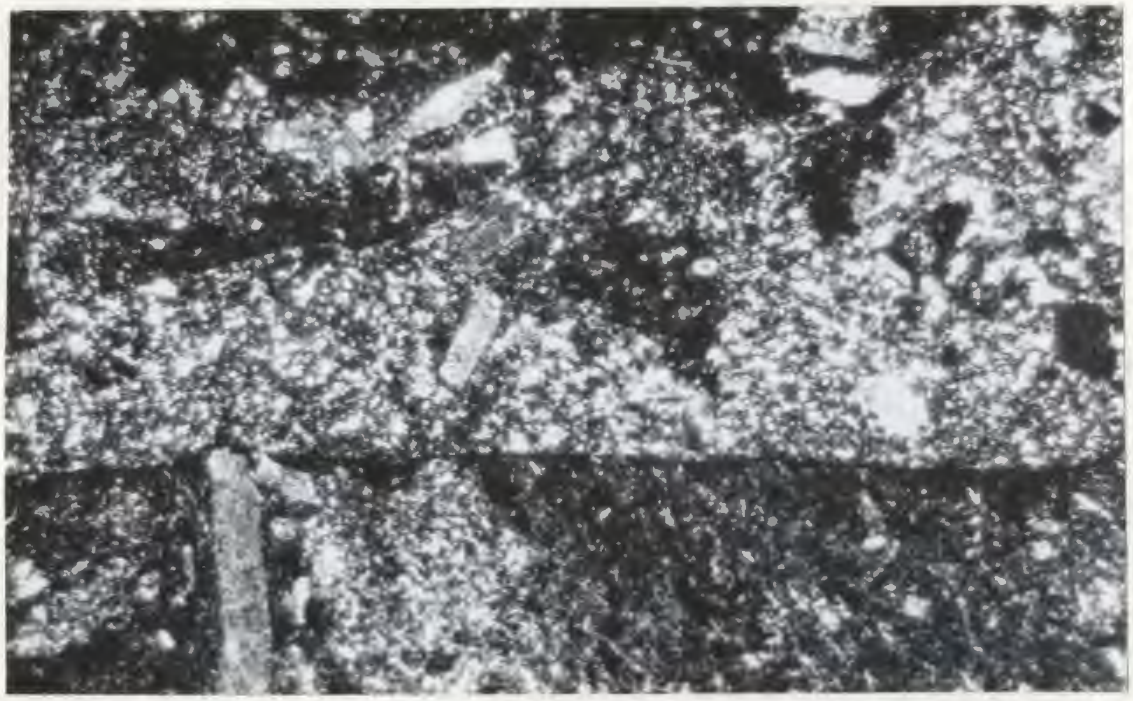

Photomicrograph 60. Same specimen as photomicrograph 59. Crossed nicols. Note turbid albite phenocryst and coarse recrystallisation.

Photomicrograph 61. Veins of albite (pale grey) and epidote (dark grey with high relief) promoting recrystallisation of iron-oxide at their margins. Compare this with devitrification textures described in photomicrographs 27-31. Plane-polarized light; field of view approx. 12mm across. Specimen H110; 3ft (0.9m) above green altered vesicular base of unit 15.

Photomicrograph 62. Electron-probe X-ray image photomicrographs showing patchy development of sericite within an albite phenocryst.

a) Na (20000 counts).

b) K (15000 counts).

c) Ca (1500 counts).

Photomicrograph 63. Electron-probe photomicrographs of K-feldspar along fractures in an albite phenocryst and partly replacing its host.

a) Plane-polarized light (x400).

b) Na (20000 counts).

c) K (10000 counts).

d) Ca (2500 counts).

Photomicrograph 64. Electron-probe photomicrographs of K-Na cryptoperthite along fractures and cleavage planes within an albite phenocryst.

a) Plane-polarized light (x400). Note rhomb of calcite (centre).

b) Na (20000 counts)

c) K (15000 counts).

d) Ca (2500 counts).

GEOLOGICAL MA

EXPLANATION

Ash-flow tuffs

Vitric tuffs (Bacon Cove Sequence)

Cooling unit

Volcanogenic sediments

Rhyolite sills

Porphyrites

Basalts

Diobase dykes

Conception Group

MAP OF COLLIERS

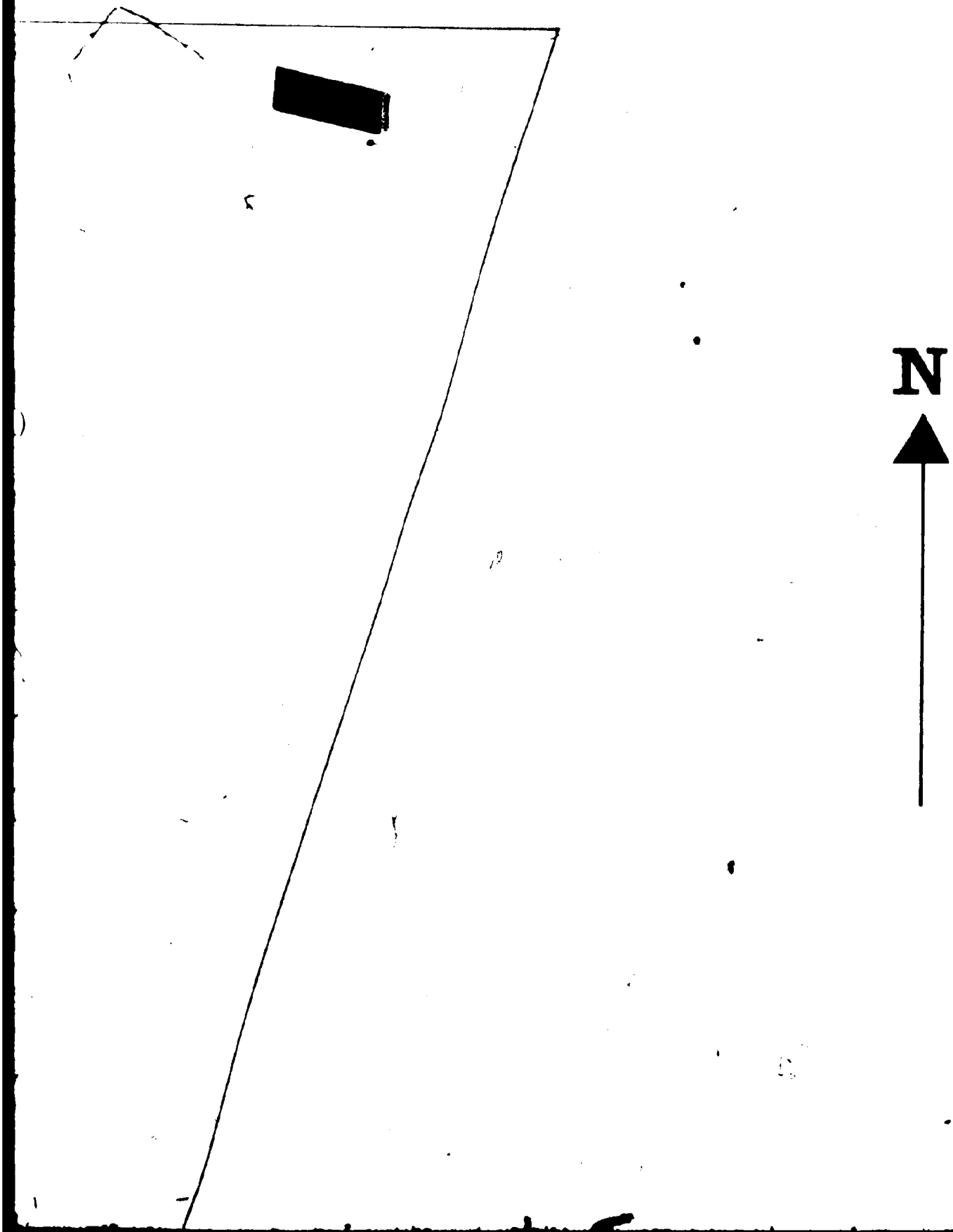

GC46a,b

S PENINSULA

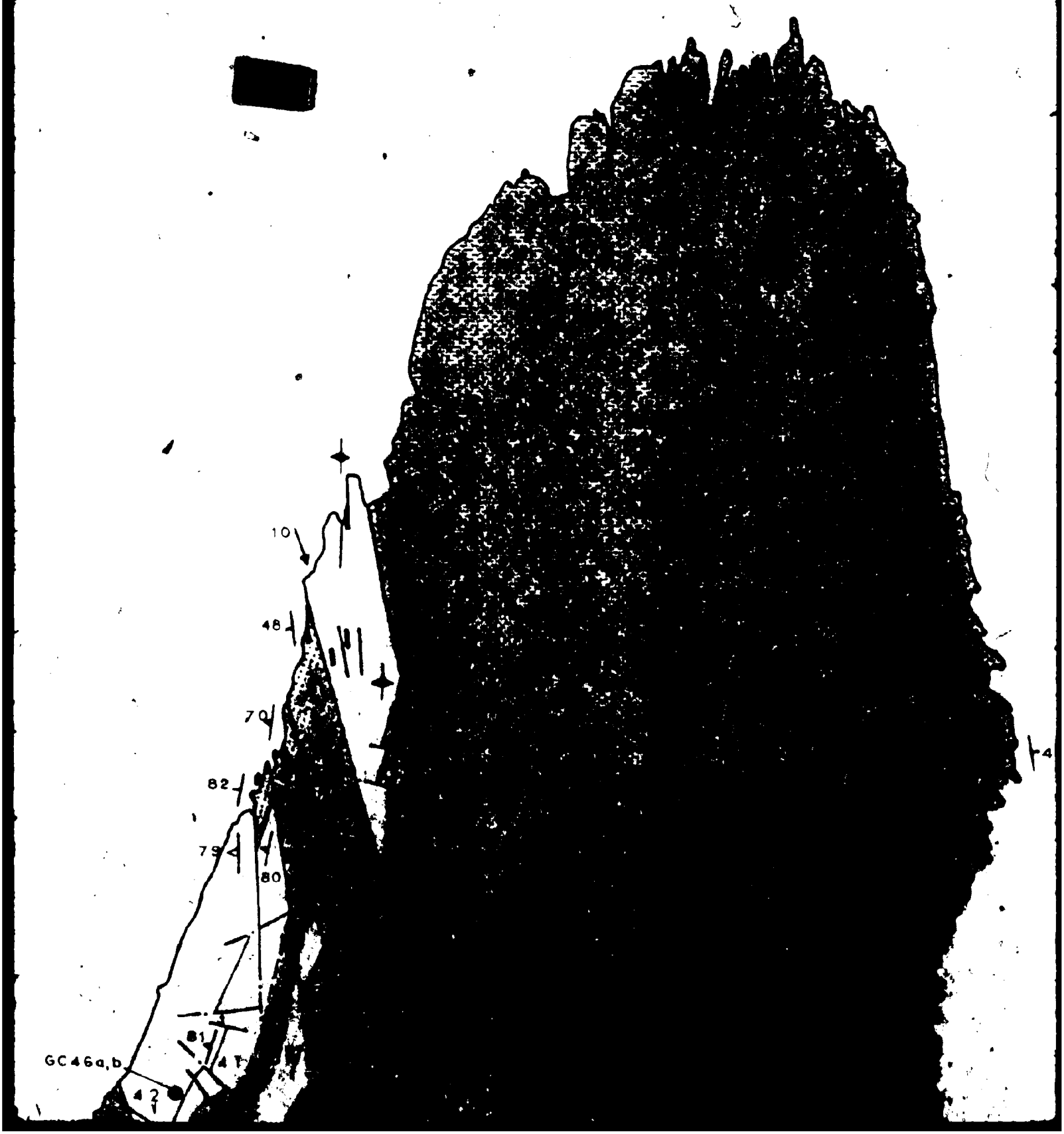

Conception Group

[redacted]

Cambrian

Fault

Geological boundary

Bedding (strike and dip)

Overturned bedding

Cleavage (vertical)

Welding (vertical)

Fold plunge

Road

Geochemical sampling site

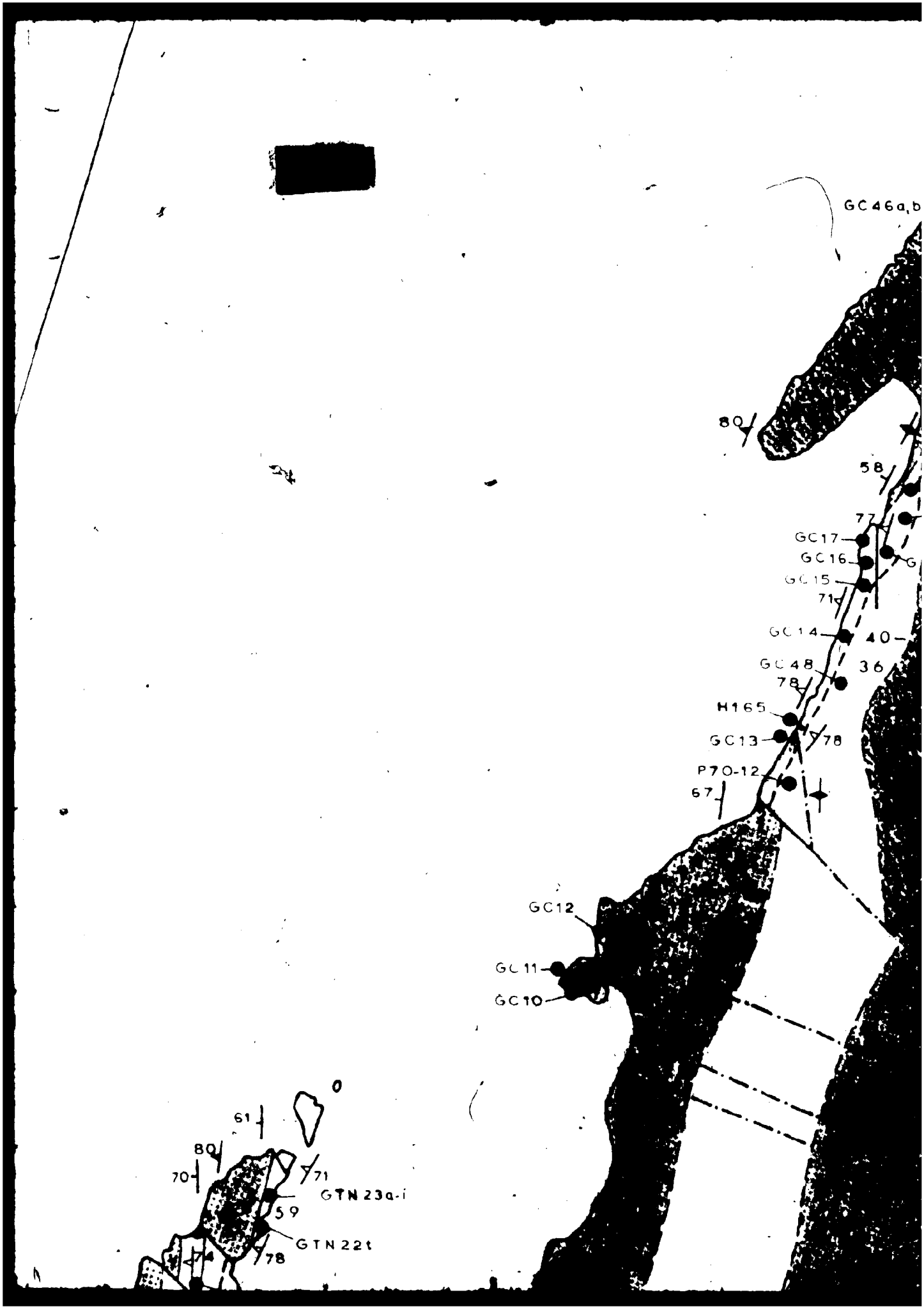
GC46a,b
80
58
77
GC17
GC16
GC15
71
GC14
40
GC48
36
78
H165
GC13
78
P70-12
67
GC12
GC11
GC10
0
61
80
70
71
GTN 23a-i
59
GTN 22t
74
78

GC46a,b
81
41
42
83
80
GC43
58
77
GC17
GC16
GC15
71
GC14
40
GC48
36
78
H165
GC13
78
P70-12
67
GC12
GC11
GC10
79
3
2
GC37a
GC38
NX1
6
2
3
GC42
53
5
6
80
1

80
81
41
42
44
83
GC43
70
3
2
GC37a
GC38
NX1
6
GC39a,
b
2
3
7
GC42
53
5
50
70
75
60
80
60

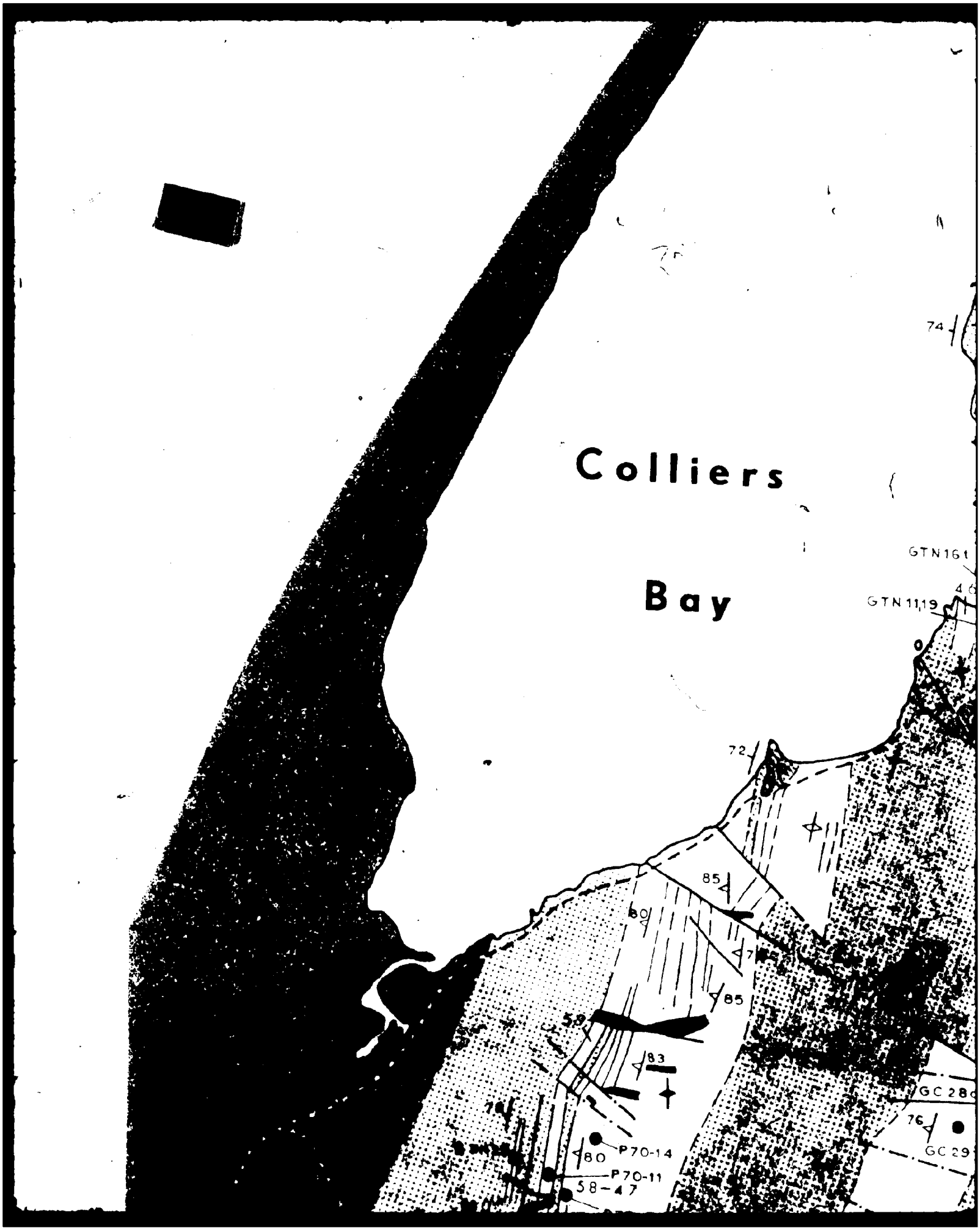
Colliers
Bay
74
GTN 161
GTN 11,19
72
85
80
85
83
74
76
GC 28
GC 29
80
P70-14
P70-11
58-47

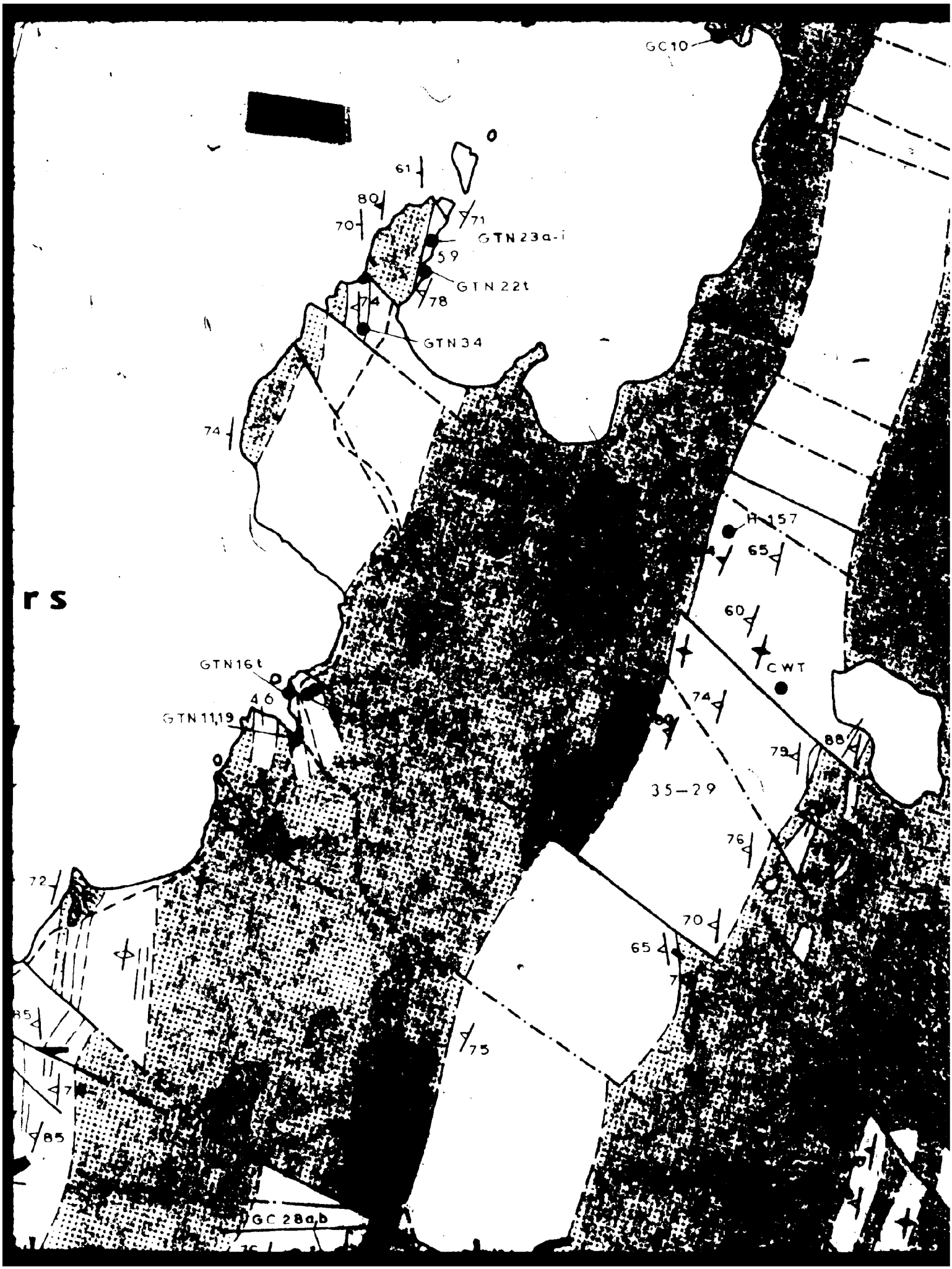
GC10
61
80
70
71
GTN23a-i
59
GTN22t
78
74
GTN34
74
H157
65
60
CWT
74
88
79
35–29
76
72
70
65
85
75
85
GC 28a,b
GTN16t
46
GTN11,19

GC11
GC10
GC42
A157
CWT
35-29
65
60
74
79
88
76
70
65
80
13
10
68
55
62
55
80
65
53

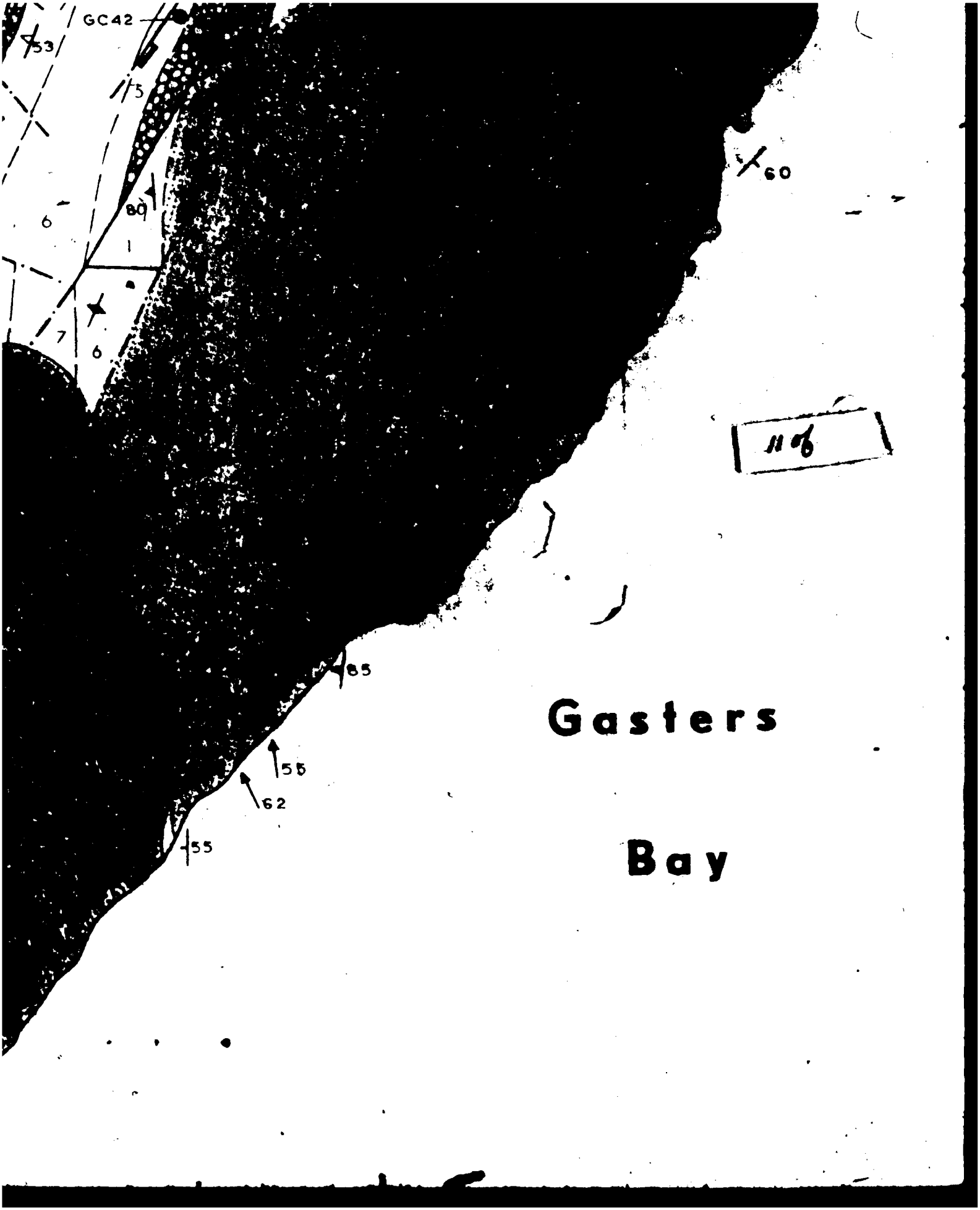
GC42
53
3
80
6
1
7
6
60
85
55
62
55
Gasters
Bay

120
85
80
71
85
59
83
78
IN 25
80
P70-14
P70-11
58-47
P70-9
60
80
85
78
26-17
15
80
76
GC23
GC22
78
72

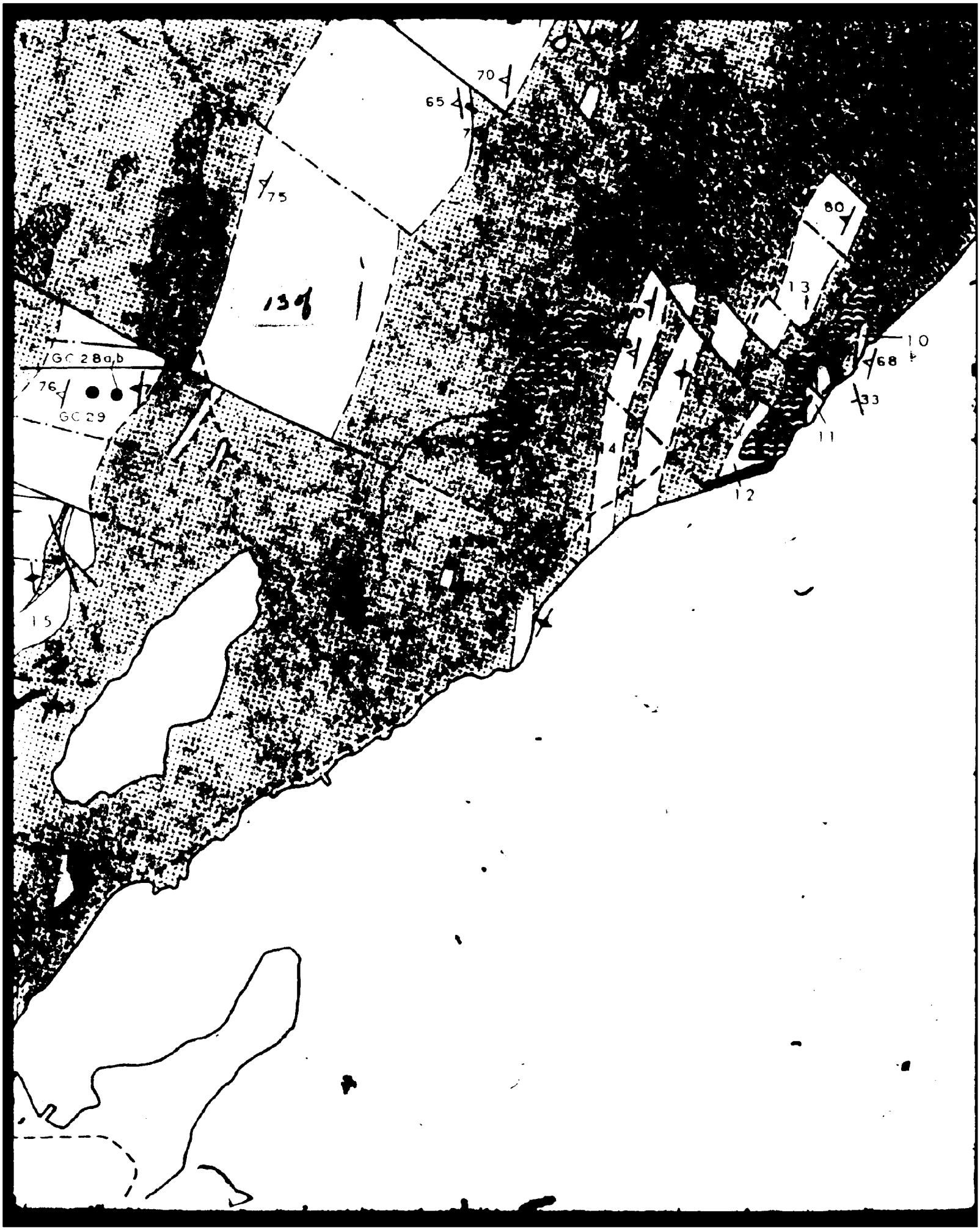
70
65
75
139
80
13
10
68
33
11
12
14
GC 28a,b
76
GC 29
15

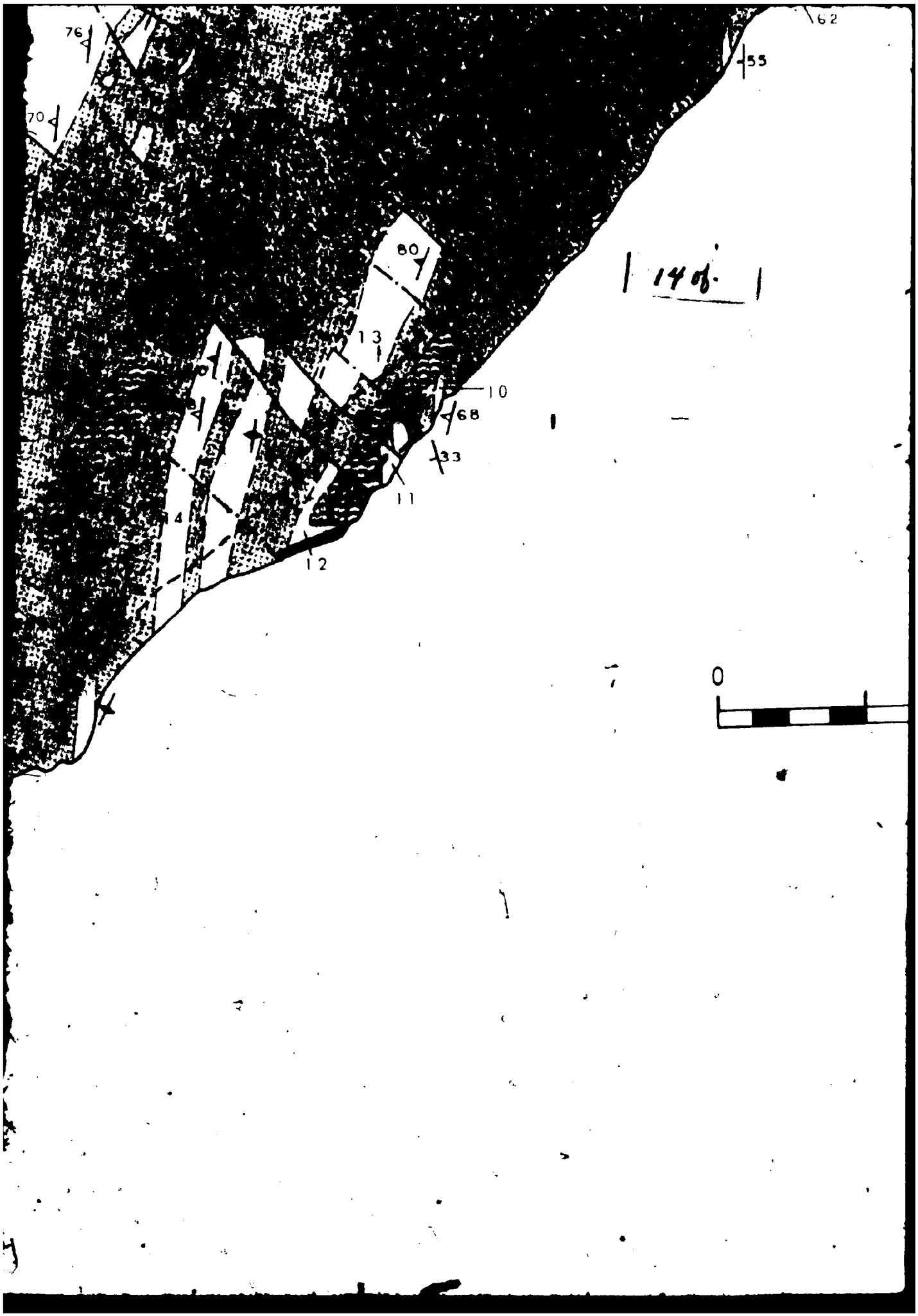
76
70
62
55
80
13
10
68
33
11
14
12
0
14 of.

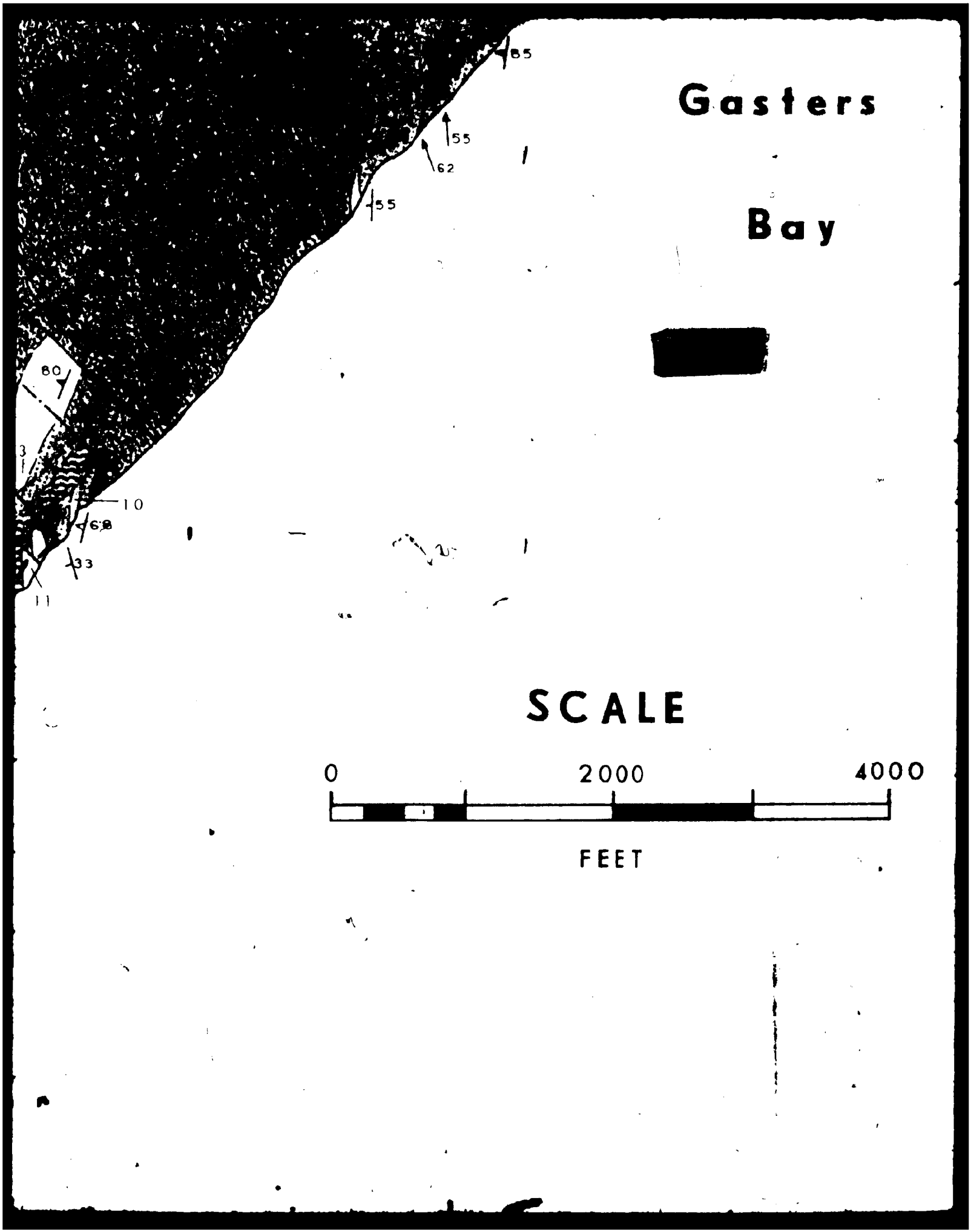
Gasters
Bay
85
55
62
55
80
3
10
68
33
11
SCALE
0
2000
4000
FEET